

1-1-1996

# Porous isotactic polypropylene from supercritical propane solution : synthesis and characterization.

Paul D. Whaley

*University of Massachusetts Amherst*

Follow this and additional works at: [https://scholarworks.umass.edu/dissertations\\_1](https://scholarworks.umass.edu/dissertations_1)

---

## Recommended Citation

Whaley, Paul D., "Porous isotactic polypropylene from supercritical propane solution : synthesis and characterization." (1996).

*Doctoral Dissertations 1896 - February 2014*. 951.

[https://scholarworks.umass.edu/dissertations\\_1/951](https://scholarworks.umass.edu/dissertations_1/951)

This Open Access Dissertation is brought to you for free and open access by ScholarWorks@UMass Amherst. It has been accepted for inclusion in Doctoral Dissertations 1896 - February 2014 by an authorized administrator of ScholarWorks@UMass Amherst. For more information, please contact [scholarworks@library.umass.edu](mailto:scholarworks@library.umass.edu).

UMASS/AMHERST



312066011493966

POROUS ISOTACTIC POLYPROPYLENE FROM  
SUPERCRITICAL PROPANE SOLUTION:  
SYNTHESIS AND CHARACTERIZATION

A Dissertation Presented

by

PAUL D. WHALEY

Submitted to the Graduate School of the  
University of Massachusetts Amherst in partial fulfillment  
of the requirements for the degree of

DOCTOR OF PHILOSOPHY

May 1996

Polymer Science and Engineering

© Copyright by Paul D. Whaley 1996

All Rights Reserved

POROUS ISOTACTIC POLYPROPYLENE FROM  
SUPERCRITICAL PROPANE SOLUTION:  
SYNTHESIS AND CHARACTERIZATION

A Dissertation Presented

by

PAUL D. WHALEY

Approved as to style and content by:



---

H. Henning Winter, Chair



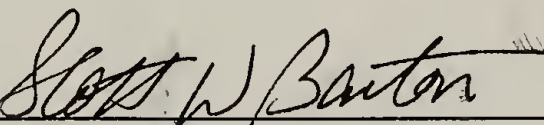
---

Paul Ehrlich, Member



---

Richard S. Stein, Member



---

Scott Barton, Member



---

Richard J. Farris, Department Head  
Department of Polymer Science and Engineering

**Dedicated**  
**to my parents**

## ACKNOWLEDGMENTS

I would like to thank Professor Paul Ehrlich for his guidance and encouragement. He consistently took an active role in my work and his training concerning the fundamentals of phase behavior was invaluable. I would also like to thank Professor Richard S. Stein for his suggestions and general thoughtfulness. His level of enthusiasm for science is approached by few and his concern for future generations is unparalleled.

I would also like to thank Professor H. Henning Winter for serving as the chair for my thesis committee and for providing laboratory space and equipment which, without, this work would not have been possible. I would also like to thank Professor Scott Barton for serving on my committee and for his encouragement and kind words.

I am grateful to Professor W. C. Conner for allowing me to use his gas adsorption equipment and for very helpful discussions concerning data analysis. I am also very grateful to Professor Greg Beaucage for performing small angle x-ray scattering measurements on porous iPP samples at various facilities.

I am grateful for discussions with Professor Mohan Srinivasarao and Drs. Sandeep Kulkarni and V. Janarthanan over the years which have broadened my scientific knowledge. The help and support of my fellow classmates, labmates, and officemates is appreciated as well as the university staff which have helped in numerous ways to make this work possible.

I would like to thank my family for supporting my pursuit of an advanced degree. I hope that I can repay them for the sacrifices they have made for me.

Finally, I would like to thank my fiancée, Judith Kaye Jackson, for her patience and understanding throughout my graduate work. Her support has helped make this thesis a reality and I look forward to our new life together.

## ABSTRACT

### POROUS ISOTACTIC POLYPROPYLENE FROM SUPERCRITICAL PROPANE SOLUTION: SYNTHESIS AND CHARACTERIZATION

MAY 1996

PAUL D. WHALEY

B.S., UNIVERSITY OF TOLEDO  
M.S., UNIVERSITY OF MASSACHUSETTS AMHERST  
Ph. D., UNIVERSITY OF MASSACHUSETTS AMHERST

Directed by: Professor H. Henning Winter

Solid-supercritical fluid (S-SCF) and liquid-vapor equilibria (cloud-point pressures) for iPP/propane systems were determined. Liquid-vapor equilibria below S-SCF equilibria temperatures for iPP/propane were obtained by studying the atactic polypropylene (aPP)/propane system. Modeling of these systems by the Sanchez-Lacombe lattice fluid theory required empirical adjustment of mixing parameters. Cloud-point pressures for polyolefins of increasing branch length and some poly(ethylene-co-octene) copolymers in propane were also determined. They decrease with increasing percentage of carbon in the branches.

Crystallization of iPP from single phase systems was achieved by controlling temperature and pressure. Under most conditions, crystallizations of un-nucleated iPP resulted in large (100+  $\mu\text{m}$ ) microspheres having poor mechanical coherency. A highly effective nucleating agent, dibenzylidene-d-sorbitol (DBS), was added to promote nucleation and coherence, but requires a cosolvent for solubilization. S-SCF equilibria for DBS in propane/1-propanol mixtures were determined as well as changes in the phase behavior of aPP/propane with the addition of an alcohol and is summarized in terms of changes in critical behavior.



Surface areas and pore size distributions (PSD) in the mesopore range (20 to ~500 Å) were determined by analysis of nitrogen adsorption-desorption isotherms. Surface areas ranged from 120-180 m<sup>2</sup>/g with most probable pore sizes, based on a cylindrical pore model, of between 100-200 Å. This pore size is supported by small angle x-ray scattering data analyzed by a model which treats the pores as a distribution of spherical aggregates. A more specific model is proposed in which the microsphere contains a dense core defined by a radius beyond which fibrillation and gas adsorption sets in. The high surface area of porous iPP is attributed to as yet unknown details of the organization of iPP lamellae on the nanoscale.

## TABLE OF CONTENTS

ACKNOWLEDGMENTS .....	v
ABSTRACT.....	vi
LIST OF TABLES .....	xiii
LIST OF FIGURES.....	xvi
Chapter	
1. INTRODUCTION.....	1
1.1 Motivation.....	1
1.2 Scope of Thesis Work.....	2
REFERENCES.....	5
2. POLYMER/SUPERCRITICAL FLUID PHASE BEHAVIOR.....	6
2.1 Background.....	7
2.1.1 Supercritical Fluids.....	7
2.1.2 Phase Separation in Supercritical Polymer Solutions.....	8
2.1.3 Previous Research .....	12
2.2 Experimental .....	15
2.2.1 Solvents .....	15
2.2.2 Polymers and Additives .....	16
2.2.3 Apparatus and Procedure .....	19
2.3 Results and Discussion.....	21
2.3.1 Polypropylene/Supercritical Fluid Systems.....	22
2.3.1.1 Isotactic Polypropylene/Propane .....	22
2.3.1.2 Atactic Polypropylene/Propane.....	23
2.3.1.3 Atactic Polypropylene/Propylene.....	23
2.3.1.4 Discussion.....	24

2.3.2	Polyolefin Branching .....	25
2.3.2.1	Structural Parameter - Branch Length .....	25
2.3.2.2	Structural Parameter - Branch Density.....	25
2.3.2.3	Correlation of Cloud-Point Pressures with Structural Parameters.....	26
2.3.2.4	Discussion.....	26
2.3.3	Ternary Systems.....	28
2.3.3.1	Ternary System Construction .....	28
2.3.3.2	Atactic Polypropylene/Propane/Alcohol .....	29
2.3.3.2.1	Atactic Polypropylene/Propane/Ethanol .....	29
2.3.3.2.2	Atactic Polypropylene/Propane/1-Propanol .....	29
2.3.3.2.3	Atactic Polypropylene/Propane/1-Butanol .....	30
2.3.3.2.4	Summary of Atactic Polypropylene/ Propane/Alcohol Systems.....	30
2.3.3.3	Dibenzylidene-d-sorbitol (DBS)/Propane/1-Propanol.....	31
2.3.3.4	Discussion.....	32
2.4	Conclusions .....	34
	REFERENCES.....	58
3.	MODELING OF PHASE BEHAVIOR.....	63
3.1	Background.....	63
3.1.1	Solution Thermodynamics .....	64
3.1.2	Polymer Solution Theories .....	66
3.1.3	Previous Modeling of LCST Behavior.....	67
3.1.4	Sanchez-Lacombe (SL) Lattice Fluid Theory.....	69
3.2	Sanchez-Lacombe (SL) Modeling of Experimental Systems .....	73
3.2.1	Dimensionless Parameter Analysis .....	74
3.2.1.1	Solution Set .....	74
3.2.1.2	Minimum $\delta$ Approach .....	76

3.2.2	Binary Systems.....	77
3.2.2.1	Sanchez-Lacombe Equation of State Parameters .....	77
3.2.2.2	Cloud-Point Isoleths for Atactic Polypropylene/ Propane.....	78
3.2.2.3	Cloud-Point Isotherms for Isotactic Polypropylene/ Propane.....	80
3.2.3	Ternary Systems.....	80
3.2.3.1	Pseudo-Binary Approach.....	80
3.2.3.2	Sanchez-Lacombe Equation of State Parameters .....	81
3.2.3.3	Cloud-Point Isoleths for Atactic Polypropylene/ Propane/1-Propanol .....	81
3.3	Conclusions .....	82
	REFERENCES.....	100
4.	FORMATION AND CHARACTERIZATION OF POROUS ISOTACTIC POLYPROPYLENE .....	104
4.1	Background.....	105
4.1.1	Thermally Induced Phase Separation (TIPS).....	105
4.1.2	Solvent Removal .....	108
4.1.3	Porous Isotactic Polypropylene by TIPS.....	109
4.2	Characterization Methods for Porous Isotactic Polypropylene.....	111
4.2.1	Microscopy and Stereological Relationships .....	112
4.2.2	Adsorption-Desorption Isotherms .....	113
4.2.2.1	Surface Areas.....	115
4.2.2.1.1	BET Theory.....	115
4.2.2.1.2	Static BET Apparatus.....	117
4.2.2.2	Porosity and Pore Size Distributions.....	118
4.2.2.2.1	Theory .....	118
4.2.2.2.2	Adsorption-Desorption Apparatus .....	122

4.2.3	Small Angle X-Ray Scattering (SAXS).....	123
4.2.3.1	Polydisperse Globular Aggregate Model.....	123
4.2.3.2	Experimental.....	125
4.3	Experimental.....	125
4.3.1	Solvents.....	125
4.3.2	Polymers and Additives.....	126
4.3.3	Apparatus.....	126
4.4	Results.....	127
4.4.1	Formation of Porous Isotactic Polypropylene (iPP).....	127
4.4.1.1	Bulk Morphology of Unnucleated iPP.....	127
4.4.1.2	Bulk Morphology of Nucleated iPP.....	129
4.4.2	Surface Area, Porosity, and Pore Size Distribution.....	130
4.4.2.1	Temperature History.....	130
4.4.2.2	Solvent.....	131
4.4.2.3	Pressure.....	132
4.4.2.4	Miscellaneous.....	133
4.4.3	Models.....	134
4.4.3.1	Lamellar Model.....	135
4.4.3.2	Fibrillation Model.....	135
4.4.3.2.1	Fibrillation Model - Temperature History.....	139
4.4.3.2.2	Fibrillation Model - Solvent.....	140
4.4.3.2.3	Fibrillation Model - Pressure.....	140
4.4.4	Discussion.....	141
4.5	Conclusions.....	149
	REFERENCES.....	181

5. CONCLUSIONS AND SUGGESTIONS FOR FUTURE WORK .....	185
5.1 Conclusions .....	185
5.1.1 Polymer/Supercritical Fluid Phase Behavior.....	185
5.1.2 Modeling of Phase Behavior .....	187
5.1.3 Formation and Characterization of Porous Isotactic Polypropylene .....	188
5.2 Suggestions for Future Work.....	189
REFERENCES.....	192
APPENDICES	
A. INDEX OF SUPERCRITICAL FLUID/POLYMER SYSTEMS.....	194
REFERENCES.....	198
B. ADSORPTION-DESORPTION ISOTHERMS AND SAXS DATA .....	201
B.1 Temperature History.....	202
B.2 Solvent.....	204
B.3 Pressure.....	206
B.4 Miscellaneous.....	208
BIBLIOGRAPHY.....	226

## LIST OF TABLES

Table	Page
2.1	Typical Property Values for Gases and Liquids Compared to Values for Supercritical Fluids Under Conditions of Polymer Miscibility..... 8
2.2	Weight-Average Molecular Weight and Polydispersity Information for Polypropylenes ..... 16
2.3	Weight-Average Molecular Weight and Polydispersity Information for Polyolefins with Different Side-Chain Branching..... 17
2.4	Weight-Average Molecular Weight, Density, and Octene Content of Poly(ethylene-co-octene) Samples ..... 18
2.5	Location of Second Critical End Point, $C_2$ , for iPP1 and iPP2, in Propane ..... 23
2.6	UCEP and LCEP Temperatures for Atactic Polypropylene/Propane/Alcohol Systems ..... 31
2.7	Critical Temperatures and Pressures for Propane/1-Propanol Mixtures..... 31
3.1	Modeling of Polymer/Solvent Systems by Polymer Solution Theories Accounting for Equation of State (EOS) Effects ..... 68
3.2	List of Solvent, Polymer, and Theory Abbreviations Used in Table 3.1 ..... 69
3.3	Sanchez-Lacombe Equation of State Parameters ..... 78
3.4	Sanchez-Lacombe Equation of State Parameters for Propane/1-Propanol Mixtures..... 81
4.1	Comparison of Peak Pore Size from Nitrogen Adsorption (Cylindrical Pore Model) and Small Angle X-Ray Scattering (Polydisperse Globular Aggregate Model) for Porous iPP at Different Isothermal Crystallization Temperatures..... 131
4.2	Comparison of Peak Pore Size from Nitrogen Adsorption (Cylindrical Pore Model) and Small Angle X-Ray Scattering (Polydisperse Globular Aggregate Model) for Porous iPP Crystallized from Different Alkanes ..... 132

4.3	Comparison of Peak Pore Size from Nitrogen Adsorption (Cylindrical Pore Model) and Small Angle X-Ray Scattering (Polydisperse Globular Aggregate Model) for Porous iPP Isothermally Crystallized at 65°C at Different Pressures.....	133
4.4	BET Surface Areas and Porosity for PP-100 and PP-DBS.....	134
A.1	LCEP Studies of Binary Polymer/Solvent Systems .....	194
A.2	LCST Studies of Binary Polymer/Solvent Systems .....	195
A.3	LCST Studies of Ternary Polymer/Solvent/Solvent Systems.....	196
A.4	Definition of Remarks - Relationship to Investigated Parameters .....	196
A.5	List of Solvent and Polymer Abbreviations Used in Tables A.1, A.2, and A.3.....	197
B.1	BET Parameters for Porous iPP on Different Dates.....	202
B.2	BET Parameters for Porous iPP Isothermally Crystallized at Different Temperatures.....	203
B.3	Adsorption-Desorption Parameters for Porous iPP Isothermally Crystallized at Different Temperatures .....	203
B.4	Hosemann Model Parameters for Porous iPP Isothermally Crystallized at Different Temperatures .....	204
B.5	BET Parameters for Porous iPP Isothermally Crystallized from Different Alkanes.....	205
B.6	Adsorption-Desorption Parameters for Porous iPP Isothermally Crystallized from Different Alkanes.....	205
B.7	Hosemann Model Parameters for Porous iPP Isothermally Crystallized from Different Alkanes.....	206
B.8	BET Parameters for Porous iPP Isothermally Crystallized at Different Pressures .....	207



<b>B.9</b>	<b>Adsorption-Desorption Parameters for Porous iPP Isothermally Crystallized at Different Pressures .....</b>	<b>207</b>
<b>B.10</b>	<b>Hosemann Model Parameters for Porous iPP Isothermally Crystallized at Different Pressures .....</b>	<b>208</b>
<b>B.11</b>	<b>BET Parameters for Porous iPP Isothermally Crystallized from Propane at Different Conditions.....</b>	<b>209</b>
<b>B.12</b>	<b>Adsorption-Desorption Parameters for Porous iPP Isothermally Crystallized from Propane at Different Conditions.....</b>	<b>209</b>

## LIST OF FIGURES

Figure	Page
2.1	Type I Phase Behavior ( $C_A$ is the critical point of the more volatile component (A), $C_B$ is the critical point of the less volatile component (B), - - - is the critical locus of the mixture, and LV denotes liquid-vapor equilibrium)..... 37
2.2	Type V Phase Behavior ( $C_A$ is the critical point of the more volatile component (A), - - - is the locus of lower critical solution temperatures (LCST), UCEP and LCEP are upper and lower critical end points, L is a single liquid phase, LV denotes liquid-vapor equilibrium, and LLV denotes liquid-liquid-vapor equilibrium) ..... 38
2.3	Type IV Phase Behavior ( $C_A$ is the critical point of the more volatile component (A), - - - is the locus of upper and lower critical solution temperatures (UCST and LCST, respectively), UCEP and LCEP are upper and lower critical end points, L is a single liquid phase, LV denotes liquid-vapor equilibrium, LL denotes liquid-liquid equilibrium, and LLV denotes liquid-liquid-vapor equilibrium) ..... 39
2.4	Crystalline Polymer/Supercritical Fluid Phase Diagram ( $T_m$ is the melting point of the pure polymer, $S_p$ -L-V denotes solid polymer-liquid-vapor equilibrium, LV denotes liquid-vapor equilibrium, $C_2$ is the second critical end point, and — is the locus of lower critical solution temperatures (L=V)) ..... 40
2.5	Variable Volume View Cell ..... 41
2.6	Overall High Pressure Phase Behavior Apparatus ..... 42
2.7	Cloud-Point Isopleths for iPP1/Propane (SCF is a single supercritical phase, LV denotes liquid-vapor equilibrium, S-SCF denotes a two phase region of solid polymer and a supercritical phase, and $C_2$ is the location of the second critical end point)..... 43
2.8	Cloud-Point Isopleths for iPP2/Propane (SCF is a single supercritical phase, LV denotes liquid-vapor equilibrium, S-SCF denotes a two phase region of solid polymer and a supercritical phase, and $C_2$ is the location of the second critical end point)..... 44
2.9	Cloud-Point Isotherms for iPP1/Propane (SCF denotes a single supercritical phase and LV denotes liquid-vapor equilibrium) ..... 45

2.10	Cloud-Point Isotherms for iPP2/Propane (SCF denotes a single supercritical phase and LV denotes liquid-vapor equilibrium) .....	46
2.11	Cloud-Point Isopleths for aPP/Propane Compared to iPP/Propane (SCF denotes a single supercritical phase and LV denotes liquid-vapor equilibrium).....	47
2.12	Cloud-Point Isopleths for aPP/Propylene Compared to aPP/Propane (SCF denotes a single supercritical phase and LV denotes liquid-vapor equilibrium).....	48
2.13	Cloud-Point Isopleths for Various Polyolefins with Different Side-Chain Branching in Propane (SCF denotes a single supercritical phase, LV denotes liquid-vapor equilibrium, * denotes data of Condo et al., 1992, and ** denotes a 70 wt. % ethylene copolymer) .....	49
2.14	Cloud-Point Isopleths for Poly(ethylene-co-octene) Copolymers with Different Octene Contents in Propane (SCF denotes a single supercritical phase, LV denotes liquid-vapor equilibrium, and * denotes data of Condo et al., 1992).....	50
2.15	Correlation of Cloud-Point Pressures of Polyolefins in Supercritical Propane with Branch Density (PE-1484 is a high density polyethylene, P(E-alt-P) is poly(ethylene-alt-propylene), aPP is atactic polypropylene, PB is poly(1-butene), PMP is poly(4-methyl-1-pentene), □ - is data of Condo et al., 1992, and O , Δ - is data of Chen et al., 1995) .....	51
2.16	Correlation of Cloud-Point Pressures of Polyolefins in Supercritical Propane with % Carbon in Branches (PE-1484 is a high density polyethylene, P(E-alt-P) is poly(ethylene-alt-propylene), aPP is atactic polypropylene, PB is poly(1-butene), PMP is poly(4-methyl-1-pentene), □ - is data of Condo et al., 1992, and O , Δ - is data of Chen et al., 1995) .....	52
2.17	Ternary Phase Behavior Diagram: Change in Critical Lines Upon Changing Polarity of Solvent (A=alkane, B=alcohol, and P=polymer).....	53
2.18	Cloud-Point Isopleths for the Ternary System: Atactic Polypropylene/Propane/Ethanol (2 wt. % Polymer Solutions) (Open symbol for 0.0 wt. % ethanol system represents the lower critical end point (LCEP)).....	54

2.19	Cloud-Point Isopleths for the Ternary System: Atactic Polypropylene/Propane/1-Propanol (2 wt. % Polymer Solutions) (Open symbols for 0.0 and 16.8 wt. % 1-propanol systems represent the lower critical end point (LCEP) and the lowest symbol for the 100 wt. % 1-propanol system represents the upper critical end point (UCEP)).....	55
2.20	Cloud-Point Isopleths for the Ternary System: Atactic Polypropylene/Propane/1-Butanol (2 wt. % Polymer Solutions) (Open symbols for 0.0, 16.8, 31.0, 47.3, and 65.4 wt. % 1-butanol systems represent upper and lower critical end points (UCEP and LCEP) and lowest points for 82.0 and 100.0 wt. % 1-butanol systems represent upper critical end points (UCEP)) .....	56
2.21	Solid-Supercritical Fluid Equilibria for Dibenzylidene-d-sorbitol in Propane/1-Propanol Mixtures (F denotes a single fluid phase and S-F denotes a solid and fluid phase) .....	57
3.1	Qualitative $\delta$ - $\zeta$ Solution Set .....	84
3.2	Pressure Dependence of $\delta$ - $\zeta$ Solution Set (MD is the solution at Minimum $\delta$ and point A represents another possible solution from the infinite set).....	85
3.3	SL Model Prediction for No Parameter Adjustment ( $\delta=0.0$ , $\zeta=1.0$ ) as Compared to the Experimental Cloud-Point Isopleth for the Atactic Polypropylene (aPP)/Propane System.....	86
3.4	$\delta$ - $\zeta$ Solution Sets for Atactic Polypropylene/Propane .....	87
3.5	$\delta$ - $\zeta$ Solutions at Minimum $\delta$ for Atactic Polypropylene/Propane .....	88
3.6	SL Model Prediction for No Parameter Adjustment ( $\delta=0.0$ , $\zeta=1.0$ ) and Minimum $\delta$ Approach as Compared to the Experimental Cloud-Point Isopleth for the Atactic Polypropylene (aPP)/Propane System. ....	89
3.7	$\delta$ - $\zeta$ Solutions at Minimum $\delta$ for Isotactic Polypropylene(iPP1)/Propane .....	90
3.8	$\delta$ - $\zeta$ Solutions at Minimum $\delta$ for Isotactic Polypropylene(iPP2)/Propane .....	91
3.9	Calculated Binodals and Spinodals for the iPP1/Propane System Using the Minimum $\delta$ Approach Compared to Experimental Cloud-Point Isotherms .....	92

3.10	Calculated Binodals and Spinodals for the iPP2/Propane System Using the Minimum $\delta$ Approach Compared to Experimental Cloud-Point Isotherms .....	93
3.11	$\delta$ - $\zeta$ Solution Sets for Atactic Polypropylene/Propane/1-Propanol (16.8 wt. % 1-Propanol) .....	94
3.12	$\delta$ - $\zeta$ Solution Sets for Atactic Polypropylene/Propane/1-Propanol (31.0 wt. % 1-Propanol) .....	95
3.13	$\delta$ - $\zeta$ Solution Sets for Atactic Polypropylene/Propane/1-Propanol (47.3 wt. % 1-Propanol) .....	96
3.14	$\delta$ - $\zeta$ Solution Sets for Atactic Polypropylene/Propane/1-Propanol (65.4 wt. % 1-Propanol) .....	97
3.15	$\delta$ Solutions at Minimum $\delta$ for Atactic Polypropylene/Propane/1-Propanol .....	98
3.16	$\zeta$ Solutions at Minimum $\delta$ for Atactic Polypropylene/Propane/1-Propanol .....	99
4.1	Temperature-Composition Phase Diagrams for Thermally Induced Phase Separation (TIPS) Processes (L denotes a single liquid phase, LL denotes liquid-liquid equilibrium, SL denotes solid-liquid equilibrium, Route A is the solidification of the polymer, and Route B is the phase separation of a single liquid phase into two liquid phases differing in polymer composition followed by solidification of the polymer).....	151
4.2	Temperature-Composition Phase Diagram for Liquid-Liquid Phase Separation (L denotes a single liquid phase, LL denotes liquid-liquid equilibrium, SL denotes solid-liquid equilibrium, - - - denotes the spinodal, Route I is liquid-liquid phase separation by nucleation and growth, and Route II is liquid-liquid phase separation by spinodal decomposition) .....	152
4.3	Types of Adsorption Isotherms .....	153
4.4	Types of Adsorption-Desorption Hysteresis for a Type IV Adsorption Isotherm .....	154
4.5	Volumetric Static BET Apparatus .....	155
4.6	Omnisorp™ 100 Adsorption-Desorption Apparatus .....	156
4.7	Temperature and Pressure Path for Crystallization of Isotactic Polypropylene from Solution in Supercritical Propane .....	157

4.8	Scanning Electron Micrograph for a 20 wt. % iPP Solution in Supercritical Propane Isothermally Crystallized at 80°C.....	158
4.9	2-D Crystallization Apparatus .....	159
4.10	Scanning Electron Micrograph for a 20 wt. % iPP Solution in Supercritical Propane Isothermally Crystallized at 80°C in 2-D Crystallization Apparatus (30µm thickness).....	160
4.11	Scanning Electron Micrograph for a 20 wt. % iPP Solution in Supercritical Propane Isothermally Crystallized at 100°C.....	161
4.12	Temperature and Pressure Path for Crystallization of Isotactic Polypropylene from Solution in Supercritical Propane/1-Propanol Mixture Containing DBS.....	162
4.13	Scanning Electron Micrograph for a 20 wt. % iPP Solution in Supercritical Propane/1-Propanol (13.9 wt. % 1-Propanol) Isothermally Crystallized at 80°C Nucleated with DBS .....	163
4.14	Surface Areas and Porosities for Porous iPP Formed by Isothermal Crystallization of 20 wt. % iPP Solutions in Supercritical Propane at Different Temperatures .....	164
4.15	Pore Size Distributions for Porous iPP Formed by Isothermal Crystallization of 20 wt. % iPP Solutions in Supercritical Propane at Different Temperatures .....	165
4.16	Surface Areas and Porosities for Porous iPP Formed by Isothermal Crystallization of 20 wt. % iPP Solutions in Different Alkanes.....	166
4.17	Pore Size Distributions for Porous iPP Formed by Isothermal Crystallization of 20 wt. % iPP Solutions in Different Alkanes.....	167
4.18	Surface Areas and Porosities for Porous iPP Formed by Isothermal Crystallization of 10 wt. % iPP Solutions at 65°C at Different Pressures .....	168
4.19	Pore Size Distributions for Porous iPP Formed by Isothermal Crystallization of 10 wt. % iPP Solutions at 65°C at Different Pressures .....	169
4.20	Pore Size Distribution for PP-100 .....	170
4.21	Pore Size Distribution for PP-DBS.....	171

4.22	Representative Polymer Lamellae.....	172
4.23	Structure for Fibrillation Model.....	173
4.24	Core Radius and Fibrillation Density as Calculated from Fibrillation Model for Porous iPP Isothermally Crystallized from Supercritical Propane at Different Temperatures .....	174
4.25	Fibrillar Surface Area and Overall Surface Area for Porous iPP Isothermally Crystallized from Supercritical Propane at Different Temperatures .....	175
4.26	Wt. % Polymer Remaining in Solution at the Time of Fibrillation for Porous iPP Isothermally Crystallized from Supercritical Propane at Different Temperatures .....	176
4.27	Core Radius and Fibrillation Density as Calculated from Fibrillation Model for Porous iPP Isothermally Crystallized from Different Alkane Solvents .....	177
4.28	Fibrillar Surface Area and Overall Surface Area for Porous iPP Isothermally Crystallized from Different Alkane Solvents .....	178
4.29	Wt. % Polymer Remaining in Solution at the Time of Fibrillation for Porous iPP Isothermally Crystallized from Different Alkane Solvents .....	179
4.30	Wide Angle X-ray Diffraction (WAXD) Data for Four Porous iPP Samples: PP-80, PP-3K, PP-3K-2, PP-5K.....	180
B.1	Reproducibility of Adsorption-Desorption Isotherms for PP-3M .....	210
B.2	Adsorption-Desorption Isotherm for PP-73.....	211
B.3	Adsorption-Desorption Isotherm for PP-77 .....	212
B.4	Adsorption-Desorption Isotherm for PP-80.....	213
B.5	Adsorption-Desorption Isotherm for PP-85.....	214
B.6	Small Angle X-Ray Scattering Curves for PP-73, PP-77, PP-80, and PP-85 .....	215
B.7	Adsorption-Desorption Isotherm for PP-Butane.....	216

B.8	Adsorption-Desorption Isotherm for PP-Heptane .....	217
B.9	Small Angle X-Ray Scattering Curves for PP-Propane (PP-73), PP-Butane, PP-Heptane .....	218
B.10	Adsorption-Desorption Isotherm for PP-3K .....	219
B.11	Adsorption-Desorption Isotherm for PP-3K-2 .....	220
B.12	Adsorption-Desorption Isotherm for PP-5K .....	221
B.13	Adsorption-Desorption Isotherm for PP-10K .....	222
B.14	Small Angle X-Ray Scattering Curves for PP-3K, PP-3K-2, and PP-5K .....	223
B.15	Adsorption-Desorption Isotherm for PP-100 .....	224
B.16	Adsorption-Desorption Isotherm for PP-DBS .....	225



# CHAPTER 1

## INTRODUCTION

### 1.1 Motivation

Several approaches exist for porous polymeric material formation, the most common being that of thermally induced phase separation (TIPS) [LeMay et al., 1990]. The TIPS process requires the use of a homogeneous polymer solution which when lowered in temperature undergoes a phase transition, either solid-liquid or liquid-liquid followed by a solid transition, to lock in a particular structure. The use of a conventional liquid solvent for the TIPS process then requires a way to remove the solvent without collapsing the structure generated in the process. Solvent removal procedures are lengthy with the most common being solvent exchange and/or freeze drying techniques [LeMay et al., 1990].

An alternative process, where the polymer is dissolved in a supercritical fluid and subsequently crystallized allows the solvent to be removed by gas escape, avoiding a second solvent removal step. Previous research has been carried out primarily on the polyethylene/propane system and the resulting structures are thought to be a result of gelation crystallization [Bush et al., 1991, Pradhan & Ehrlich, 1995].

The use of solvents is being discouraged because of environmental regulations and this impacts the polymer industry [Cavanaugh & Nauman, 1995]. The TIPS process requires large quantities of solvent and solvent extraction creates a mixed solvent which must be separated to recycle. Processing from a supercritical fluid solution has the advantage that a single solvent or solvent system is used and can be recycled by compressing the vapor stream.

## 1.2 Scope of Thesis Work

The goal of this research is to better understand the crystallization of polymers from supercritical fluids (SCF). Few polymers are known to be soluble in supercritical fluids although continuing research is identifying additional polymers soluble in supercritical fluids. The additional constraint of polymer crystallinity further limits the number of available systems to those similar to polyethylene in supercritical alkanes or alkenes. Systems of possible interest would include crystallizable polyethylene copolymers and other crystalline polyolefins such as isotactic polypropylene (iPP) and isotactic poly(4-methyl-1-pentene) in supercritical alkane or alkene solvents. Previous exploratory research on porous iPP generated by crystallization from its solutions in supercritical propane produced morphologies that are thought to be generated by gelation crystallization [Pradhan & Ehrlich, 1995]. The morphologies obtained were those of porous microspheres and such a well defined morphology lends itself to further study. Therefore, the crystalline polymer/SCF system chosen for study was that of isotactic polypropylene in supercritical propane.

The logical progression of this research was to define the phase behavior of the iPP/propane system, carry out formation of porous iPP, and characterize the porous iPP. In addition, thermodynamic modeling of some of the systems was also attempted to verify conclusions from other researchers.

Chapter 2 provides some background on supercritical fluids, the types of pressure-temperature phase diagrams for polymer/solvent systems, and a literature survey of previously studied polymer/supercritical fluid systems highlighting major findings. The experimental phase behavior of two different fractions of iPP and one fraction of atactic polypropylene in supercritical propane was determined. The dependence of polymer branching, both branch length and branch density, on the cloud-point pressures in supercritical propane was determined and correlated with branching parameters. The use of polar nucleating agents to alter the porous iPP morphology required the use of polar

cosolvents to obtain dispersion of the nucleating agent. Therefore, the dissolution of a highly effective nucleating agent for iPP, dibenzylidene-d-sorbitol (DBS), in propane/1-propanol mixtures was determined. The addition of a polar cosolvent will alter the phase behavior of the polymer and this initiated the investigation of ternary systems of the type aPP/propane/alcohol. These systems display interesting phase behavior which can be qualitatively predicted from the phase behavior of the aPP/propane and aPP/alcohol binary systems.

Chapter 3 describes the efforts to model the phase behavior of some of the polymer supercritical fluid systems described in Chapter 2. Previous thermodynamic modeling of polymer/supercritical fluid systems is reviewed and selection of the Sanchez-Lacombe lattice fluid (LF) theory for modeling the nonpolar systems presented in Chapter 2 is justified. An analysis of the dimensionless parameters of the LF theory is presented and a procedure is proposed for selection of dimensionless parameters. Values for the dimensionless parameters required in order to fit experimental cloud-point pressures are determined for the aPP/propane and iPP/propane systems. Calculated binodals and spinodals for the iPP/propane system are compared to experimental cloud-point isotherms for this system. An extension of the modeling to the ternary system, aPP/propane/1-propanol, is also attempted.

Chapter 4 provides a background on thermally induced phase separation (TIPS), subsequent solvent removal procedures, and a literature survey of the TIPS process applied to the formation of porous isotactic polypropylene (iPP). The formation of porous iPP and the obtained morphologies, as determined by scanning electron microscopy, as a function of processing variables and the addition of nucleating agents is presented. Characterization methods applicable to porous iPP samples are described. This includes surface areas, porosities, and pore size distributions obtained by measurement of nitrogen adsorption-desorption isotherms. Additional analysis of small angle x-ray scattering data is used to support pore structures obtained from the adsorption isotherms. Results for

surface areas and pore structures are presented for a variety of different processing conditions. Models based on the morphology are proposed and attempts are made to link results with long-standing theories of polymer crystallization and the unique behavior of iPP crystallization.

Chapter 5 summarizes the important findings and discusses conclusions from this work. Also discussed are suggestions for future work to advance and improve upon the findings in this research.

Appendix A indexes the polymer/supercritical fluid systems which have been studied by various researchers. Appendix B contains the raw nitrogen adsorption-desorption isotherms and small-angle x-ray scattering data used for analysis of surface areas, porosities, and pore size distributions as discussed in Chapter 4.

## REFERENCES

Bush, P. J., D. Pradhan, and P. Ehrlich, "Lamellar Structure and Organization in Polyethylene Gels Crystallized from Supercritical Solution in Propane," *Macromolecules*, **24**, 1439 (1991).

Cavanaugh, T. J., and E. B. Nauman, "The Future of Solvents in the Polymer Industry," *Trends Polym. Sci.*, **3**, 48, (1990).

LeMay, J. D., R. W. Hopper, L. W. Hrubesh, and R. W. Pekala, "Low-Density Microcellular Materials," *MRS Bull.*, **15**, 19 (1990).

Pradhan, D., and P. Ehrlich, "Morphologies of Microporous Polyethylene and Polypropylene Gels Crystallized from Solution in Supercritical Propane," *J. Polym. Sci. Part B: Polym. Phys.*, **33**, 1053 (1995).

## CHAPTER 2

### POLYMER/SUPERCritical FLUID PHASE BEHAVIOR

Most processes for the formation of porous polymeric materials require phase separation of polymer solutions whereby a continuous polymer phase imbibed with solvent results [LeMay et al., 1990]. The morphology of the continuous polymer depends on the type of phase separation. Therefore, knowledge of the phase behavior is a prerequisite for determining appropriate processing conditions. Additionally, removal of the imbibed solvent must preserve the polymer morphology obtained by phase separation. Solvent removal is usually achieved by solvent extraction or freeze-drying techniques, but these procedures are lengthy and can degrade the polymer structure.

The focus of this work is the formation of porous isotactic polypropylene (iPP) created by polymer crystallization from homogeneous supercritical fluid/polymer solutions. The use of a supercritical fluid allows the solvent to be removed by gas escape under low or zero surface tension conditions resulting in a solvent-free material unperturbed by solvent removal [Bush et al., 1991; LeMay et al., 1990; Pradhan & Ehrlich, 1995; Sawyer & Grubb, 1987].

The purpose of this chapter is to establish the phase behavior of supercritical fluid/polymer systems, in particular that of iPP/propane, to determine appropriate processing conditions for carrying out crystallization from a single supercritical phase to obtain porous iPP. Controlling the porous iPP morphology requires the use of nucleating agents. Therefore, the dissolution of a highly effective polar nucleating agent for iPP, dibenzylidene-d-sorbitol, in propane/1-propanol mixtures is presented. Changes in the phase behavior of ternary atactic polypropylene (aPP)/propane/alcohol systems with solvent mixture polarity is also presented. Additionally, changes in cloud-point pressures with polymer branching are systematically studied by variation of branch length and branch density and correlated with branching parameters.

## 2.1 Background

Relevant background information includes the properties of supercritical fluids and their application to polymers. General pressure-temperature phase diagrams for polymer/solvent systems are discussed. Since crystallizable polymers are utilized for material formation, crystalline polymer/supercritical fluid phase behavior is also discussed. A literature review of polymer/supercritical fluid phase behavior highlighting important results is presented. These results include the dependence of the phase behavior on polymer molecular weight, solvent, polymer structure, and polarity.

### 2.1.1 Supercritical Fluids

Supercritical fluids (SCFs) are gases or liquids at temperatures and pressures above their critical point. The critical point is the temperature and pressure along the vapor pressure curve at which the liquid and vapor phases become indistinguishable. Critical points for many pure components are available [Reid et al., 1987].

Interest in SCFs is a result of their enhanced solvating power when compared to gases. This is a partial result of the SCF density being greater than that of a gas as shown in Table 2.1 [McHugh & Krukonis, 1986]. Other advantageous properties of the SCF include diffusion coefficients and viscosities intermediate to those of a gas and liquid as shown in Table 2.1 [McHugh & Krukonis, 1986]. Additionally, the liquid-vapor surface tension goes to zero at the critical point [McHugh & Krukonis, 1986].

The ability to "tune" the SCF solvating power by both temperature and pressure has led to many extraction applications [McHugh & Krukonis, 1986]. Polymers are completely miscible in SCFs at sufficient pressures [Ehrlich & Kurpen, 1963] and this forms a basis for polymer separations using SCFs. Examples include molecular weight fractionation [Zhao et al., 1995; McHugh & Krukonis, 1986], fractionation of high density polyethylene resins with respect to branching [Watkins et al., 1991], and compositional fractionation of copolymers [Elsbernd et al., 1990; McHugh & Krukonis, 1986].

Immiscibility of polymers in supercritical fluids can also be utilized. Additive extraction from polymers benefits from the enhanced diffusional characteristics of the supercritical fluid [Cotton et al., 1993].

Table 2.1 Typical Property Values for Gases and Liquids Compared to Values for Supercritical Fluids Under Conditions of Polymer Miscibility

Property	Gas	Supercritical Fluid	Liquid
Density ( $\text{g/cm}^3$ )	$10^{-3}$	0.5-0.9	1.0
Diffusion Coefficient ( $\text{cm}^2/\text{s}$ )	$10^{-1}$	$10^{-3}$ - $10^{-4}$	$10^{-5}$
Viscosity (cP)	$10^{-3}$	$10^{-2}$ - 0.10	1.0

### 2.1.2 Phase Separation in Supercritical Polymer Solutions

The phase diagrams of binary systems can be classified into five types according to the pressure-temperature (P-T) projections of critical lines as predicted by application of the van der Waals equation to mixtures [Scott & Van Konynenburg, 1970]. Type I phase behavior is the simplest and occurs in mixtures of chemically similar low molecular weight components while for polymer/solvent systems, Type IV and V phase behavior is commonly observed.

Type I phase behavior is shown in Figure 2.1. In this system, a single critical locus, dashed line of Figure 2.1, connects the critical points,  $C_A$  and  $C_B$ , of the two components. This type of phase behavior occurs when the components are chemically similar and asymmetry in molecular size is low. The system ethane/heptane is an example of Type I phase behavior [Smith & Van Ness, 1987].

For chemically similar components, as the asymmetry in molecular size of the two components increases, the phase behavior changes from Type I to Type V. The asymmetry required for Type V phase behavior does not require the second component to



be a high polymer and for ethane occurs with hydrocarbons as low as  $C_{24}$  through  $C_{32}$  [Freeman & Rowlinson, 1960]. The P-T projections of critical lines in a Type V system are shown in Figure 2.2. The critical points of the pure components are denoted as  $C_A$  and  $C_B$  where A is the more volatile component. For polymeric systems,  $C_B$  would not exist or would exist at such high temperatures to place it off the figure when drawn to scale and, therefore, is not shown in Figure 2.2. The dashed line of Figure 2.2 is known as the lower critical solution temperature (LCST). The LCST is the temperature at which two fluid phases critically merge to form a single phase with a reduction in temperature of the system. As shown in Figure 2.2, the LCST does not start at the critical point of the more volatile component,  $C_A$ , but the LCST and  $C_A$  are connected by a branch denoting a three phase line of liquid-liquid-vapor (LLV). The critical mixture curve starts at  $C_A$  and connects with a point on the LLV line called the upper critical end point (UCEP). The LLV line extends from the UCEP to the lower critical end point (LCEP) where it meets the LCST. For polymers, the UCEP and  $C_A$  are virtually identical and the LLV line falls on the vapor pressure curve of the more volatile component. This results because the solubility of the polymer in the liquid phase is so small as to not cause an experimentally significant vapor pressure reduction.

Type IV phase behavior also occurs in systems where a large asymmetry in molecular size exists but the difference from Type V systems is the chemical dissimilarity of the components. The P-T projections of critical lines in a Type IV system are shown in Figure 2.3. Type IV phase behavior includes all the features of the Type V system previously described, but also includes an upper critical solution temperature (UCST). The UCST is the temperature at which two fluid phases critically merge to form a single phase with an increase in temperature of the system. The UCST, like the LCST, meets a LLV line at an UCEP. The low polymer solubility in the liquid phase results in an experimentally indistinguishable vapor pressure lowering and therefore the LLV line lies directly on the vapor pressure curve of the more volatile component.

The UCST is relatively pressure insensitive in comparison to the LCST. The reasons for this are related to the differences in origins of the phase separation. The UCST is enthalpic in origin and depends on the chemical dissimilarity of the components. Pressure has the minor effect of bringing chemical components in closer proximity which will alter the phase separation temperature only slightly. However, in extreme cases, pressure can dramatically modify solvent properties and this can modify phase separation behavior. The poly(ethylene oxide) (PEO)/water system is an example of a system whose phase behavior is uniquely altered by pressure [Cook et al., 1992]. The LCEP of the PEO/water system is approximately 100°C with the LCST shifting to slightly higher temperatures (~104°C) as pressure is increased to 1.5 kbar. Pressures higher than 1.5 kbar lower the phase separation temperature and at 4.3 kbar the polymer is insoluble in the experimental temperature window of 30-100°C. This unique phase behavior is due to a reduction in the degree of hydrogen bonding by water with increasing pressure. Since hydrogen bonding controls the solubility of the PEO/water system, the disruption of hydrogen bonding by pressure leads to phase separation.

The LCST is entropic in origin and results from a free volume dissimilarity between the polymer and solvent. In the region of the critical point, the free volume of the solvent can be changed quite dramatically by altering pressure. Therefore, the LCST has a larger pressure dependence as shown in Figures 2.2 and 2.3. The slope of the LCST, in the vicinity of the LCEP, is always positive and will eventually become zero and then negative. The change of the LCST branch to a negative slope actually makes the system have a high temperature UCST branch. In the polyethylene/ethane [Ehrlich & Kurpen, 1963] and polyethylene/ethylene [de Loos et al., 1983] systems, the slope is negative and is referred to as a UCST. However, the origin of the phase separation is entropic in nature. The point at which the LCST goes through a maximum in pressure was generally thought to occur at approximately the critical temperature of the solvent [Ehrlich & Kurpen, 1963] but this seems to be the case only for polyethylene in n-alkanes. For

polymeric systems, all these LCST features are not obtainable experimentally because of apparatus limitations, polymer degradation at high temperatures, or polymer crystallization.

For crystallizable polymers, a solid phase interrupts the bulk of the phase diagram below the melting point of the polymer in the solvent. The phase diagram for a crystallizable polymer/solvent system is shown in Figure 2.4 for a system where the polymer melting point in the solvent is above the critical point of the solvent. Solid-supercritical fluid (S-SCF) is shown in Figure 2.4 to be relatively insensitive to pressure. This is a matter of convenience as it is expected that S-SCF equilibria would be sensitive to the solvent quality which is a function of the state variables, T and P. Studies to determine the slope of S-SCF equilibria line have not been performed due to experimental time constraints and experimental accuracy. Time constraints occur because S-SCF equilibria for polymers can only be measured on slow heating due to the large supercoolings for crystallizable polymers. Fluid-phase equilibria (L-V) can be observed only at temperatures above S-SCF equilibria. A three phase point (S-L-V) called the second critical end point,  $C_2$ , links S-SCF equilibria to L-V equilibria at the critical composition.  $C_2$  is difficult to measure experimentally and, therefore, is found by extrapolation of S-SCF equilibria with L-V equilibria at the critical composition. L-V equilibria at the critical composition are referred to as the LCST. The critical composition can be determined by the measurement of phase volumes or observation of dew and bubble points [de Loos et al., 1983]. A three phase line (S-L-V) links  $C_2$  with the melting temperature of the pure polymer,  $T_m$ . S-L-V equilibria can not be measured by optical methods. A three-dimensional representation of Figure 2.4 including the composition axis is available for the polyethylene/propane system [Condo et al., 1992].

### 2.1.3 Previous Research

Lower critical solution temperature (LCST) behavior in alkane/polyolefin systems was reported and it was suggested that this phenomena is universal for polymer/solvent systems [Freeman & Rowlinson, 1960]. The lower critical endpoint (LCEP) is located at a temperature below the critical point of the solvent. For a given polymer in a series of chemically similar solvents, the change in location of the LCEP is commensurate with the change in the critical temperature of the solvent [Cowie & McEwen, 1974]. The existence of a universal LCST phenomena and the relation to the solvent critical temperature suggests that corresponding state theories can be used to describe the LCST. Experimental research on the pressure-temperature (P-T) projections of the LCST has focused on the effect of polymer molecular weight, solvent, polymer structure, and polarity on the phase diagrams.

Polymer molecular weight has a large influence on polymer/solvent phase behavior. Increasing polymer molecular weight increases the UCEP and decreases the LCEP [Zeman & Patterson, 1972] thereby increasing the region of immiscibility. Both the UCEP and LCEP reach a limiting value at high molecular weight. The high molecular weight limit is referred to as the  $\theta$  temperature [Flory, 1953].  $\theta$  temperatures are found by plotting the reciprocal UCEP and LCEP temperatures as a function of  $M_w^{-1/2}$  and extrapolating to infinite molecular weight ( $M_w^{-1/2} = 0$ ) [Zeman et al., 1972]. In some binary systems, as the polymer molecular weight is increased, the UCEP and LCEP become identical and a further increase in polymer molecular weight causes a merging of the UCST and LCST [Zeman & Patterson, 1972; Chen & Radosz, 1992]. The merged UCST and LCST has been referred to as a U-LCST [Chen & Radosz, 1992]. Recent experiments with nearly monodisperse polymers of different molecular weight have shown how the LCST depends on polymer molecular weight [Chen & Radosz, 1992]. The low polydispersity of their samples allow a controlled analysis of molecular weight effects in supercritical fluid/polymer systems because phase behavior diagrams, particularly the

critical composition, are changed by polydispersity [Koningsveld & Staverman, 1968a,b,c]. As polymer molecular weight is increased, the phase separation pressure (cloud-point pressure or upper critical solution pressure (UCSP)) at constant temperature is increased but reaches a limiting value at infinite polymer molecular weight [Zeman & Patterson, 1972, Chen & Radosz, 1992].

The choice of solvent dramatically alters phase behavior and has been shown, for polyethylene in n-alkanes, that an increase in solvent molecular weight decreases the upper critical solution pressure (UCSP) or cloud-point pressures at a specific temperature [Ehrlich & Kurpen, 1963]. Qualitatively, this effect has been shown to be related to the solubility parameter of the solvent. For lower molecular weight solvents, a higher pressure is required to reach a certain value of the solubility parameter particularly those solvents that are supercritical [Ehrlich & Kurpen, 1963]. Additionally, the effect of solvent molecular weight has been studied for nearly monodisperse poly(ethylene-alt-propylene) in n-alkenes [Chen & Radosz, 1991]. The amorphous nature of this polymer allowed investigation of the phase behavior to temperatures at least as low as the LCEP and in some systems, to a merging of the UCST and LCST verifying that these systems are Type IV as expected from the chemical dissimilarity between solvent and polymer.

Polymer structural parameters, the branch content and branch length, can have a significant effect on the cloud-point pressures. Increasing the branching results in dramatically lower cloud-point pressures as compared to the linear analog. This has been shown by varying the butene content (ethyl branches) of poly(ethylene-co-butene) copolymers [Chen et al., 1995]. These studies provide a direct relation of cloud-point pressures with known polymer structural parameters. Other studies are aimed at deducing the relative level of structural branching from cloud-point pressures in a particular solvent. In a study of a fractionated polyethylene, it was concluded that a decreasing degree of sample crystallinity could be correlated to the decrease in cloud-point pressure in propane and ethane [Hasch et al. 1993a]. The authors state that an increase in the amount of

branching is responsible for lowering sample crystallinity and this branching results in lowering of cloud-point pressures. However, the degree of crystallinity should not be used to correlate fluid phase equilibria particularly when the degree of crystallinity in polymers is a large function of sample thermal history. No additional data (NMR, IR, etc.) are given to support the increase in branching. An additional problem with this study is that cloud-point measurements are also subject to molecular weight and molecular weight distribution considerations [Koningsveld & Staverman, 1968a,b,c]. The phase equilibria for the polymers used in this study are a function of both molecular weight and branching.

Branching also changes the location of the LCEP in a given solvent. The LCEP shifts to higher temperatures with increased branch content. The LCEP of polyethylene in n-pentane is 353 K while that for polypropylene in n-pentane is 422 K and random poly(ethylene-co-propylene) copolymers have LCEPs between these two limits [Charlet & Delmas, 1981]. Increasing the branch length also shifts the LCEP to higher temperatures. The LCEP of poly(1-pentene) in n-pentane is 433 K and shifts to 441 K for poly(4-methyl-1-pentene) in n-pentane [Charlet et al., 1981].

The effect of a polar component, either polar copolymers or polar solvents, on the phase behavior is significant. In nonpolar solvent/polar copolymer systems, the cloud point pressures increase as the polar comonomer content increases. Using a polar cosolvent can help decrease the cloud point pressures up to a point where the polar component of the polymer and the polar cosolvent are balanced in polarity and amount. Additional polar cosolvent then increases the cloud point pressures as the medium becomes too polar for the nonpolar portion of the polymer [Hasch et al., 1993b]. However, trends in these systems should be viewed carefully as most copolymers make the system a ternary system where intra- and intermolecular interactions are present and interaction energies between solvent and both components of the copolymer must be estimated. Also, most copolymers previously studied contain a crystallizable component,

usually polyethylene, which does not allow the measurement of fluid-fluid phase equilibria at temperatures below S-SCF equilibria. The importance of ternary systems and the associated phase behavior is of importance for fractionation of polar copolymers. Synthesis of polar copolymers, particularly those copolymers of ethylene, give a distribution of polar comonomer content in the polymer. The ability to tune a solvent by varying the polarity allows one to perform fractionations based on polar comonomer content [Meilchen et al., 1991].

Additional polymer/supercritical fluid phase behavior research has addressed combinations of the aforementioned variables [Haschets & Shine, 1993; Gregg et al., 1994a,b; Hasch et al., 1992; Hasch et al., 1993a,b; Lee et al., 1994; Meilchen et al., 1991; Zeman et al., 1972; Zeman & Patterson, 1972]. Additional data on ternary systems (fluid/fluid/polymer) are available [McClellan & McHugh, 1985; Seckner et al., 1988; Meilchen, et al., 1992; Kiran et al., 1993; Kiamos & Donohue, 1994; McHugh & Guckes, 1985; Suresh et al., 1994]. Reviews of supercritical polymer solutions and polymer-fluid interactions [Ehrlich, 1992] as well as data on phase equilibria specific to high pressure polyethylene processes [Folie & Radosz, 1995] are available. Appendix A contains tables listing various binary and ternary supercritical fluid(s)/polymer systems which have been studied.

## 2.2 Experimental

### 2.2.1 Solvents

Propane and propylene (CP grade, 99.0+% minimum purity) were obtained from Merriam-Graves and used as received. Ethanol (U.S.P. grade) was obtained from Pharmco and used as received. 1-propanol and 1-butanol (certified grade) were obtained from Fisher Scientific and used as received.

## 2.2.2 Polymers and Additives

The phase behavior in supercritical propane of various polyolefins described in this study is divided into three categories: polypropylenes (isotactic and atactic), polyolefins with different branch length, and poly(ethylene-co-octene) copolymers of different branch density (various octene contents).

Weight-average molecular weight ( $M_w$ ) and polydispersity ( $M_w/M_n$ ) information for the polypropylenes used in this study are listed in Table 2.2, as is the origins of these samples. All polypropylene samples were free of stabilizers and additives. The isotactic polypropylenes (iPP) contained less than 2 wt. % xylene solubles (atactic polypropylene) but have an unspecified isotactic pentad fraction. The isotactic polypropylenes were used as received. Atactic polypropylene (aPP) was filtered while in toluene solution with the toluene being subsequently removed by vacuum-stripping.

Table 2.2 Weight-Average Molecular Weight and Polydispersity Information for Polypropylenes

Sample Designation	$M_w$	$M_w/M_n$
isotactic polypropylene (iPP1) <sup>1</sup>	29,000	2.0
isotactic polypropylene (iPP2) <sup>2</sup>	290,000	4.4
atactic polypropylene (aPP) <sup>1</sup>	400,000	2.0

1 - obtained from Dr. Howard Turner of Exxon Chemical, Baytown, TX

2 - obtained from Dr. Jean News of Himont Corporation, Wilmington, DE

Table 2.3 contains weight-average molecular weight and polydispersity information for the polyolefins used in the study of branch length as a structural parameter. The origins of these samples are listed in Table 2.3. The poly(ethylene-co-propylene) (PEP) contains 70 weight percent ethylene and the poly(4-methyl-1-pentene) (PMP), on which no molecular weight information was made available, contains an



unspecified amount of copolymer. The PMP is a commercial grade with the product designation RT-18 and has a melt flow rate of 26 g/10 min (ASTM D1238 test method at test conditions of 260°C and 5 kg).

Table 2.3 Weight-Average Molecular Weight and Polydispersity Information for Polyolefins with Different Side-Chain Branching

Sample Designation	$M_w$	$M_w/M_n$
polyethylene (NBS 1484) <sup>1</sup>	119,600	1.19
poly(ethylene-co-propylene), PEP <sup>2</sup>	153,000	2.8
atactic polypropylene (aPP) <sup>3</sup>	400,000	2.0
poly(1-butene), PB <sup>4</sup>	570,000	n.a.*
poly(4-methyl-1-pentene), PMP <sup>5</sup>	n.a.*	n.a.*

1 - data of Condo et al., 1992

2 - obtained from Dr. S. J. Chen of Exxon Chemical, Annandale, NJ

3 - obtained from Dr. Howard Turner of Exxon Chemical, Baytown, TX

4 - obtained from Aldrich Chemical

5 - obtained from Mitsui Plastics, White Plains, NY

\* not available

Table 2.4 lists the weight-average molecular weight, density, and octene content of the polymers used in the study of branch density as a structural parameter. The poly(ethylene-co-octene) (P(E-co-O)) copolymers were graciously donated by Yvonne Akpalu of the University of Massachusetts - Amherst. Samples were given to her by Dr. Herve Marand of Virginia Polytechnic Institute and State University who obtained them from Dr. Steve Chum of the Dow Chemical Corporation in Freeport, Texas. The weight-average molecular weight is obtained by a relation between melt index and weight average molecular weight for polymers containing no long chain branching. The weight average molecular weight of the branched copolymer,  $M_w^{\text{branch}}$ , is then obtained by the following relationship

$$M_w^{\text{branch}} = \frac{M_w^{\text{linear}}}{1 - \frac{2}{n}W} \quad (2.1)$$

where  $M_w^{\text{linear}}$  is the weight average molecular weight of the linear polymer,  $n$  is the number of carbons in the 1-alkene comonomer, and  $W$  is the mass fraction of 1-alkene in the copolymer [Scholte et al., 1984]. The octene content of these copolymers are estimated from a linear relationship between polymer density at 25°C and octene content as measured by IR.

Table 2.4 Weight-Average Molecular Weight, Density, and Octene Content of Poly(ethylene-co-octene) Samples.

Sample Designation	$M_w$	Density (g/cc)	Mole % Octene
PE (NBS 1484) <sup>1</sup>	119,600	n.a.*	n.a.*
P(E-co-O)-1	99,300	0.9350	0.38
P(E-co-O)-2	94,600	0.9100	2.10
P(E-co-O)-3	143,600	0.9020	3.30
P(E-co-O)-4	151,800	0.8850	5.30
P(E-co-O)-5	111,300	0.8750	6.60
P(E-co-O)-6	159,700	0.8700	7.40
P(E-co-O)-7	203,400	0.8630	8.4

<sup>1</sup> - data of Condo et al., 1992

\* not available

Dibenzylidene-d-sorbitol (DBS), an effective nucleating agent for isotactic polypropylene [Thierry et. al, 1992], was obtained from Milliken Chemical (Spartanburg, N.C.) under the product name Millad<sup>®</sup> 3905. Millad<sup>®</sup> 3905 contains a minimum of 96% DBS and was used as received.

Antioxidants were used when obtaining phase equilibria of aPP/1-propanol and aPP/1-butanol as these mixtures were not easily purged of oxygen and because high temperatures were required for dissolution. Irganox 1010<sup>®</sup> was obtained from Ciba-Geigy and was used at approximately 0.5 wt. % based on the polymer weight.

### 2.2.3 Apparatus and Procedure

A schematic of the variable volume view cell used to measure high-pressure phase behavior is shown in Figure 2.5. The apparatus used for this work is a slight modification from the one used by Condo et al., 1992. The cell is a cylindrical vessel constructed of 316SS with an inner diameter of 0.75 in. (1.9 cm) and an outer diameter of 2.5 in. (6.35 cm) which allows operation at pressures of at least 10,000 psi (~690 bar). The cell is fitted with a piston which is moved by a hydraulic fluid system and allows one to vary the system volume and pressure. Four ports exist for introducing solvent into the cell and for direct temperature measurement with thermocouple probes. The view cell is fitted with a window (annealed Pyrex) placed in a window keeper and is located at one end of the view cell. A brass retaining nut holds the window keeper in place. The view cell is part of the overall apparatus shown in Figure 2.6.

The piston with o-rings is placed into the barrel of the view cell. The view cell is then filled with the appropriate amount of polymer and a magnetic stir bar. The window, window keeper with o-rings, and brass retaining nut are put into place. The cell is then placed in a thermostatted oven and connected to the hydraulic fluid line. The solvent feed line and a thermocouple probe are connected to two of the four access ports. The other two access ports are fitted with standard high pressure plugs. Solvent is then introduced

from a lecture cylinder into a Jerguson gauge which is used as a liquid level measuring device. After obtaining the liquid level, which is converted to a volume, the contents of the Jerguson gage are transferred to the view cell. The view cell is then isolated by closing the valve in the solvent supply line. The system volume is then adjusted by moving the piston back and forth using a hydraulic fluid system. This system uses silicon oil as the pressure transmitting fluid and a pressure generator (High Pressure Equipment (HIP), Model 50-6-15) as the volume displacing device. Pressure is then monitored by a transducer (Lima-Baldwin) in the hydraulic fluid line. This pressure is corrected for the pressure drop across the piston to give the sample pressure. Vapor pressures of the supercritical solvent measured with the transducer on the hydraulic side were found to be approximately 1 bar higher than the true vapor pressure. Therefore, this correction was applied below the critical temperature while above the critical temperature a standard correction of 1 bar was applied. Agitation in the system is provided by a rotating magnet outside of the cell which couples to the stir bar inside the cell. In some cases, phase equilibria measurements below room temperature were required and for this a cooling jacket for the view cell was built and fluid from a chiller was circulated through the jacket.

The overall apparatus has many design advantages. The variable volume view cell allows the user to perform the phase equilibria on a particular concentration of the system over a desired range of temperature and pressure in one run. Also, at typical working volumes, the path length of the light that is reflected back into the borescope is quite long and the cloud point can be detected by the eye. In view cells of this type, the cloud point is best defined as the pressure and temperature at which the mixture becomes so opaque that it is no longer possible to see the stir bar. Visual detection of the cloud point has been compared to the decrease in intensity of a laser beam passing through the system and both techniques give values within the limits of experimental error [Meilchen et al., 1991].

The disappearance of a solid phase, optically, on very slow heating ( $<0.1^{\circ}\text{C}/\text{min}$ ) is denoted as S-SCF equilibria. Due to large supercoolings of crystallizable polymers,

measurement of S-SCF equilibria is not possible on cooling. Cloud-point pressures are measured at constant temperature while slowly lowering pressure and recording the onset of turbidity.

### 2.3 Results and Discussion

The binary system of isotactic polypropylene (iPP)/propane was studied first. Cloud-point isopleths as well as S-SCF equilibria were obtained for two different molecular weight iPP fractions. Extensions of the phase behavior below the S-SCF equilibria of the iPP/propane system were made by studying the completely amorphous polymer, atactic polypropylene, in propane. The effect of introducing chemical dissimilarity on the aPP/propane system was determined by substituting propylene as the solvent.

Previous research has showed how different solvents change the cloud-point pressures of the polyethylene/solvent system [Ehrlich & Kurpen, 1963]. A complimentary study to determine how structural parameters such as branch length and branch density change the phase behavior of polyolefins in supercritical propane was performed. Branch length was studied by determining the cloud-point pressures for homopolymer polyolefins having different branch lengths in supercritical propane. Branch density was studied by determining the cloud-point pressures for poly(ethylene-co-octene) copolymers differing in octene content in supercritical propane. Correlation of cloud-point pressures with the structural parameters is presented for materials studied here and in the literature. Additional structural parameters that may alter the cloud-point pressures are also discussed.

Ternary systems consisting of aPP in propane/alcohol mixtures were also investigated. Three different alcohols (ethanol, 1-propanol, and 1-butanol) were chosen which have the characteristic that the UCEP of the aPP/alcohol system is much higher than the LCEP of the aPP/propane system. The word cosolvent will be used in describing

the alcohols because at appropriate temperatures and pressures they can solubilize aPP. However, the alcohols chosen are nonsolvents for aPP at ambient conditions. Mixture compositions ranging from pure propane to pure alcohol are investigated for 1-propanol and 1-butanol. The ethanol content in solvent mixtures goes from pure propane up to 47 wt. % ethanol. The phase behavior of such ternary systems is of importance for the processing of iPP with polar nucleating agents. Such polar cosolvents are necessary for the dispersion for polar nucleating agents but the effect on the polymer phase behavior has to be investigated.

Dispersion of polar nucleating agents such as dibenzylidene sorbitol (DBS) is crucial in solution crystallization of isotactic polypropylene. The appropriate amount of polar cosolvent was chosen by studying the phase behavior of the ternary system, DBS/propane/1-propanol, at low 1-propanol content. Low content of 1-propanol is preferred to keep the mixture supercritical and to insure that the crystallization of DBS occurs prior to isotactic polypropylene crystallization. Coherency of the resultant iPP matrix can be achieved if there is successful dispersion of DBS and DBS crystallizes to form a network structure prior to iPP crystallization. The amount of 1-propanol controls this process and also controls whether the iPP undergoes liquid-liquid phase separation when quenched to carry out crystallizations.

### 2.3.1 Polypropylene/Supercritical Fluid Systems

#### 2.3.1.1 Isotactic Polypropylene/Propane

Figures 2.7 and 2.8 show cloud-point isopleths (constant composition) and S-SCF equilibria for two different molecular weight isotactic polypropylenes, iPP1 and iPP2, respectively, in propane. The location of the second critical endpoint,  $C_2$ , is obtained by the intersection of the S-SCF with the intersection of the cloud-point isopleth for the critical composition. Experimental determination of the critical composition was made by noting for which composition the liquid and vapor phase volumes were identical. The

location of  $C_2$  is shown in Figures 2.7 and 2.8 and Table 2.5 lists the values of the state variables at  $C_2$ . Cloud-point isotherms for iPP1/propane and iPP2/propane are shown in Figures 2.9 and 2.10, respectively, for three temperatures: 135°C, 145°C, 155°C

Table 2.5. Location of Second Critical End Point,  $C_2$ , for iPP1 and iPP2, in Propane

	P (bar)	T (°C)	Critical Polymer Wt. Fraction
$C_2$ (iPP1)	175	109	0.15
$C_2$ (iPP2)	250	130	0.075

### 2.3.1.2 Atactic Polypropylene/Propane

The amorphous nature of atactic polypropylene (aPP) allows phase equilibria to be determined at temperatures below the S-SCF equilibria in iPP/propane systems. Figure 2.11 shows the cloud-point isopleth for 2 wt. % aPP in propane as compared to the critical composition isopleths for the iPP fractions. The cloud-point isopleth for aPP/propane is traced in pressure-temperature space to a lower critical end point (LCEP) of 279 K.

### 2.3.1.3 Atactic Polypropylene/Propylene

Chemical dissimilarity was introduced into the system by changing the solvent from propane to propylene. The cloud-point isopleth for the aPP/propylene system is shown in Figure 2.12 as a comparison to the aPP/propane system. The cloud-point isopleth for the aPP/propylene system is shifted to slightly lower temperatures than that for the aPP/propane system.

#### 2.3.1.4 Discussion

Based on the phase diagram of aPP/propane, in the experimental temperature window, the system displays Type V behavior characterized by a LCEP of 279 K. In the experimental temperature window, the aPP/propylene system displays Type V behavior with the cloud-point isopleths shifted, at constant pressure, to temperatures slightly below those for aPP/propane. This shift is commensurate with the decrease in the critical point of propylene (92°C) as compared to propane (97°C). The LCEP of the aPP/propylene system, if it exists, is at a temperature below those experimentally obtainable. Chemical dissimilarity in the aPP/propylene system is expected to make this system exhibit Type IV phase behavior characterized by an UCEP and a LCEP. In the experimental temperature window, there is no evidence for this and this system appears to be that of a Type V system.

The experimental critical polymer weight fraction for both iPP/propane systems is larger than the critical composition predicted by theory for the respective molecular weight fractions [Flory, 1953]. This can be attributed to the polydispersity of the iPP samples which shifts the critical composition to higher values [Koningsveld & Staverman, 1968a,b,c]. Additionally, the experimental critical polymer concentration does not correspond to the maximum cloud-point pressure as shown in the cloud-point isotherms shown in Figures 2.9 and 2.10. Again, this can be attributed to the polydispersity of the iPP fractions [Koningsveld & Staverman, 1968a,b,c]. In polymer/supercritical fluid systems, the shift of the critical point to a point below the maximum of the cloud-point isotherm has been well documented for a polydisperse polyethylene in ethylene [de Loos et al., 1983].



### 2.3.2 Polyolefin Branching

Cloud-point pressures for polyolefins differing in branch length and branch density in propane are presented and correlation of cloud-point pressures with structural parameters is presented.

#### 2.3.2.1 Structural Parameter - Branch Length

The cloud-point pressures in the same supercritical solvent, propane, are presented for polyolefins containing branches of different length. A highly linear polyethylene [Condo et. al., 1992] serves as the component containing no side-chain branching. Side-chain branching is then introduced and increases in the following order: poly(ethylene-co-propylene) copolymer (PEP), atactic polypropylene homopolymer (aPP), poly (1-butene) (PB), and poly(4-methyl-1-pentene) (PMP). Figure 2.13 shows cloud-point isopleths in propane for the five polymers (PE, PEP, aPP, PB, PMP) at compositions close to critical. The cloud-point pressures decrease substantially as the branch length increases. In the case of PEP/propane, the cloud point pressure decreases relative to PE/propane and does so as a function of the branch density (# of methyl branches/100 ethyl units in main chain). Therefore, branch density reduces cloud-point pressures. This is presented in the next section.

#### 2.3.2.2 Structural Parameter - Branch Density

The effect of branch density (# of branches/100 ethyl units in main chain) in reducing the cloud-point pressures was studied by using the copolymer, poly(ethylene-co-octene), whose composition ranged from polyethylene homopolymer to a copolymer containing 30 wt. % octene. Cloud-point isopleths for 5 wt. % polymer solutions are shown in Figure 2.14. The cloud-point pressures decrease as the octene content in the copolymer increases.

### 2.3.2.3 Correlation of Cloud-Point Pressures with Structural Parameters

Two structural parameters, branch length and branch density, have a similar effect on cloud-point pressures. The study of polyolefins (PE, PP, PB, and PMP) in supercritical propane shows that branch length has the effect of lowering the cloud-point pressures. These samples have the same branch density which is defined as the # of branches per 100 ethyl units in the main chain [Chen et al., 1995]. The study of poly(ethylene-co-octene) copolymers in supercritical propane shows that increasing the branch density lowers the cloud-point pressures at constant branch length (hexyl). Correlation of the cloud-point pressures with branch density has been attempted for poly(ethylene-co-butene) and it was concluded that the cloud-point pressures at a single temperature are a linear function of butene content (branch density) [Chen et al., 1995]. Figure 2.15 shows the correlation of cloud-point pressures with branch density for the polyolefins studied here and those available in literature [Condo et al., 1992; Chen et al., 1995]. This plot shows a linear correlation for a given copolymer series (same branch unit) but that polymers with longer branches further reduce the cloud-point pressures at equivalent branch density. Therefore, the correlation must include both branch density and branch length. The % of carbon contained in the branches is such a measure. At constant branch density, the % of carbon in the branches will go up as branch length increases. Figure 2.16 shows the correlation of cloud-point pressures with the % carbon in the branches for the polyolefins studied here and those available in the literature [Condo et al., 1992; Chen et al., 1995].

### 2.3.2.4 Discussion

Cloud-point pressures are very sensitive to the structural parameters of the polymer and the study of polyolefin systems allows a systematic study to be performed that focuses solely on structure independent of changes in chemical composition. Increasing either branch density or branch length reduces the cloud-point pressures. The dependence of cloud-point pressures on polyolefin structural parameters shows how

fractionations of branched materials can be performed. Fractionation of high density polyethylene resins from supercritical solution has been attempted [Watkins et al., 1991].

The correlation of cloud-point pressures, at constant temperature, with the % carbon contained in the branches appears to work quite well and suggests universal behavior for polyolefins of differing structure. Other structural parameters, unaccounted for in this correlation, may be of importance. Molecular weight and molecular weight distribution, tacticity, and distribution of branches are three additional factors that need to be considered. Comparisons between branched samples should be performed independent of molecular weight. Therefore, the molecular weight should be high enough to be approximate the phase behavior at infinite molecular weight. The molecular weight of the samples studied here are close to that infinite molecular weight limit. Additionally, the molecular weight distribution, ideally, would be monodisperse. Cloud-point pressures are influenced by polydispersity [Koningsveld & Staverman, 1968a,b,c] and this complicates the analysis of trends of cloud-point pressures with structural parameters. Tacticity may also effect the cloud-point pressures as was seen in the aPP and iPP studies (Section 2.3.1.2). The % carbon contained in the branches for these two samples is the same but the density of the samples may be different. The molecular weight of the aPP and iPP fractions studied in this research were not identical. Further studies on identical molecular weight samples differing only in tacticity should be performed. The distribution of branches may also play a role in the location of cloud-point pressures. As shown in Figure 2.16, the points labeled PE, aPP, P(E-alt-P), PB, PMP are for homopolymers which have periodically regular branching along the main chain. The remaining points are for copolymers which have a distribution in branch points along the main chain. Cloud-point pressures for copolymers are at slightly higher values suggesting that phase separation may be occurring because of longer ethylene blocks present in the backbone. A possible test of this would be phase behavior studies of a diblock polyolefin with an ethylene block and a branched block.

### 2.3.3 Ternary Systems

The amorphous nature of aPP allows one to study the phase behavior over a wide temperature window and therefore, a greater understanding of ternary systems can be obtained. The effect of adding a polar cosolvent in differing compositions to a nonpolar binary system is systematically studied for the aPP/propane/alcohol system. The alcohols chosen for study were ethanol, 1-propanol, and 1-butanol.

Predictions of the phase behavior for the ternary system are presented based on the phase behavior of the binary polymer/solvent systems. These predictions are then tested for three different ternary systems.

#### 2.3.3.1 Ternary System Construction

The phase behavior of the ternary system can qualitatively be predicted from the binary systems of the polymer and solvent. The aPP/propane system is of Type V phase behavior while the aPP/alcohol system is Type IV. For the aPP/alcohol systems studied, the UCEP is at a temperature greater than the LCEP of the aPP/propane system. Figure 2.17 shows the overlap of the binary phase diagrams in this case. (A = alkane, B= alcohol, P= polymer). As the content of the alcohol (B) is increased, the UCEP and LCEP of the system shifts to higher temperatures. However, the relative shift of the LCEP and UCEP with composition is not the same. At some composition, the LCEP and UCEP can become identical and at slightly higher alcohol compositions neither an UCEP or a LCEP exist and pressures above the vapor pressure must be applied to solubilize the polymer.

Merging of the UCST and LCST can occur by increasing polymer molecular weight (Section 2.1.3) or changing solvent quality. However, there is a major difference between the two cases for merged U-LCSTs. If a merging of the UCST and LCST occurs with increasing polymer molecular weight, the merging remains at all higher polymer molecular weights. In contrast, if a merging of the UCST and LCST occurs for some solvent mixture and the binary alcohol/polymer system has a separate UCEP and LCEP,

then a range of solvent mixture compositions will display U-LCST merging. If the binary alcohol/aPP system has a merged U-LCST, all solvent mixtures above a critical mixture composition will result in U-LCST type phase behavior.

### 2.3.3.2 Atactic Polypropylene/Propane/Alcohol

Cloud-point pressures for three different aPP/propane/alcohol systems are presented. The three different alcohols are ethanol, 1-propanol, and 1-butanol. Each ternary system displays unique phase behavior as a function of solvent mixture composition.

#### 2.3.3.2.1 Atactic Polypropylene/Propane/Ethanol

Figure 2.18 shows cloud-point isopleths for the aPP/propane/ethanol system ranging from the aPP/propane system to aPP in a solvent mixture of ethanol/propane containing 47.3 wt. % ethanol. The polymer concentration is fixed at 2 wt. % for each system. For the solvent mixture with the lowest ethanol content (16.8 wt. %), the LCEP disappears in the experimental temperature window and the system may be of the U-LCST type. At the two higher ethanol compositions, a definite merging of the UCST and LCST has occurred.

#### 2.3.3.2.2 Atactic Polypropylene/Propane/1-Propanol

Figure 2.19 shows cloud-point isopleths for the aPP/propane/1-propanol system ranging from the aPP/propane system to the aPP/1-propanol system. The polymer concentration is fixed at 2 wt. % for each system. For the solvent mixture with the lowest 1-propanol content (16.8 wt. %), a separate LCST branch is observed (and presumably an UCST branch at temperatures below that obtained experimentally). For higher 1-propanol compositions, a merging of the UCST and LCST is observed which requires that for some solvent mixture composition, the UCEP and LCEP must be identical. The

lowest pressure at which miscibility is observed initially increases and then decreases as the 1-propanol content is increased.

#### 2.3.3.2.3 Atactic Polypropylene/Propane/1-Butanol

Figure 2.20 shows cloud-point isopleths for the aPP/propane/1-butanol system ranging from the aPP/propane system to the aPP/1-butanol system. The polymer concentration is fixed at 2 wt. % for each system. As the composition of the alcohol in the mixture is increased, the LCEP and UCEP increases but at no composition does the UCST and LCST merge. The LCEP and UCEP in the system with 47.3 wt. % 1-butanol are only separated by 18°C. This system is a case where the UCEP of the aPP/alcohol (1-butanol) system (~ 149°C) is at a temperature above the LCEP of the aPP/propane (~ 6°C) and no merging of UCST and LCST behavior occurs as a function of solvent composition in the ternary system, aPP/propane/1-butanol.

#### 2.3.3.2.4 Summary of Atactic Polypropylene/Propane/Alcohol Systems

Table 2.6 lists the temperature of the UCEP and LCEP for the three atactic polypropylene (aPP)/propane/alcohol systems presented above as a function of solvent mixture composition. Table 2.6 also lists for which solvent mixture compositions U-LCST behavior exists.

The phase behavior of the binary solvent mixtures were studied for the propane/1-propanol series. In no case was there evidence of liquid-liquid phase separation of this system in the temperature region used in the ternary experiments. Approximate critical temperatures and pressures for propane/1-propanol mixtures are shown in Table 2.7. The binary systems of propane/ethanol and propane/1-butanol were not studied.

Table 2.6 UCEP and LCEP Temperatures for Atactic Polypropylene/Propane/Alcohol Systems

wt. % alcohol	ethanol		1-propanol		1-butanol	
	UCEP (°C)	LCEP (°C)	UCEP (°C)	LCEP (°C)	UCEP (°C)	LCEP (°C)
0.0	None	6	None	6	None	6
16.8	U-LCST	U-LCST	OTW	17	OTW	22
31.0	U-LCST	U-LCST	U-LCST	U-LCST	OTW	40
47.3	U-LCST	U-LCST	U-LCST	U-LCST	43	61
65.4	NM	NM	U-LCST	U-LCST	85	149
82.0	NM	NM	U-LCST	U-LCST	115	OTW
100.0	NM	NM	178	OTW	149	OTW

NM = not measured

OTW = outside experimental temperature window

Table 2.7 Critical Temperatures and Pressures for Propane/1-Propanol Mixtures

wt. % 1-propanol	Critical Temperature (°C)	Critical Pressure (bar)
0.0*	96.7	42.5
16.8	114.5	49.9
31.0	134.9	59.9
47.3	160.8	66.8
65.4	OTW	OTW
82.0	NM	NM
100.0*	263.6	51.7

\* - data from Reid et al., 1987

NM = not measured

OTW = outside experimental temperature window

### 2.3.3.3 Dibenzylidene-d-sorbitol (DBS)/Propane/1-Propanol

The dispersion of polar nucleating agents in a nonpolar polymer or nonpolar polymer/solvent system requires very high temperatures or small quantities of a polar cosolvent. The temperature and pressure dependence of the dissolution of dibenzylidene-

d-sorbitol (DBS) in propane/1-propanol mixtures is shown in Figure 2.21. The amount of DBS was fixed at 0.0025g DBS per ml of solution at room temperature.

#### 2.3.3.4 Discussion

The prediction of the phase behavior of ternary systems of the type aPP/propane/alcohol from the binary systems is qualitatively possible. Merging of the UCST and LCST with changes in the mixture polarity are predicted. For the ternary system with ethanol, this merging occurs at low ethanol content (<16.8 wt. %). For the aPP/propane/1-propanol system, the merging occurs at a slightly higher alcohol composition of between 16.8 and 31.0 wt. %. No merging occurs in the ternary system containing 1-butanol.

Based on the construction of the ternary system from the binary systems, merging of the UCST and LCST requires a specific relative location of the critical end points for the binary polymer/solvent systems. Merging is only possible for a system where the UCEP of the one binary system, aPP/alcohol, is at a temperature above the LCEP of the other binary system, aPP/propane. However, the relative location is necessary but is not a sufficient condition for UCST and LCST merging as is seen in the case of the ternary system containing 1-butanol where no merging occurs. Therefore, an additional factor is required for UCST and LCST merging and is that of the relative shift of the UCST and LCST as a function of solvent mixture composition. For the n-alcohol series, the solvent's critical point, and corresponding LCEP for the aPP/alcohol series, increases with increasing molecular weight. At the same time, the location of the UCEP for the aPP/alcohol series decreases with increases in the molecular weight of the n-alcohol. For propane/alcohol mixtures, the relative shift of the LCST and UCST with composition is the key to UCST and LCST merging.

For the aPP/propane/ethanol system, the shift of the LCST with composition is small while the UCST increases dramatically with increasing ethanol content. At some



point, the UCST is shifted to higher temperatures than the LCST branch and a merging of the UCST and LCST occurs. Based on the shift of the UCST with ethanol composition, the UCST of the aPP/ethanol system might be higher than the critical temperature of ethanol and the binary system (aPP/ethanol) would be of the U-LCST type. For the aPP/propane/1-propanol system, the LCST shift becomes greater than that for the system containing ethanol while the shift of the UCST with composition is reduced as compared to the ethanol system. For the aPP/propane/1-butanol system, the shift in the LCST with composition increases while the shift in the UCST decreases and no merging occurs. It is expected that all ternary systems of the type, aPP/propane/alcohol, which contain an alcohol higher than 1-butanol will display the characteristics of the aPP/propane/1-butanol system.

An additional feature of the ternary system, aPP/propane/1-propanol, is the possible reemergence of the UCEP and LCEP at a 1-propanol composition slightly above the highest studied here (82 wt. %). This is possible because the aPP/1-propanol system has a separate UCEP at  $\sim 178^{\circ}\text{C}$  and a LCEP which was above the experimental apparatus temperature limit. Therefore, merging of the UCST and LCST occurs for a range of solvent compositions.

The ternary system of dibenzylidene-d-sorbitol (DBS)/propane/1-propanol behaves as expected. As the 1-propanol content is increased, the temperature and pressure of solid-fluid equilibria is decreased. The increased polarity of the solvent mixture as the 1-propanol content is increased lowers the dissolution temperatures for the polar DBS. Low amounts of 1-propanol ( $\sim 15$  wt. %) allow the dissolution of DBS in the processing window for iPP/propane systems. Cosolvent can be added to control the temperature at which the DBS crystallizes from the solution as compared to the crystallization of iPP.

## 2.4 Conclusions

The phase behavior studies show that the polypropylene/propane system is a Type V system. For atactic polypropylene (aPP)/propane, the LCEP of the system is at 279K. Cloud-point pressures as well as S-SCF equilibria for the isotactic polypropylene (iPP)/propane system were determined and this allowed an estimation of the second critical end point,  $C_2$ . Introducing chemical dissimilarity by the use of the solvent propylene increased the phase separated region of the aPP/propylene system as compared to the aPP/propane system. In the experimental temperature window, the aPP/propylene system appears to be a Type V system but it is expected to be Type IV because of the chemical dissimilarity. The polypropylenes studied have different molecular weights and, as expected, the cloud-point pressures increase with increasing molecular weight. However, the exact relationship between cloud-point pressure and molecular weight is difficult to determine because the phase behavior is altered by the polydispersity and tacticity of the polypropylene samples.

Additionally, polyolefin structural parameters, branch length and branch density, drastically change the cloud-point pressures in a single supercritical solvent. Increasing either the branch length or branch density reduce the cloud-point pressures as compared to the linear polyolefin counterpart, high density polyethylene. Decreasing cloud-point pressures correlate well with the increasing % of carbons in the branches. The dramatic changes in phase behavior with branch content suggest that branching based separations could be performed from such supercritical polymer solutions.

The study of the ternary system, atactic polypropylene (aPP)/propane/alcohol, details the transition of a Type V system, aPP/propane, to a Type IV system, aPP/alcohol, as a function of solvent mixture composition. The uniqueness of this type of system is that the LCEP of the aPP/propane system is at a temperature below that of the UCEP of the aPP/alcohol. This relative location of the critical end points allows the possibility of a merging of the UCST and LCST into a U-LCST at certain solvent mixture compositions.

For the aPP/propane/ethanol system the occurrence of a U-LCST occurs at propane/ethanol mixtures containing as low as 16.8 wt. % ethanol. Phase behavior of the aPP/ethanol system was not experimentally obtainable but this binary system is expected to have a merged U-LCST based on the phase behavior in propane/ethanol mixtures. This is due to the shift of the UCST to temperatures above the critical point of ethanol. As the 1-propanol content is increased in the aPP/propane/1-propanol system, the transition to U-LCST behavior occurs at a 1-propanol content slightly above 16.8 wt. %. This merging of the UCST and LCST occurs for all higher 1-propanol mixture compositions. However, the aPP/1-propanol system has an UCEP and presumably a LCEP (not determined experimentally). Therefore, at some 1-propanol mixture composition above the highest studied here (82 wt. %), the reemergence of an UCEP and LCEP is expected. The aPP/propane/1-butanol system does not show a merging of the UCST and LCST at any mixture composition studied. At 47.3 wt. % 1-butanol, the UCEP and LCEP come within 18°C of each other. The UCST is generally not very pressure sensitive as stated in Section 2.1.2. The 1-butanol/propane mixtures show this pressure independence at high 1-butanol content. However, as the 1-butanol content is decreased, the UCST becomes pressure sensitive around the UCEP. This is due to overlap of entropic (free volume) based phase separation with enthalpic based phase separation. When this overlap is very large, a merging of the UCST and LCST can occur as shown in the aPP/propane/ethanol and aPP/propane/1-propanol systems.

Currently, a great deal of interest exists in using supercritical carbon dioxide as a solvent for polymers [Tuminello et al., 1995]. Based on the research carried out here, two relevant points should be considered when embarking on the quest for polymer solubility in supercritical carbon dioxide. First, the critical temperature of CO<sub>2</sub> is 31°C. Therefore, the LCEP of a high molecular weight polymer in CO<sub>2</sub> would be much lower. The pressure dependence of the LCST branch would require that at ambient conditions (~20°C) pressure be raised above the vapor pressure to obtain polymer miscibility. The

extent to which pressure must be raised is then a function of polymer structural parameters, branch length and branch density, as discussed in Section 2.3.2. Polymer/CO<sub>2</sub> research suggests this as the case because solubility can be obtained with long side-chain fluoropolymers [Shaffer & DeSimone, 1995]. However, the research on ternary systems presented here reveals that chemical incompatibility of polymer and solvent cause an UCST with the UCST shifting to higher temperatures as the unfavorable interactions are increased (Section 2.3.3.2). Therefore, the polymer may be insoluble in CO<sub>2</sub> at any temperature. Synthesis efforts to make polymers that are soluble in CO<sub>2</sub> will require a high degree of chemical compatibility between CO<sub>2</sub> and the polymer.

Controlling the morphology of isotactic polypropylene requires the addition of a nucleating agent. One of the most effective nucleating agents for isotactic polypropylene is dibenzylidene-d-sorbitol (DBS) [Thierry et al., 1992]. Dispersion of the DBS is required to promote the efficiency of the nucleating agent. Due to the polar nature of DBS, solubilization under reasonable processing conditions requires a polar cosolvent. Therefore, the temperature and pressure dependence of DBS solubilization in propane/1-propanol mixtures was determined. The DBS solubilization study showed that DBS solubility is obtained at the appropriate temperatures for making homogeneous iPP/propane solutions at low contents of 1-propanol (~ 15 wt. %) in propane. This level of 1-propanol promotes crystallization of DBS prior to reaching S-SCF equilibrium for the iPP/propane system upon quenching such homogeneous solutions. From the study of the ternary system, aPP/propane/1-propanol (Section 2.3.3.2.2) it was also determined that this level of 1-propanol does not shift the UCST into the temperature window used for isothermal iPP crystallizations. Therefore, small amounts of 1-propanol allow crystallization of iPP to proceed from a single phase instead of undergoing liquid-liquid phase separation prior to crystallization.

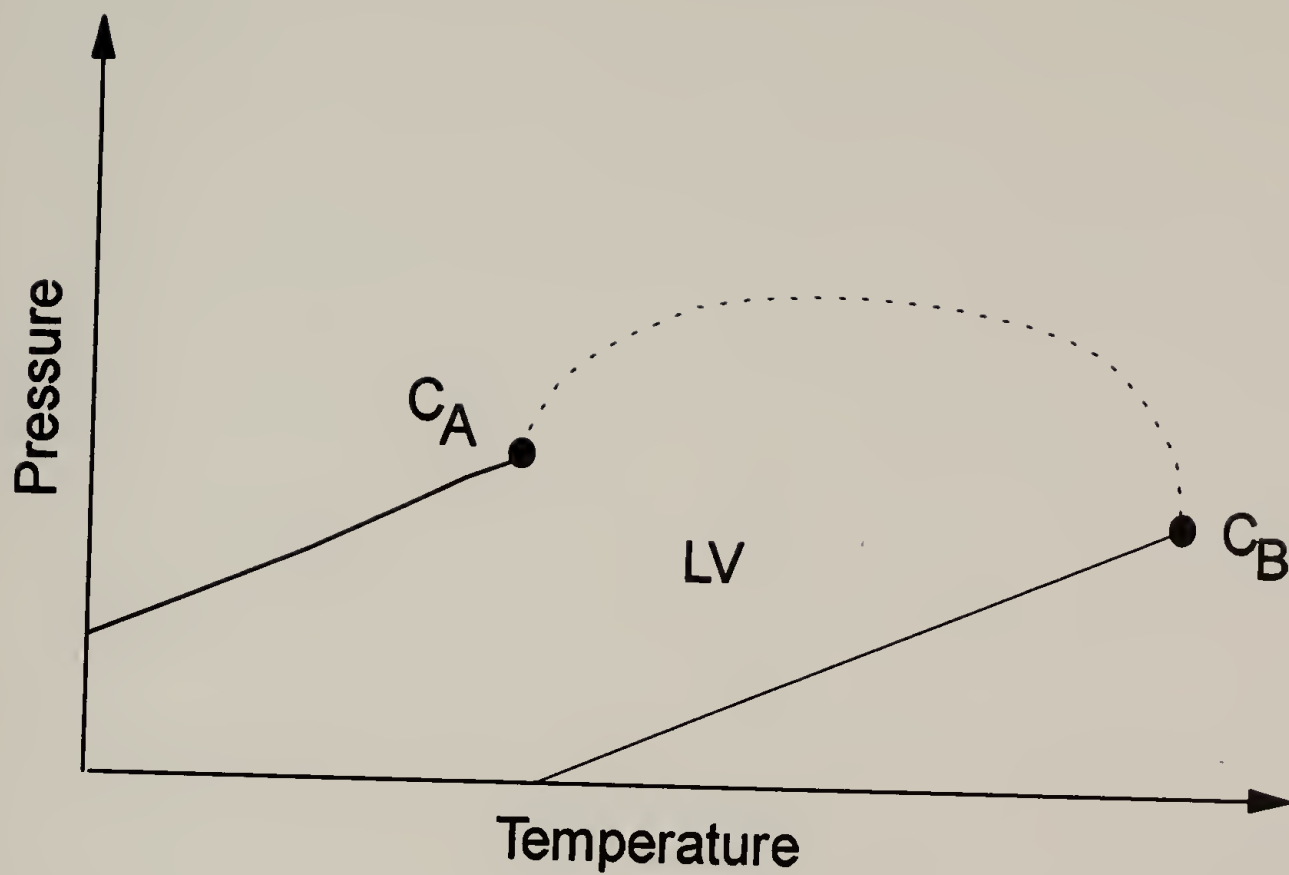


Figure 2.1 Type I Phase Behavior ( $C_A$  is the critical point of the more volatile component (A),  $C_B$  is the critical point of the less volatile component (B), - - - is the critical locus of the mixture, and LV denotes liquid-vapor equilibrium)

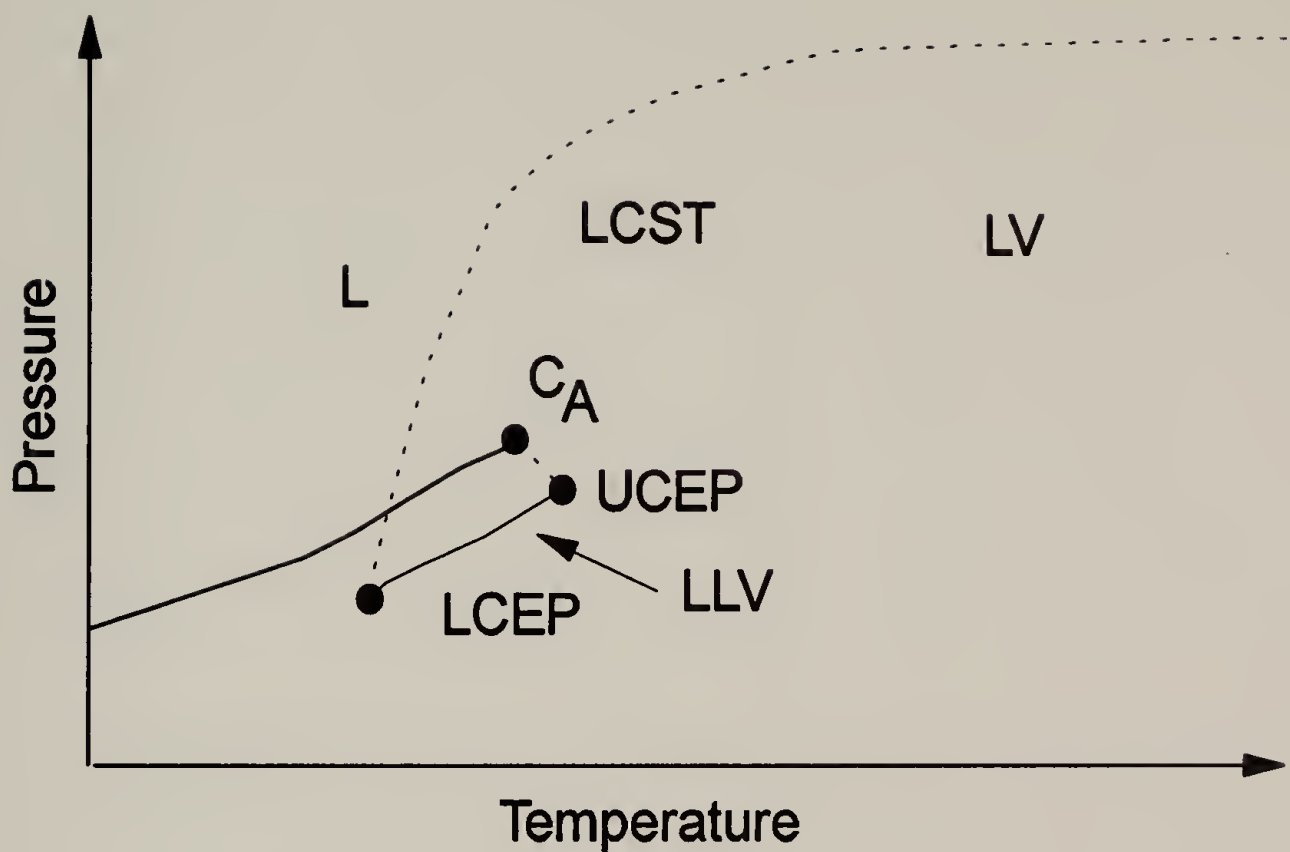


Figure 2.2 Type V Phase Behavior ( $C_A$  is the critical point of the more volatile component (A), - - - is the locus of lower critical solution temperatures (LCST), UCEP and LCEP are upper and lower critical end points, L is a single liquid phase, LV denotes liquid-vapor equilibrium, and LLV denotes liquid-liquid-vapor equilibrium)

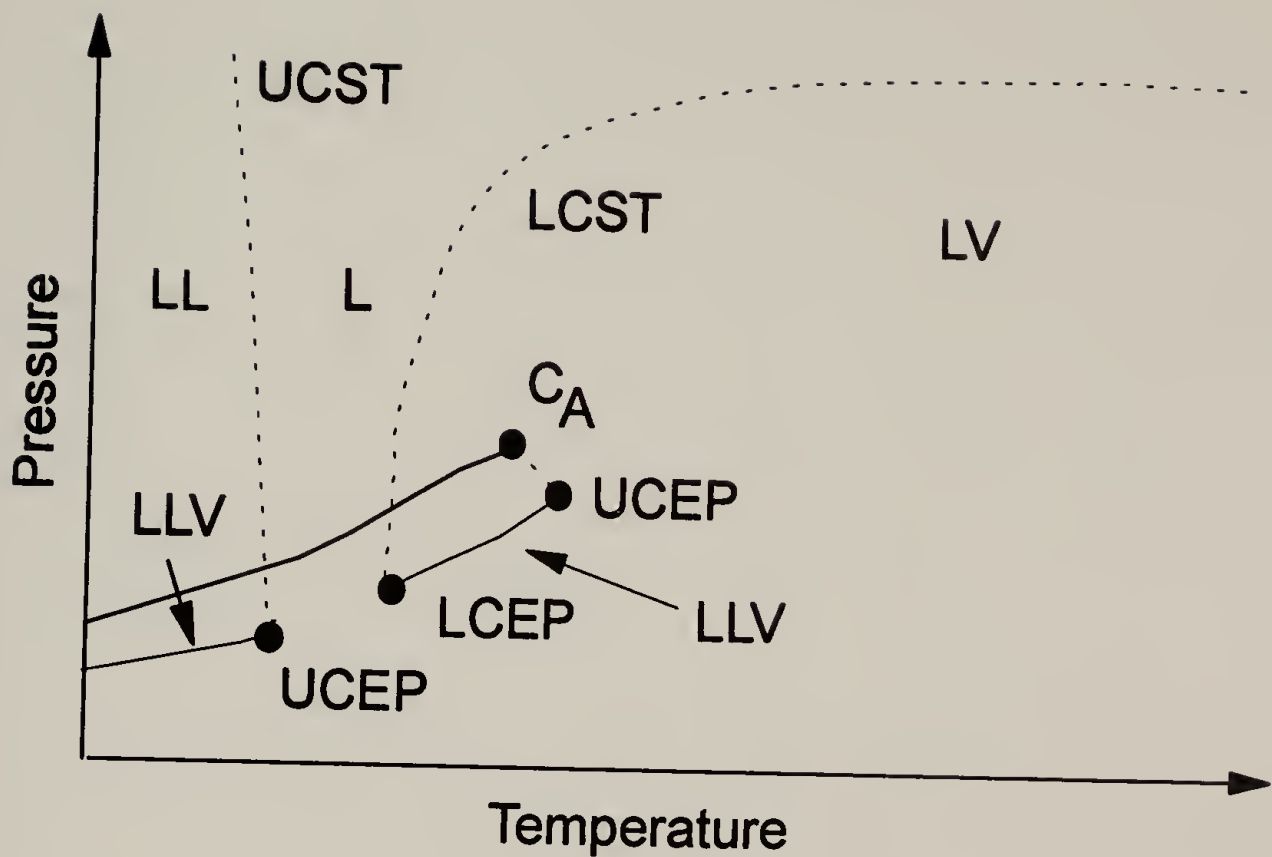


Figure 2.3 Type IV Phase Behavior ( $C_A$  is the critical point of the more volatile component (A), - - - is the locus of upper and lower critical solution temperatures (UCST and LCST, respectively), UCEP and LCEP are upper and lower critical end points, L is a single liquid phase, LV denotes liquid-vapor equilibrium, LL denotes liquid-liquid equilibrium, and LLV denotes liquid-liquid-vapor equilibrium)

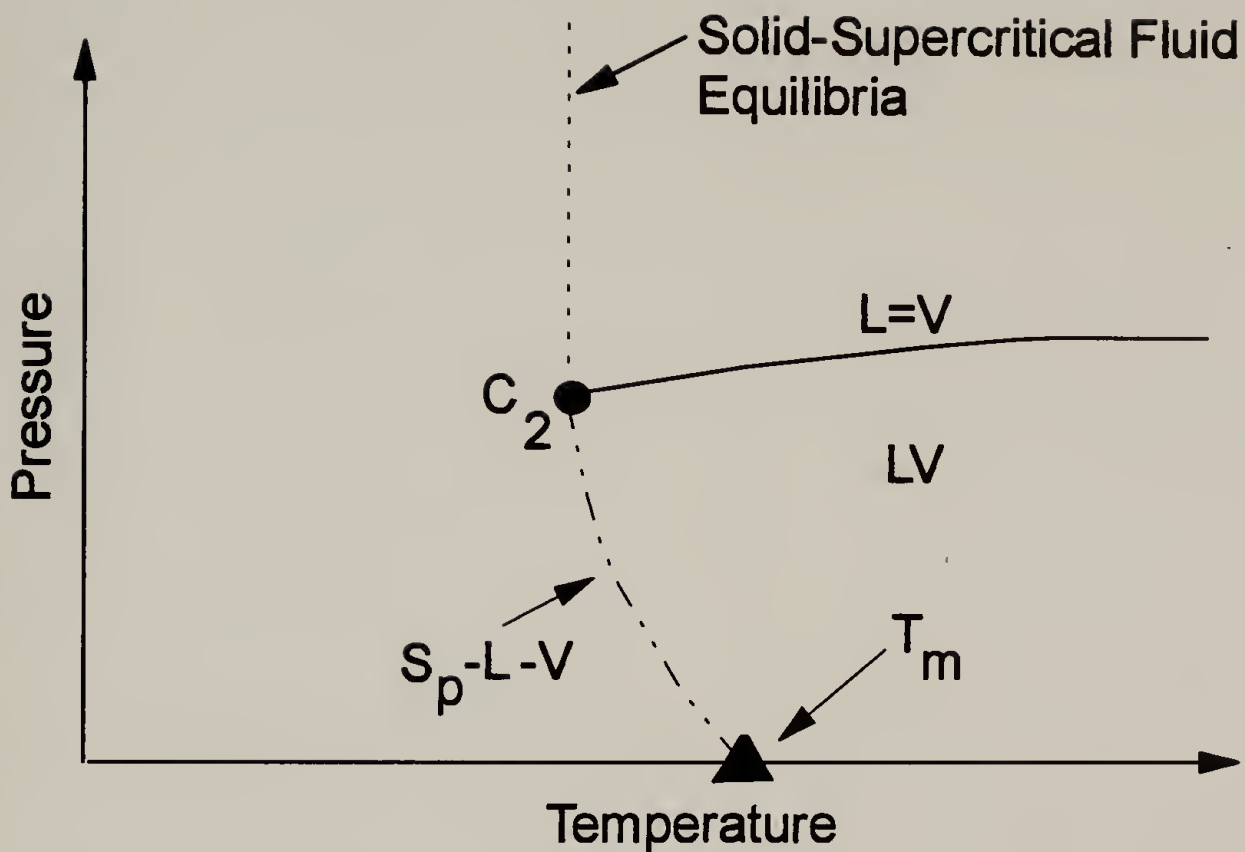
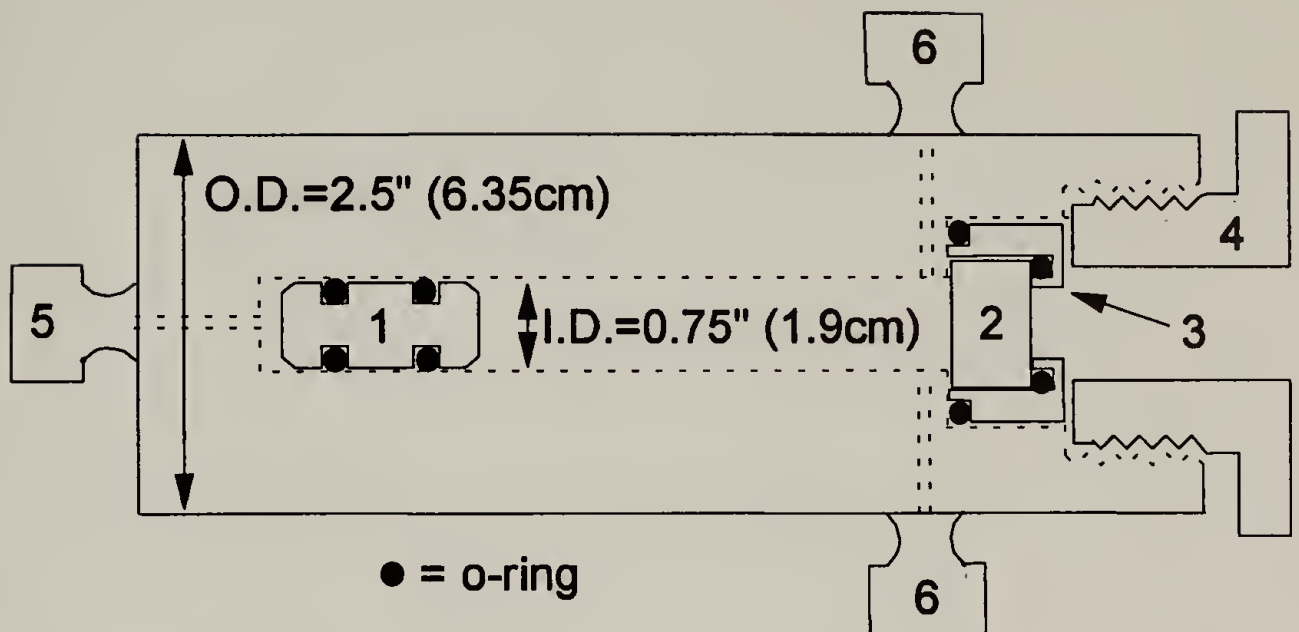


Figure 2.4 Crystalline Polymer/Supercritical Fluid Phase Diagram ( $T_m$  is the melting point of the pure polymer,  $S_p-L-V$  denotes solid polymer-liquid-vapor equilibrium,  $LV$  denotes liquid-vapor equilibrium,  $C_2$  is the second critical end point, and — is the locus of lower critical solution temperatures ( $L=V$ ))





1 - piston

2 - annealed pyrex window

3 - window keeper

4 - brass retaining nut

5 - hydraulic port

6 - feed and temperature  
probe ports

Figure 2.5 Variable Volume View Cell

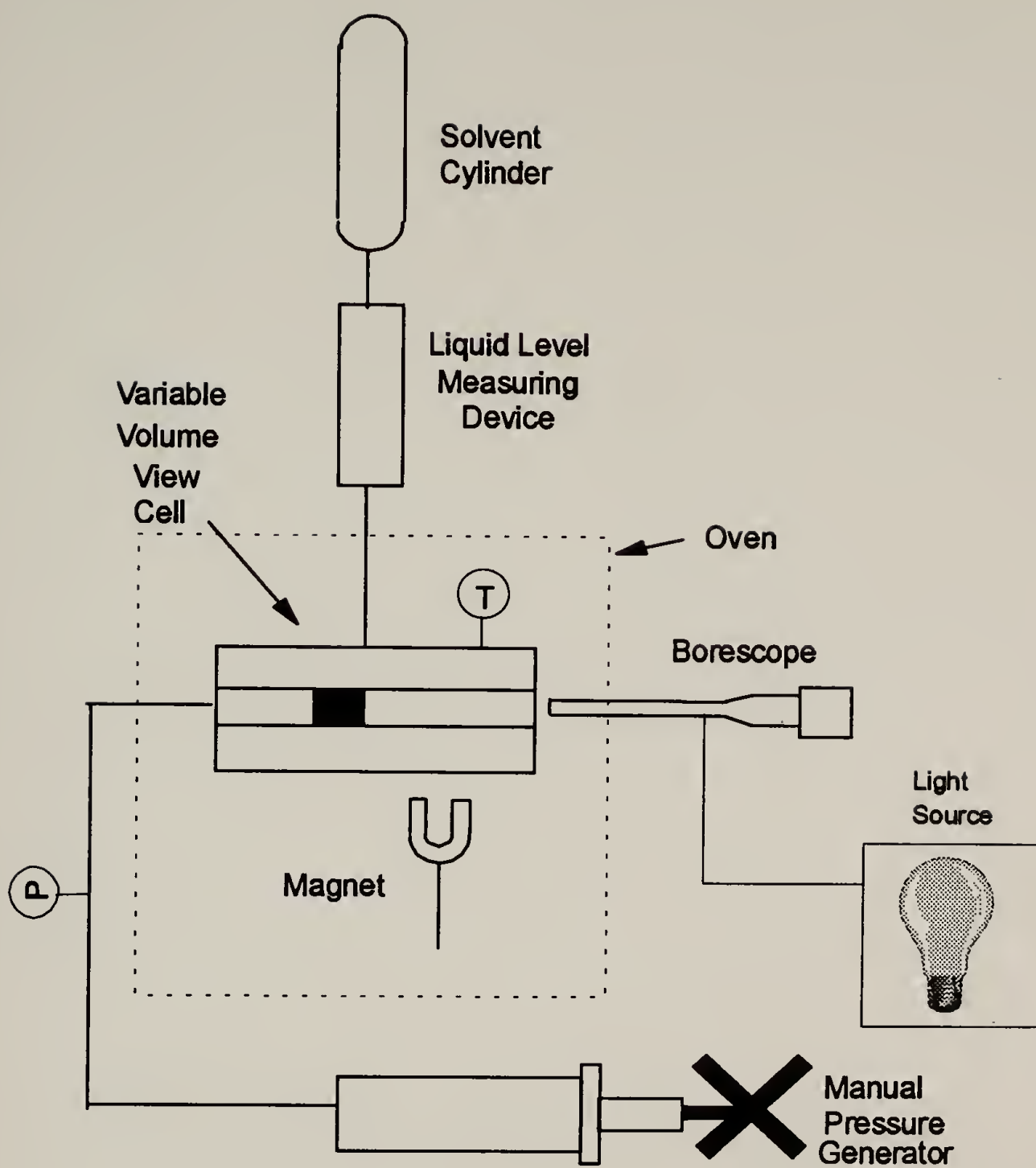


Figure 2.6 Overall High Pressure Phase Behavior Apparatus

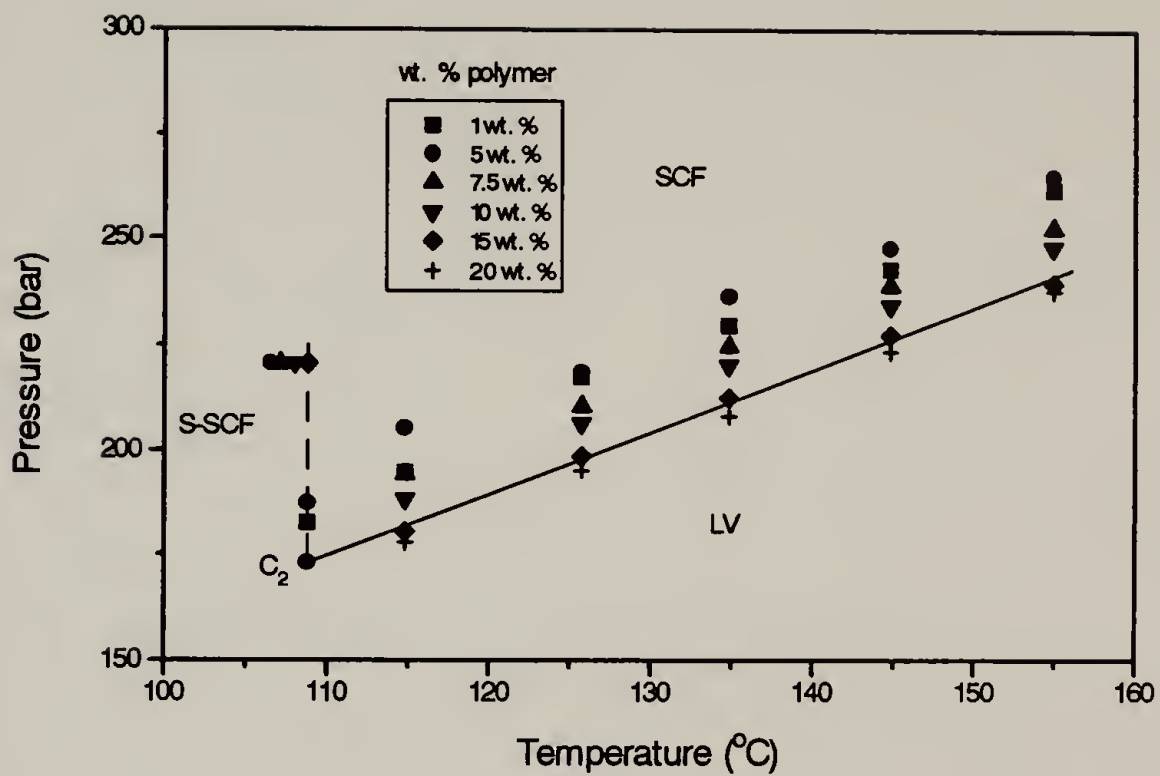


Figure 2.7 Cloud-Point Isoleths for iPP1/Propane (SCF is a single supercritical phase, LV denotes liquid-vapor equilibrium, S-SCF denotes a two phase region of solid polymer and a supercritical phase, and C<sub>2</sub> is the location of the second critical end point)

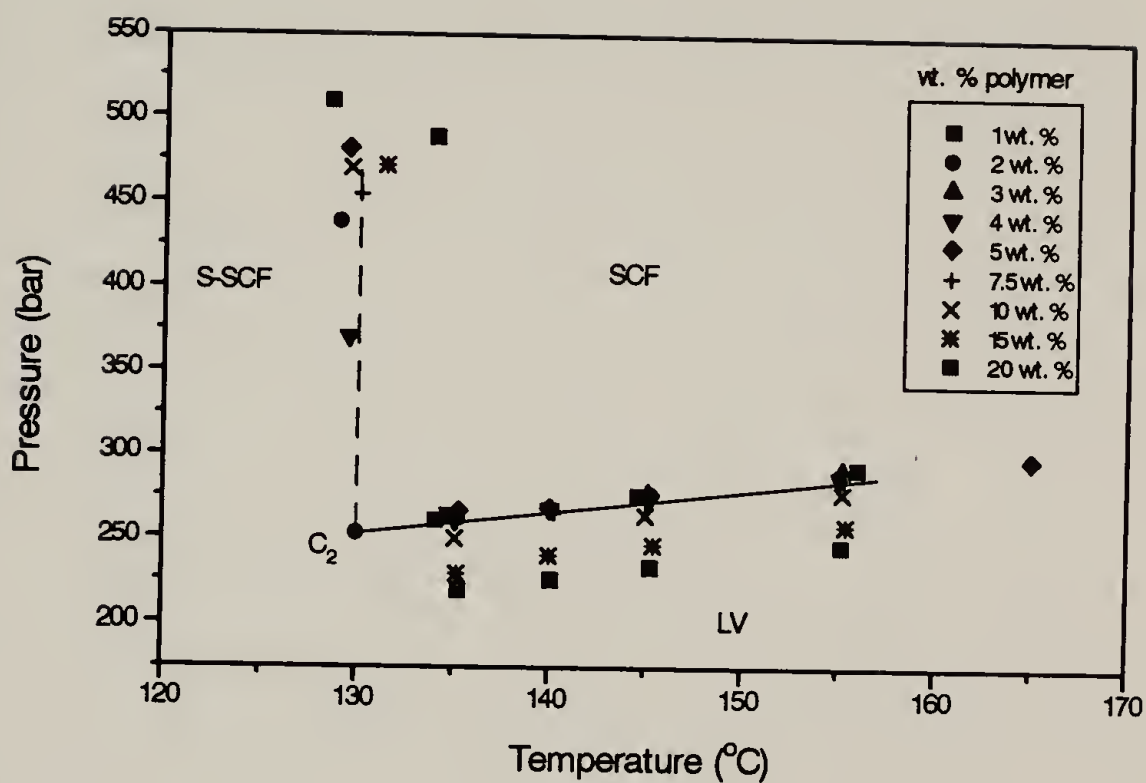


Figure 2.8 Cloud-Point Isopleths for iPP2/Propane (SCF is a single supercritical phase, LV denotes liquid-vapor equilibrium, S-SCF denotes a two phase region of solid polymer and a supercritical phase, and C<sub>2</sub> is the location of the second critical end point)

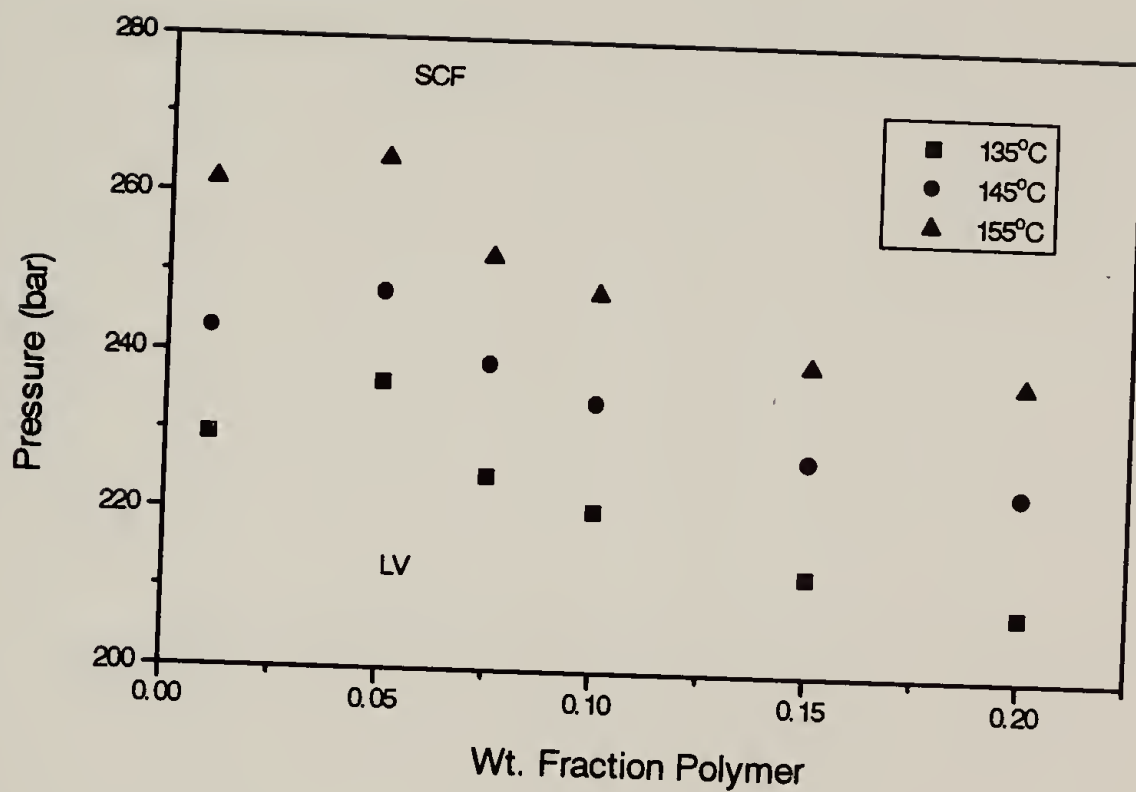


Figure 2.9 Cloud-Point Isotherms for iPP1/Propane (SCF denotes a single supercritical phase and LV denotes liquid-vapor equilibrium)

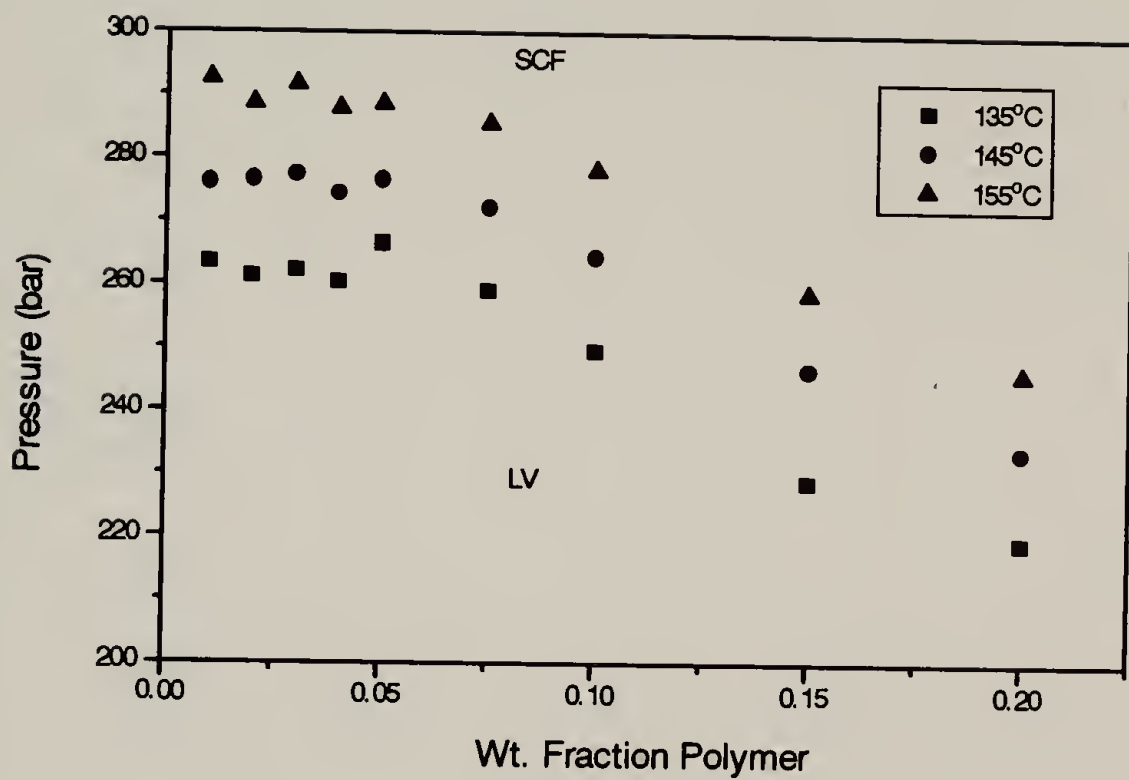


Figure 2.10 Cloud-Point Isotherms for iPP2/Propane (SCF denotes a single supercritical phase and LV denotes liquid-vapor equilibrium)

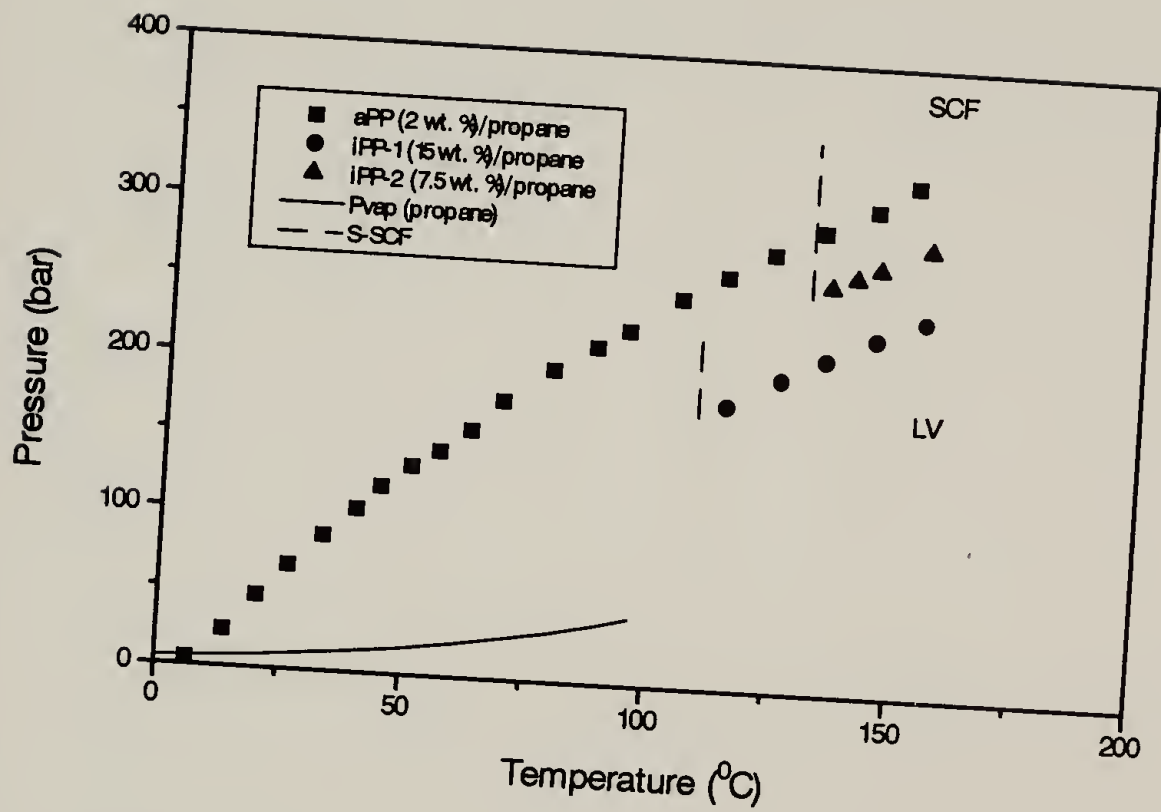


Figure 2.11 Cloud-Point Isopleths for aPP/Propane Compared to iPP/Propane (SCF denotes a single supercritical phase and LV denotes liquid-vapor equilibrium)

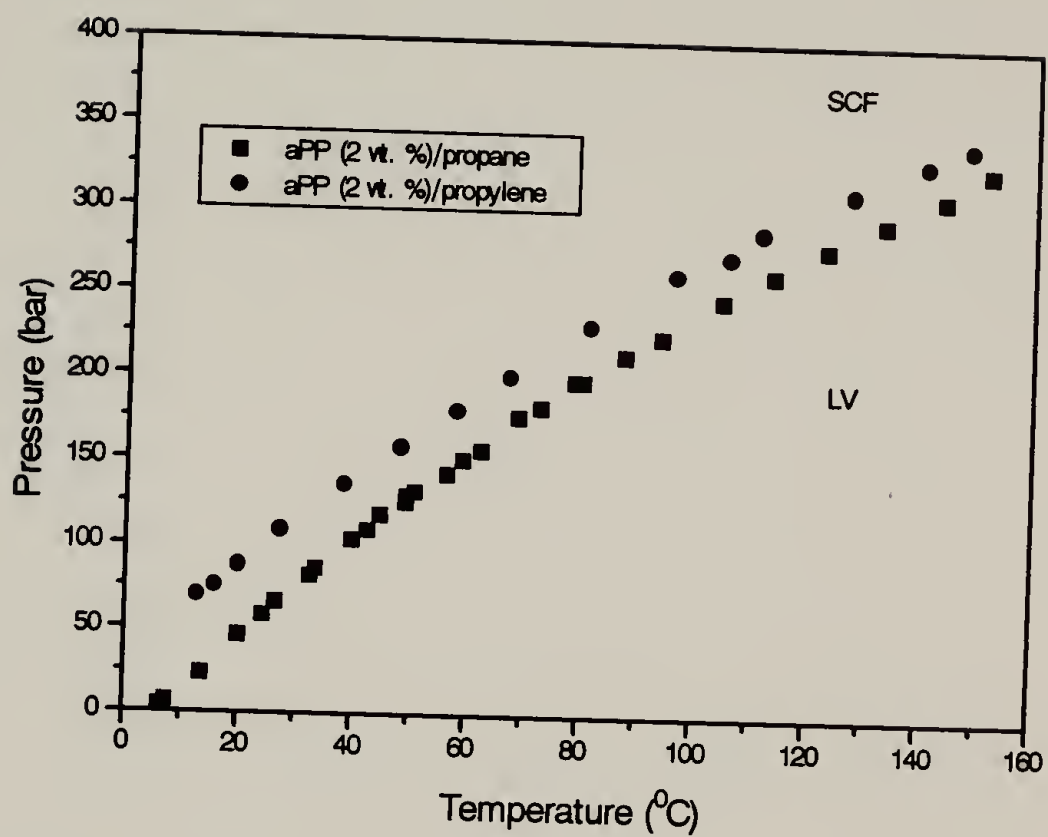


Figure 2.12 Cloud-Point Isopleths for aPP/Propylene Compared to aPP/Propane (SCF denotes a single supercritical phase and LV denotes liquid-vapor equilibrium)



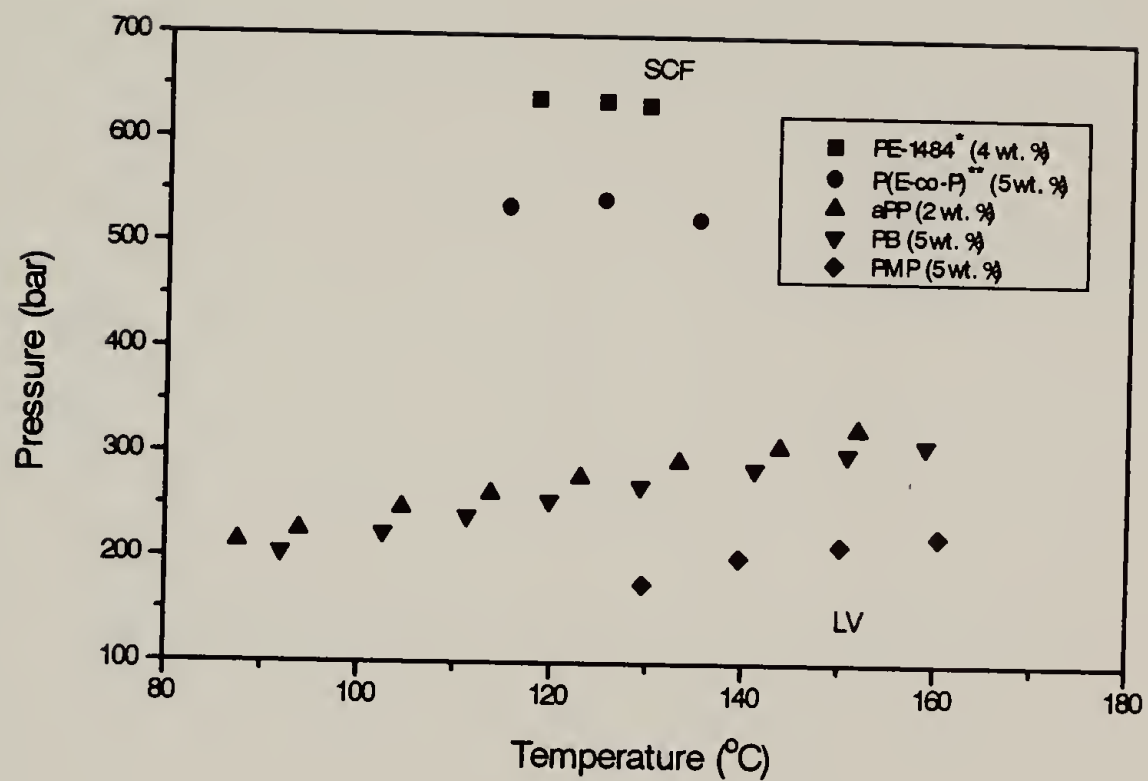


Figure 2.13 Cloud-Point Isopleths for Various Polyolefins with Different Side-Chain Branching in Propane (SCF denotes a single supercritical phase, LV denotes liquid-vapor equilibrium, \* denotes data of Condo et al., 1992, and \*\* denotes a 70 wt. % ethylene copolymer)

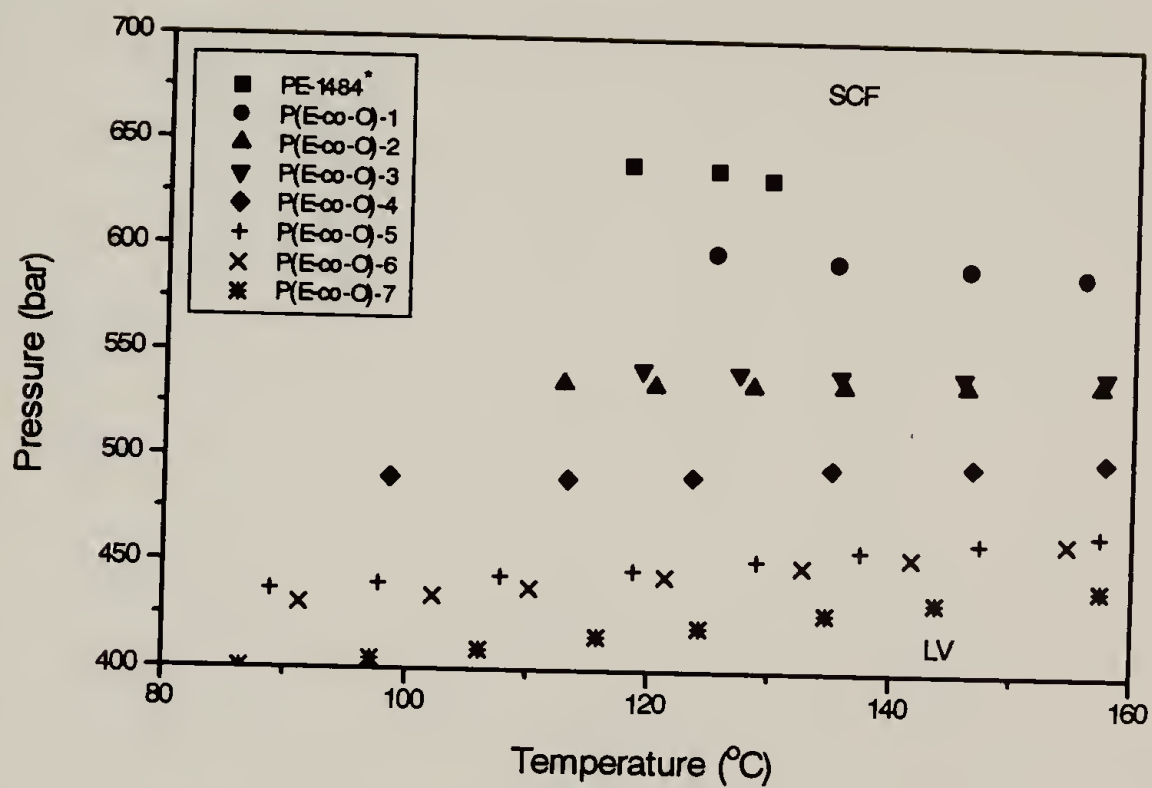


Figure 2.14 Cloud-Point Isopleths for Poly(ethylene-co-octene) Copolymers with Different Octene Contents in Propane (SCF denotes a single supercritical phase, LV denotes liquid-vapor equilibrium, and \* denotes data of Condo et al., 1992)

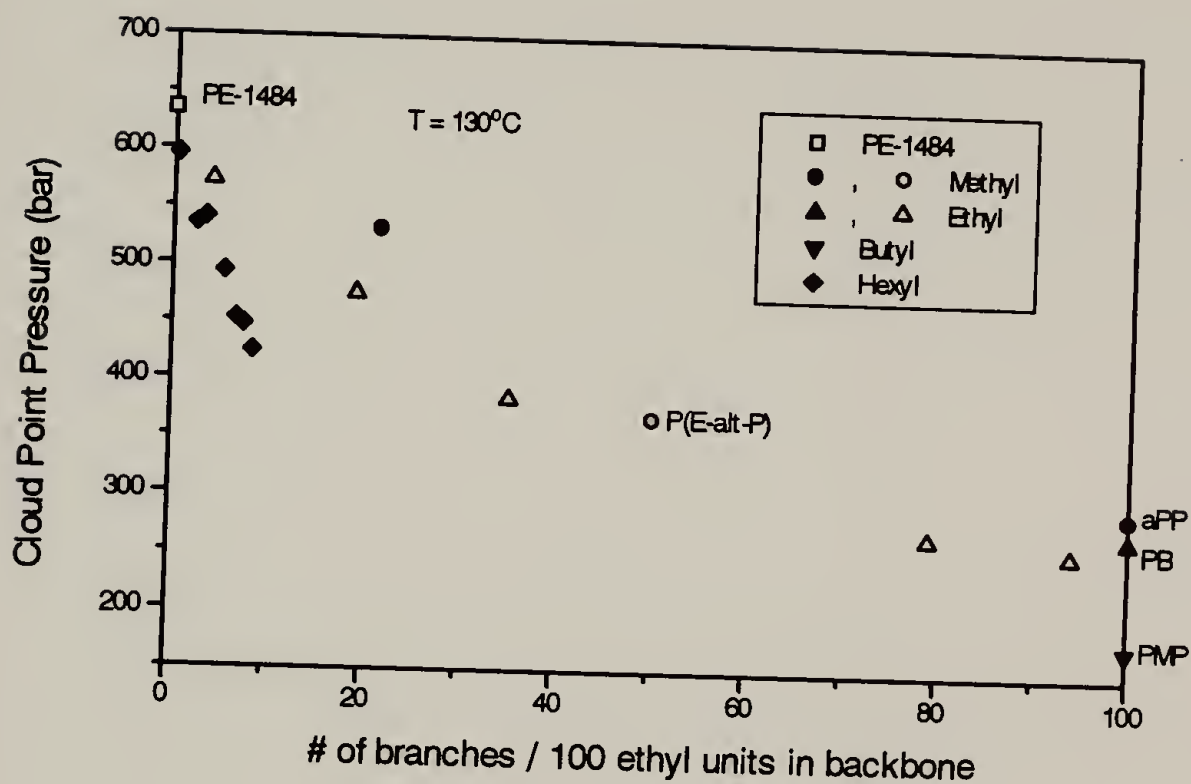


Figure 2.15 Correlation of Cloud-Point Pressures of Polyolefins in Supercritical Propane with Branch Density (PE-1484 is a high density polyethylene, P(E-alt-P) is poly(ethylene-alt-propylene), aPP is atactic polypropylene, PB is poly(1-butene), PMP is poly(4-methyl-1-pentene),  $\square$  - is data of Condo et al., 1992, and O,  $\Delta$  - is data of Chen et al., 1995)

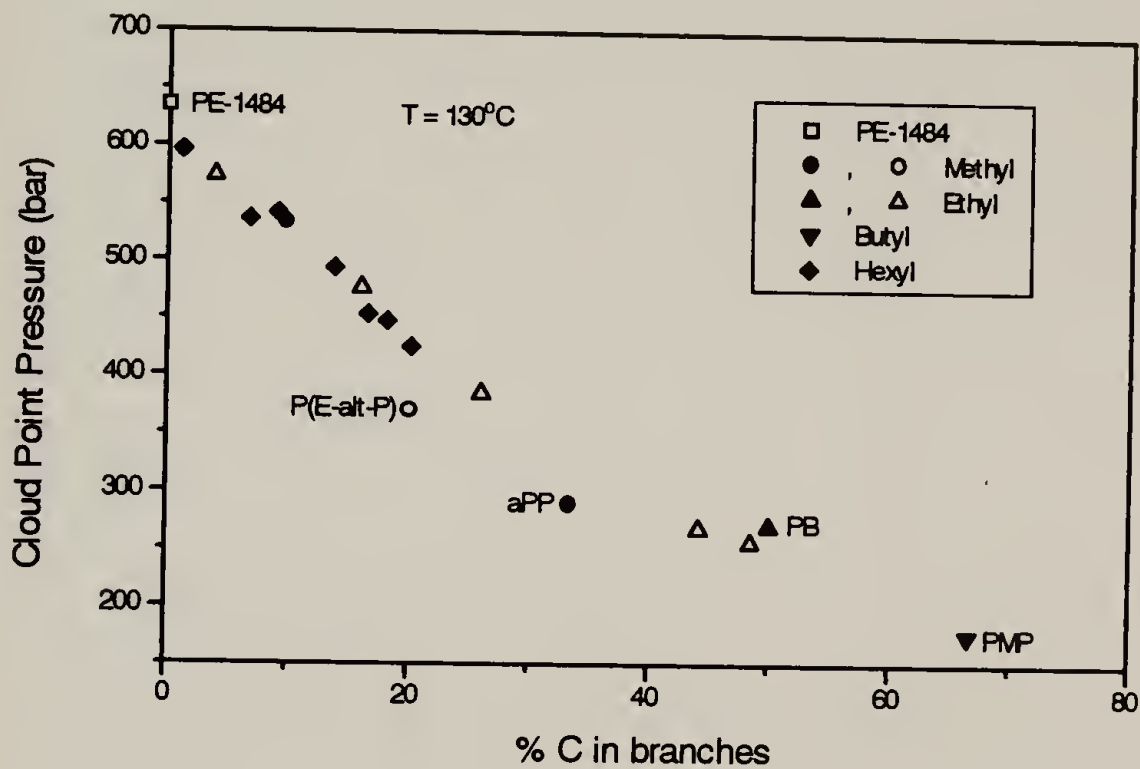


Figure 2.16 Correlation of Cloud-Point Pressures of Polyolefins in Supercritical Propane with % Carbon in Branches (PE-1484 is a high density polyethylene, P(E-alt-P) is poly(ethylene-alt-propylene), aPP is atactic polypropylene, PB is poly(1-butene), PMP is poly(4-methyl-1-pentene),  $\square$  - is data of Condo et al., 1992, and  $\circ$ ,  $\Delta$  - is data of Chen et al., 1995)

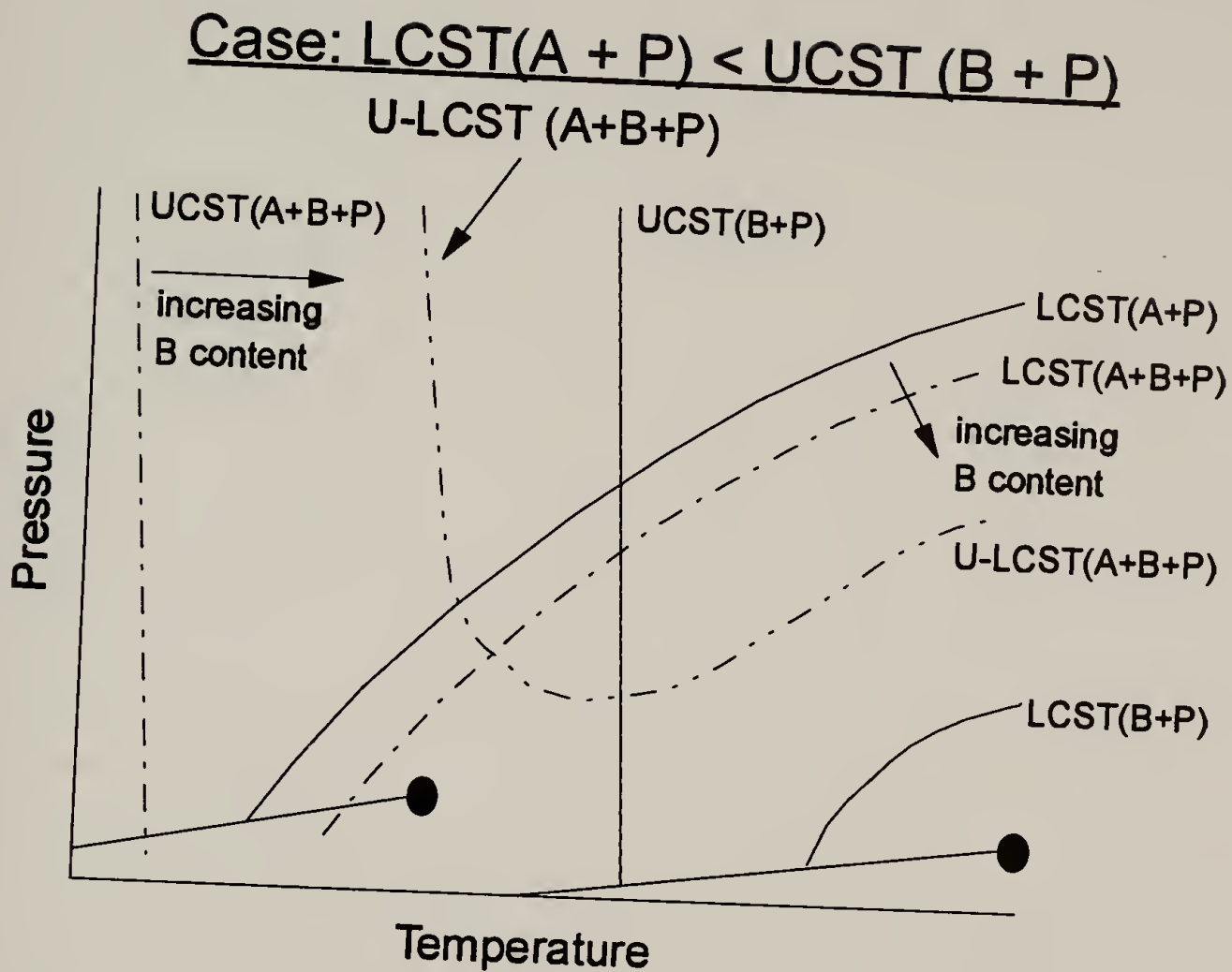


Figure 2.17 Ternary Phase Behavior Diagram: Change in Critical Lines Upon Changing Polarity of Solvent (A=alkane, B=alcohol, and P=polymer)

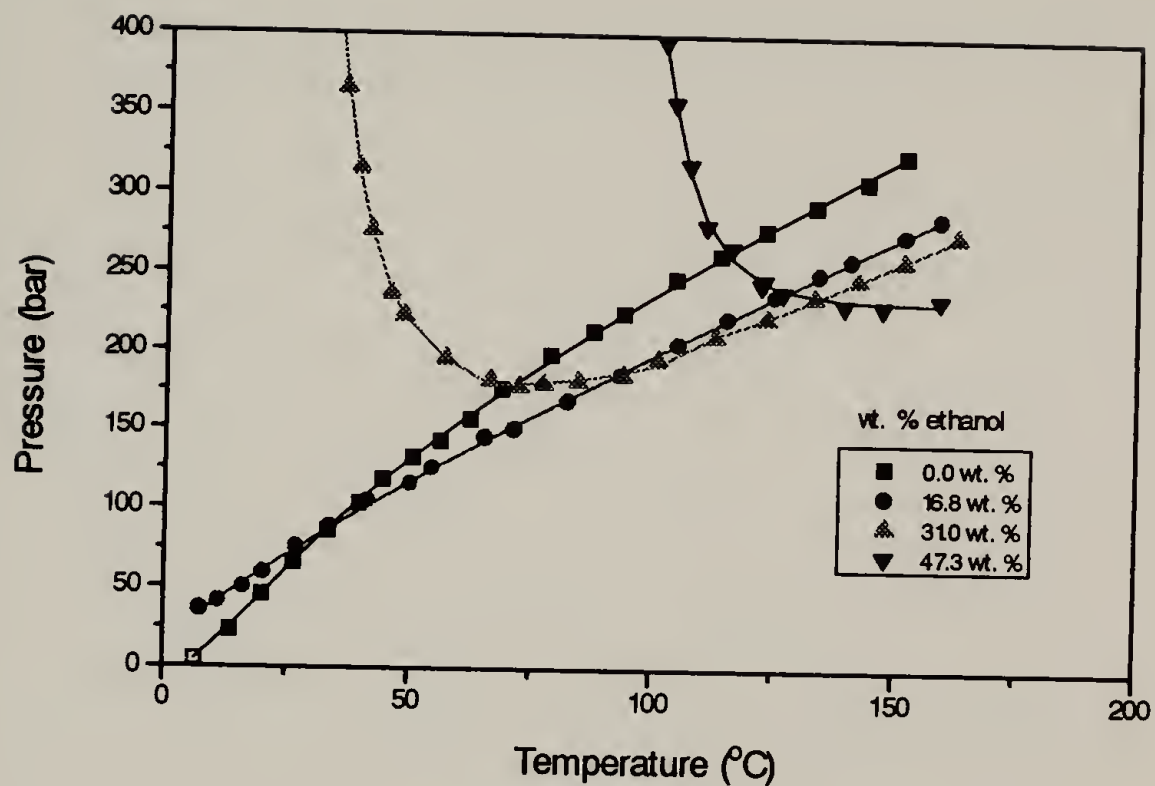


Figure 2.18 Cloud-Point Isoleths for the Ternary System: Atactic Polypropylene/Propane/Ethanol (2 wt. % Polymer Solutions) (Open symbol for 0.0 wt. % ethanol system represents the lower critical end point (LCEP))

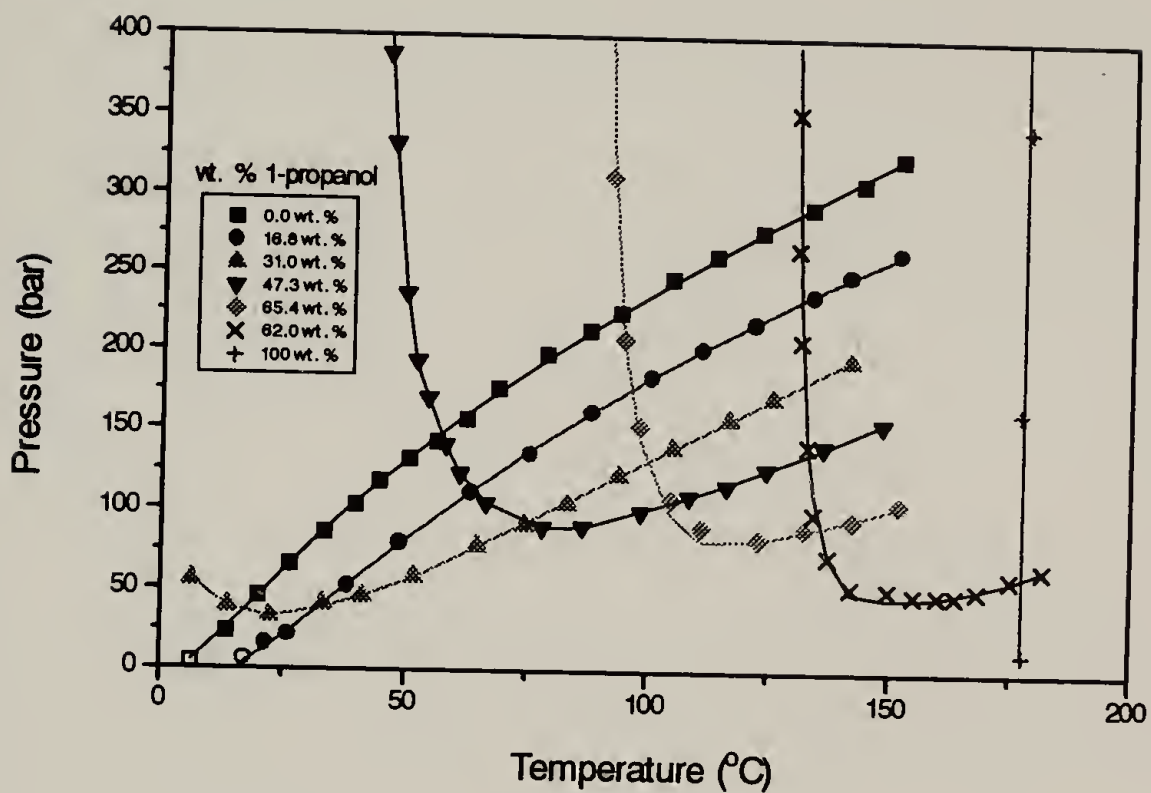


Figure 2.19 Cloud-Point Isopleths for the Ternary System: Atactic Polypropylene/Propane/1-Propanol (2 wt. % Polymer Solutions) (Open symbols for 0.0 and 16.8 wt. % 1-propanol systems represent the lower critical end point (LCEP) and the lowest symbol for the 100 wt. % 1-propanol system represents the upper critical end point (UCEP))

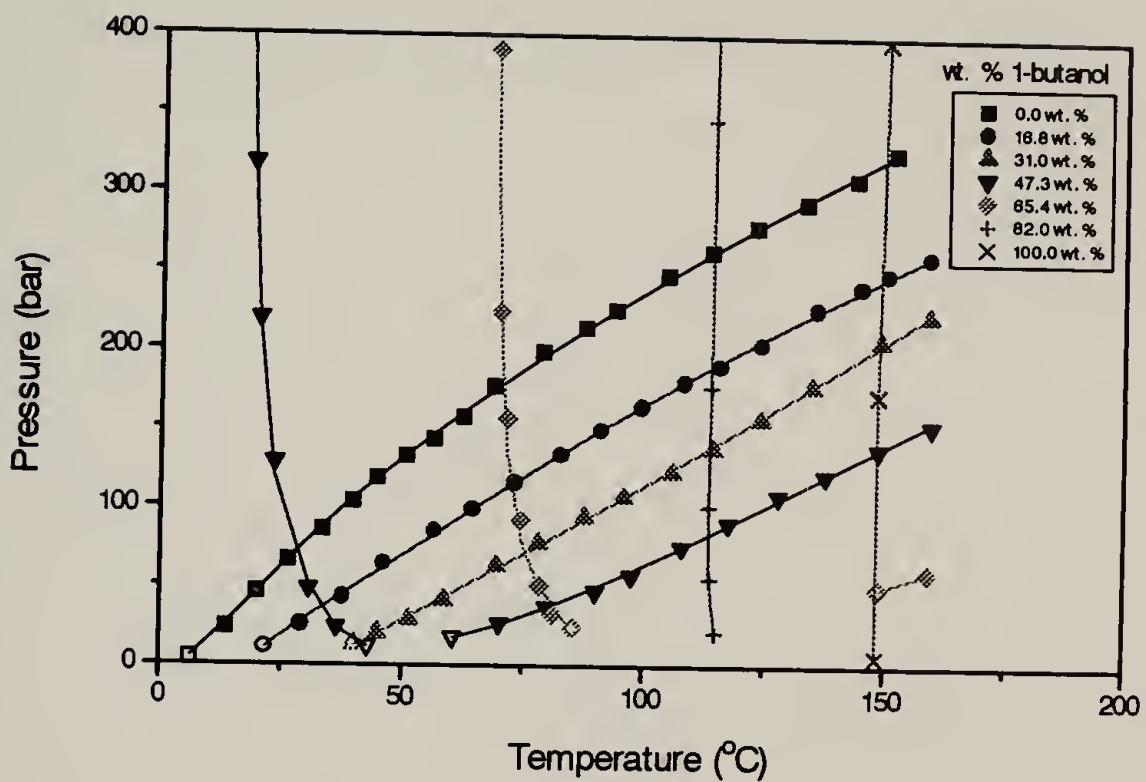


Figure 2.20 Cloud-Point Isopleths for the Ternary System: Atactic Polypropylene/Propane/1-Butanol (2 wt. % Polymer Solutions) (Open symbols for 0.0, 16.8, 31.0, 47.3, and 65.4 wt. % 1-butanol systems represent upper and lower critical end points (UCEP and LCEP) and lowest points for 82.0 and 100.0 wt. % 1-butanol systems represent upper critical end points (UCEP))



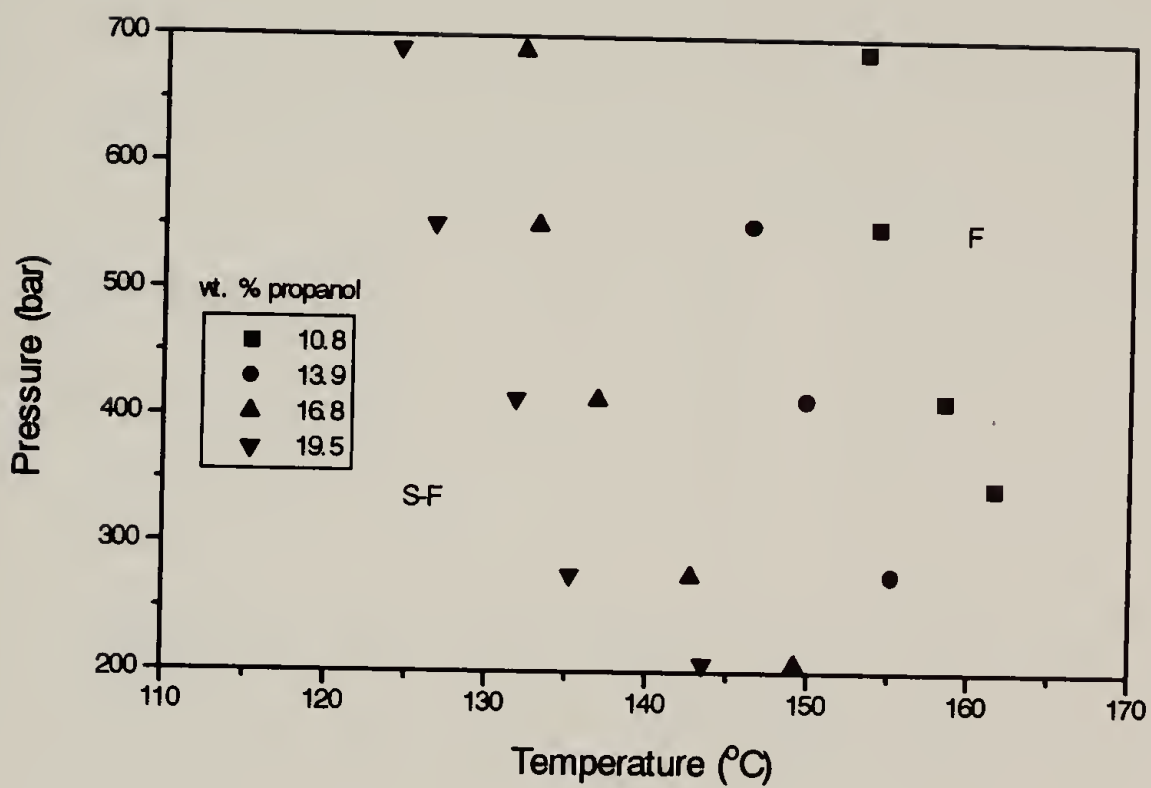


Figure 2.21 Solid-Supercritical Fluid Equilibria for Dibenzylidene-d-sorbitol in Propane/1-Propanol Mixtures (F denotes a single fluid phase and S-F denotes a solid and fluid phase)

## REFERENCES

- Bush, P. J., D. Pradhan, and P. Ehrlich, "Lamellar Structure and Organization in Polyethylene Gels Crystallized from Supercritical Solution in Propane," *Macromolecules*, **24**, 1439 (1991).
- Charlet, G., and G. Delmas, "Thermodynamic Properties of Polyolefin Solutions at High Temperature: 1. Lower Critical Solubility Temperatures of Polyethylene, Polypropylene and Ethylene-Propylene Copolymers in Hydrocarbon Solvents," *Polymer*, **22**, 1181 (1981).
- Charlet, G., R. Ducasse, and G. Delmas, "Thermodynamic Properties of Polyolefin Solutions at High Temperature: 2. Lower Critical Solubility Temperatures for Polybutene-1, Polypropylene-1, and Poly(4-methylpentene-1) in Hydrocarbon Solvents and the Determination of the Polymer Solvent Interaction-parameter for PB1 and one Ethylene-Propylene Copolymer," *Polymer*, **22**, 1190 (1981).
- Chen, S., and M. Radosz, "Density-Tuned Polyolefin Phase Equilibria. 1. Binary Solutions of Alternating Poly(ethylene-propylene) in Subcritical and Supercritical Propylene, 1-Butene, and 1-Hexene. Experiment and Flory-Patterson Model," *Macromolecules*, **25**, 3089 (1992).
- Chen, S., I. G. Economou, and M. Radosz, "Density-Tuned Polyolefin Phase Equilibria. 2. Multicomponent Solutions of Alternating Poly(ethylene-propylene) in Subcritical and Supercritical Olefins. Experiment and SAFT Model," *Macromolecules*, **25**, 4987 (1992).
- Chen, S., M. Banaszak, and M. Radosz, "Phase Behavior of Poly(ethylene-1-butene) in Subcritical and Supercritical Propane: Ethyl Branches Reduce Segment Energy and Enhance Miscibility," *Macromolecules*, **28**, 1812 (1995).
- Condo, P. D., E. J. Colman, and P. Ehrlich, "Phase Equilibria of Linear Polyethylene with Supercritical Propane," *Macromolecules*, **25**, 750 (1992).
- Cook, R. L., H. E. King, and D. G. Peiffer, "Pressure-Induced Crossover from Good to Poor Solvent Behavior for Polyethylene Oxide in Water," *Phys. Rev. Lett.*, **69**(21), 3072 (1992).
- Cotton, N. J., K. D. Bartle, A. A. Clifford, and C. J. Dowle, "Rate and Extent of Supercritical Fluid Extraction of Additives from Polypropylene: Diffusion, Solubility, and Matrix Effects," *J. Appl. Polym. Sci.*, **48**, 1607 (1993).
- Cowie, J. M. G., and I. J. McEwen, "Lower Critical Solution Temperatures of Polypropylene Solutions," *J. Polym. Sci.: Polym. Phys. Ed.*, **12**, 441 (1974).

de Loos, T. W., W. Poot, and G. A. M. Diepen, "Fluid Phase Equilibria in the System Polyethylene + Ethylene. 1. Systems of Linear Polyethylene + Ethylene at High Pressure," *Macromolecules*, **16**, 111 (1983).

Ehrlich, P., "Supercritical Polymer Solutions and Polymer-Fluid Interactions at High Pressure," *Chemtracts-Macromol. Chem.*, **3**, 1 (1992).

Ehrlich, P., and J. J. Kurpen, "Phase Equilibria of Polymer-Solvent Systems at High Pressures Near Their Critical Loci: Polyethylene with n-Alkanes," *J. Polym. Sci., Pt. A*, **1**, 3217 (1963).

Elsbernd, C. S., J. M. DeSimone, A. M. Hellstern, S. D. Smith, P. M. Gallagher, V. J. Krukonis, and J. E. McGrath, "The Application of Supercritical Fluids in the Fractionation and Characterization of Siloxane Oligomers and Graft Copolymers," *Polym. Prepr. (Am. Chem. Soc., Div. Polym. Chem.)*, **31**(1), 673 (1990).

Flory, P. J., *Principles of Polymer Chemistry*, Cornell University Press: Ithaca (1953).

Folie, B. and M. Radosz, "Phase Equilibria in High-Pressure Polyethylene Technology," *Ind. Chem. Eng. Res.*, **34**, 1501 (1995).

Freeman, P. I., and J. S. Rowlinson, "Lower Critical Points in Polymer Solutions," *Polymer*, **1**, 20 (1960).

Gregg, C. J., F. P. Stein, and M. Radosz, "Phase Behavior of Telechelic Polyisobutylene (PIB) in Subcritical and Supercritical Fluids. 1. Inter- and Intra-Association Effect for Blank, Monohydroxy, and Dihydroxy PIB (1K) in Ethane, Propane, Dimethyl Ether, Carbon Dioxide, and Chlorodifluoromethane," *Macromolecules*, **27**, 4972 (1994a).

Gregg, C. J., F. P. Stein, and M. Radosz, "Phase Behavior of Telechelic Polyisobutylene (PIB) in Subcritical and Supercritical Fluids. 2. PIB Size, Solvent Polarity, and Inter- and Intra-Association Effect for Blank, Monohydroxy, and Dihydroxy PIB (11K) in Ethane, Propane, Carbon Dioxide, and Dimethyl Ether," *Macromolecules*, **27**, 4981 (1994b).

Hasch, B. M., M. A. Meilchen, S. Lee, and M. A. McHugh, "High-Pressure Phase Behavior of Mixtures of Poly(Ethylene-co-Methyl Acrylate) with Low-Molecular Weight Hydrocarbons," *J. Polym. Sci.: Part B: Polym. Phys.*, **30**, 1365 (1992).

Hasch, B. M., S. Lee, M. A. McHugh, J. J. Watkins, and V. J. Krukonis, "The Effect Of Backbone Structure on the Cloud Point Behavior of Polyethylene-Ethane and Polyethylene-Propane Mixtures," *Polymer*, **34**(12), 2554 (1993a).

Hasch, B. M., M. A. Meilchen, S. Lee, and M. A. McHugh, "Cosolvency Effects on Copolymer Solutions at High Pressure," *J. Polym. Sci.: Part B: Polym. Phys.*, **31**, 429 (1993b).

- Haschets, C. W., and A. D. Shine, "Phase Behavior of Polymer-Supercritical Chlorodifluoromethane Solutions," *Macromolecules*, **26**, 5052 (1993).
- Kiamos, A. A., and M. D. Donohue, "The Effect of Supercritical Carbon Dioxide on Polymer-Solvent Mixtures," *Macromolecules*, **27**, 357 (1994).
- Kiran, E., W. Zhuang, and Y. L. Sen, "Solubility and Demixing of Polyethylene in Supercritical Binary Fluid Mixtures: Carbon-Dioxide-Cyclohexane, Carbon Dioxide-Toluene, Carbon Dioxide-Pentane," *J. Appl. Polym. Sci.*, **47**, 895 (1993).
- Koningsveld, R., and A. J. Staverman, "Liquid-Liquid Phase Separation in Multicomponent Polymer Solutions. I. Statement of the Problem and Description of Methods of Calculation," *J. Polym. Sci. Pt. A-2*, **6**, 305 (1968a).
- Koningsveld, R., and A. J. Staverman, "Liquid-Liquid Phase Separation in Multicomponent Polymer Solutions. II. The Critical State," *J. Polym. Sci. Pt. A-2*, **6**, 325 (1968b).
- Koningsveld, R., and A. J. Staverman, "Liquid-Liquid Phase Separation in Multicomponent Polymer Solutions. III. Cloud-Point Curves," *J. Polym. Sci. Pt. A-2*, **6**, 349 (1968c).
- Lee, S., M. A. LoStracco, and M. A. McHugh, "High-Pressure, Molecular Weight-Dependent Behaviour of (Co)polymer-Solvent Mixtures: Experiments and Modeling," *Macromolecules*, **27**, 4652 (1994).
- LeMay, J. D., R. W. Hopper, L. W. Hrubesh, and R. W. Pekala, "Low-Density Microcellular Materials," *MRS Bulletin*, **15**(12), 19 (1990).
- McClellan, A. K., and M. A. McHugh, "Separating Polymer Solutions Using High Pressure Lower Critical Solution Temperature (LCST) Phenomena," *Polym. Eng. and Sci.*, **25**(17), 1088 (1985).
- McHugh, M. A., and T. L. Guckes, "Separating Polymer Solutions with Supercritical Fluids," *Macromolecules*, **18**, 674 (1985).
- McHugh, M. A., and V. Krukoniš, *Supercritical Fluid Extraction: Principles and Practice*, Butterworths: Boston (1986)
- Meilchen, M. A., B. M. Hasch, and M. A. McHugh, "Effect of Copolymer Composition on the Phase Behavior of Poly(ethylene-co-methyl acrylate) with Propane and Chlorodifluoromethane," *Macromolecules*, **24**, 4874 (1991).

- Meilchen, M. A., B. M. Hasch, S. Lee, and M. A. McHugh, "Poly(ethylene-co-methyl acrylate)-solvent-cosolvent Phase Behavior at High Pressures," *Polymer*, **33**, 1922 (1992).
- Pradhan, D., and P. Ehrlich, "Morphologies of Microporous Polyethylene and Polypropylene Gels Crystallized from Solution in Supercritical Propane," *J. Polym. Sci. Part B: Polym. Phys.*, **33**, 1053 (1995).
- Reid, R. C., J. M. Prausnitz, and B. E. Poling, *The Properties of Gases and Liquids*, 4th. Ed., Mc-Graw Hill: New York (1987).
- Sawyer, L. C., and D. T. Grubb, *Polymer Microscopy*, Chapman and Hall: New York (1987).
- Scholte, TH. G., H. L. J. Meijerlink, H. M. Schoffeleers, and A. M. G. Brands, "Mark-Houwink Equation and GPC Calibration for Linear Short-Chain Branched Polyolefins, Including Polypropylene and Ethylene-Propylene Copolymers," *J. Appl. Polym. Sci.*, **29**, 3763 (1984).
- Scott, R. L., and P. H. Van Konynenburg, "Van der Waals and Related Models for Hydrocarbon Mixtures," *Disc. Faraday Soc.*, **49**, 87 (1970).
- Seckner, A. J., A. K. McClellan, and M. A. McHugh, "High-Pressure Solution Behavior of the Polystyrene-Toluene-Ethane System," *AIChE J.*, **34**(1), 9 (1988).
- Shaffer, K. A., and J. M. DeSimone, "Chain Polymerization in Inert Near- and Supercritical Fluids," *Trends. Polym. Sci.*, **5**(3), 146 (1995).
- Smith, J. M., and H. C. Van Ness, *Introduction to Chemical Engineering Thermodynamics*, 4th Ed., McGraw-Hill: New York (1987).
- Suresh, S. J., R. M. Enick, and E. J. Beckman, "Phase Behavior of Nylon 6/Trifluoroethanol/Carbon Dioxide Mixtures," *Macromolecules*, **27**, 348, (1994).
- Thierry, A., B. Fillon, C. Straupé, B. Lotz, and J. C. Wittman, "Polymer Nucleating Agents: Efficiency Scale and Impact of Physical Gelation," *Progr. Colloid Polym. Sci.*, **87**, 28 (1992).
- Tuminello, W. H., G. T. Dee, and M. A. McHugh, "Dissolving Perfluoropolymers in Supercritical Carbon Dioxide," *Macromolecules*, **28**, 1506 (1995).
- Watkins, J. J., V. J. Krukonis, P. D. Condo, D. Pradhan, and P. Ehrlich, "Fractionation of High Density Polyethylene in Propane by Isothermal Pressure Profiling and Isobaric Temperature Profiling," *J. Supercritical Fluids*, **4**, 24 (1991).

Zeman, L., and D. Patterson, "Pressure Effects in Polymer Solution Phase Equilibria. II. Systems Showing Upper and Lower Critical Solution Temperatures," *J. Phys. Chem.*, **76(8)**, 1214 (1972).

Zeman, L., J. Biros, G. Delmas, and D. Patterson, "Pressure Effects in Polymer Solution Phase Equilibria. I. The Lower Critical Solution Temperature of Polyisobutylene and Polydimethylsiloxane in Lower Alkanes," *J. Phys. Chem.*, **76(8)**, 1206 (1972).

Zhao, X., R. Watkins, and S. W. Barton, "Strategies for Supercritical CO<sub>2</sub> Fractionation of Polydimethylsiloxane," *J. Appl. Polym. Sci.*, **55**, 773 (1995).

## CHAPTER 3

### MODELING OF PHASE BEHAVIOR

Predicting polymer solution phase behavior has received a great deal of theoretical interest [Flory, 1953; Flory et al., 1964a,b; Sanchez-Lacombe, 1978]. Predictions by polymer solution theories must be compared to experimental phase behavior observations. Such comparisons will help test polymer solution theories and possibly suggest ways in which theories may be reformulated or improved.

The purpose of this chapter is to compare predictions by polymer solution theories with some of the experimental data presented in Chapter 2. The specific polymer solution theory applied here is the lattice fluid theory of Sanchez-Lacombe (SL). Predictions by the SL theory will be compared to experimental data for the atactic polypropylene/propane and isotactic polypropylene/propane systems. An analysis of the mixing parameters inherent in the theory is included. Application of SL theory to the atactic polypropylene/propane/1-propanol system is also presented.

#### 3.1 Background

Relevant background information includes the basics of solution thermodynamics detailing mixture miscibility criteria as well as definition of the binodal, spinodal, and mixture critical point. Polymer solution thermodynamics as well as important developments leading to the application of equations of state (EOS) theories to predict lower critical solution temperature (LCST) behavior are discussed. A literature review of EOS modeling of LCST behavior in polymer/solvent systems is presented and reasons for selecting the Sanchez-Lacombe (SL) lattice fluid theory to model the polymer solutions in this thesis are discussed. Finally, an overview of the SL theory is presented along with the appropriate equations.

### 3.1.1 Solution Thermodynamics

A necessary condition for miscibility of components in a mixture requires that the Gibbs free energy change of mixing,  $\Delta G_{\text{mix}}$ , be negative. Miscibility over the whole composition range requires that  $\Delta G_{\text{mix}}$  as a function of composition always have positive curvature. For a binary mixture, this miscibility criterion can be stated as

$$\frac{\partial^2 \Delta G_{\text{mix}}}{\partial x^2} > 0 \quad (3.1)$$

where  $x$  is a measure of composition (i.e. mole fraction).

If equation 3.1 is violated for any composition, the single phase system becomes unstable. Properties of interest in the phase separated system are the composition of the phases in equilibrium at constant temperature and pressure (binodal) and the conditions at incipient phase separation i.e., the cloud-points, including the critical point.

For obtaining the binodal and mixture critical point, it is helpful to define a partial molar quantity called the chemical potential. The chemical potential of species  $i$ ,  $\mu_i$ , is obtained by differentiating  $\Delta G_{\text{mix}}$  with respect to the number of moles of species  $i$  and is given by

$$\mu_i = \left. \frac{\partial \Delta G_{\text{mix}}}{\partial n_i} \right|_{T, P, n_i'} \quad (3.2)$$

where the subscript  $n'$  indicates that all other mole numbers except  $n_i$  are held constant.

Analogous to equation 3.1, a stability criterion can be written in terms of the chemical potential and is given by



$$\frac{\partial \mu_1}{\partial x_1} > 0, \frac{\partial \mu_2}{\partial x_2} > 0 \quad (3.3)$$

Equilibrium between two phases in a two component system requires that the chemical potential of species  $i$  be equal in each of the phases and is given by

$$\begin{aligned} \mu_1' &= \mu_1'' \\ \mu_2' &= \mu_2'' \end{aligned} \quad (3.4)$$

where the prime and double prime superscripts represent the two different phases. In addition to this requirement, the stability criterion (equation 3.3) must be met at those phase compositions. Compositions which provide a solution to equation 3.4 and also satisfy the stability criterion represent the binodal.

Compositions for which the derivative of the chemical potential with respect to composition is zero represents the spinodal and is given by

$$\frac{\partial \mu_1}{\partial x_1} = 0 \quad (3.5)$$

In a phase separated system, two compositions will satisfy this condition with compositions between these two limits being unstable compositions.

Conditions for incipient phase separation at the mixture critical point are found by determining the solution to the following equation:

$$\frac{\partial \mu_1}{\partial x_1} = \frac{\partial^2 \mu_1}{\partial x_1^2} = 0 \quad (3.6)$$

At the mixture critical point, the compositions of both the binodal and spinodal become equal.

### 3.1.2 Polymer Solution Theories

The classical theory of polymer solutions may be considered to be the Flory-Huggins theory. This lattice theory predicts the existence of an upper critical solution temperature (UCST) based on the  $\chi$  parameter [Flory, 1953]. For polymers of infinite molecular weight, phase separation occurs when  $\chi \geq 1/2$ . In the original Flory-Huggins theory,  $\chi$  is a measure of the enthalpic polymer-solvent interactions whose value decreases with increasing temperature. Therefore, the Flory-Huggins theory only predicts UCST behavior.

Phase separation of polymer solutions upon heating was found in alkane/polyolefin systems [Freeman & Rowlinson, 1960] and is referred to as lower critical solution temperature (LCST) behavior. LCST behavior is now accepted as a universal property of polymer/solvent systems whose origins are either equation of state (EOS) dissimilarity between the polymer and solvent (compressibility) or specific interactions between components (hydrogen bonding) [Sanchez & Balazs, 1989; Sanchez, 1993]. Since the Flory-Huggins theory only predicts the existence of an UCST, new polymer solution theories were necessary to predict LCST behavior. Equations of state applied to mixtures have successfully predicted LCST behavior occurring as a result of compressibility effects [Sanchez & Lacombe, 1978; Flory et al., 1964a,b; Patterson & Delmas, 1969] and specific interactions [Panayiotou & Sanchez, 1991; Sanchez & Balazs, 1989].

### 3.1.3 Previous Modeling of LCST Behavior

The prediction of the LCST by equation of state theories has been attempted in many systems. In most cases, theoretical predictions are qualitatively correct but exact representation of experimental data requires the use of fitting parameters. Table 3.1 is a sampling of research where various theories have been applied to model LCST behavior. Table 3.2 lists abbreviations for solvents, polymers, and theories used in Table 3.1

Researchers have suggested that modeling of LCST behavior in nonpolar polymer/solvent systems by the Sanchez-Lacombe (SL) lattice fluid theory requires only a single temperature dependent adjustment parameter [Hasch et al., 1992; Hasch et al., 1993b]. Such results suggest that the SL theory would prove to be an appropriate model for the polypropylene/propane systems presented in Chapter 2. Therefore, specific details about this theory are presented as background information to provide a basis for subsequent modeling.

Table 3.1 Modeling of Polymer/Solvent Systems by Polymer Solution Theories Accounting for Equation of State (EOS) Effects

Polymer	Solvent	Theory	Reference
PE	ethylene	FH*	deLoos et al., 1983
P(E-alt-P)	propylene, 1-butene, 1-hexene	FP	Chen & Radosz, 1992
P(E-alt-P)	propylene, 1-butene, 1-hexene, and mixtures	SAFT	Chen et al., 1992
telechelic PIB (OH endcapped)	ethane, propane, dimethyl ether, carbon dioxide, CDFM	SAFT	Gregg et al., 1994a,b
P(E-co-MA)	ethylene, propylene, ethane, propane	SL	Hasch et al., 1992
PE, P(E-co-MA)	propane/acetone	SL	Hasch et al., 1993a
PE	ethane, propane	SL	Hasch et al., 1993b
PE, P(E-co-MA)	ethane, propane, butane, ethylene, propylene, 1-butene, CDFM, dimethyl ether	SAFT	Hasch et al., 1996
PMMA, PCL	CDFM	SL	Haschets & Shine, 1993
PE	dimethyl ether	SAFT	Lee et al., 1994
P(E-co-MA)	butane	SAFT	Lee et al., 1994
P(E-co-AA)	butene	SAFT	Lee et al., 1994
PE	ethylene	PHC	Liu & Prausnitz, 1980
P(E-co-MA)	CDFM, propane	SL	Meilchen et al., 1991
PE	alkanes	FP	Patterson & Delmas, 1969
PS	acetone	FP	Siow et al., 1972
Nylon 6	TFEtOH/carbon dioxide	SAFT, SLP	Suresh et al., 1994
PE	ethylene, FTCEM	FOVE	Walsh & Dee, 1988
PE	n-pentane/carbon dioxide	SL	Xiong & Kiran, 1994
PE	n-butane, n-pentane	SAFT, SL	Xiong & Kiran, 1995
PDMS, PIB	alkanes	FP	Zeman et al., 1972
PS	acetone, methyl acetate	FP	Zeman & Patterson, 1972

Table 3.2 List of Solvent, Polymer, and Theory Abbreviations Used in Table 3.1

<u>Solvent</u>	
CDFM	chlorodifluoromethane
FTCM	fluorotrichloromethane
TFEtOH	trifluoroethanol
<u>Polymer</u>	
Nylon 6	polycaprolactam
PCL	polycaprolactone
PDMS	polydimethyl siloxane
PE	polyethylene
P(E-co-AA)	poly(ethylene-co-acrylic acid)
P(E-co-MA)	poly(ethylene-co-methyl acrylate)
P(E-alt-P)	poly(ethylene-alt-propylene)
PIB	polyisobutylene
PMMA	poly(methyl methacrylate)
PS	polystyrene
<u>Theory</u>	
FH*	Flory-Huggins (pressure dependent $\chi$ )
FOVE	Flory-Orwoll-Vrij-Eichinger
FP	Flory-Patterson
PHC	Perturbed-Hard-Chain
SAFT	Statistical Associating Fluid Theory
SL	Sanchez-Lacombe
SLP	Sanchez-Lacombe-Perram

#### 3.1.4 Sanchez-Lacombe (SL) Lattice Fluid Theory

The Sanchez-Lacombe (SL) lattice fluid model characterizes a fluid by three equation of state parameters,  $T^*$ ,  $P^*$ , and  $\rho^*$ , otherwise known as the characteristic temperature, pressure, and density, respectively [Sanchez & Lacombe, 1976]. The equation of state (EOS) for a Sanchez-Lacombe lattice fluid is given by

$$\tilde{\rho}^2 + \tilde{P} + \tilde{T} \left[ \ln(1 - \tilde{\rho}) + \left(1 - \frac{1}{r}\right) \tilde{\rho} \right] = 0 \quad (3.7)$$

where the reduced temperature, pressure, volume and density are defined by

$$\tilde{T} = \frac{T}{T^*}, \quad \tilde{P} = \frac{P}{P^*}, \quad \tilde{v} = \frac{1}{\tilde{\rho}} = \frac{V}{V^*} \quad (3.8)$$

The relationship between the characteristic parameters and molecular level parameters is given by

$$\epsilon^* = kT^*, \quad v^* = \frac{kT^*}{P^*}, \quad r = \frac{MP^*}{kT^* \rho^*} = \frac{M}{\rho^* v^*} \quad (3.9)$$

where  $\epsilon^*$  is the interaction energy per mer,  $v^*$  is the close-packed mer volume,  $r$  is the number of sites on the lattice that the molecule occupies,  $M$  is molecular weight, and  $k$  is the Boltzmann constant. For polymeric materials, the equation of state reduces to

$$\tilde{\rho}^2 + \tilde{P} + \tilde{T} [\ln(1 - \tilde{\rho}) + \tilde{\rho}] = 0 \quad (3.10)$$

since  $r \rightarrow \infty$ . Equation of state parameters are generally determined from a knowledge of the PVT behavior of a fluid. However, for polymers, the corresponding states nature of equation 3.10 allows determination of the equation of state parameters from other experimentally determined parameters [Sanchez and Lacombe, 1977]. These parameters are the density, thermal expansion coefficient, and compressibility measured at atmospheric pressure and the same temperature.

The equations of state for a pure fluid can then be applied to fluid mixtures utilizing mixing rules which determine cross-terms from pure component properties. The first application of the SL EOS to polymer solutions characterized the binary mixture with a single dimensionless energy parameter [Sanchez and Lacombe, 1978]. A later extension relaxed the theory to characterize a binary mixture with two parameters [Sanchez, 1980]. In addition to the dimensionless energy parameter, a dimensionless volume parameter was introduced in the two parameter model. These empirical dimensionless parameters provide a measure of the deviation of cross-terms predicted by mixing rules to those required to predict the experimental fluid mixture properties.

The dimensionless energy parameter,  $\zeta$ , is defined by

$$\zeta = \frac{\epsilon_{12}^*}{(\epsilon_{11}^* \epsilon_{22}^*)^{1/2}} \quad (3.11)$$

while the dimensionless volume parameter is defined by

$$\delta = \frac{2v_{12}^*}{(v_{11}^* + v_{22}^*)} - 1 \quad (3.12)$$

where the 11 and 22 subscripts refer to the pure component parameters while 12 subscripts refer to the mixture cross-terms.  $\delta$  is a measure of the deviation of closed-packed mixing from ideal mixing, or

$$\delta \begin{cases} < 0 & , & v^* < v_{\text{ideal}}^* \\ = 0 & , & v^* = v_{\text{ideal}}^* \\ > 0 & , & v^* > v_{\text{ideal}}^* \end{cases} \quad , \quad \text{where} \quad v_{\text{ideal}}^* = \phi_1 v_1^* + \phi_2 v_2^* \quad (3.13)$$

while  $\zeta$  expresses the deviation of the polymer-solvent mer-mer interaction energy from the geometric mean of the pure component interaction energies which is consistent with the commonly invoked Lorentz-Berthelot rule [Rowlinson & Swinton, 1982]. Therefore, values of  $\zeta$  other than unity represent a deviation from the Lorentz-Berthelot rule.

Applying equation 3.2 to the appropriate free energy of mixing expression [Lacombe & Sanchez, 1976], gives the following expression for the chemical potential [Sanchez, 1980]

$$\mu_i = RT \left[ \ln(\phi_i) + \left(1 - \frac{r_i}{r}\right) \right] + r_i \left\{ -\rho \left[ \varepsilon^* + \frac{\partial \varepsilon^*}{\partial \phi_i} \right]_{\phi} + P\bar{v} \left[ \frac{\partial v^*}{\partial \phi_i} \right]_{\phi} - v^* \right\} + RT\bar{v} \left[ (1 - \bar{\rho}) \ln(1 - \bar{\rho}) + \frac{\bar{\rho}}{r_i} \ln \bar{\rho} \right] \quad (3.14)$$

where  $\phi_i$  is the volume fraction of species  $i$  and  $R$  is the universal gas constant.

The partial derivatives in equation 3.14 must be evaluated for the specific proposed mixing rules. The proposed mixing rules for the molecular size parameter, mer-mer interaction energy, and average mer volume are given by [Sanchez, 1980]

$$\frac{1}{r} = \sum_i \frac{\phi_i}{r_i} \quad (3.15a)$$

$$\varepsilon^* = \sum_i \sum_j \phi_i \phi_j \frac{v_{ij}^* \varepsilon_{ij}^*}{v^*} \quad (3.15b)$$



$$v^* = \sum_i \sum_j \phi_i \phi_j v_{ij}^* \quad (3.15c)$$

After evaluation of the partial derivatives of equations 3.15b and 3.15c, the following expression for the chemical potential is given by [Meilchen et al., 1991]

$$\mu_i = RT \left[ \ln(\phi_i) + \left(1 - \frac{r_i}{r}\right) \right] + r_i \left\{ \begin{aligned} & -\rho \left[ \frac{2}{v^*} \left( \sum_{j=1}^c \phi_j v_{ij}^* \varepsilon_{ij}^* - \varepsilon^* \sum_{j=1}^c \phi_j v_{ij}^* \right) + \varepsilon^* \right] + P\bar{v} \left[ 2 \sum_{j=1}^c \phi_j v_{ij}^* - v^* \right] \\ & + RT\bar{v} \left[ (1 - \bar{\rho}) \ln(1 - \bar{\rho}) + \frac{\bar{\rho}}{r_i} \ln \bar{\rho} \right] \end{aligned} \right\} \quad (3.16)$$

Equation 3.16 is preferred because the chemical potential expression of Sanchez (1980) contains some errors.

This chemical potential expression is then used to find the binodal (equation 3.4), spinodal (equation 3.5), and the mixture critical point (equation 3.6). An efficient routine based on a graphical representation of the chemical potential as a function of composition has been proposed for solving binodal compositions [Lacombe & Sanchez, 1976].

### 3.2 Sanchez-Lacombe (SL) Modeling of Experimental Systems

Prior to application of the Sanchez-Lacombe (SL) lattice fluid theory to experimental systems, an analysis of the dimensionless parameters is presented. Cloud-point data for the binary systems, atactic polypropylene/propane and isotactic polypropylene/propane will then be modeled. An extension of the modeling to the

ternary system, atactic polypropylene/propane/1-propanol, by a pseudo-binary approach will also be presented.

### 3.2.1 Dimensionless Parameter Analysis

The generalized two dimensionless parameter theory is used to model some of the experimental data of Chapter 2 as it provides a very flexible approach. However, the two dimensionless parameter theory introduces two issues. First, a unique value of  $\zeta$  and  $\delta$  can not be found to describe the experimental mixture critical points over the entire temperature and pressure range studied. In other words, a solution set, a line in  $\zeta$ - $\delta$  space, exists which describes the experimental mixture critical point. Second, a systematic way of selecting a value of  $\zeta$  and  $\delta$  from the solution set must be developed.

The procedure for obtaining the solution set is presented and then the general features of the solution set are discussed. Criteria for selecting systematic values of  $\zeta$  and  $\delta$  from the solution set based on the change of the solution set with pressure are proposed.

#### 3.2.1.1 Solution Set

The procedure to determine the set of values of the dimensionless parameters which describe incipient phase separation is as follows

- A. Obtain the characteristic parameters for the pure components. If not available in the literature, they must be obtained by fitting PVT data to the equation of state or, for polymers without known PVT data, from a procedure based on a corresponding state approach [Sanchez & Lacombe, 1977].
- B. Select values for the dimensionless energy and volume parameters,  $\zeta$  and  $\delta$ .
- C. Calculate the characteristic parameters,  $T^*$ ,  $P^*$ , and  $\rho^*$ , for all mixture compositions.

- D. Determine  $\tilde{\rho}$  by solving the equation of state (equation 3.7) for all mixture compositions at the appropriate T and P. The precision to which  $\tilde{\rho}$  must be determined is at least 1 part in  $10^{10}$ . This precision is required to insure stability of future numerical derivative calculations
- E. Calculate the chemical potential for each species at all mixture compositions using equation 3.16.
- F. Numerically evaluate the stability criterion (equation 3.3). If the stability criterion is violated at any composition, phase separation occurs at that T and P with the selected values of  $\zeta$  and  $\delta$ . If the stability criterion is satisfied for all compositions, complete miscibility occurs at that T and P with the selected values of  $\zeta$  and  $\delta$ .
- G. Adjust  $\zeta$  and  $\delta$  and repeat the procedure starting at B until a solution set of  $\zeta$  and  $\delta$  is found that describes a system which is on the verge of violating the stability criterion at a single composition, the mixture critical point. An efficient routine for determining the solution set is to fix one of the dimensionless parameters while adjusting the other. Once a solution is found, step the value of the fixed dimensionless parameter and then repeat the procedure.

A qualitative example of a solution set that describes values of  $\zeta$  and  $\delta$  which predict incipient instability of the system at a given T and P is shown in Figure 3.1 as a line. The regions of  $\zeta$  and  $\delta$  which predict phase separation and complete miscibility are also indicated in Figure 3.1. As can be seen from Figure 3.1, the solution set is not singular because two solutions to one of the dimensionless parameters can occur at a fixed value of the other dimensionless parameter. The linear branch of the solution set represents points where the chemical potential function becomes very flat with respect to composition. Small changes in either  $\zeta$  and  $\delta$ , result in enormous changes in the composition at which the stability criterion is violated. Therefore, solutions along this

linear branch may not properly describe experimental observations. Criteria for selecting a single value for  $\zeta$  and  $\delta$  are developed in the next section.

### 3.2.1.2 Minimum $\delta$ Approach

The value of  $\zeta$  and  $\delta$  that is selected from the solution set must satisfy the following criteria:

1. The value of  $\zeta$  and  $\delta$  must predict a system at the point of incipient instability at the experimental cloud-point temperature and pressure determined for compositions close to the critical composition.
2. Upon decreasing pressure at constant temperature, the value of  $\zeta$  and  $\delta$  must predict phase separation.
3. Upon increasing pressure at constant temperature, the value of  $\zeta$  and  $\delta$  must predict complete miscibility.

Figure 3.2 shows what happens to the solution set as a function of pressure. The solution set describing incipient phase separation at the experimental cloud-point pressures and temperatures is labelled  $P=P_{\text{exp}}$  in Figure 3.2. At  $P>P_{\text{exp}}$ , the solution set describing incipient phase separation shifts to the left and slightly upward while for  $P<P_{\text{exp}}$ , the solution set shifts to the right and slightly downward. The value of  $\zeta$  and  $\delta$  denoted by point A in Figure 3.2 lies on the solution set for  $P_{\text{exp}}$ . If the  $\zeta$  and  $\delta$  value at point A are used to describe the phase behavior of the system at higher and lower pressures, the reverse trend of the phase behavior from that observed experimentally is predicted. For  $P>P_{\text{exp}}$ , point A is outside the miscibility region while for  $P<P_{\text{exp}}$ , point A is in the miscibility region of the  $\zeta$ - $\delta$  solution set. Therefore, solutions along this linear branch of the solution sets are unable to predict the pressure dependence of the phase behavior.

This is probably related to the flatness of the chemical potential with respect to composition in that region of  $\zeta$ - $\delta$  values (Section 3.2.1.1).

The value of  $\zeta$  and  $\delta$  denoted as MD in Figure 3.2 lies on the solution set for  $P=P_{\text{exp}}$  at the minimum value of  $\delta$ . Solutions at MD accurately represent the experimental phase behavior observations. For  $P>P_{\text{exp}}$ , point MD is inside the miscibility region while for  $P<P_{\text{exp}}$  point MD is outside the miscibility region of the  $\zeta$ - $\delta$  solution set. The selection of the point at minimum  $\delta$  is arbitrary but qualitatively predicts the pressure dependence of the phase behavior and provides a consistent location on the solution set. Locating the value of  $\zeta$  and  $\delta$  at minimum  $\delta$  and subsequent modeling with this value of  $\zeta$  and  $\delta$  will be referred to as the minimum  $\delta$  approach. Currently, elimination of the adjustable  $\delta$  parameter is favored [Sanchez, 1996] but without this adjustability, modeling of the experimental data would not be possible over the entire temperature window when using the SL theory.

### 3.2.2 Binary Systems

The modeling of binary systems with the two dimensionless parameter theory of Sanchez-Lacombe is presented. First, modeling of the cloud-point isopleths for the atactic polypropylene/propane system is presented. Binodals and spinodals for the isotactic polypropylene/propane system are calculated after modeling the critical cloud-point isopleths. The calculated binodals are compared to the experimental cloud-point isotherms.

#### 3.2.2.1 Sanchez-Lacombe Equation of State Parameters

Table 3.3 lists the characteristic parameters for the Sanchez-Lacombe equation of state for propane and isotactic polypropylene. The characteristic parameters for atactic polypropylene are not available in the literature because PVT data for this polymer is

unavailable. Therefore, when modeling the phase behavior of atactic polypropylene systems, the characteristic parameters for isotactic polypropylene are used.

Table 3.3 Sanchez-Lacombe Equation of State Parameters

Fluid	$T^*$ (K)	$P^*$ (MPa)	$\rho^*$ (kg/m <sup>3</sup> )
propane <sup>1</sup>	371.0	314.0	690.0
isotactic polypropylene (iPP) <sup>2</sup>	771.0	281.0	852.0

1 - Sanchez & Lacombe, 1978

2 - Rodgers & Sanchez, 1993

### 3.2.2.2 Cloud-Point Isopleths for Atactic Polypropylene/Propane

The predicted lower critical solution temperatures (LCST) for the atactic polypropylene/propane system are shown in Figure 3.3 for no adjustment to the dimensionless energy and volume parameters ( $\delta=0.0$ ,  $\zeta=1.0$ ) in the SL model. The model prediction is compared to the experimental LCST in Figure 3.3. The lower critical end point (LCEP) of the system is predicted with reasonable accuracy. The experimental LCEP is 279 K while the LCEP predicted by the SL model is 271 K. However, the pressure dependence of the LCST is not adequately described and temperature dependent adjustment of the dimensionless parameters is necessary.

For six experimental cloud-point temperatures and pressures for the atactic polypropylene/propane system, the  $\delta$ - $\zeta$  solution sets determined from the procedure outlined in Section 3.2.1.1 are shown in Figure 3.4. Values from the  $\delta$ - $\zeta$  solution sets corresponding to minimum  $\delta$  are selected using the criteria proposed in Section 3.2.1.2. The temperature dependence of  $\delta$  and  $\zeta$  at minimum  $\delta$  are shown in Figure 3.5.  $\delta$ , the

dimensionless volume parameter, is a linear function of temperature while  $\zeta$ , the dimensionless energy parameter, decreases with increasing temperature and then reaches a constant value. Modeling the LCST after fitting appropriate temperature dependent expressions for  $\delta$  and  $\zeta$  results in a good agreement between model prediction and experimental results as shown in Figure 3.6. The quality of the fit could be improved by modeling more experimental points and by improving the equational forms used to describe the temperature dependence of  $\zeta$  and  $\delta$ . At temperatures as low as 200K, there is no prediction of an upper critical solution temperature (UCST) in this system. This is in agreement with the expected behavior for chemically similar systems such as atactic polypropylene/propane. Additionally, the model predicts miscibility as the pressure is increased above the experimental cloud-point pressures in the temperature range of 200 to 500 K at pressures up to 1000 bar.

Previous research on nonpolar supercritical fluid/polyethylene solutions has revealed only the need for a temperature dependent adjustment of the dimensionless volume parameter [Hasch et al., 1992; Hasch et al., 1993b]. However, this is not the case for the atactic polypropylene/propane system as can be seen from the  $\delta$ - $\zeta$  solution sets shown in Figure 3.4. If the dimensionless energy parameter is left unadjusted, fits to the data are not possible at temperatures above 387K. An alternate approach is to fix the dimensionless volume parameter and vary the dimensionless energy parameter. This approach is less successful as fits to the cloud-point isopleth data are not possible at temperatures above 310K. In contrast to previous studies on nonpolar supercritical fluid/polyethylene systems, these results suggest that in order to fit the cloud-point isopleth of the aPP/propane system temperature dependent adjustment of both dimensionless parameters is necessary.

### 3.2.2.3 Cloud-Point Isotherms for Isotactic Polypropylene/Propane

$\delta$ - $\zeta$  solutions sets required to model critical cloud-point isopleths for the iPP1/propane and iPP2/propane systems were determined and the minimum  $\delta$  values obtained. Values of  $\delta$  and  $\zeta$  at minimum  $\delta$  are shown in Figures 3.7 and 3.8 for iPP1/propane and iPP2/propane, respectively. With the values of  $\delta$  and  $\zeta$  at minimum  $\delta$ , the binodal and spinodal curves at different temperatures were calculated by using Equations 3.4 and 3.5. Figure 3.9 compares the cloud-point isotherms for the iPP1/propane with model predictions at three temperatures, 135°C, 145°C, and 155°C. Figure 3.10 does the same comparison for the iPP2/propane system. The binodal does not match the cloud-point isotherms in either the iPP1/propane and iPP2/propane systems and is the result of polymer polydispersity [Koningsveld & Staverman, 1968a,b].

### 3.2.3 Ternary Systems

The modeling of a ternary system introduces additional complexity as compared to a binary system. The addition of a third component requires that four additional cross-terms be estimated by mixing rules. In total, six fitting parameters exist for the ternary mixture as compared to two fitting parameters for binary systems. An alternative approach is to model the ternary system as a pseudo-binary system [Kiran et al., 1993].

#### 3.2.3.1 Pseudo-Binary Approach

This approach requires the formation of a pseudo-solvent whose characteristic parameters are determined from the mixing rules defined in equations 3.15a-c and without adjustment to the dimensionless parameters. Characteristic parameters of the pseudo-solvent depend on the solvent mixture composition due to the mixing rule dependence on volume fraction. The pseudo-solvent/polymer phase behavior can then be modeled as a binary system with the procedures previously discussed (Sections 3.2.1.1 and 3.2.1.2).



### 3.2.3.2 Sanchez-Lacombe Equation of State Parameters

Table 3.4 shows the equation of state parameters of the pseudo-solvent for different propane/1-propanol mixtures. The pure 1-propanol equation of state parameters were obtained from the literature and come from a slightly modified expression for the equation of state as compared to the SL EOS (equation 3.7) [Panayiotou & Sanchez, 1991]. The SL EOS parameters for 1-propanol are available in the literature [Sanchez & Lacombe, 1976].

Table 3.4 Sanchez-Lacombe Equation of State Parameters for Propane/1-Propanol Mixtures

(wt. % 1-propanol)	T* (K)	P* (MPa)	$\rho^*$ (kg/m <sup>3</sup> )
0.00	371.0	314.0	690.0
16.8	383.8	315.4	713.5
31.0	395.8	316.4	734.6
47.3	411.2	317.6	760.4
65.4	430.8	318.6	791.3
100	478.0	320.0	858.0

### 3.2.3.3 Cloud-Point Isoleths for Atactic Polypropylene/Propane/1-Propanol

$\delta$ - $\zeta$  solutions sets required to model critical cloud-point isopleths for the different ternary systems were determined by modeling the pseudo solvent/aPP binary system. The  $\delta$ - $\zeta$  solution sets at several temperatures for the various ternary systems can be found in Figures 3.11 to 3.14. As the 1-propanol content is increased, the  $\delta$ - $\zeta$  solution sets become less well-behaved to a point where solution sets cannot be obtained. This is probably a result of the inadequacy of forming a pseudo-solvent without parameter adjustment or that modeling of UCST is quite difficult in the theoretical framework [Sanchez & Lacombe, 1978]. The values of  $\zeta$  and  $\delta$  at minimum  $\delta$  for all the ternary systems are shown in

Figures 3.15 and 3.16, respectively. The linear trend of  $\delta$  with temperature breaks down at higher 1-propanol content. The temperature dependence of  $\zeta$  becomes more complex as the content of 1-propanol is increased. However, the value of  $\zeta$  does increase as the content of 1-propanol is increased suggesting that the interaction energy adjustment is larger for more polar solvent mixtures. An additional problem is the use of the EOS parameters for 1-propanol from a modified equation of state that attempts to account for hydrogen bonding [Panayiotou & Sanchez, 1991]. It is doubtful that the use of the appropriate EOS parameters for 1-propanol [Sanchez & Lacombe, 1976] would result in simple temperature trends of  $\delta$  and  $\zeta$ . Additionally, temperature dependent adjustment of both dimensionless parameters will probably still be required as is the case for binary systems studied here (Sections 3.2.2.2 and 3.2.2.3).

### 3.3 Conclusions

The modeling of phase equilibria for nonpolar supercritical polymer solutions can be achieved with the Sanchez-Lacombe Lattice Fluid theory. For the aPP/propane system, modeling of the data requires the use of two dimensionless adjustment parameters. Previous research suggested that only one temperature dependent adjustable parameter, the dimensionless volume term,  $\delta$ , is required for nonpolar supercritical polymer solutions [Hasch et al., 1992; Hasch et al., 1993b]. The method proposed here, called the minimum  $\delta$  approach, is to select the combination of  $\zeta$  and  $\delta$  occurring at minimum  $\delta$  from the entire solution set. This combination of  $\zeta$  and  $\delta$  gives the best agreement with the pressure dependence of the phase transitions. For solutions obtained by the minimum  $\delta$  approach for the atactic polypropylene/propane system,  $\delta$  obeys a linear temperature dependence, while  $\zeta$  decreases with increasing temperature and then reaches a constant value at higher temperatures. Binodals for two different isotactic polypropylene fractions in supercritical propane were calculated and compared to

experimental cloud-point isotherms. The disagreement between experiment and theory is probably a result of the polymer polydispersity [Koningsveld & Staverman, 1968a,b].

The modeling of ternary systems by a pseudo-binary approach was attempted for the aPP/propane/1-propanol system. Solutions of the LF equations can be obtained but the temperature dependence of  $\delta$  and  $\zeta$  begin to deviate from the simple behavior found in the aPP/propane system. The deviation becomes more pronounced as the 1-propanol content increases and could be due to several factors. The first factor is the failure to adjust the dimensionless parameters to determine the characteristic parameters of the pseudo solvent. Modeling of the phase behavior of the propane/1-propanol system could provide insights on how to adjust these parameters [Xiong & Kiran, 1994]. The second factor is the modeling of LCST behavior at low 1-propanol content and U-LCST behavior at higher 1-propanol content.  $\delta$  and  $\zeta$  at minimum  $\delta$  may be simple functions of temperature when describing LCST behavior only and may become more complex in order to predict U-LCST behavior. Finally, the dependency of  $\delta$  and  $\zeta$  was selected to be temperature dependent when in fact such parameters may also be pressure dependent.

In all the binary and ternary systems studied, the values of  $\zeta$  selected by the minimum  $\delta$  approach are significantly greater than unity. In most liquid-liquid mixtures, adjustment of  $\zeta$  to values below unity is required to obtain agreement between model predictions and experimental results [Rowlinson & Swinton, 1982]. The origins for the different adjustments required in supercritical fluid/polymer systems versus most liquid-liquid systems are unknown but may be related to the high pressures, the polymeric nature of one of the components, and/or densities in supercritical systems which are lower than conventional liquids.

Further tests of thermodynamic theories will require information in addition to the thermodynamic phase behavior of the system. Without further information, selection of adjustable parameters, dimensionless energy and volume, is arbitrary. Any adjustable parameter trends should also be regarded as arbitrary.

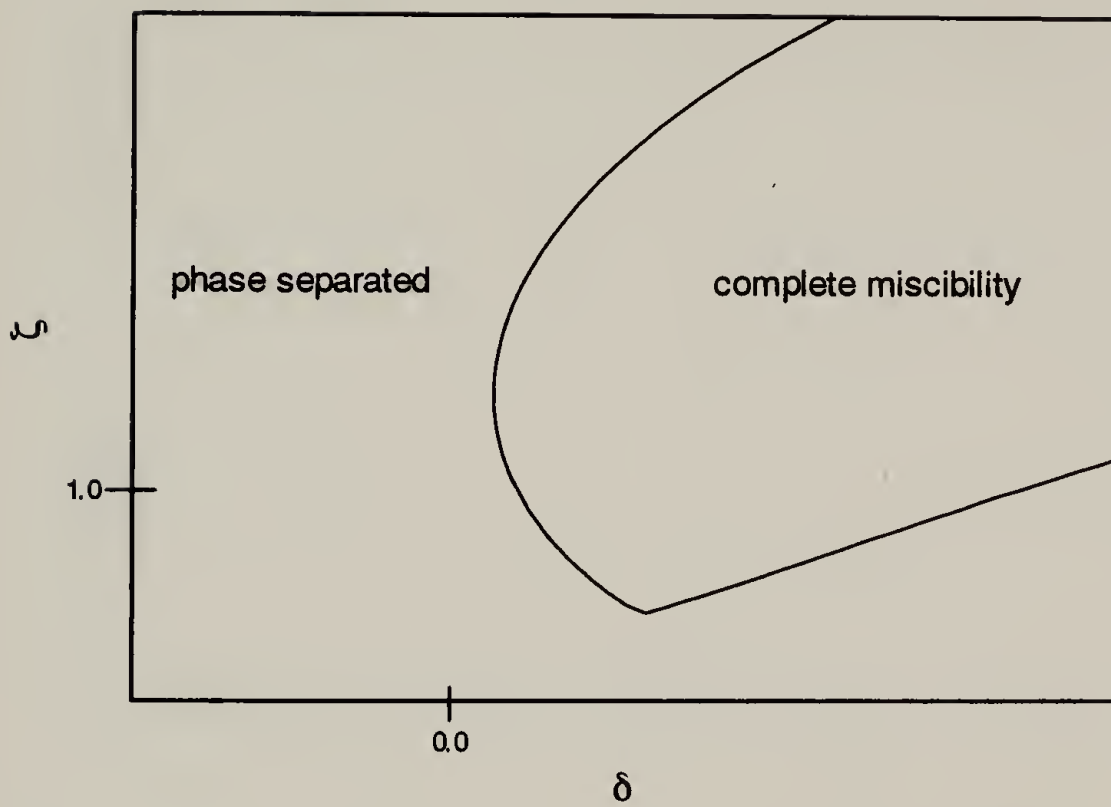


Figure 3.1 Qualitative  $\delta$ - $\zeta$  Solution Set

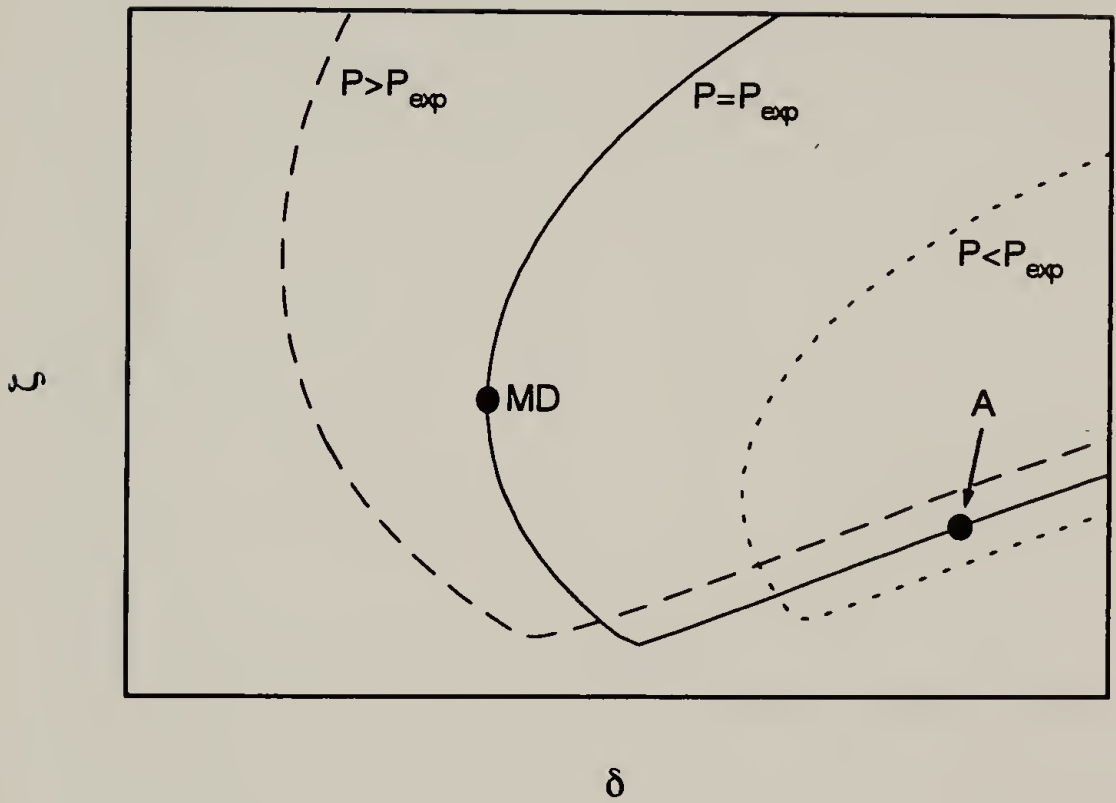


Figure 3.2 Pressure Dependence of  $\delta$ - $\zeta$  Solution Set (MD is the solution at Minimum  $\delta$  and point A represents another possible solution from the infinite set)

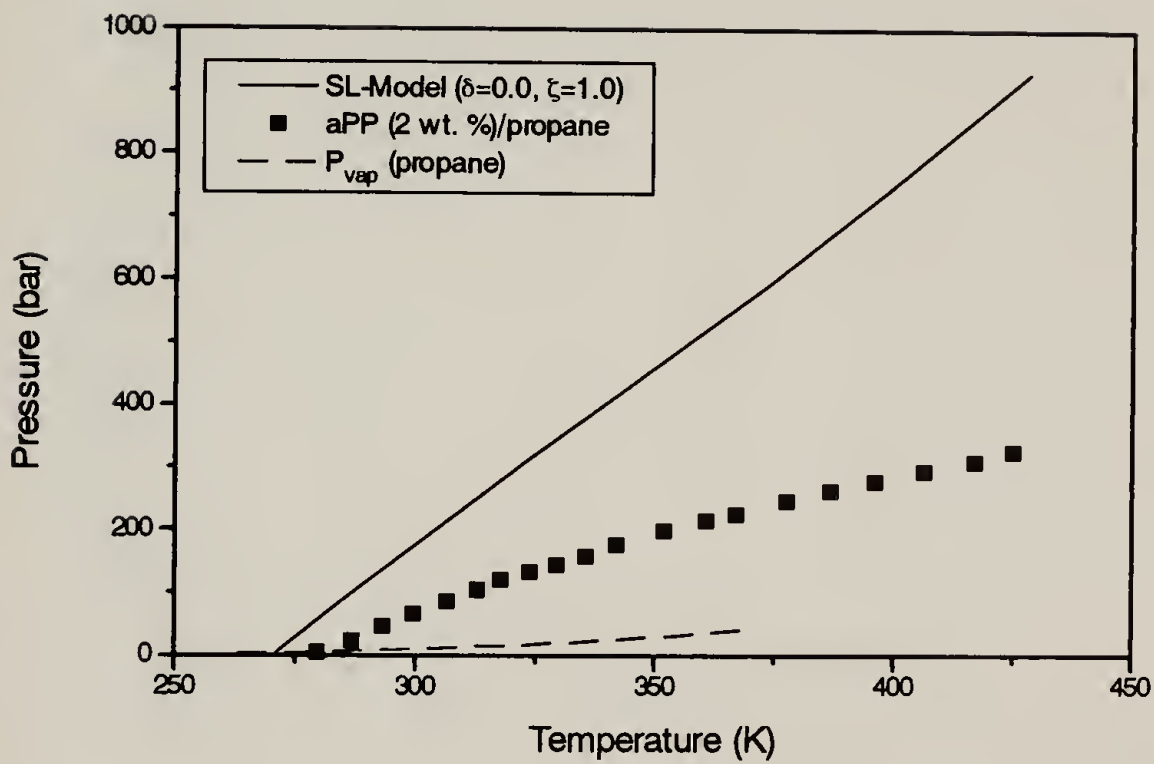


Figure 3.3 SL Model Prediction for No Parameter Adjustment ( $\delta=0.0, \zeta=1.0$ ) as Compared to the Experimental Cloud-Point Isopleth for the Atactic Polypropylene (aPP)/Propane System

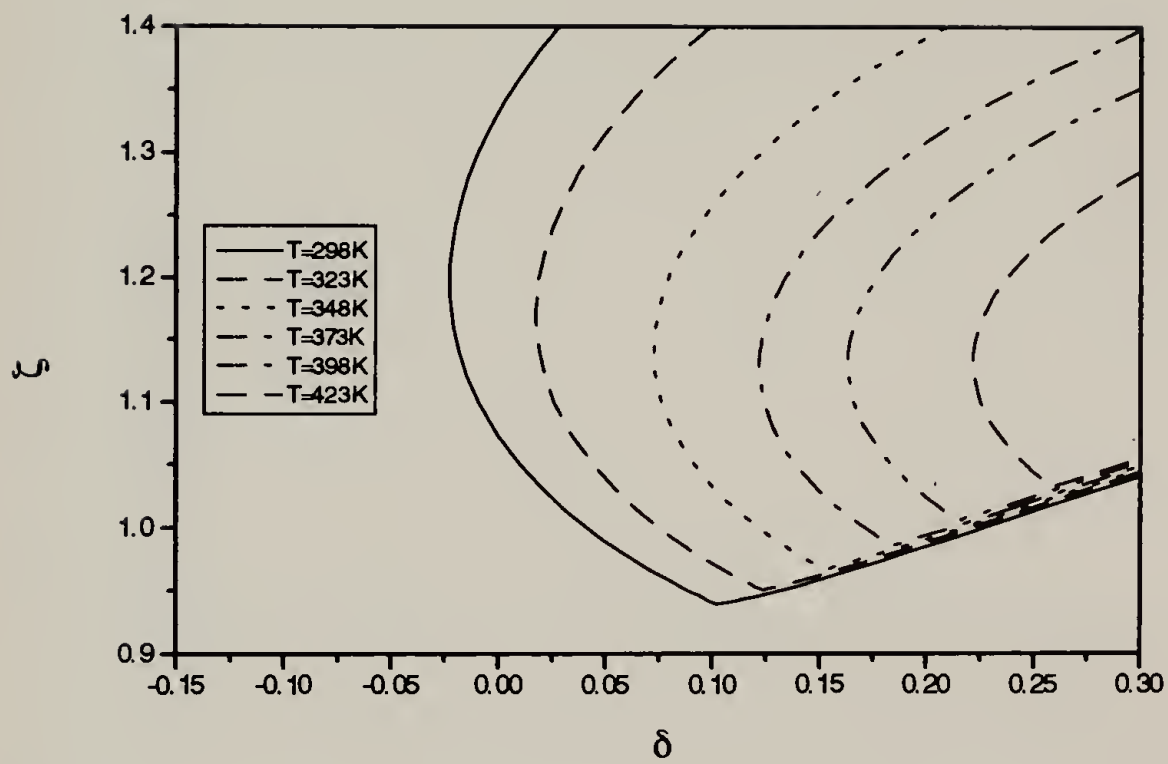


Figure 3.4  $\delta$ - $\zeta$  Solution Sets for Atactic Polypropylene/Propane

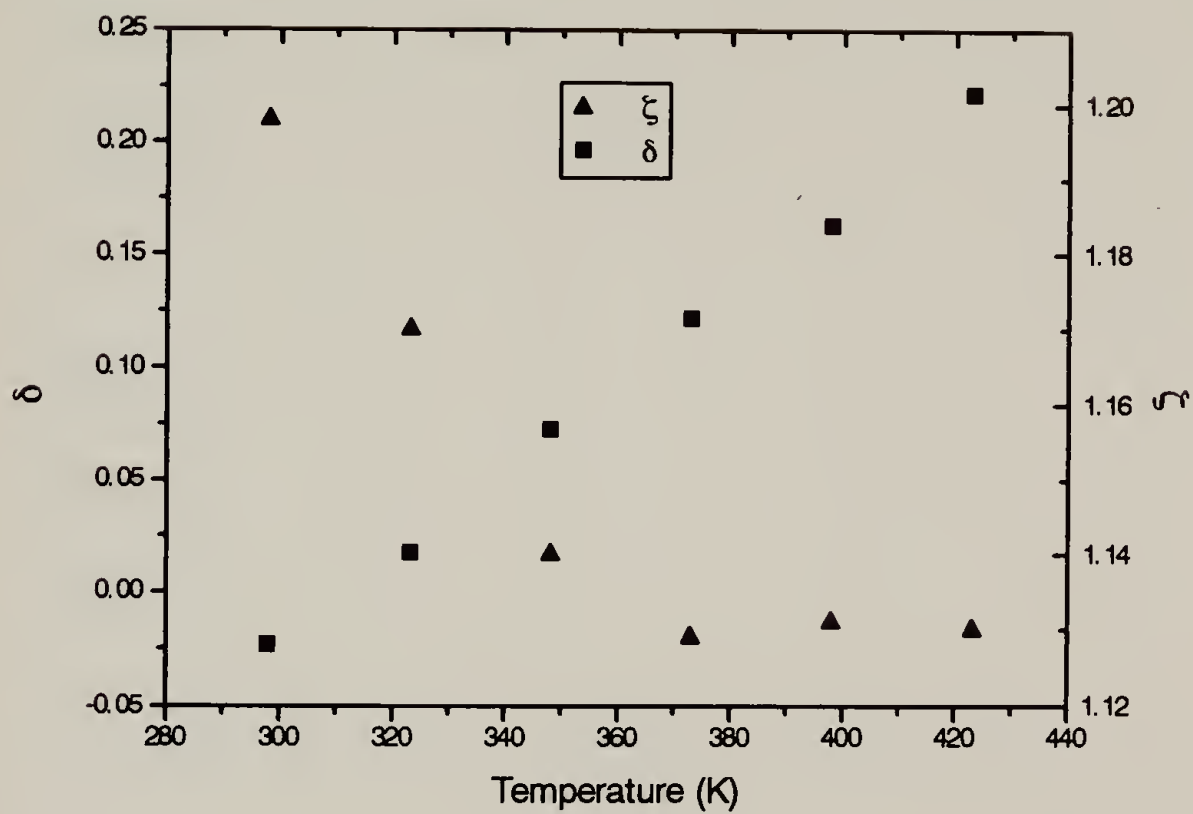


Figure 3.5  $\delta$ - $\zeta$  Solutions at Minimum  $\delta$  for Atactic Polypropylene/Propane



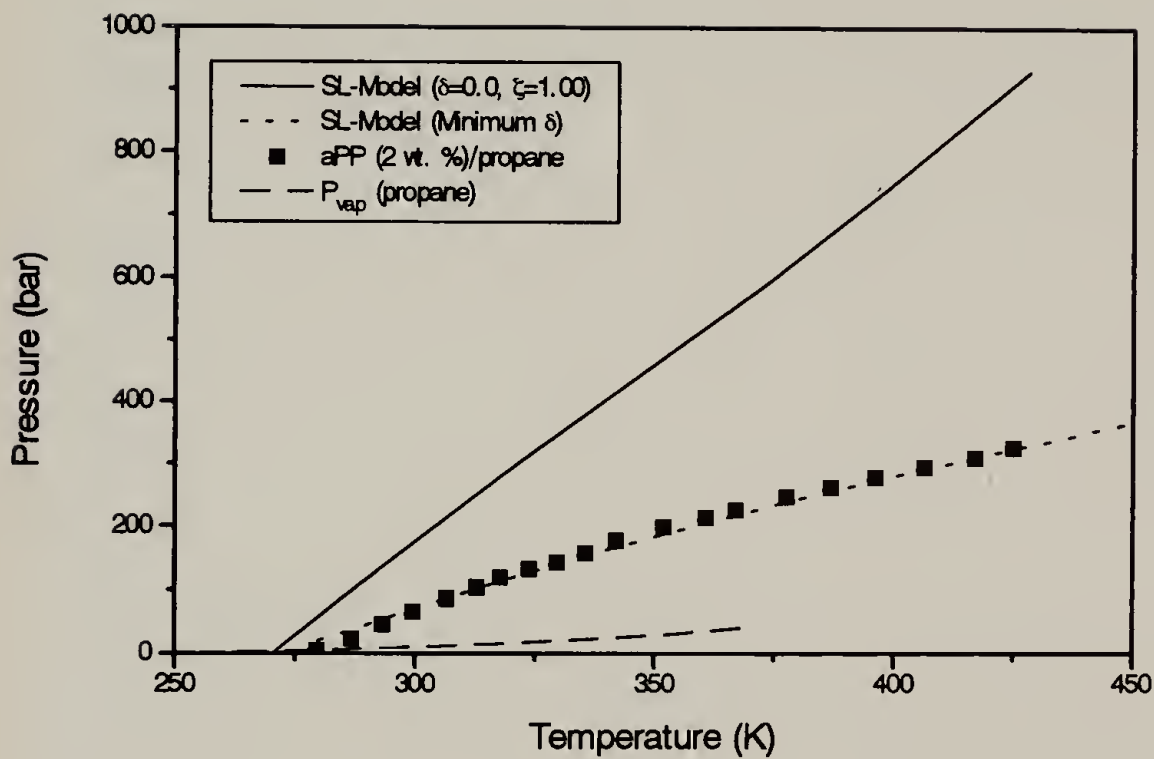


Figure 3.6 SL Model Prediction for No Parameter Adjustment ( $\delta=0.0, \zeta=1.0$ ) and Minimum  $\delta$  Approach as Compared to the Experimental Cloud-Point Isopleth for the Atactic Polypropylene (aPP)/Propane System

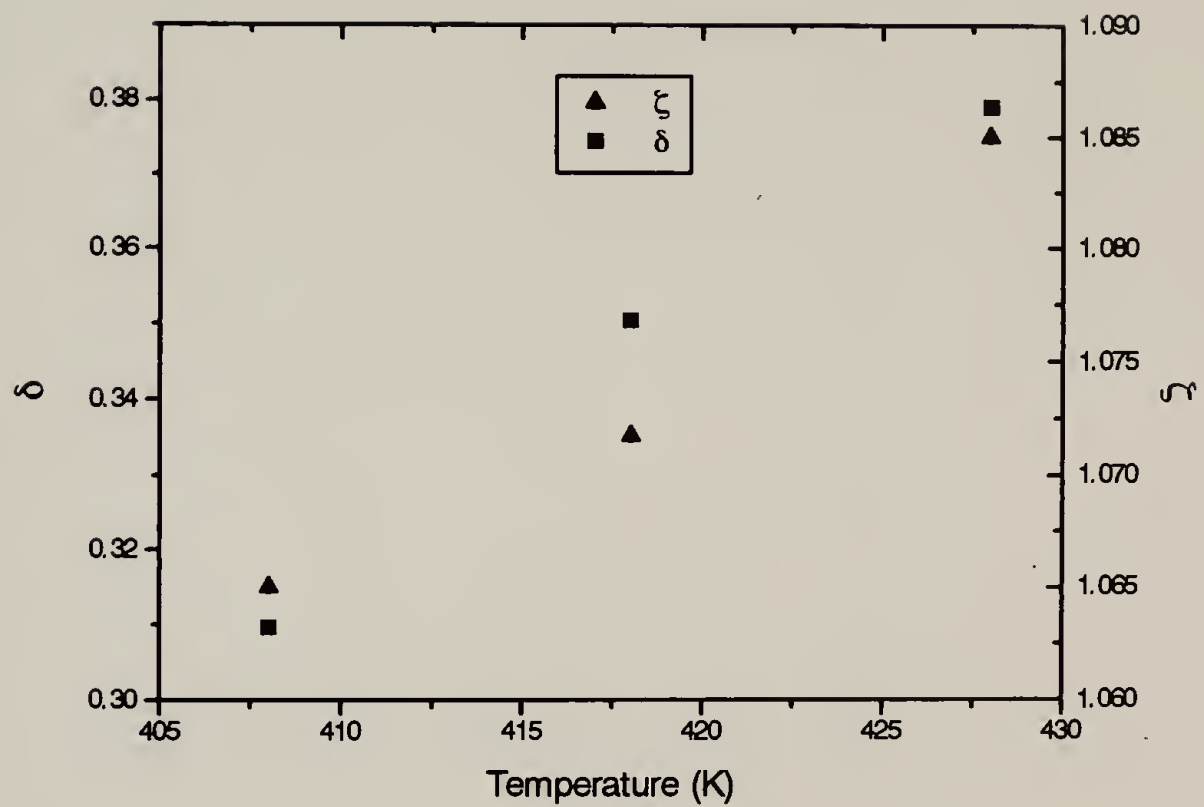


Figure 3.7  $\delta$ - $\xi$  Solutions at Minimum  $\delta$  for Isotactic Polypropylene(iPP1)/Propane

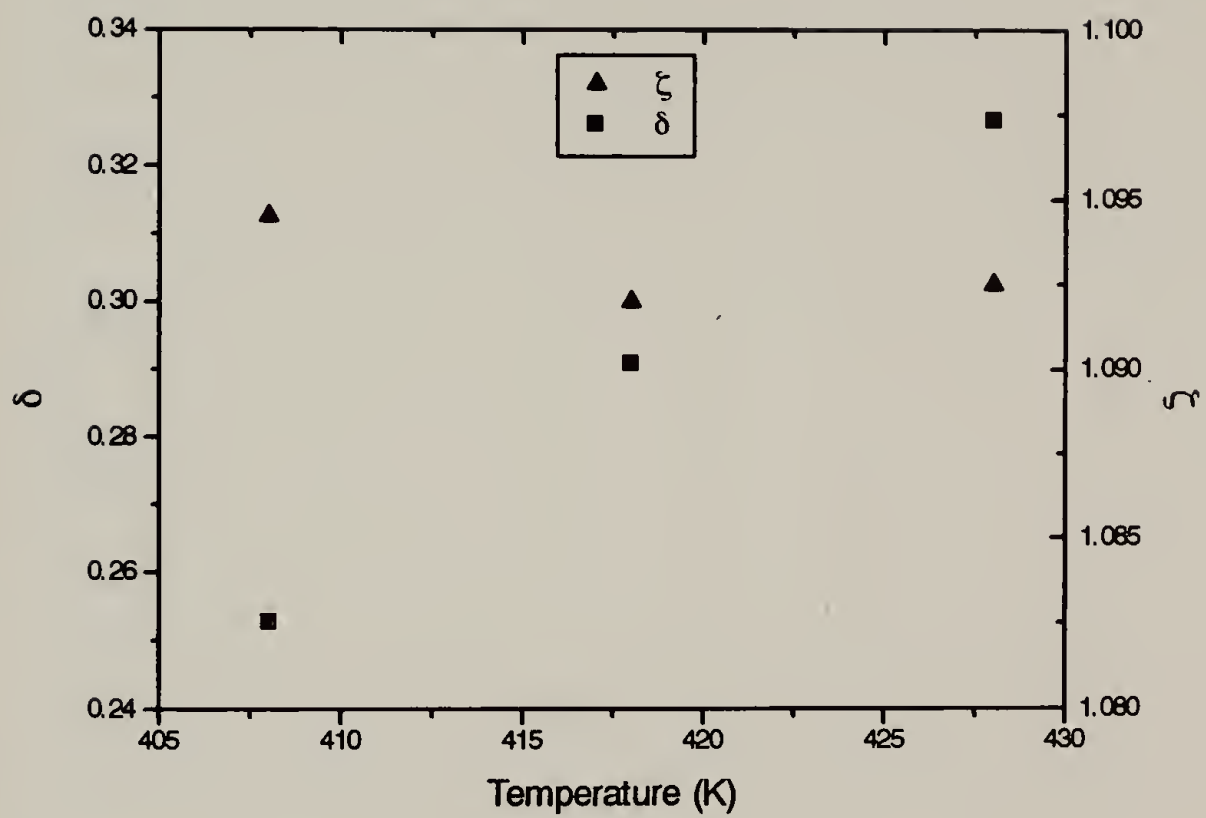


Figure 3.8  $\delta$ - $\zeta$  Solutions at Minimum  $\delta$  for Isotactic Polypropylene(iPP2)/Propane

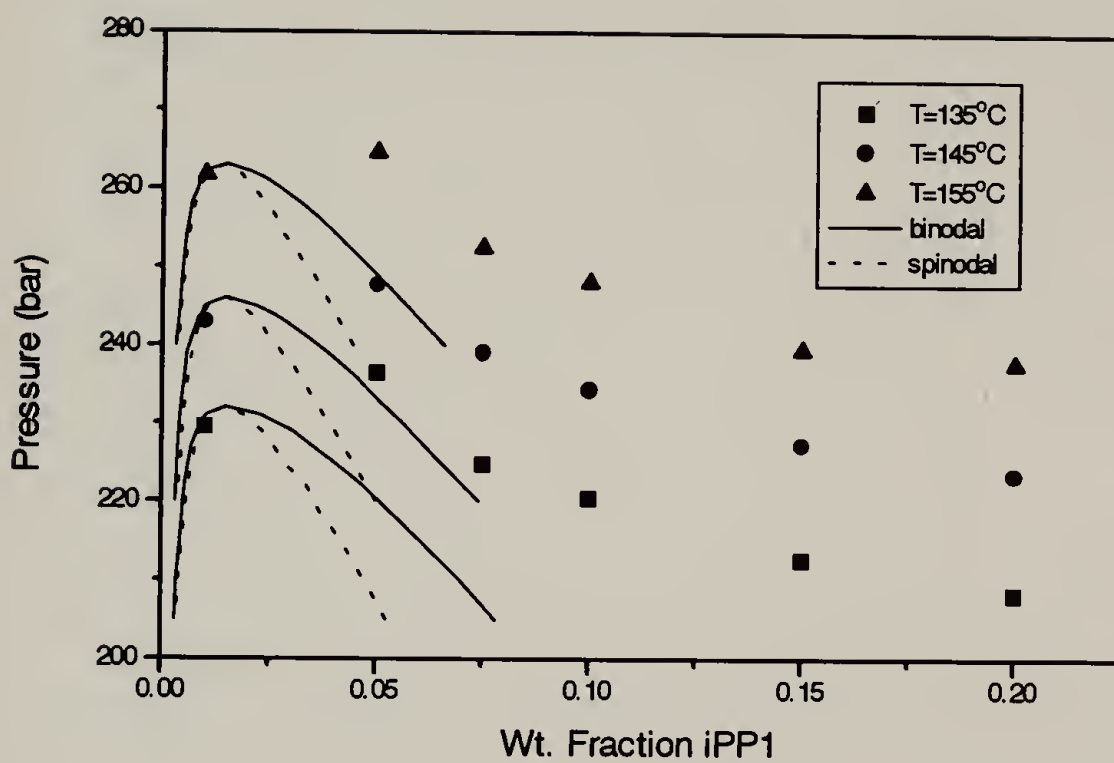


Figure 3.9 Calculated Binodals and Spinodals for the iPP1/Propane System Using the Minimum  $\delta$  Approach Compared to Experimental Cloud-Point Isotherms

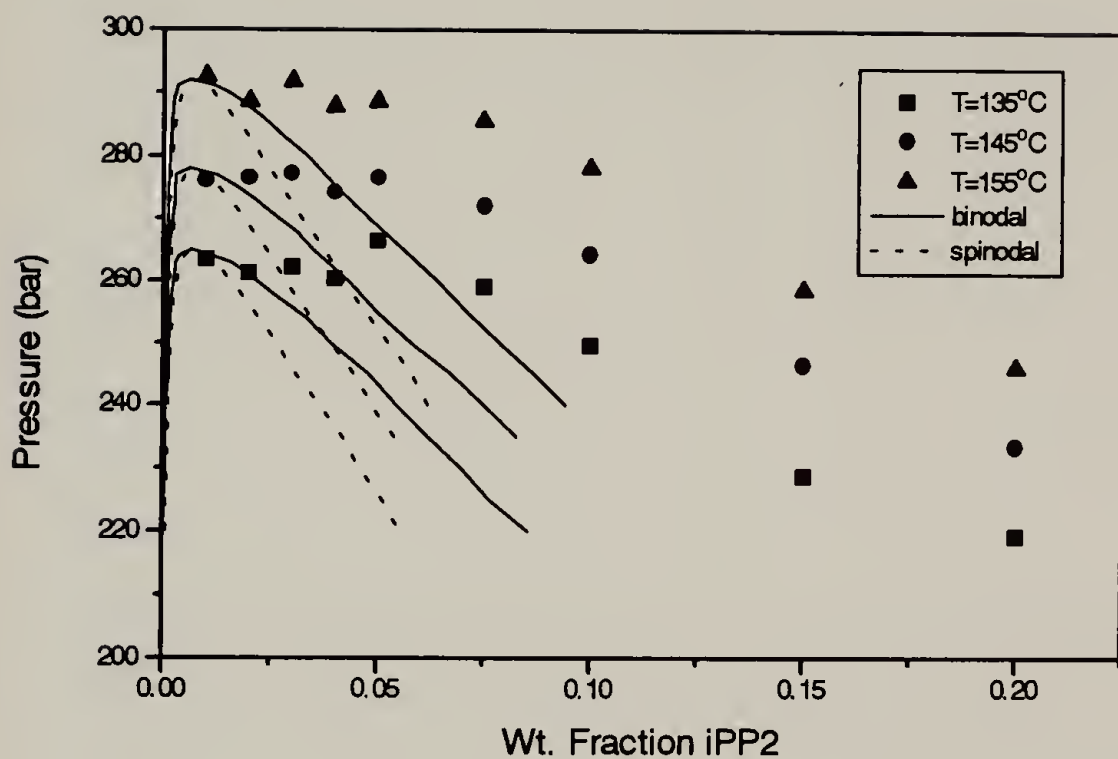


Figure 3.10 Calculated Binodals and Spinodals for the iPP2/Propane System Using the Minimum  $\delta$  Approach Compared to Experimental Cloud-Point Isotherms

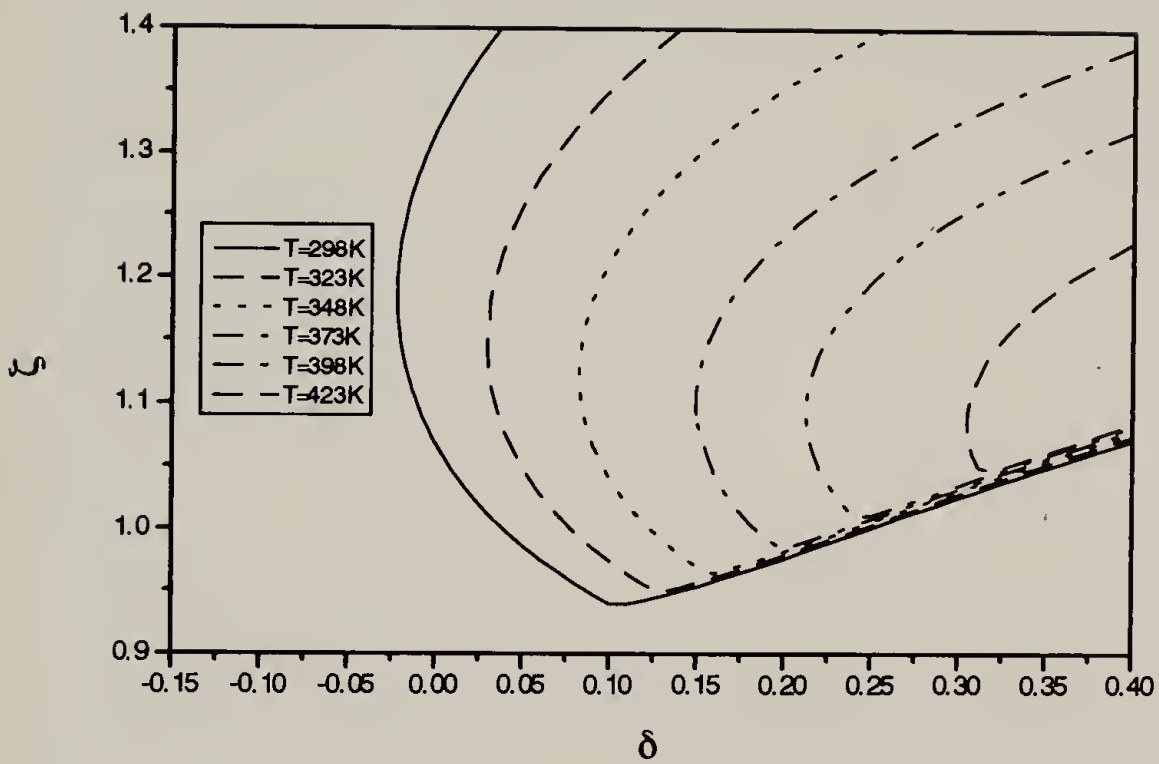


Figure 3.11  $\delta$ - $\zeta$  Solution Sets for Atactic Polypropylene/Propane/1-Propanol (16.8 wt. % 1-Propanol)

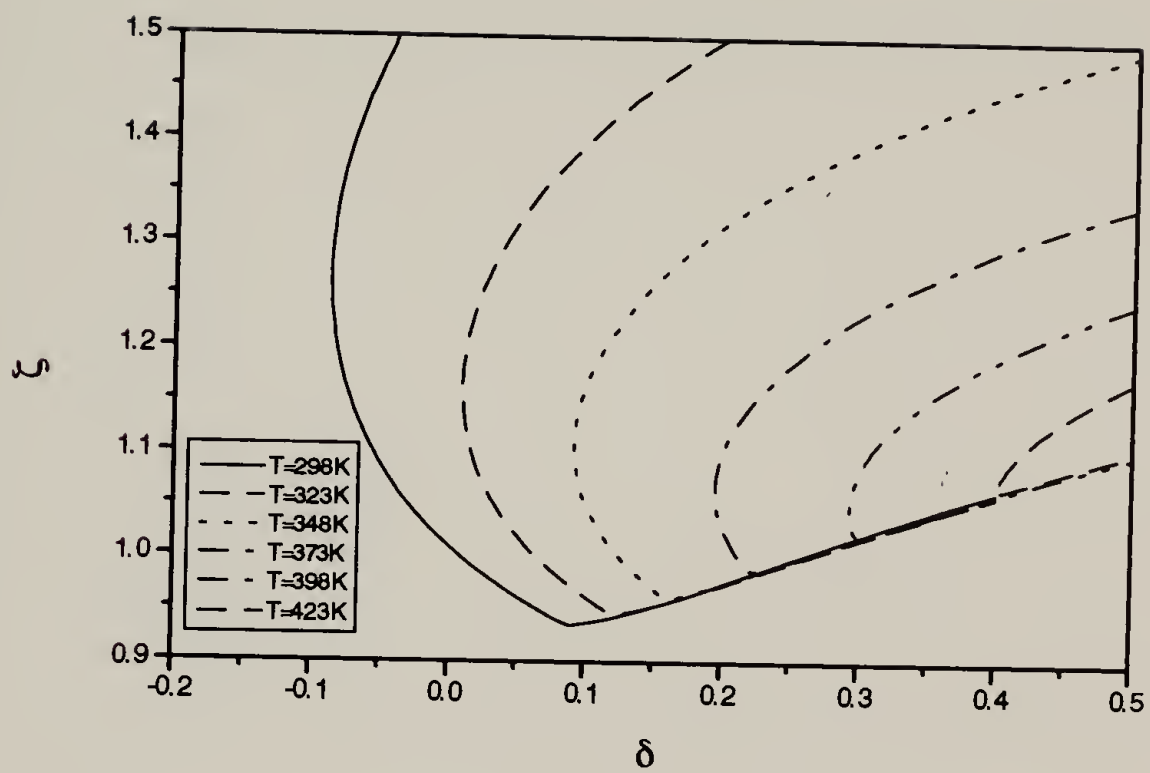


Figure 3.12  $\delta$ - $\zeta$  Solution Sets for Atactic Polypropylene/Propane/1-Propanol (31.0 wt. % 1-Propanol)

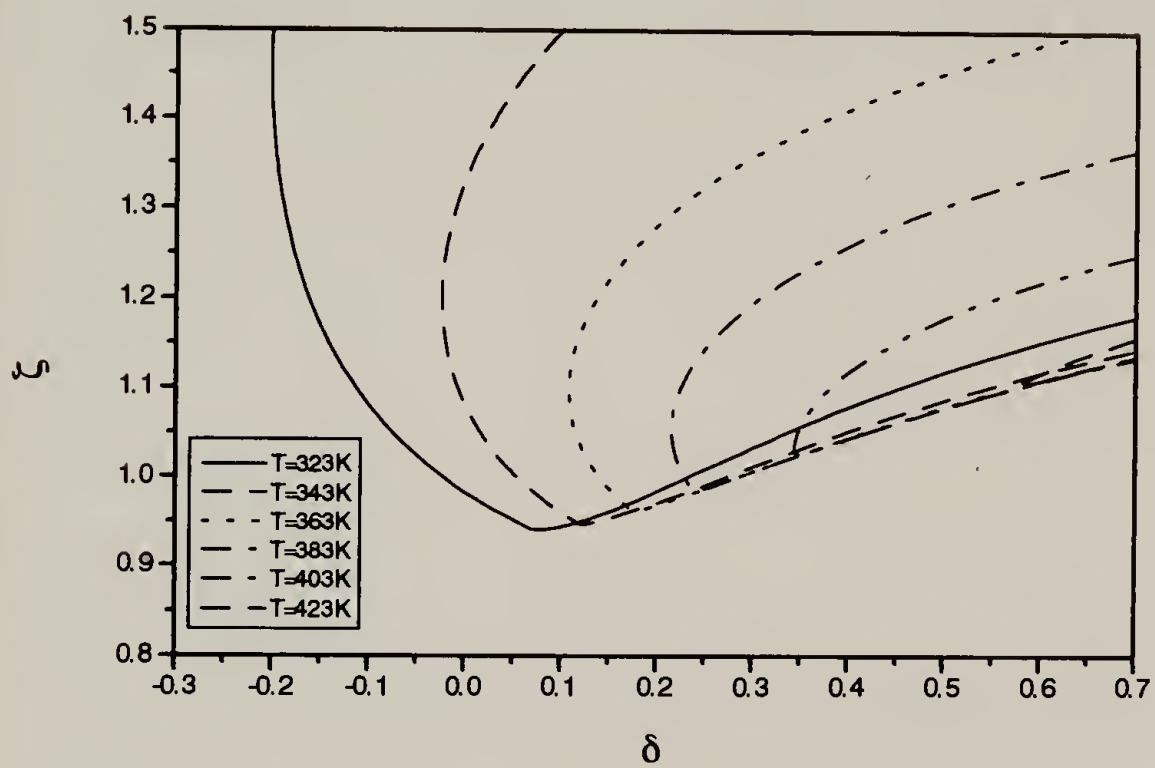


Figure 3.13  $\delta$ - $\xi$  Solution Sets for Atactic Polypropylene/Propane/1-Propanol (47.3 wt. % 1-Propanol)



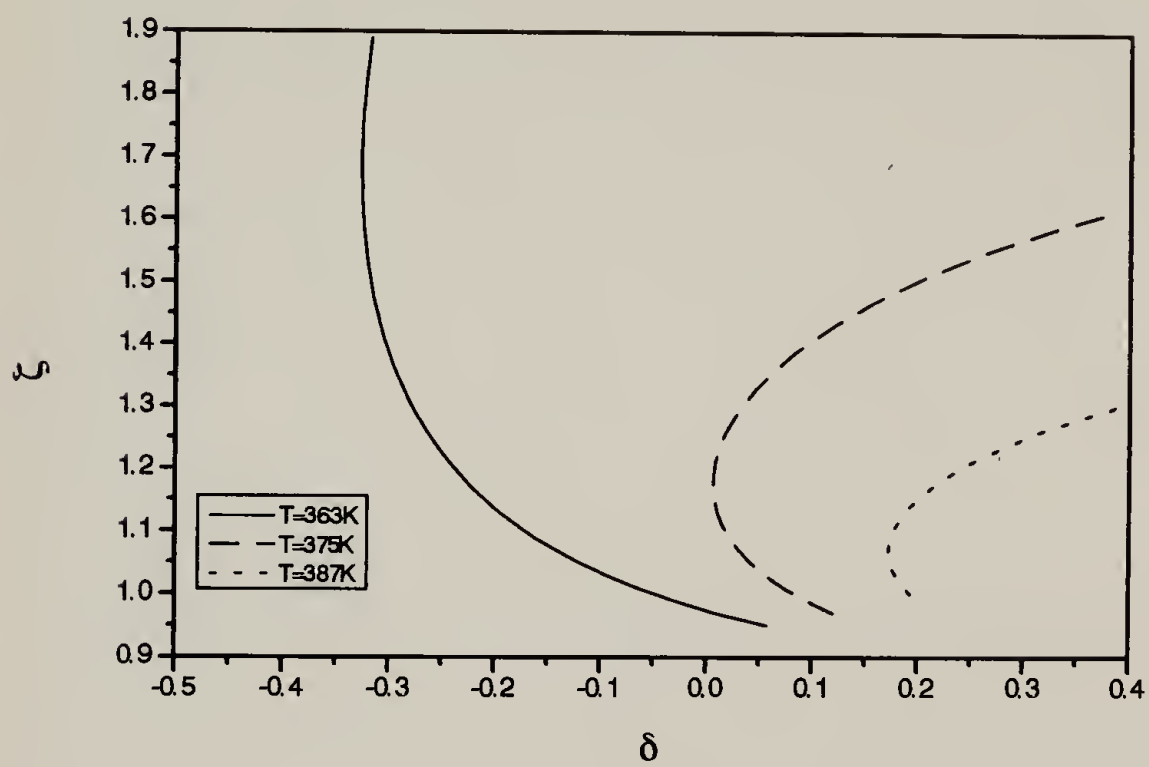


Figure 3.14  $\delta$ - $\zeta$  Solution Sets for Atactic Polypropylene/Propane/1-Propanol (65.4 wt. % 1-Propanol)

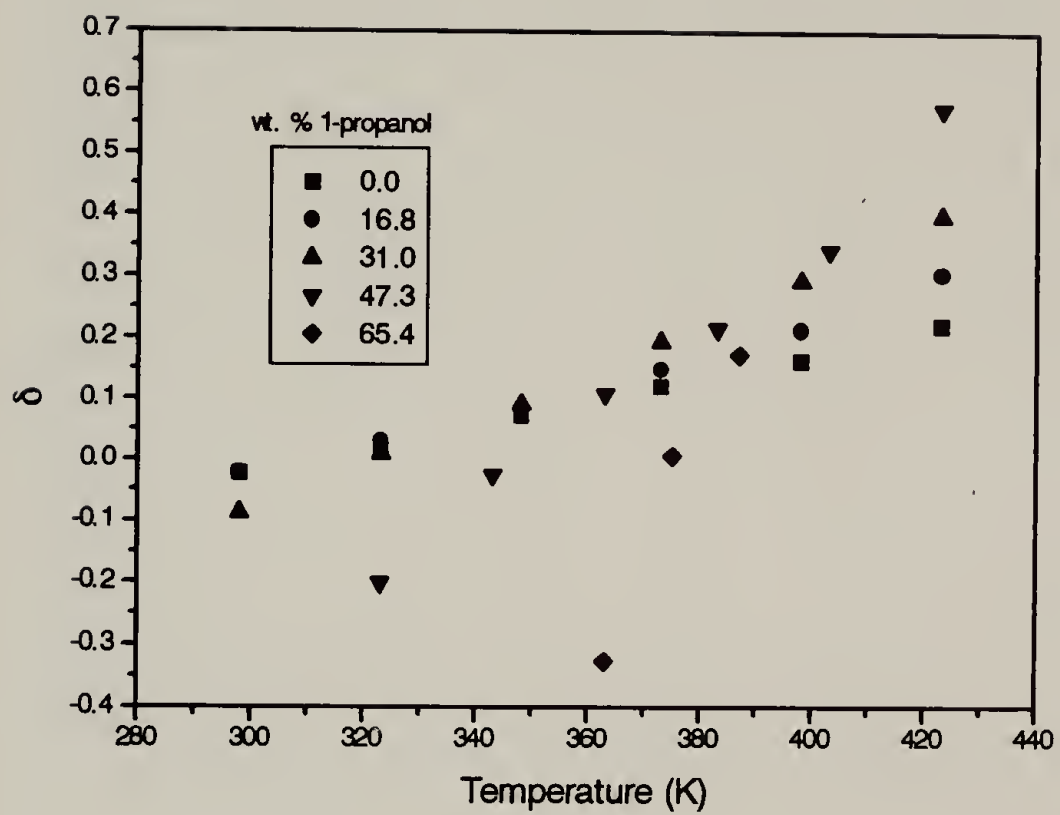


Figure 3.15  $\delta$  Solutions at Minimum  $\delta$  for Atactic Polypropylene/Propane/1-Propanol

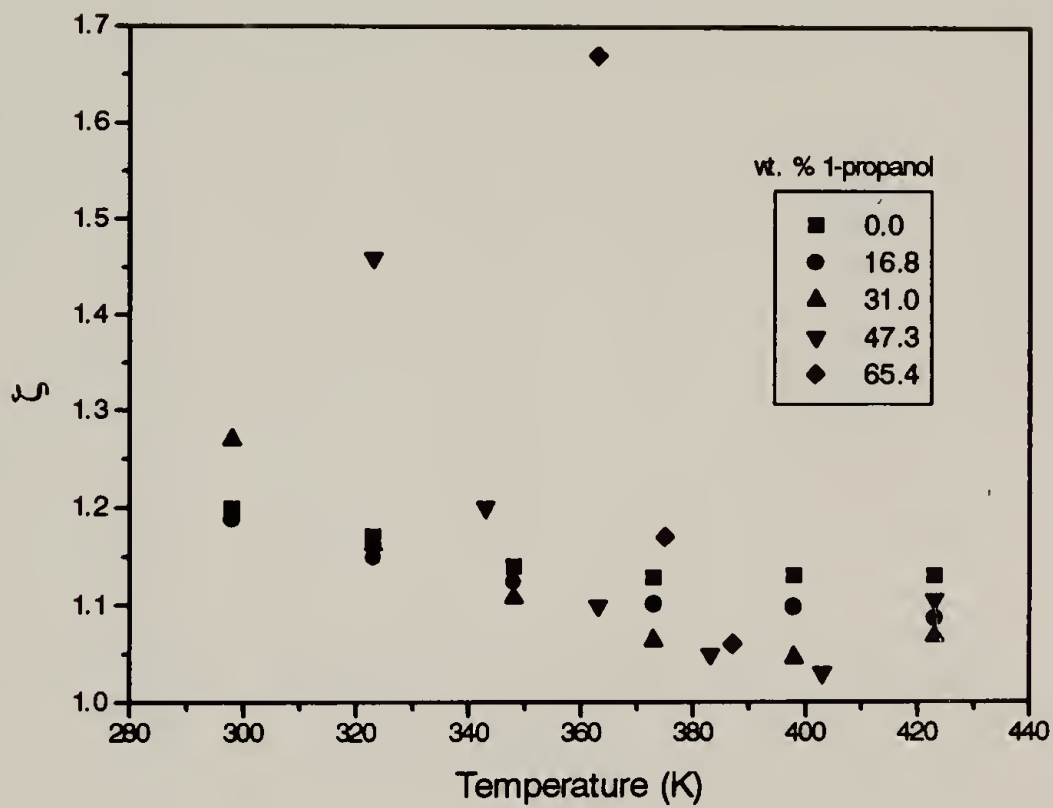


Figure 3.16  $\zeta$  Solutions at Minimum  $\delta$  for Atactic Polypropylene/Propane/1-Propanol

## REFERENCES

- Chen, S., and M. Radosz, "Density-Tuned Polyolefin Phase Equilibria. 1. Binary Solutions of Alternating Poly(ethylene-propylene) in Subcritical and Supercritical Propylene, 1-Butene, and 1-Hexene. Experiment and Flory-Patterson Model," *Macromolecules*, **25**, 3089 (1992).
- Chen, S., I. G. Economou, and M. Radosz, "Density-Tuned Polyolefin Phase Equilibria. 2. Multicomponent Solutions of Alternating Poly(ethylene-propylene) in Subcritical and Supercritical Olefins. Experiment and SAFT Model," *Macromolecules*, **25**, 4987 (1992).
- de Loos, T. W., W. Poot, and G. A. M. Diepen, "Fluid Phase Equilibria in the System Polyethylene + Ethylene. 2. Calculation of Cloud Point Curves for Systems of Linear Polyethylene + Ethylene," *Macromolecules*, **16**, 117 (1983).
- Flory, P. J., *Principles of Polymer Chemistry*, Cornell University Press: Ithaca (1953).
- Flory, P. J., R. A. Orwoll, and A. Vrij, "Statistical Thermodynamics of Chain Molecule Liquids. I. An Equation of State for Normal Paraffin Hydrocarbons," *J. Am. Chem. Soc.*, **86**, 3507 (1964a).
- Flory, P. J., R. A. Orwoll, and A. Vrij, "Statistical Thermodynamics of Chain Molecule Liquids. II. Liquid Mixtures of Normal Paraffin Hydrocarbons," *J. Am. Chem. Soc.*, **86**, 3515 (1964b).
- Freeman, P. I., and J. S. Rowlinson, "Lower Critical Points in Polymer Solutions," *Polymer*, **1**, 20 (1960).
- Gregg, C. J., F. P. Stein, and M. Radosz, "Phase Behavior of Telechelic Polyisobutylene (PIB) in Subcritical and Supercritical Fluids. 1. Inter- and Intra-Association Effect for Blank, Monohydroxy, and Dihydroxy PIB (1K) in Ethane, Propane, Dimethyl Ether, Carbon Dioxide, and Chlorodifluoromethane," *Macromolecules*, **27**, 4972 (1994a).
- Gregg, C. J., F. P. Stein, and M. Radosz, "Phase Behavior of Telechelic Polyisobutylene (PIB) in Subcritical and Supercritical Fluids. 2. PIB Size, Solvent Polarity, and Inter- and Intra-Association Effect for Blank, Monohydroxy, and Dihydroxy PIB (11K) in Ethane, Propane, Carbon Dioxide, and Dimethyl Ether," *Macromolecules*, **27**, 4981 (1994b).
- Hasch, B. M., M. A. Meilchen, S. Lee, and M. A. McHugh, "High-Pressure Phase Behavior of Mixtures of Poly(Ethylene-co-Methyl Acrylate) with Low-Molecular Weight Hydrocarbons," *J. Polym. Sci.: Part B: Polym. Phys.*, **30**, 1365 (1992).
- Hasch, B. M., M. A. Meilchen, S. Lee, and M. A. McHugh, "Cosolvency Effects on Copolymer Solutions at High Pressure," *J. Polym. Sci.: Part B: Polym. Phys.*, **31**, 429 (1993a).

Hasch, B. M., S. Lee, M. A. McHugh, J. J. Watkins, and V. J. Krukonis, "The Effect Of Backbone Structure on the Cloud Point Behavior of Polyethylene-Ethane and Polyethylene-Propane Mixtures," *Polymer*, **34**(12), 2554 (1993b).

Hasch, B. M., S. Lee, and M. A. McHugh, "Strengths and Limitations for Calculating Polar Copolymer-Solvent Phase Behavior," *J. Appl. Polym. Sci.*, **59**, 1107 (1996).

Haschets, C. W., and A. D. Shine, "Phase Behavior of Polymer-Supercritical Chlorodifluoromethane Solutions," *Macromolecules*, **26**, 5052 (1993).

Kiran, E., Y. Xiong, and W. Zhuang, "Modeling Polyethylene Solutions in Near and Supercritical Fluids Using the Sanchez-Lacombe Model," *J. Supercritical Fluids*, **6**, 193 (1993).

Koningsveld, R., and A. J. Staverman, "Liquid-Liquid Phase Separation in Multicomponent Polymer Solutions. II. The Critical State," *J. Polym. Sci. Pt. A-2*, **6**, 325 (1968a).

Koningsveld, R., and A. J. Staverman, "Liquid-Liquid Phase Separation in Multicomponent Polymer Solutions. III. Cloud-Point Curves," *J. Polym. Sci. Pt. A-2*, **6**, 325 (1968b).

Lacombe, R. H., and I. C. Sanchez, "Statistical Thermodynamics of Fluid Mixtures," *J. Phys. Chem.*, **80**, 2568 (1976).

Lee, S., M. A. LoStracco, and M. A. McHugh, "High-Pressure, Molecular Weight-Dependent Behaviour of (Co)polymer-Solvent Mixtures: Experiments and Modeling," *Macromolecules*, **27**, 4652 (1994).

Liu, D. D., and J. M. Prausnitz, "Calculation of Phase Equilibria for Mixtures of Ethylene and Low-Density Polyethylene at High Pressures," *Ind. Eng. Process Des. Dev.*, **19**, 205 (1980).

Meilchen, M. A., B. M. Hasch, and M. A. McHugh, "Effect of Copolymer Composition on the Phase Behavior of Poly(ethylene-co-methyl acrylate) with Propane and Chlorodifluoromethane," *Macromolecules*, **24**, 4874 (1991).

Panayiotou C., and I. C. Sanchez, "Hydrogen Bonding in Fluids: An Equation-of-State Approach," *J. Phys. Chem.*, **95**, 10090 (1991).

Patterson, D., and G. Delmas, "Critical State in Chain-Molecule Mixtures," *Trans. Faraday Soc.*, **65**, 708 (1969).

Rodgers, P. A., and I. C. Sanchez, "Improvement to the Lattice-Fluid Prediction of Gas Solubilities in Polymer Liquids," *J. Polym. Sci. Pt. B. Polym. Phys.*, **31**, 273 (1993).

Rowlinson, J. S., and F. L. Swinton, *Liquids and Liquid Mixtures*, 3rd Ed., Butterworths: London (1982).

Sanchez, I. C., "Statistical Thermodynamics of Bulk and Surface Properties of Polymer Mixtures," *J. Macromol. Sci.-Phys.*, **B17(3)**, 565 (1980).

Sanchez, I. C., "Equation of State Thermodynamics of Polymer and Related Solutions," in *Models for Thermodynamic and Phase Equilibria Calculations*, S. I. Sandler, ed., Marcel Dekker: New York (1993).

Sanchez, I. C., personal communication, (1996).

Sanchez, I.C., and A. C. Balazs, "Generalization of the Lattice-Fluid Model for Specific Interactions," *Macromolecules*, **22**, 2325 (1989).

Sanchez, I. C., and R. H. Lacombe, "An Elementary Molecular Theory of Classical Fluids. Pure Fluids," *J. Phys. Chem.*, **80**, 2352 (1976).

Sanchez, I. C., and R. H. Lacombe, "An Elementary Equation of State for Polymer Liquids," *J. Polym. Sci., Polym. Lett. Ed.*, **15**, 71 (1977).

Sanchez, I. C., and R. H. Lacombe, "Statistical Thermodynamics of Polymer Solutions," *Macromolecules*, **11**, 1145 (1978).

Siow, K. S., G. Delmas, and D. Patterson, "Cloud-Point Curves in Polymer Solutions with Adjacent Upper and Lower Critical Solution Temperatures," *Macromolecules*, **5**, 29 (1972).

Suresh, S. J., R. M. Enick, and E. J. Beckman, "Phase Behavior of Nylon 6/Trifluoroethanol/Carbon Dioxide Mixtures," *Macromolecules*, **27**, 348 (1994).

Walsh, D. J., and G. T. Dee, "Calculations of the Phase Diagrams of Polyethylene Dissolved in Supercritical Solvents," *Polymer*, **29**, 656 (1988).

Xiong, Y., and E. Kiran, "Prediction of High-Pressure Phase Behavior in Polyethylene/n-pentane/Carbon Dioxide Ternary System with the Sanchez-Lacombe Model," *Polymer*, **35**, 4408 (1994).

Xiong, Y., and E. Kiran, "Comparison of Sanchez-Lacombe and SAFT Model in Predicting Solubility of Polyethylene in High-Pressure Fluids," *J. Appl. Polym. Sci.*, **55**, 1805, (1995).

Zeman, L., and D. Patterson, "Pressure Effects in Polymer Solution Phase Equilibria. II. Systems Showing Upper and Lower Critical Solution Temperatures," *J. Phys. Chem.*, **76(8)**, 1214 (1972).

Zeman, L., J. Biros, G. Delmas, and D. Patterson, "Pressure Effects in Polymer Solution Phase Equilibria. I. The Lower Critical Solution Temperature of Polyisobutylene and Polydimethylsiloxane in Lower Alkanes," *J. Phys. Chem.*, **76(8)**, 1206 (1972).

## CHAPTER 4

### FORMATION AND CHARACTERIZATION OF POROUS ISOTACTIC POLYPROPYLENE

Porous polymeric materials, such as membranes and filters, are widely used in separation processes. These applications require materials, in film or hollow fiber form, which have open cell morphologies and, depending on the specific application, with pore sizes between 0.1 and 30  $\mu\text{m}$ . Widely used processes to make these materials utilize phase separation of polymer solutions induced by temperature or by introduction of a nonsolvent [LeMay et al., 1990]. The phase separation is accompanied by gelation and/or crystallization of the polymer locking in a particular morphology. These solvent based processes trap solvent in the polymer matrix which must be removed in a subsequent processing step. Solvent extraction and freeze-drying techniques are utilized for solvent removal. These techniques are lengthy procedures which can damage the pore structures generated during phase separation. Solvent extraction by a supercritical fluid, critical point drying, is a route that can preserve the pore structure [LeMay et al., 1990; Sawyer & Grubb, 1987].

Crystallization from supercritical polymer solutions is a novel approach for the formation of porous polymeric materials [Bush et al., 1991; Pradhan & Ehrlich, 1995]. This approach has the advantage that solvent removal is achieved by gas escape. This reduces the processing time and the amount of solvent used as compared to conventional solvent extractions. Depending on the polymer/solvent system, gas escape can be done above or slightly below the critical point of the solvent. At these conditions, structural preservation of the polymer matrix is possible [Bush et al., 1991; Pradhan & Ehrlich, 1995]. This structural preservation may be the result of the low- or zero surface tension properties of near- or supercritical fluids.



The purpose of this chapter is to evaluate the process of producing porous polymeric materials by crystallization of isotactic polypropylene (iPP) from its solutions in supercritical propane. The detailed phase behavior presented in Section 2.3.1 provides information on the thermodynamic limits appropriate for carrying out crystallizations from a single-phase supercritical solution. Porous iPP samples are generated by varying process variables such as temperature, pressure, solvent, and nucleating agents. The morphology of porous iPP is presented and mechanical integrity controlled by the use of a nucleating agent. Surface area, porosity, and pore size distributions for the porous iPP are obtained by analysis of nitrogen adsorption isotherms. Small angle x-ray scattering (SAXS) measurements are used to substantiate the pore size distributions obtained from nitrogen adsorption. The model used to interpret SAXS data and obtain a pore size distribution is discussed. A model is proposed to relate the morphology of the porous iPP with the surface area, porosity, and pore size distributions.

#### 4.1 Background

The formation of porous polymeric materials by crystallization of supercritical polymer solutions is similar, in some respects, to a conventional process called thermally induced phase separation (TIPS). Therefore, the TIPS process is reviewed and methods for solvent removal from porous polymeric materials are presented. A literature review of TIPS applied to isotactic polypropylene is also presented.

##### 4.1.1 Thermally Induced Phase Separation (TIPS)

The thermally induced phase separation (TIPS) process consists of the following steps:

1. A homogeneous polymer solution is made by blending the polymer and a high boiling solvent at the appropriate temperature conditions.

2. The temperature of the solution is lowered to induce phase separation whereby gelation and/or crystallization of the polymer results in a polymer matrix imbued with solvent.
3. The solvent is removed by first exchanging the high boiling solvent with a low boiling solvent followed by evaporative drying and/or freeze-drying to produce a solvent-free microporous structure.

In commercial production of TIPS materials, the solution is extruded through a shaping die for making hollow fibers or flat sheets. Since the phase separation is controlled by temperature, heat transfer limits the thickness of useful materials which can be obtained by this process.

The choice of solvent is important because solvent quality determines the type of phase separation and the temperature onset of this phase separation. The Flory  $\chi$  parameter is a measure of solvent quality [Flory, 1953]. For a crystalline polymer/solvent system where  $\chi < 1/2$ , for polymers of infinite molecular weight, the temperature composition phase diagram will contain a solid-liquid phase transition known as the melting point depression curve. If  $\chi > 1/2$  above the melting point depression curve for the crystalline polymer/solvent system, a region of liquid-liquid phase separation will occur in the temperature-composition diagram. Since  $\chi$  normally decreases with increasing temperature, the liquid-liquid immiscibility region will close yielding a single phase solution. Therefore, depending on solvent quality, the TIPS process can either occur by a transition of the liquid phase into a solid-liquid phase (Route A) or by a transition of a single liquid phase into two liquid phases of differing polymer concentration followed by crystallization and/or gelation (Route B). Figure 4.1 shows the two routes on temperature-composition phase diagrams. The morphology of the microporous structure is highly dependent on the phase separation history of the system.

For crystallizable polymer/solvent systems undergoing solid-liquid phase separation, control over morphology is achieved by variation of thermal history, polymer molecular weight and distribution, and addition of nucleating agents. These are the same parameters used to control the morphology of melt crystallized polymers. In addition, solution parameters such as the solvent and polymer concentration will play a role in determining the final microporous structure.

For crystallizable polymer/solvent systems undergoing liquid-liquid phase separation prior to crystallization, control over morphology is highly dependent on the liquid-liquid phase separation process. Liquid-liquid phase separation occurs by two different routes: nucleation and growth as well as spinodal decomposition. In Figure 4.2, the phase diagram in temperature-concentration space is shown with these two routes marked as I and II. Route I (nucleation and growth) occurs in the region between the binodal and spinodal curves, also known as the metastable region. Route II (spinodal decomposition) occurs at the spinodal curve. Phase separation in this region is instantaneous as this region is unstable. The resultant morphologies of materials produced by liquid-liquid phase separation followed by crystallization depends on which route is used. Also, since nucleation and growth is a rate process, cooling rates will be very important in the resultant morphology. Slower cooling rates and systems held in the two phase region, isothermally, give rise to the coalescence of the structure and larger cell sizes result [Tsai & Torkelson, 1990a]. Additionally, high viscosity polymer solutions slow nucleation and growth and quenching into the spinodal region can be accomplished [Tsai & Torkelson, 1990b].

Since solid-liquid phase separation occurs from a homogeneous polymer solution, morphology and homogeneity is controlled by factors relating to crystallization (i.e. degree of supercooling, concentration, addition of nucleating agents, etc.). For crystallizable polymers, liquid-liquid phase separation processes have additional complicating factors which result from the growth mechanisms encountered (nucleation

and growth or spinodal decomposition) and their composition and cooling rate dependence. The additional variables that alter the morphologies obtained from liquid-liquid phase separation processes generally forces one to study solid-liquid phase separation processes first and then liquid-liquid phase separation processes, if possible.

#### 4.1.2 Solvent Removal

The TIPS process traps solvent which must be removed from the polymer matrix. Solvent removal techniques which preserve the structure of the polymer matrix formed in the TIPS process must be utilized. Three of the most common methods are evaporative drying, freeze-drying, and critical point drying.

Removal of solvent by evaporation is referred to as evaporative drying. Solvent evaporation should be possible at mild conditions. The TIPS process often use very high boiling solvents which have an insignificant vapor pressure and, therefore, solvent exchanges are performed to replace this solvent with a relatively low boiling solvent. Evaporation of the low boiling solvent can cause a collapse of the polymer matrix due to a finite liquid-vapor surface tension. Therefore, selection of the low boiling solvent must be made by trial and error to see which solvent can be evaporated from the polymer matrix with minimal structural collapse. Evaporative drying is useful for only a handful of very strong porous polymeric materials [LeMay et al., 1990]. In addition to structural collapse, increased solvent use and processing time required for solvent exchanges can be disadvantageous from an economical and environmental standpoint.

Freeze-drying requires that the sample be cooled to conditions where the solvent freezes and is removed at its sublimation pressure [Sawyer & Grubb, 1987]. The TIPS process often does not use a solvent which has reasonable sublimation conditions. Therefore, solvent exchanges have to be performed. In addition to the increased solvent use from solvent exchanges, processing time is increased because diffusion of the sublimed solvent through the polymer matrix is rate limiting.

Supercritical fluid (SCF) extraction is performed by placing the sample in a high pressure vessel and filling the vessel with a supercritical fluid (typically CO<sub>2</sub>) which extracts the solvent out of the matrix. A low or zero liquid-vapor surface tension allows the removal of the near- or supercritical fluid without collapse of the polymer matrix, a process referred to by some as critical point drying. [LeMay et al., 1990; Sawyer & Grubb, 1987] A limitation to this technique is that the SCF must be miscible with the solvent or solvent exchanges must be done prior to supercritical fluid extraction.

Processing directly from a supercritical fluid would bypass the very time consuming processes of solvent exchanges and/or freeze-drying. The formation of porous, mechanically self-supporting polyethylene foams by crystallization of supercritical polymer solutions is possible [Bush et al., 1991; Pradhan & Ehrlich, 1995]. The solvent in this process, propane, is removed by gas escape. Even at ambient temperatures, gas escape occurs without collapse of the crystalline polyethylene network. The liquid-vapor surface tension of the solvent is sufficiently low as to not damage the morphology.

#### 4.1.3 Porous Isotactic Polypropylene by TIPS

The literature on the application of TIPS for forming porous isotactic polypropylene (iPP) is reviewed. This will allow a comparison between the morphologies obtained by conventional TIPS processes with those obtained by crystallization of supercritical polymer solutions. The bulk of the literature on porous iPP formation by TIPS processes is the result of work from a single laboratory [Lloyd et al., 1990; Lloyd et al., 1991; Kim & Lloyd, 1991; Lim et al., 1991; Kim et al., 1991; Alwattari & Lloyd, 1991; McGuire et al., 1993] along with some patents [Castro, 1985; Vitzthum & Davis, 1984; Lopatin et al., 1989]. Published literature often contains information only about the bulk morphology of the porous structure. Mechanical properties of iPP membranes, surface areas, and pore size distributions are usually not available in the published literature.

For polymer/solvent systems undergoing solid-liquid transitions, the morphology of isotactic polypropylene is that of impinged spherulites [Lloyd et al., 1990]. Larger spherulites, and a corresponding decrease in the number of spherulites are obtained at higher crystallization temperatures or slower cooling rates [Lloyd et al., 1990; Lim et al., 1991; McGuire et al., 1993]. The spherulite center is a solid core while its surface texture is attributed to branched lamellae that form when the concentration of polymer in solution is depleted [Lloyd et al., 1990]. Solvents with higher mobility diffuse out of the growing spherulite and into the interspherulitic regions [Kim et al., 1991]. For iPP concentrations up to 50 wt. % (~50 vol. %), the spherulitic morphology results in poor bulk mechanical coherency because of the low polymer concentration and low number of tie chains in the interspherulitic region [Lloyd et al., 1990]. To improve mechanical integrity, nucleating agents were added to reduce spherulite sizes. Low concentrations of dibenzylidene sorbitol (DBS) or adipic acid effectively reduces spherulite size and produces mechanically coherent membranes at iPP concentrations below 50 wt. % [Lloyd et al., 1990; Lim et al., 1991; McGuire et al., 1993]. Higher iPP concentrations (~80 wt. %) could also be used to increase mechanical coherency but this results in the loss of microporosity [Lloyd et al., 1990].

Morphologies obtained by liquid-liquid phase separation are different than those obtained by solid-liquid phase separation [Lloyd et al, 1991; Kim & Lloyd, 1991]. In slowly cooled *n,n*-bis(2-hydroxyethyl) tallowamine (TA)/iPP solutions, the morphology obtained is that of a cellular structure while quenching of those same solutions result in a lacy structure [Lloyd et al., 1991]. The difference between the two is a result of coarsening of the liquid-liquid phase separated structure [Tsai & Torkelson, 1990a]. At high concentrations of iPP, the TA/iPP system undergoes solid-liquid phase separation instead of liquid-liquid phase separation, which results in spherulitic morphologies [Lloyd et al., 1991]. Quenching yields dense spherulites while slow cooling yields spherulitic structures with some small cellular features which may be a result of liquid-liquid phase

separation occurring as the polymer concentration decreases during crystallization [Lloyd et al., 1991].

Crystallization of the solvent occurring prior to or competing with iPP crystallization was also studied [Kim et al., 1991; Alwattari & Lloyd, 1991]. For the hexamethylbenzene/iPP system, crystallization of the hexamethylbenzene occurs prior to iPP crystallization. Extraction of hexamethylbenzene crystals embedded in the iPP matrix results in a needle-like pore morphology [Alwattari & Lloyd, 1991].

The specific surface areas of porous iPP generated by TIPS process (liquid-liquid phase separation of iPP/n,n-bis(2-hydroxyethyl)tallowamine solutions) are reported in one patent [Castro, 1985]. For five different porosities between 29-90%, the specific surface areas are in the range of 88-100 m<sup>2</sup>/g. Heat treatment results in significant reductions in the specific surface area.

#### 4.2 Characterization Methods for Porous Isotactic Polypropylene

Many techniques exist for the characterization of porous materials. However, most techniques are limited to a particular range of pore sizes while others require mechanically coherent materials. Therefore, researchers often limit themselves to characterizing the bulk morphology with techniques such as scanning electron microscopy (SEM).

The characterization methods applicable to porous isotactic polypropylene (iPP) formed by crystallization from supercritical propane are presented. First, the study of porous iPP by microscopic methods, optical and electron, is discussed and stereological relationships allowing a quantitative cell size determination are presented. The general characteristics of adsorption isotherms are then presented. The apparatuses used to obtain adsorption isotherms and the theories utilized to calculate surface area, porosity, and pore size distribution are presented. Pore structural analysis is complimented by small angle x-

ray scattering (SAXS) measurements interpreted by a two phase model where the pores are represented as polydisperse globular aggregates.

#### 4.2.1 Microscopy and Stereological Relationships

Polarized optical microscopy can yield information about the spherulitic habit in melt crystallized isotactic polypropylene (iPP) [Padden & Keith, 1959]. Scattering at polymer/void interfaces in porous iPP significantly reduces light transmission and prevents structural observation in transmission optical microscopy. Imbibing the pores with a fluid that closely matches the index of refraction of iPP would reduce the scattering allowing observation by optical microscopy. Toluene, under most conditions, provides a sufficient match of refractive index.

Scanning electron microscopy (SEM) is an excellent tool for observation of the bulk morphology in porous materials. Preparation of the porous materials for analysis is minimal and requires freeze fracturing, at temperatures below  $T_g$ , and then sputter coating with a conductive layer of metal [Sawyer & Grubb, 1987].

In porous materials, SEM allows a qualitative measurement of the average distance between surfaces of the solid phase. However, SEM is a 2-dimensional image of a 3-dimensional structure. Therefore, quantitative determination of cell sizes from micrographs is time consuming and rarely utilized. Stereological relationships exist to relate the surface area per unit volume,  $S_v$ , to the average distance between solid phases,  $d$  [Aubert, 1988]. This relationship is given by

$$\langle d \rangle = \frac{4}{S_v} \quad (4.1)$$

For spherical cells,  $d$  is a ratio of the third to second moment and is given by



$$\langle d \rangle = \frac{\sum n_i d_i^3}{\sum n_i d_i^2} \quad (4.2)$$

where  $n_i$  is the number of cells of dimension  $d_i$  [Aubert, 1988]. Therefore, large cells are weighted very heavily.

If the surfaces of the material are accessible to gas adsorption (open pores), the specific surface area in  $\text{m}^2/\text{g}$ ,  $S_{\text{sp}}$ , can be measured (Section 4.2.2.1). With knowledge of the porosity,  $\epsilon$ ,  $S_v$  is given by

$$S_v = S_{\text{sp}} \rho_m (1 - \epsilon) \quad (4.3)$$

where  $\rho_m$  is the density of the solid phase.

#### 4.2.2 Adsorption-Desorption Isotherms

Physical adsorption of vapors, gases below the critical point, on solid surfaces is a result of attractive forces between solid and gas which, in most all cases, is fully reversible. Adsorption is a function of pressure, temperature, the nature of the solid, and solid-gas interactions and is often represented as adsorption isotherms where the quantity of gas adsorbed is a function of relative pressure (pressure divided by the saturated vapor pressure of the gas).

Adsorption isotherms can be classified into five types [Brunauer et al., 1940] as shown in Figure 4.3. Types I-III represent adsorption onto non-porous adsorbents while Type IV and V isotherms are extensions of Type II and III isotherms, respectively, for porous adsorbents in which capillary condensation occurs. Type I isotherms, or Langmuir isotherms, are found in systems where adsorption is limited to a few molecular layers [Gregg & Sing, 1982]. The other isotherms are characterized by multilayer adsorption

where the isotherm shape at low relative pressures depends on the strength of adsorbate-adsorbent interactions relative to the strength of adsorbate-adsorbate interactions. The knee in the low relative pressure region of Type II and IV isotherms results from strong adsorbent-adsorbate interactions where the first layer forms easily but the formation of subsequent layers becomes less favorable because of weaker adsorbate-adsorbate interactions. In Type III and V isotherms, formation of the initial adsorbed layer is not favored because of weak adsorbent-adsorbate interactions. Stronger adsorbate-adsorbate interactions cause adsorption to become more favorable as more adsorbed layers are present and this leads to the upswing in Type III and V isotherms. For Type IV and V isotherms, at high relative pressures, capillary condensation takes place in pores of  $\sim 20\text{-}1000\text{\AA}$ .

Capillary condensation is not always reversible and therefore, leads to hysteresis loops. During adsorption, capillary condensation occurs in progressively larger pores. During desorption (lowering relative pressure), the desorption occurs from progressively smaller pores. If a large pore is blocked by a smaller one, desorption of the large pore will not occur until the relative desorption pressure of the smaller pore is reached. Recent research suggests that if pore blocking does not exist, there is no adsorption-desorption hysteresis [Schmidt et al., 1995]. This is in contrast to theories that propose different mechanisms for pore filling and emptying as being responsible for the hysteresis [Cohan, 1938].

Hysteresis loops, based on Type IV isotherms, can be classified into five types as shown in Figure 4.4. These hysteresis loops can be attributed to specific pore models [Mikhail & Robens, 1983]. Type A and E are the most important because Type A is associated with the simplest pore model, cylindrical pores, while Type E corresponds to a system with pores having narrow necks and wide bodies. Type A corresponds to cylindrical pores open at both ends and where both the adsorption and desorption branch are steep. Breadth of the adsorption and desorption branch in pore filling and desorption

are an indication that a distribution in pore sizes exists and is referred to as non-ideal Type A behavior. Type E hysteresis loops result from narrow pores which act as bottlenecks for the desorption of liquid from larger pores.

Despite extensive research in the pore size analysis of systems, no satisfactory theory of hysteresis exists. For example, a hysteresis loop cannot be attributed to a unique pore shape and a distributions of pore sizes and shapes probably exist within a particular adsorbent [Mikhail & Robens, 1983]. Also, for powders, pores are formed by the packing of the powder and it is difficult to separate the contribution of these pores from the internal pores of the material [Mikhail & Robens, 1983].

Adsorption isotherms allow estimation of surface areas, porosity, and pore size distributions. Determination of surface areas from the low relative pressure region ( $0.05 < P/P_0 < 0.3$ ) and pore size distributions from the high relative pressure region ( $0.7 < P/P_0 < 1.0$ ) of the adsorption isotherm is discussed.

#### 4.2.2.1 Surface Areas

Most adsorbate-adsorbent systems have adsorption isotherms of Type II or IV. Surface areas can be calculated from these isotherms using the BET theory [Gregg & Sing, 1982; Lowell & Shields, 1984]. The relevant equations for determining the surface area by the BET theory are presented. The volumetric apparatus utilized to measure the adsorption isotherm required for BET calculations is also described.

##### 4.2.2.1.1 BET Theory

Researchers extended theories of monolayer adsorption to multilayer adsorption using several simplifying assumptions. This resulted in the BET theory which is named after the founders [Brunauer et al., 1938]. The simplifying assumptions have led to several criticisms of the BET theory but the theory is still widely used to calculate surface

area [Gregg & Sing, 1982; Lowell & Shields, 1984]. The BET equation allows determination of the number of molecules required to form a monolayer from a multilayer adsorption isotherm even though the adsorbent is never covered by exactly one adsorbate layer [Lowell & Shields, 1984]. The monolayer coverage can easily be converted into a surface area.

The BET equation expressed in terms of the volume of gas adsorbed,  $V_a$ , as a function of relative pressure ( $P/P_0$ , where  $P$  is pressure and  $P_0$  is the saturated vapor pressure of the adsorbate) is given by

$$\frac{1}{V_a \left[ \left( \frac{P_0}{P} \right) - 1 \right]} = \frac{1}{V_m C} + \frac{C-1}{V_m C} \left( \frac{P}{P_0} \right) \quad (4.4)$$

where  $V_m$  is the volume of gas required to form a monolayer and  $C$  is the BET constant [Brunauer et al., 1938]. From the slope,  $s$ , and intercept,  $i$ , of the BET equation,  $V_m$  and  $C$  are given by

$$V_m = \frac{1}{s+i} \quad (4.5)$$

$$C = \frac{s}{i} + 1 \quad (4.6)$$

The BET  $C$  constant is mathematically related to the heat of adsorption whose value is related to the isotherm type [Gregg & Sing, 1982; Lowell & Shields, 1984]. BET  $C$  values less than 2 give rise to a Type III isotherm where applicability of the BET theory is questioned [Gregg & Sing, 1982; Lowell & Shields, 1984]. BET  $C$  values between 20

and 1000 are related to Type II isotherms and represent values in the ideal range for surface area calculations.

Due to the theoretical assumptions, the BET equation is generally only applicable in the relative pressure range of  $0.05 < P/P_0 < 0.30$  [Gregg & Sing, 1982; Lowell & Shields, 1984]. Fits of the BET equation in this relative pressure region yield straight lines and give good values for the monolayer coverage,  $V_m$ . The BET surface area or specific surface area,  $S_{sp}$  in  $m^2/g$ , can then be calculated from  $V_m$ , when expressed in  $cm^3$  (STP)  $g^{-1}$ , by using the relation

$$S_{sp} = \frac{V_m}{22414} N\sigma \times 10^{-18} \quad (4.7)$$

where 22414 is the number of  $cm^3$  per mol at STP conditions,  $N$  is Avogadro's number ( $6.023 \times 10^{23}$  molecules/mol), and  $\sigma$  is the cross-sectional area ( $nm^2$ ) of the adsorbate [Lowell & Shields, 1984]. The most common adsorbate is nitrogen whose cross-sectional area is  $0.162 nm^2$  at 77 K [Lowell & Shields, 1984].

#### 4.2.2.1.2 Static BET Apparatus

A schematic of the volumetric static BET apparatus used for this work is shown in Figure 4.5. Use of the apparatus was provided by Dr. W. C. Conner of the Chemical Engineering Department. Initially, the entire system, except for the gas bulbs, is evacuated. Helium (Ultra High Purity grade, 99.999% minimum purity) is introduced through valve A, with valve B closed, into a manifold containing five bulbs of known volume. Valve A is then closed and equilibrium pressures are recorded as the mercury level is raised to fixed points between each of the volumetric bulbs. Valve B is opened and the pressure trace recorded with the sample tube immersed in a fluid at the adsorption temperature. The system is evacuated and the procedure repeated for the adsorbate. The

adsorbate is nitrogen (Ultra High Purity grade, 99.999% minimum purity) and the adsorption temperature is that of liquid nitrogen (~ 77 K) for all experiments performed in this thesis. The pressure traces obtained with the non-adsorbing helium allows the calculation of the sample dead volume. With the sample dead volume known, the pressure trace for the adsorbate can be converted into a volumetric quantity adsorbed. In the case of nitrogen as the adsorbate, the saturated adsorbate vapor pressure,  $P_0$ , is atmospheric pressure. Impurities or dissolved oxygen in the liquid nitrogen can alter the saturated vapor pressure but the resulting error in the calculated value for the surface area is small [Lowell & Shields, 1984].

#### 4.2.2.2 Porosity and Pore Size Distributions

The relevant equations for the determination of pore sizes and pore size distribution are presented along with the apparatus used to determine adsorption-desorption isotherms to a relative pressure of unity.

##### 4.2.2.2.1 Theory

Condensation of vapor in small pores, also known as capillary condensation, occurs because the equilibrium vapor pressure of a liquid on a curved surface,  $P$ , is lower than the vapor pressure of that same liquid on a plane surface,  $P_0$ . The Kelvin equation describes this relationship and is given by

$$\ln\left(\frac{P}{P_0}\right) = -\frac{2\gamma\bar{V}}{r_k RT} \cos\theta \quad (4.8)$$

where  $r_k$  is the Kelvin radius,  $R$  is the gas constant,  $T$  is the absolute temperature,  $\gamma$  is the surface tension,  $\bar{V}$  is the molar volume of the liquid, and  $\theta$  is the contact angle of liquid in

contact with the pore wall [Gregg & Sing, 1982; Lowell & Shields, 1984]. Equation 4.8 is applicable for a cylindrical meniscus of the liquid in contact with its vapor. For nitrogen,  $\bar{V}$  is known and universal values for  $\gamma$  and  $\theta$  are assumed unless better values for a specific adsorbate-adsorbent system are known [Lowell & Shields, 1984].

With the Kelvin equation, calculation of the pore size distribution is straightforward. Prior to the occurrence of capillary condensation, multilayer adsorption has occurred on the surfaces of the adsorbent. The statistical thickness of this adsorbed layer and how it changes with relative pressure must be determined. Experimental fits of the adsorption data in the relative pressure range,  $0.3 < P/P_0 < 0.7$ , to the Halsey equation can give this information [Gregg & Sing, 1982; Halsey, 1948]. The statistical thickness,  $t$ , is given by

$$t = H_{\text{con}} \left( \frac{1}{\ln \left( \frac{P_0}{P} \right)} \right)^{\frac{1}{H_{\text{exp}}}} \quad (4.9)$$

where  $H_{\text{con}}$  is the Halsey constant and  $H_{\text{exp}}$  is the Halsey exponent.

The pore radius,  $r_p$ , is given by

$$r_p = r_k + t \quad (4.10)$$

where  $r_k$  and  $t$  are simple functions of the relative pressure,  $P/P_0$ , as given by equations 4.8 and 4.9.

The analysis of adsorption-desorption isotherms to obtain pore size distributions assuming cylindrical pores is straightforward. Analysis of the adsorption branch is

preferred because the desorption branch is a result of pore blocking effects (Section 4.2.2) and, therefore, the adsorption branch should more accurately describe the true nature of the porous system. However, the following procedure could be applied to either the adsorption or desorption branch.

Between two points on the adsorption isotherm, the change in the amount of gas adsorbed at STP conditions,  $\Delta V_{\text{gas}}$ , can be related to a change in a liquid volume,  $\Delta V_{\text{liq}}$ , by

$$\Delta V_{\text{liq}} = \Delta V_{\text{gas}} \left( \frac{\bar{V}}{V_{\text{STP}}} \right) \quad (4.11)$$

where  $\bar{V}$  is the molar volume of the adsorbate and  $V_{\text{STP}}$  is the  $\text{cm}^3$  per mol at STP conditions.

Assuming cylindrical pores, the differential pore volume between two points on the adsorption isotherm,  $dV_p$ , is given by

$$dV_p = \left( \frac{\bar{r}_p}{\bar{r}_k} \right)^2 \left[ \Delta V_{\text{liq}} - (\Delta t \Sigma S) \right] \quad (4.12)$$

where  $\bar{r}_p$  and  $\bar{r}_k$  are the average pore radius and Kelvin radius,  $\Delta t$  is the change in statistical thickness between the points on the adsorption isotherm, and  $\Sigma S$  is a surface area summation. The product  $\Delta t \Sigma S$  is a measure of the amount of adsorbed gas required to thicken the adsorbed layer on surfaces located in pores where capillary condensation has not occurred. Calculation of  $\Sigma S$  is detailed after definition of the surface area for cylindrical pores. The pore surface area,  $S_p$ , can be calculated for cylindrical pores by the following equation



$$S_p = \frac{2dV_p}{\bar{r}_p} \quad (4.13)$$

The calculation of the surface area summation should start at a point where the available surface area is zero or, in other words, at the point where all capillaries are filled with liquid adsorbate. Surface area is then generated as pores are emptied and can be calculated by equation 4.13. If calculation of the surface area proceeded from the relative pressure where capillary condensation started to take place, the surface area would start at some value and should decrease to zero once all the pores are filled. This starting surface area would have to be estimated. Therefore, calculation of the pore volume by either the adsorption or desorption branch should be done working from the highest relative pressure to lower relative pressures.

The pore size distribution is then calculated taking the incremental pore volume,  $dV_p$ , divided by the difference in pore radius,  $\Delta r_p$ , between the two points on the adsorption isotherm. A plot of  $dV_p / \Delta r_p$  versus  $r_p$  gives the pore size distribution. The cumulative pore volume can then be calculated by the summation of  $dV_p$  or by integration of the pore size distribution. An alternative method for calculating pore volume is to assume that the pore volume is equal to the quantity of adsorbed gas at a relative pressure of 0.99. If the total pore volume,  $V_p$ , is on a per gram basis of the material, the porosity,  $\epsilon$ , is given by

$$\epsilon = \frac{V_p}{V_m + V_p} \quad (4.14)$$

where  $V_m$  is the specific volume of the material (adsorbent).

#### 4.2.2.2 Adsorption-Desorption Apparatus

A schematic of the adsorption-desorption apparatus used for this work is shown in Figure 4.6. Use of the apparatus was provided by Dr. W. C. Conner of the Chemical Engineering Department. The instrument is a Omnisorp™ 100 built by Omicrom Technology Corporation (Berkeley Heights, NJ). Adsorption-desorption experiments, depending on the amount of sample and its pore volume characteristics, take about 24 hours. Therefore, data acquisition and instrument control is performed by computer (Mac II computer, Centrel data acquisition software, and  $\mu$ Mac-1050 data acquisition board).

In this apparatus, helium or adsorbate is continuously metered in with the use of a mass flow controller (Brooks Instruments, Model 5850E). The mass flow controller operates in the 0 to 5 cc(STP)/min range. The flow rate generally chosen during experimental runs is in the 0.3-0.5 cc(STP)/min range. The sample tube is immersed in liquid nitrogen whose level is controlled by an automated filling system consisting of a liquid level probe and a portable liquid nitrogen dewar. Initially, the system is evacuated. Adsorbate (Nitrogen, Ultra High Purity grade, 99.999% minimum purity) is metered into the system and the pressure recorded as a function of time. When a relative pressure very close to unity is reached, inlet flow is stopped and desorption is started. The direction of flow through the mass flow controller is manipulated by opening and closing certain valves so that the gas in the system flows to vacuum. The pressure and time is recorded and the run finished when the relative pressure reaches  $\sim 0.30$ . After evacuating the system, a flow experiment is performed with helium (Ultra High Purity grade, 99.999% minimum purity) to allow calculation of the sample dead volume. With the sample dead volume, the quantity of gas adsorbed is calculated from the adsorbate run. The calculation of dead volume and quantity of gas adsorbed depends on an accurately calibrated flow controller. This calibration was performed using flow experiments into sample bulbs of different volumes with the entire system at a constant temperature. The calibrated flow rate in standard  $\text{cm}^3/\text{min}$  was then calculated for both helium and nitrogen.

### 4.2.3 Small Angle X-Ray Scattering (SAXS)

Small angle x-ray scattering on random two phase materials can yield information about the size of the heterogeneity. For two phase systems with sharp boundaries, a correlation length which describes the size of the heterogeneity can be obtained [Debye & Bueche, 1949; Debye et al., 1957]. However, the porous isotactic polypropylene under investigation in this thesis has a pore size distribution and a more appropriate model would account for this distribution in structure. From scattering experiments, it is impossible to independently obtain both a size distribution and a shape [Glatter, 1982]. Therefore, either a size distribution or shape has to be assumed and because a size distribution is desired, a shape has been assumed. The model chosen is that for a two phase system where one of the phases is composed of polydisperse globular aggregates [Hosemann & Bagchi, 1962]. The relevant equations for the polydisperse globular aggregate model and the apparatuses used to perform SAXS measurements are presented.

#### 4.2.3.1 Polydisperse Globular Aggregate Model

The polydisperse globular aggregate model assumes a Maxwell distribution of spheres which is given by

$$M(y) = \left(\frac{y}{y_0}\right)^n \exp\left[-\left(\frac{y}{y_0}\right)^2\right] \frac{K(n)}{y_0} \quad (4.15)$$

where  $y_0$  is the radius of the sphere and  $n$  is the Maxwell distribution exponent and  $K(n)$  is given by

$$\frac{1}{K_n} = \frac{1}{2} \Gamma\left(\frac{n+1}{2}\right) = \frac{1}{2} \left(\frac{n-1}{2}\right)! \quad n \geq -1 \quad (4.16)$$

where  $\Gamma$  is the gamma function [Hosemann & Bagchi, 1962].

The observed scattered intensity,  $I_{\text{obs}}$ , for this type of system is given by

$$I_{\text{obs}} = \Delta\rho^2 N_c v_c \left[ 1 + \frac{1}{5} (q y_o)^2 \right]^{-\frac{1}{2}(n+4)} \quad (4.17)$$

where  $\Delta\rho$  is the density difference between the two phases (electron density in the case of x-ray scattering),  $N_c$  is the number of particles,  $v_c$  is the average volume of the particles, and  $q$  is the scattering vector given by

$$q = \frac{4\pi \sin\left(\frac{\theta}{2}\right)}{\lambda} \quad (4.18)$$

where  $\theta$  is the scattering angle and  $\lambda$  is the wavelength of the radiation [Hosemann & Bagchi, 1962].

A suggested method for determining the Maxwell distribution parameters from experimental data is to analyze  $q^2 I_{\text{obs}} - q$  plots [Hosemann & Bagchi, 1962]. Multiplying equation 4.17 by  $q^2$  gives

$$q^2 I_{\text{obs}} = A_o \frac{q^2}{\left[ 1 + \frac{(q y_o)^2}{5} \right]^{\frac{1}{2}(n+4)}} \quad (4.19)$$

where  $A_0$  is a constant. Fits of equation 4.19 to experimental scattering data will give the Maxwell distribution parameters,  $y_0$  and  $n$ , and a value for  $A_0$ . The Maxwell distribution of spheres can then be compared to the pore size distribution obtained from analysis of nitrogen adsorption isotherms.

#### 4.2.3.2 Experimental

All x-ray scattering measurements on porous isotactic polypropylene (iPP) samples were performed by Dr. Greg Beaucage of the University of Cincinnati, Department of Materials Science and Engineering. Measurements were made at Sandia National Labs and Oak Ridge National Labs (ORNL). At Sandia, wide angle x-ray diffraction (WAXD), Kratky small angle x-ray scattering (SAXS), and Bonse-Hart SAXS were performed while pinhole SAXS was performed at ORNL. X-ray scattering measurements for porous iPP samples later identified as PP-3K, PP-3K-2, PP-5K, and PP-80 were obtained at Sandia while those identified as PP-73, PP-77, PP-85, PP-Butane, and PP-Heptane were obtained at ORNL. The Kratky SAXS data presented in this thesis is that obtained after desmearing of the experimental SAXS data. The absolute intensities were measured in all cases and normalized to the sample thickness and therefore, comparisons can be made between samples. However, the sample thickness is not an easily measured quantity because of the non-film like morphology of the porous iPP. Therefore, significant errors in the normalized absolute intensity could result from thickness deviations.

### 4.3 Experimental

#### 4.3.1 Solvents

Propane and butane (CP grade, 99.0+% minimum purity) were obtained from Merriam-Graves and used as received. 1-propanol (certified grade) and heptane (certified grade) were obtained from Fisher Scientific and used as received.

#### 4.3.2 Polymers and Additives

A commercial isotactic polypropylene, Himont 6824PM, was used for the crystallization studies and was provided by the Millipore Corporation. The sample has an estimated  $M_w$  above 600,000, a broad molecular weight distribution, contains heat stabilizing additives, and is distributed as a very finely ground powder. The high molecular weight was chosen in an attempt to promote coherency in the crystallized iPP. The finely ground powder facilitated the mixing of the polymer to make a homogeneous solution as compared to pellets which agglomerate and form a viscous phase which is hard to disperse. The use of iPP containing heat stabilizers was helpful to insure that long mixing times would not degrade the polymer.

Dibenzylidene sorbitol (DBS), an effective nucleating agent for isotactic polypropylene [Thierry et al., 1990; Thierry et al., 1992], was obtained from Milliken Chemical (Spartanburg, N.C.) under the product name Millad<sup>®</sup> 3905. Millad<sup>®</sup> 3905 contains a minimum of 96% DBS and was used as received.

#### 4.3.3 Apparatus

The high pressure view cell used for phase behavior measurements (Section 2.2.2) was fitted with a cooling jacket so that crystallizations could be carried out at various thermal histories. Heating tapes were used to heat the cell to temperatures required to obtain homogeneous solutions. To carry out isothermal crystallization or to quench the sample, fluid from a circulating bath was circulated through the cooling jacket. Additionally, the external rotating magnet was placed on a translating stage to promote mixing along the cell axis in order to achieve uniform dispersions.

## 4.4 Results

The application of the characterization methods discussed in Section 4.2 to porous isotactic polypropylene (iPP) formed by crystallization of supercritical propane solutions is presented. The temperature and pressure routes for the formation of porous iPP are detailed first. The bulk morphology of unnucleated and nucleated systems is then presented. Surface areas, porosities, and pore size distributions calculated from nitrogen adsorption isotherms are presented as well as pore size distributions obtained by interpretation of small angle x-ray scattering (SAXS) data with the polydisperse globular aggregate model. Surface areas, porosities, and pore size distributions are presented as a function of the processing variables: temperature, pressure, and solvent. Models are proposed to relate the surface area, porosity, and pore size distribution to the observed bulk morphologies.

### 4.4.1 Formation of Porous Isotactic Polypropylene (iPP)

The temperatures and pressures required to carry out crystallizations of isotactic polypropylene from solutions in supercritical propane are defined by the phase diagrams presented in Section 2.3.1. The research here focused on crystallization of iPP by traversing the solid-supercritical fluid phase boundary in iPP/propane systems. Figure 4.7 shows the temperature-pressure route used in carrying out such crystallizations. A homogeneous solution is quenched to temperatures much lower than the S-SCF equilibrium temperature of the iPP2/propane system. The pressure is kept above the cloud-point pressures for the atactic polypropylene/propane system to insure that liquid-vapor phase separation does not compete with crystallization.

#### 4.4.1.1 Bulk Morphology of Unnucleated iPP

Under most crystallization conditions, the iPP morphology is that of highly porous spherulites. Crystallization of a 20 wt. % iPP solution in propane at 80°C and 6000 psi

(PP-80) resulted in the morphology shown in Figure 4.8. When the pores imbibe an index of refraction-matching fluid, such as toluene, polarized optical microscopy reveals a maltese cross indicative of a spherulitic morphology [Padden & Keith, 1959]. Of interest was the interior structure of these microspheres. Attempts to embed the microspheres in epoxy and section them using a cryomicrotome proved unsuccessful. This may be related to the inability of the epoxy to enter the small pores of the material (Section 4.4.2). To determine the interior morphology, a 2-D crystallization apparatus was constructed, as shown in Figure 4.9, and inserted into the pressure cell. 2-D crystallizations carried out at the same conditions for PP-80 revealed a dense core which changed to a fibrillated growth at some radius as shown in Figure 4.10. This transition in morphology also occurs in 3-dimensional microspheres based on confocal microscopy studies [Kulkarni, 1994].

Crystallization of a 20 wt. % iPP solution in supercritical propane at 100°C and 6000 psi (PP-100) resulted in the random lamellar morphology shown in Figure 4.11. At polymer concentrations lower than those presented here for iPP, the occurrence of a lamellar structure at high crystallization temperatures and spherulites (dendrites) at lower temperatures is observed for solution crystallizations of polyethylene [Wunderlich, 1973].

The mechanical coherency of any of the iPP materials produced by crystallization from supercritical propane is very poor. This agrees with previous research on un-nucleated iPP [Lloyd et al., 1990] and is probably a result of low nucleation at high crystallization temperatures and high diluent (propane) mobility allowing solvent to diffuse out of growing spherulites and into the interspherulitic regions [Kim et al., 1991]. Mechanical coherency of porous iPP can be promoted by the addition of nucleating agents [Lloyd et al., 1990; Lim et al., 1991; McGuire et al., 1993]. The addition of nucleating agents to the iPP/propane system is discussed in the next section.



#### 4.4.1.2 Bulk Morphology of Nucleated iPP

Dibenzylidene-d- sorbitol (DBS) has been evaluated as a nucleating agent for polyolefins and has been determined to be highly effective for polypropylene [Fillon et al., 1993a,b; Thierry et al., 1990; Thierry et al., 1992]. DBS crystallizes in the form of small fibers which cause gelation at very low concentrations. This gelation is an excellent state of dispersion for the nucleating agent and in addition the small fibers provide large surface areas for nucleation [Thierry et al., 1990; Thierry et al., 1992]. Therefore, incorporation of DBS into iPP/propane systems was attempted. Solubilization of the DBS is required to create a homogeneous dispersion. Solubilization of DBS in the experimental temperature and pressure window requires small amounts of a cosolvent. 1-propanol was selected as the cosolvent and solid-supercritical fluid equilibria for the DBS/propane/1-propanol system were studied and results presented in Section 2.3.3.3. The cloud-point pressures of the aPP/propane/1-propanol system were studied and results presented in Section 2.3.3.2.2. The phase behavior of the ternary system shows that at low 1-propanol content iPP crystallization from a single phase polymer solution can take place without liquid-liquid phase separation occurring in the experimental temperature window used for iPP crystallizations.

The temperature and pressure route for the DBS modified system is shown in Figure 4.12. A homogeneous solution of DBS and iPP in a propane/1-propanol mixture is obtained at high temperatures. The temperature of the system is reduced to induce gelation crystallization of the DBS and then crystallization of the iPP at lower temperatures. The pressure is maintained above the cloud-point pressures of the aPP/propane/1-propanol system at similar 1-propanol content. The crystallization of a 20 wt. % iPP solution in propane/1-propanol (13.9 wt. % 1-propanol) at 80°C and 6000psi (PP-DBS) resulted in the morphology shown in Figure 4.13. The quantity of DBS added to the system was 2 wt. % based on the weight of the polymer. Spherulite sizes are dramatically reduced which supports previous researchers findings in conventional

solvent/iPP systems [Lloyd et al., 1990; Lim et al., 1991; McGuire et al., 1993]. More importantly, coherency is substantially enhanced. The sample presented in Figure 4.13 shrunk slightly during solvent removal, but with optimization of the 1-propanol content, DBS content, and temperature history, it is expected that shrinkage could be minimized. The addition of 1-propanol to propane increases the critical temperature and 1-propanol has a higher surface tension than propane at the solvent removal conditions. These factors could contribute to structural collapse during the solvent removal process. Shrinkage could be minimized by lowering the 1-propanol content, by using a lower alcohol such as methanol, or by reducing the DBS content thereby requiring less cosolvent.

#### 4.4.2 Surface Area, Porosity, and Pore Size Distribution

The bulk morphology provides some clues as to the mechanism for crystallization of isotactic polypropylene from supercritical propane. Initial surface area studies suggested that iPP crystallized from supercritical propane has relatively high surface areas ( $\sim 120\text{-}180\text{m}^2/\text{g}$ ). Therefore, the effect of processing variables such as temperature, pressure and solvent on the surface area were studied. Such surface area studies suggested that pore size distributions might also provide some useful information. In obtaining this information, an estimate of the porosity, for pore sizes  $< 1000 \text{ \AA}$ , can also be determined. Small angle x-ray scattering from porous iPP is analyzed by a polydisperse globular aggregate model to obtain a pore size distribution which is compared to pore size distributions determined from nitrogen adsorption isotherms.

##### 4.4.2.1 Temperature History

Isothermal crystallizations of 20 wt. % iPP solutions in supercritical propane were performed at four temperatures (73, 77, 80, and 85°C) at a constant pressure of 6000psi with the samples identified as PP-73, PP-77, PP-80, PP-85. Crystallizations in this temperature range resulted in spherulitic morphologies. The original nitrogen adsorption-

desorption isotherms and SAXS data for these samples can be found in Appendix B. Appendix B also lists key parameters obtained from BET analysis, pore size distribution analysis, and polydisperse globular aggregate analysis. The surface areas and porosities for these samples are shown in Figure 4.14. The surface areas and porosities increase with decreasing crystallization temperature or higher degrees of supercooling. The pore size distributions calculated from nitrogen adsorption isotherms for these samples are shown in Figure 4.15. The pore size distribution in these samples is almost identical. Table 4.1 compares the peak in the pore size distribution from the analysis of nitrogen adsorption isotherms and from small angle x-ray scattering data analyzed with the polydisperse globular aggregate model.

Table 4.1 Comparison of Peak Pore Size from Nitrogen Adsorption (Cylindrical Pore Model) and Small Angle X-Ray Scattering (Polydisperse Globular Aggregate Model) for Porous iPP at Different Isothermal Crystallization Temperatures

Sample	Peak Pore Size, $r_D$ (Å) (Nitrogen Adsorption)	Peak Pore Size, $y_0$ (Å) (SAXS)
PP-73	98	93.2
PP-77	98	91.3
PP-80	102	80.3
PP-85	89	83.9

#### 4.4.2.2 Solvent

In addition to crystallization from supercritical propane, crystallizations were carried out from two other solvents, butane and heptane, and the samples identified as PP-Butane and PP-Heptane. The original nitrogen adsorption-desorption isotherms and SAXS data for these samples can be found in Appendix B. Appendix B also lists key parameters obtained from BET analysis, pore size distribution analysis, and polydisperse globular aggregate analysis. The surface areas and porosities of porous iPP formed by

crystallization in these different solvents are shown in Figure 4.16 as compared to a sample formed by crystallization from propane, PP-73. Both surface area and porosity increase as the molecular weight of the solvent is decreased. The pore size distributions calculated from nitrogen adsorption isotherms for these samples are shown in Figure 4.17. The area under the pore size distribution curves is equal to the pore volume and clearly shows that the lower the alkane, the higher the sample porosity. The pore size distributions are very similar, as is the case for crystallization at different temperatures. Table 4.2 compares the peak in the pore size distribution from the analysis of nitrogen adsorption isotherms and from small angle x-ray scattering data analyzed with the polydisperse globular aggregate model.

Table 4.2 Comparison of Peak Pore Size from Nitrogen Adsorption (Cylindrical Pore Model) and Small Angle X-Ray Scattering (Polydisperse Globular Aggregate Model) for Porous iPP Crystallized from Different Alkanes

Sample	Peak Pore Size, $r_D$ (Å) (Nitrogen Adsorption)	Peak Pore Size, $y_0$ (Å) (SAXS)
PP-Propane (PP-73)	98	93.2
PP-Butane	81	73.4
PP-Heptane	85	74.5

#### 4.4.2.3 Pressure

Isothermal crystallizations of 10 wt. % iPP solutions in supercritical propane were performed at three pressures (3000, 5000, and 10000psi) at a constant temperature of 65°C and the samples identified as PP-3K, PP-3K-2, PP-5K, PP-10K, respectively. The porous iPP formed at these temperatures and pressures has a spherulitic morphology. The original nitrogen adsorption-desorption isotherms and SAXS data for these samples can be found in Appendix B. SAXS data is not available for PP-10K. Appendix B also lists key

parameters obtained from BET analysis, pore size distribution analysis, and polydisperse globular aggregate analysis. The surface areas and porosities for these samples are shown in Figure 4.18. Both surface area and porosity do not appear to correlate with pressure. The pore size distributions calculated from nitrogen adsorption isotherms for these samples are shown in Figure 4.19. The pore size distribution in these samples is almost equivalent. Table 4.3 compares the peak in the pore size distribution from the analysis of nitrogen adsorption isotherms and from small angle x-ray scattering data analyzed with the polydisperse globular aggregate model.

Table 4.3 Comparison of Peak Pore Size from Nitrogen Adsorption (Cylindrical Pore Model) and Small Angle X-Ray Scattering (Polydisperse Globular Aggregate Model) for Porous iPP Isothermally Crystallized at 65°C at Different Pressures

Sample	Peak Pore Size, $r_D$ (Å) (Nitrogen Adsorption)	Peak Pore Size, $y_0$ (Å) (SAXS)
PP-3K	210	109.5
PP-3K-2	176	98
PP-5K	183	93
PP-10K	210	*

\* - SAXS data not available for this sample

#### 4.4.2.4 Miscellaneous

Surface areas, porosities, and pore size distributions on two other porous iPP samples were determined. These samples are the 20 wt. % iPP isothermally crystallized at 100°C (PP-100) whose morphology was presented in Section 4.4.1.1 and the 20wt. % iPP sample containing DBS (PP-DBS) whose morphology was presented in Section 4.4.1.2. The original nitrogen adsorption-desorption isotherms for these samples can be found in Appendix B. Appendix B also lists key parameters obtained from BET analysis

and pore size distribution analysis. The BET surface areas and porosities for these two samples are listed in Table 4.4. Figure 4.20 and 4.21 show the pore size distributions for PP-100 and PP-DBS, respectively. The peak in the pore size distribution for PP-100 is ~200 Å which is double that found in the temperature history and solvent trends (Sections 4.4.2.1 and 4.4.2.2). The peak in the pore size distribution for PP-DBS is in the vicinity of 65 Å. Small angle x-ray scattering was not performed on either sample.

Table 4.4 BET Surface Areas and Porosity for PP-100 and PP-DBS

Sample	BET Surface Area, (m <sup>2</sup> /g)	Porosity, ε
PP-100	125.5	0.363
PP-DBS	87	0.190

#### 4.4.3 Models

The surface area of the porous iPP formed by crystallization from supercritical propane is relatively large. The surface areas of crystallizable polymers are expected to be limited by the formation of lamellae. A model which predicts the surface area for lamellar materials in terms of a lamellar thickness is presented. Several problems exist with this simple model because it does not account for the amorphous fraction of the polymer, accessibility of lamellar surfaces to gas adsorption, and structural heterogeneities. A second model, based on the fibrillation of the growing spherulite is proposed to calculate surface areas and porosities of the fibrillated structure as well as the onset of this fibrillation.

#### 4.4.3.1 Lamellar Model

Crystallization of polymers into the form of lamellae will be an inherent limitation to the formation of high surface area materials. A polymer lamellae is shown in Figure 4.22 with a lamellar thickness,  $t$ . In the case where the lateral dimensions  $a$  and  $b$  are much larger than  $t$ , the surface area to volume ratio of a lamellae,  $S_v^{\text{lamellae}}$ , is given by

$$S_v^{\text{lamellae}} = \frac{\text{Surface Area}}{\text{Volume}} = \frac{2ab}{abt} = \frac{2}{t} \quad (4.20)$$

and the specific surface area of the lamellae,  $S_{sp}^{\text{lamellae}}$ , is given by

$$S_{sp}^{\text{lamellae}} = \frac{\text{Surface Area}}{\text{Volume} \times \text{Density}} = \frac{2ab}{abt\rho} = \frac{2}{t\rho} \quad (4.21)$$

If a density of  $1 \text{ g/cm}^3$  and a lamellar thickness of  $100\text{\AA}$  is assumed,  $S_{sp}^{\text{lamellae}}$  is  $200\text{m}^2/\text{g}$ . This model assumes that the lamellae form as a single layer with their surfaces freely accessible. However, stacking of lamellae occurs in most crystallizations, except for dilute solution crystallizations, and thus would reduce the specific surface area. Additionally, this model does not account for the amorphous fraction of the polymer which can be in the vicinity of 50%. Therefore, the lamellar model gives an estimate of the order of magnitude of the specific surface area.

#### 4.4.3.2 Fibrillation Model

The morphology of the porous iPP formed by crystallization from supercritical propane results in a heterogeneous structure. Under most conditions, this heterogeneous structure is in the form of spherulites which have a transition from a dense core (no

porosity) to a fibrillated structure (high porosity). The dense core contributes very little to the overall surface area while the fibrillated structure has a large surface area. The larger the dense core relative to the fibrillated structure, the lower the specific surface area.

Ideally, one would like to determine the specific surface area of the fibrillated structure alone. The fibrillation model proposed is an attempt to determine the surface area and porosity of the fibrillated structure as well as the onset of fibrillation.

The basic spherulite morphology with the dense core (black) and the fibrillated structure (grey) is shown in Figure 4.23. The relative radius at which the transition from a dense core to a fibrillated structure occurs is denoted as  $r_{\text{core}}$ . The maximum radius of the sphere is unity. Two assumptions are made in this model. The first is that the density of the core is that of nonporous polypropylene and that the fibrillation density is a constant value,  $\rho_{\text{fib}}$ . The second is that the surface area per unit volume ratio is zero for the core and is equal to  $(S/V)_{\text{fib}}$  throughout the fibrillated structure.

With these assumptions, equations to determine  $\rho_{\text{fib}}$  and  $r_{\text{core}}$  from the experimental porosity, surface area, and pore size distributions for the bulk material can be formulated. The bulk density is given by

$$\rho_{\text{bulk}} = \rho_{\text{PP}}(1 - \epsilon) = \rho_{\text{PP}}r_{\text{core}}^3 + \rho_{\text{fib}}(1 - r_{\text{core}}^3) \quad (4.22)$$

Equation 4.22 can be solved for  $\rho_{\text{fib}}$  to give

$$\rho_{\text{fib}} = \rho_{\text{PP}} \left( 1 - \frac{\epsilon}{(1 - r_{\text{core}}^3)} \right) \quad (4.23)$$



A second equation relating  $\rho_{\text{fib}}$  and  $r_{\text{core}}$  is required. Equation 4.1 can be used to find another relationship using the second assumption concerning the surface to volume ratio. This relationship is given by

$$\langle d \rangle = \frac{4}{\left(\frac{S}{V}\right)_{\text{fib}}} = \frac{4(1 - r_{\text{core}}^3)}{S_{\text{sp}}\rho_{\text{PP}}(1 - \varepsilon)} \quad (4.24)$$

Equation 4.24 can be solved for  $r_{\text{core}}$  to give

$$r_{\text{core}} = \left(1 - \frac{\langle d \rangle S_{\text{sp}}\rho_{\text{PP}}(1 - \varepsilon)}{4}\right)^{\frac{1}{3}} \quad (4.25)$$

Equations 4.25 and 4.23 can be solved for  $\rho_{\text{fib}}$  which is given by

$$\rho_{\text{fib}} = \rho_{\text{PP}} \left(1 - \frac{4\varepsilon}{\langle d \rangle S_{\text{sp}}\rho_{\text{PP}}(1 - \varepsilon)}\right) \quad (4.26)$$

The porosity of the fibrillated structure,  $\varepsilon_{\text{fib}}$ , is then given by

$$\varepsilon_{\text{fib}} = \frac{\rho_{\text{PP}} - \rho_{\text{fib}}}{\rho_{\text{PP}}} \quad (4.27)$$

The specific surface area of the fibrillated structure,  $S_{\text{sp}}^{\text{fib}}$ , is given by

$$S_{sp}^{fib} = \frac{S_{sp}\rho_{PP}(1-\epsilon)}{\rho_{fib}(1-r_{core}^3)} \quad (4.28)$$

or by

$$S_{sp}^{fib} = \frac{4}{\rho_{fib}\langle d \rangle} \quad (4.29)$$

and should be equal to or greater than the specific surface area of the bulk,  $S_{sp}$ .

Equations 4.25 and 4.26 set limits for the value of  $\langle d \rangle$ . Since  $r_{core}$  cannot be negative, equation 4.25 gives the condition that the maximum  $\langle d \rangle$ ,  $\langle d \rangle_{max}$ , is given by

$$\langle d \rangle_{max} = \frac{4}{S_{sp}\rho_{PP}(1-\epsilon)} \quad (4.30)$$

Similarly,  $\rho_{fib}$  cannot be negative and equation 4.26 gives the condition that the minimum value of  $\langle d \rangle$ ,  $\langle d \rangle_{min}$ , is given by

$$\langle d \rangle_{min} = \frac{4\epsilon}{S_{sp}\rho_{PP}(1-\epsilon)} \quad (4.31)$$

If the value of  $\langle d \rangle$  obtained from pore size distributions exceeds  $\langle d \rangle_{max}$ , the value of  $r_{fib}$  would be zero and, therefore, the material has no dense core. The porosity, specific surface area of the fibrillated structure, and fibrillation density would thus be the same as the bulk material.

Based on the fibrillated model structure, a relative mass of the core versus the fibrillated region can be extracted. The relative mass of the core and fibrillated structure are given by

$$m_{\text{core}} \propto \rho_{\text{PP}} r_{\text{core}}^3, \quad m_{\text{fib}} \propto \rho_{\text{fib}} (1 - r_{\text{core}}^3) \quad (4.32)$$

The weight percent of polymer remaining in solution at the time of fibrillation,  $\text{wt}\%(\text{fib})$ , is then given by

$$\text{wt}\%(\text{fib}) = \text{wt}\%(\text{initial soln}) \frac{m_{\text{core}}}{(m_{\text{core}} + m_{\text{fib}})} \quad (4.33)$$

#### 4.4.3.2.1 Fibrillation Model - Temperature History

Figure 4.24 shows the core radius and fibrillation density,  $r_{\text{core}}$  and  $\rho_{\text{fib}}$ , as a function of the isothermal crystallization conditions for the porous iPP. The results show that the onset of fibrillation occurs at a smaller relative radius for lower crystallization temperatures. The fibrillation density,  $\rho_{\text{fib}}$ , is relatively constant over the range of crystallization temperatures. The specific surface area of the fibrillar structure is compared to the overall specific surface area in Figure 4.25. This figure shows that the surface area of the fibrillated structure, within experimental error, is constant over the range of crystallization temperatures while the overall surface area is increasing. Figure 4.26 shows the wt. % of polymer in solution at the onset of fibrillation. This figure shows that the amount of polymer remaining in solution at the onset of fibrillation is higher for decreasing crystallization temperature.

#### 4.4.3.2.2 Fibrillation Model - Solvent

Figure 4.27 shows the core radius and density,  $r_{\text{core}}$  and  $\rho_{\text{fib}}$ , as a function of the alkane solvent from which porous iPP was generated. The results show that the onset of fibrillation occurs at a smaller relative radius for lower molecular weight solvents. The fibrillation density,  $\rho_{\text{fib}}$ , does not exhibit a trend with solvent size but is very similar in value despite large differences in  $r_{\text{core}}$ . The specific surface area of the fibrillar structure is compared to the overall specific surface area in Figure 4.28. This figure shows that the surface area of the fibrillated structure is lower for crystallizations from propane than from butane and heptane. The surface area calculation for the fibrillated structure (Equation 4.28) relies heavily on the cube of the core radius. As the core radius gets closer to unity for PP-Butane and PP-Heptane, the calculation of fibrillar surface area is subject to large errors because of the assumptions made in the proposed theory. Figure 4.29 shows the wt. % of polymer in solution at the onset of fibrillation. This figure shows that the amount of polymer remaining in solution at the onset of fibrillation is higher for decreasing molecular weight.

#### 4.4.3.2.3 Fibrillation Model - Pressure

The fibrillation model applied to porous iPP formed by isothermal crystallization of 10 wt.% solutions at 65°C and different pressures is a case where  $\langle d \rangle$  is greater than  $\langle d \rangle_{\text{max}}$  and therefore  $r_{\text{core}}$  is zero (equation 4.30). The instantaneous fibrillation of these 10 wt. % systems is in line with the results of the temperature series (Section 4.4.3.2.1) that suggest that fibrillation always occurs prior to the polymer solution concentration reaching 10 wt. %.

#### 4.4.4 Discussion

Porous isotactic polypropylene (iPP) as formed by crystallization of a single phase solution in supercritical propane appears to have a morphology qualitatively similar with that of porous iPP formed by thermally induced phase separation (solid-liquid) processes from conventional solvents. The morphology is that of relatively large ( $100+ \mu\text{m}$ ) porous microspheres [Section 4.4.1.1 and Lloyd et al., 1990]. In both systems, the mechanical coherency is low due to the small amount of tie chains present at impinging spherulites. Lower coherency is expected when solvent mobility is higher because the solvent diffuses to the interspherulitic regions which results in a lower concentration of polymer tie chains at the impinging spherulites [Kim et al., 1991]. More detailed comparisons between the literature work and the porous iPP presented in this thesis is difficult because literature studies focus on crystallizations at high cooling rates ( $> 10 \text{ K/min}$ ) [Kim et al., 1991] while the work in this thesis concentrates on isothermal crystallizations of iPP.

Literature studies and this thesis work suggest that the formation of coherent materials from iPP is difficult to attain and is a result of the characteristics of iPP and its crystallization behavior. The low nucleation density in iPP results in large microspheres having mechanically weak interspherulitic regions. Highly coherent iPP can be formed by the addition of nucleating agents which reduce spherulite sizes improving mechanical coherency [Lloyd et al., 1990]. Dibenzylidene-d-sorbitol (DBS) has been found to be a highly effective nucleating agent for iPP [Thierry et al., 1990; Thierry et al., 1992]. For nucleation of iPP from solution, the key issues are the dispersion of DBS and its gelation prior to iPP crystallization. The polar nature of DBS requires the use of a cosolvent in order to solubilize DBS in the processing window used for the iPP/propane system. The temperatures for dispersion and subsequent gelation are controlled by the amount of the polar cosolvent. 1-propanol was selected as the polar cosolvent. The crystallization of iPP from propane containing a small amount of 1-propanol and DBS results in a morphology consisting of very small spherulites ( $< 5 \mu\text{m}$ ) having good mechanical

coherency (Section 4.4.1.2). This morphology is consistent with nucleated iPP formed by solid-liquid phase separation from conventional solvents [Lloyd et al., 1990; McGuire et al., 1993].

Specific surface areas have been reported for porous iPP formed by liquid-liquid phase separation of iPP/n,n-bis(2-hydroxyethyl)tallowamine (TA) solutions [Castro, 1985]. Specific surface areas of 90-100 m<sup>2</sup>/g, independent of porosity, were reported. These specific surface areas are of similar magnitude to those found for the porous iPP formed by crystallization from propane presented in this thesis. Pore sizes, determined by mercury porosimetry, are approximately 0.5 μm [Castro, 1985]. Such features are an order of magnitude above those obtainable from analysis of nitrogen adsorption isotherms and are too large to account for such high values of specific surface area. Smaller features in this porous iPP must be responsible for these surface areas. Threadlike morphologies generated by spinodal decomposition, a growth mechanism for systems undergoing liquid-liquid phase separation, can account for high specific surface areas [Aubert, 1988; Aubert, 1990]. SEM studies of porous iPP generated by liquid-liquid phase separation of its solutions in TA suggest that cellular structures are present at the size scale found in mercury porosimetry and not a threadlike morphology [Castro, 1985]. Therefore, a feature smaller than those seen by SEM or calculated from mercury porosimetry measurements must account for the bulk of the surface area found in these studies. A mechanism operating on the nanoscale and inherent in the crystallization of iPP from solution or in the bulk may be responsible for the large surface areas.

The crystallization behavior of isotactic polypropylene continues to be a topic of current research because of its industrial importance and because its behavior is quite complex and not fully understood. Isotactic polypropylene crystallizes in a number of crystal modifications with the most common being the α (monoclinic), β (hexagonal), and γ (triclinic) forms [Turner-Jones et al., 1964]. The particular crystal modification is a function of temperature [Padden & Keith, 1959], pressure [Pae, 1968], solvent [Sauer et

al., 1965; Khoury, 1966], molecular weight [Turner-Jones et al., 1964; Lotz et al., 1986], and stereospecificity [Turner-Jones et al., 1964]. The presence of two different crystal habits in a given sample is common. Small quantities of a second crystal habit have been shown to be responsible for the different spherulite types found in melt crystallized isotactic polypropylene [Padden & Keith, 1959].

A long standing puzzle has been the crystallization of iPP in a lath-like habit from solution [Sauer et al., 1965; Khoury, 1966]. The discovery of such a habit was thought to occur by epitaxial overgrowth occurring on the  $\alpha$  phase substrate with an abrupt change in the chain direction [Khoury, 1965]. Later research suggests that this branching may be initiated by  $\gamma$  phase material because of the relative fit of this crystal at the boundary layer of  $\alpha$  phase material [Padden & Keith, 1973]. A contributing factor to this branching, initiated by  $\gamma$  phase material, is the segregation of stereoirregular species. Such stereoirregular species crystallize preferentially in the  $\gamma$  phase [Turner-Jones et al., 1964]. A critical concentration (temperature dependent) of stereoirregular polymer may be required to initiate the branching [Padden & Keith, 1973]. More recent research has suggested that both  $\alpha$  and  $\gamma$  lamella can branch off of a parent  $\alpha$  lamella [Lotz et al., 1986]. The angle of the parent  $\alpha$  lamella with respect to the branched  $\gamma$  lamella is  $40^\circ$  but the chain axis in the two phases are parallel. The branched  $\alpha$  lamella makes an angle of  $80^\circ$  with respect to the parent  $\alpha$  lamella with the chain axis orientation epitaxial. Recent research has now suggested that the  $\gamma$  phase material is composed of two non-parallel chain orientations in the unit cell [Lotz et al., 1991].

This type of branching, regardless of the mechanism or crystal modification, could produce features that would account for the high specific surface areas found in porous iPP as formed by crystallization from supercritical propane. For porous iPP, the specific surface area is in the range of 120-180  $\text{m}^2/\text{g}$ . This is near the limit of 200  $\text{m}^2/\text{g}$  for sheets of iPP with a lamellar thickness of 100 Å (Section 4.4.3.1). Specific surface areas approaching the theoretical limit suggests three possibilities concerning the nanostructure

of porous iPP. First, the amount of material in stacked lamella must be relatively small. A sheet of iPP two lamella thick would result in a specific surface area of ca.  $100 \text{ m}^2/\text{g}$  based on a lamellar thickness of  $100 \text{ \AA}$ . This value for specific surface area is below that observed experimentally. Alternatively, the lamellar dimensions would be different from those proposed in the lamellar model (Section 4.4.3.1). Instead of a sheet, geometries in which the lateral surface area can not be neglected may exist. If a needle-like habit of growth exists instead of a infinite sheet-like growth, the theoretical limit for the specific surface area could be substantially higher than the lamellar estimate of  $200 \text{ m}^2/\text{g}$  [Section 4.4.3.1]. The SAXS data analyzed by a model structure consisting of disk-like lamellar platelets of radius,  $R$ , and thickness,  $t$ , give values of  $R$  between  $130\text{-}340 \text{ \AA}$  and values of  $t$  between  $55\text{-}84 \text{ \AA}$  [Beaucage, 1995]. This type of structure would give specific surface areas from  $300 \text{ m}^2/\text{g}$  to in excess of  $400 \text{ m}^2/\text{g}$ . However, no microscopy results exist to support this type of structure. Additionally, the contribution of the amorphous phase, which constitutes ca. 50% of the material, could also be important. Some structural feature of this phase might contribute significantly to the overall surface area. Samples are stored above  $T_g$  of the iPP and one would expect changes to occur in the amorphous phase over time that would reduce the surface area. Surface areas studied over a period of months showed no significant decay in the value of the specific surface area (Appendix B). Therefore, both limited stacking of lamella and needle-like growths are probably occurring in the porous iPP formed by crystallization from supercritical propane. The extent to which each contribute to surface area can not be determined.

The similarity of the pore size distributions of the porous iPP within the temperature, solvent, and pressure series, is noteworthy. This similarity exists for pore radii of  $20\text{-}1000 \text{ \AA}$ , defined as mesopores, as determined by analysis of nitrogen adsorption isotherms. These mesopores are thought to be intraspherulitic and porosities determined by nitrogen adsorption are limited to information about mesopores. Characteristics of pores larger than mesopores, macropores, are not known at this time



but their presence could contribute significantly to porosity but insignificantly to surface area. In the samples prepared from 20 wt. % iPP solutions at different crystallization temperatures, the pore size distributions were nearly identical with a peak pore radius of ca. 100 Å. Crystallization of iPP from butane and heptane also gave similar pore size distributions and peak pore radii with the only difference being a smaller population of such pores for these solvents as compared to propane. Samples prepared from 10 wt. % iPP solutions at constant temperature but different pressures gave pore size distributions that were nearly identical having a peak pore radius of ca. 200 Å. These small scale pores could be a result of the branching habit of iPP spherulites. The distributions in all cases are relatively broad but continuous suggesting that this 3-dimensional network of pores may be a result of local growth environments. Solution concentration and/or the presence of specific crystal phases may be controlling the pore size distributions.

Wide angle x-ray diffraction (WAXD) analysis to determine the amount and/or presence of  $\alpha$  and  $\gamma$  phases were performed on four of the samples presented in this thesis. Figure 4.30 shows the diffraction patterns for four porous iPP samples: PP-80, PP-3K, PP-3K-2, and PP-5K. PP-80 shows evidence of some  $\gamma$  phase material but the others contain an experimentally immeasurable quantity of  $\gamma$  phase material. The PP-3K, PP-3K-2, and PP-5K samples have a peak pore radius of 200 Å while PP-80 has a peak pore radius of ca. 100 Å. Crystallization times were shorter for the samples PP-3K, PP-3K-2, and PP-5K (isothermal crystallization temperatures of 65°C) than for PP-80. Longer crystallization times would allow molecular weight segregation to occur and this low molecular weight material might crystallize, preferentially, in the  $\gamma$  phase [Turner-Jones et al., 1964; Lotz et al., 1986]. The difference in pore size distribution may be related to the regular serration of the branching which occurs for  $\gamma$  phase material as evidenced by crystallization in thin films [Padden & Keith, 1966]. However, the solution concentrations from which the porous iPP is generated is quite different. PP-3K, PP-3K-2, and PP-5K were made by crystallization of 10 wt. % iPP solutions while PP-80 was prepared from a

20 wt. % iPP solution. If larger cells result as the polymer is depleted, lower initial weight fractions would give larger pore sizes as is the case for these porous iPP samples. Since crystallization of 20 wt. % iPP solutions in butane and n-heptane resulted in the same pore size distribution as obtained for 20 wt. % iPP solutions in propane, depletion of the polymer in solution during growth might control the pore size distribution. The pore volumes, obtained by integration of pore size distribution curves (Section 4.2.2.2.1), of porous iPP samples should be related to the openness of spherulite textures. Increases in porosity are linked to increases in surface area which suggest a "two structure" system of porous and nonporous material. Such a "two structure" system is the basis of the fibrillation model (Section 4.4.3.2).

Phenomenological treatment of spherulitic crystallization suggests that the openness of spherulite texture is related to the concentration of impurities [Keith & Padden, 1964]. Impurities can be low molecular weight species (solvents) and/or stereoirregular polymer. The coarseness of spherulite texture is related to the segregation of impurities between crystalline fibers. The size of these crystalline fibers,  $\delta$ , is given by

$$\delta = \frac{D}{G} \quad (4.34)$$

where  $D$  is the diffusion coefficient of the impurity and  $G$  is the radial growth rate of the spherulite [Keith & Padden, 1964]. Additionally, the noncrystallographic branching in the spherulite increases with decreasing  $\delta$  [Keith & Padden, 1964].

For the crystallization of iPP from solution in propane, the diffusion coefficient of the impurity, propane, is roughly constant for the range of temperatures utilized for isothermal crystallizations. However, the radial growth rate would be expected to increase with increasing degree of supercooling. Therefore,  $\delta$  would decrease with increasing supercooling and more open textures should be obtained. Porosities for porous

iPP increase with increasing degree of supercooling (Section 4.4.2.1). A decrease in  $\delta$  with increasing supercooling also suggests the formation of higher surface area iPP because of the formation of smaller crystalline fibers as well as increased noncrystallographic branching. Alternatively, a smaller  $\delta$  may decrease  $r_{\text{core}}$ , the onset of fibrillation, and increase specific surface areas. Porous iPP crystallized at higher degrees of supercooling results in higher surface areas (Section 4.4.2.1). The higher surface areas are also not inconsistent with the idea that decreases in lamellar thickness are expected for higher degrees of supercooling [Lauritzen & Hoffman, 1960]

Relationships between the phenomenological treatment of spherulites and porous iPP generated by crystallization from different solvents are more difficult to determine. The diffusion coefficient for the solvents decrease with increasing molecular weight. Direct comparison between samples prepared from propane, butane, and n-heptane could be made if the growth rate was equivalent or known. Information is not available on the actual growth rates in these different solvents and, therefore, the value of  $\delta$  is not known and trends of surface area and porosity with  $\delta$  cannot be established. The porosities suggest that there is a more open structure for crystallizations from propane (Section 4.4.2.2). However, the issue of collapse of pores during solvent removal is a complicating factor for samples prepared from butane and n-heptane.

The openness of spherulitic texture is related to the concentration of impurity [Keith & Padden, 1964]. In porous iPP generated by crystallization of 10 wt. % iPP solutions from supercritical propane at different pressures (Section 4.4.2.3), pore volumes are approximately twice the pore volumes found for crystallizations of 20 wt. % iPP solutions at different temperatures (Section 4.4.2.1). Since the peak pore radius is ca. 200 Å for the 10 wt. % iPP solutions and 100 Å for the 20 wt. % iPP solutions, depletion of the polymer during crystallization may be responsible for the pore size distribution. Changes of  $\delta$  with pressure are hard to predict and, therefore, trends with surface area can

not be established. No experimental correlation between pressure and surface area seems to exist for the samples presented in Section 4.4.2.3.

The next issue is the observed transition from a nonporous core to a fibrillated structure where spherulite branching occurs. Solvent, impurity, is segregated between the branches and when it is removed becomes the location of the pores. The application of the fibrillation model to the samples prepared in this research tries to relate the onset of the fibrillation to the measured parameters of surface area, porosity, and pore size distribution. For porous iPP samples prepared by isothermal crystallization at different temperatures, the fibrillation model predicts that the onset of fibrillation occurs at a smaller relative radius for higher supercoolings. Similarly, the onset of fibrillation in porous iPP samples obtained by crystallization from different solvents occurs at a smaller relative radius for crystallizations from lower molecular weight solvents. For porous iPP formed by crystallization of 10 wt.% iPP solutions at the same isothermal crystallization temperature but different pressures, the fibrillation model predicts that fibrillation is instantaneous.

The fibrillation model allows the calculation of the polymer solution concentration at the time of fibrillation. In all cases, for crystallizations of 20 wt.% iPP solutions in propane at different temperatures, fibrillation occurs at polymer concentrations above 10 wt. %. In the pressure series, the initial polymer concentration was 10 wt. %. In all samples prepared in the pressure series, the fibrillation model predicts that the core radius is zero. The onset of fibrillation in both the temperature and pressure series suggest that a critical polymer concentration (temperature dependent) is required for fibrillation to occur. Once fibrillation occurs, a polymer structure is formed which, after solvent is removed, is the location of mesopores.

The exact mechanism responsible for fibrillated growth is unknown for the systems studied here. The large number of possible variables that may alter growth characteristics along with insufficient information about in-situ crystallization kinetics makes this problem

difficult to resolve. The uniqueness of the systems studied in this research is the use of a supercritical fluid diluent from which crystallization takes place. The special thermodynamic properties of the supercritical solvent (low densities, low viscosities, high compressibilities, high diffusion coefficients) may play a role in the onset of fibrillation. Instabilities at the spherulite growth front, caused by thermal gradients which can induce large density changes in supercritical fluids, may be a contributing factor to the onset of fibrillation.

#### 4.5 Conclusions

Porous iPP formed by crystallization of single phase solutions in supercritical propane results in morphologies very similar to those obtained by the conventional thermally induced phase separation (liquid to solid) process. Under most crystallization conditions, large microspheres which are spherulitic in habit are obtained for unnucleated systems. Nucleation of iPP with dibenzylidene-d-sorbitol (DBS) results in very small spherulites having good mechanical coherency. One area of difference may be the specific surface areas of porous iPP obtained from crystallization in supercritical propane. Comparisons with the literature cannot be made because of the lack of this information for porous iPP produced by TIPS.

Habits inherent in iPP crystallization (homoepitaxy) are probably responsible for the small pore sizes and the high specific surface areas of porous iPP as formed by crystallization from supercritical propane. These specific surface areas are quite large, 120-180 m<sup>2</sup>/g and represent a relatively efficient use of the material in applications requiring high surface areas. Controlling factors such as solution concentration, temperature, pressure, and polymer characteristics (molecular weight and stereospecificity) need to be studied in greater detail.

The supercritical solution process allows preservation of nanoscale structural features by removing the solvent by gas escape at near- or supercritical conditions. The

solvent free polymer matrix whose structure is unperturbed by solvent removal can be studied in detail and relations between processing conditions and structural characteristics can be made. The nanoscale features of the porous iPP prepared in this research is a potential candidate for adsorption based separations. The utility of these materials in such applications would have to be tested but a concentration dependence of pore size distributions suggests that adsorbents could be tailored with specific pore sizes.

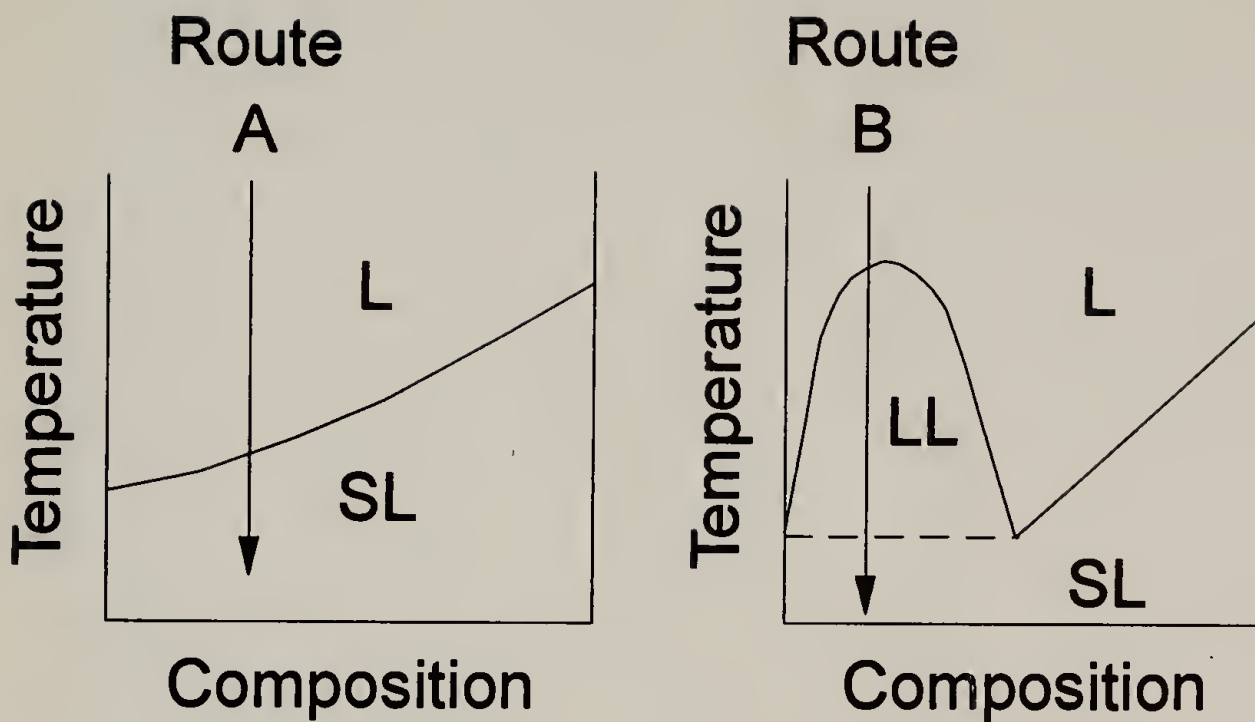


Figure 4.1 Temperature-Composition Phase Diagrams for Thermally Induced Phase Separation (TIPS) Processes (L denotes a single liquid phase, LL denotes liquid-liquid equilibrium, SL denotes solid-liquid equilibrium, Route A is the solidification of the polymer, and Route B is the phase separation of a single liquid phase into two liquid phases differing in polymer composition followed by solidification of the polymer)

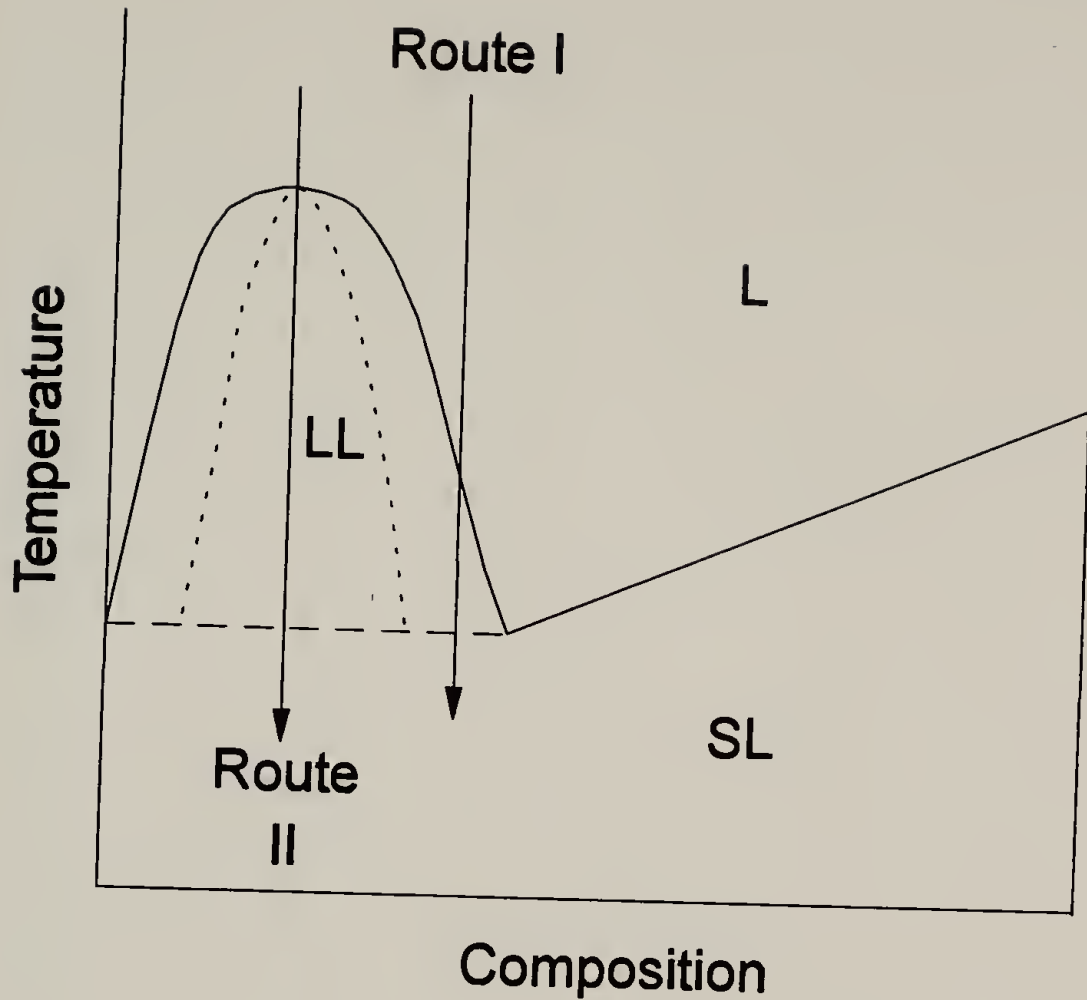


Figure 4.2 Temperature-Composition Phase Diagram for Liquid-Liquid Phase Separation (L denotes a single liquid phase, LL denotes liquid-liquid equilibrium, SL denotes solid-liquid equilibrium, - - - denotes the spinodal, Route I is liquid-liquid phase separation by nucleation and growth, and Route II is liquid-liquid phase separation by spinodal decomposition)



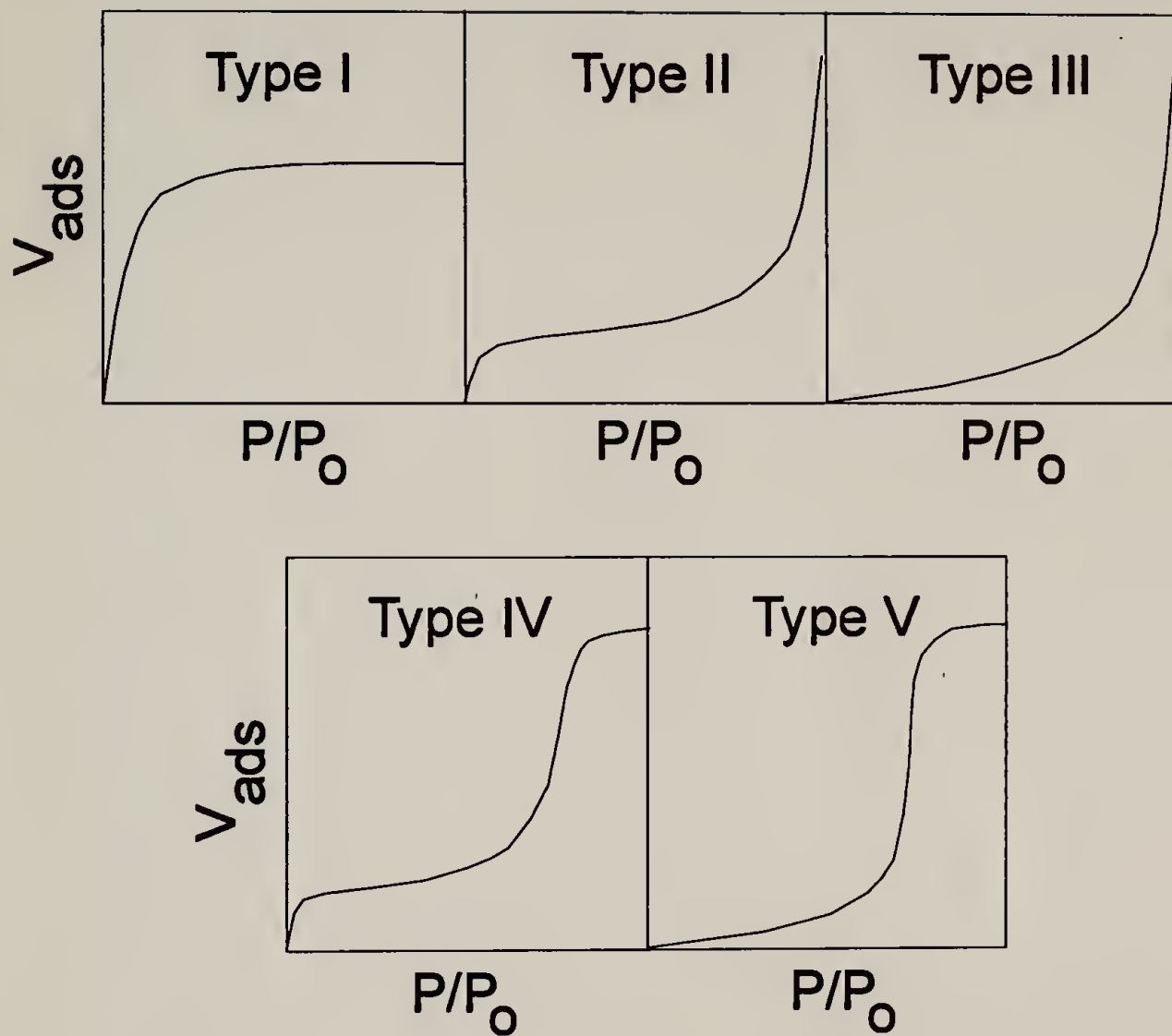


Figure 4.3 Types of Adsorption Isotherms

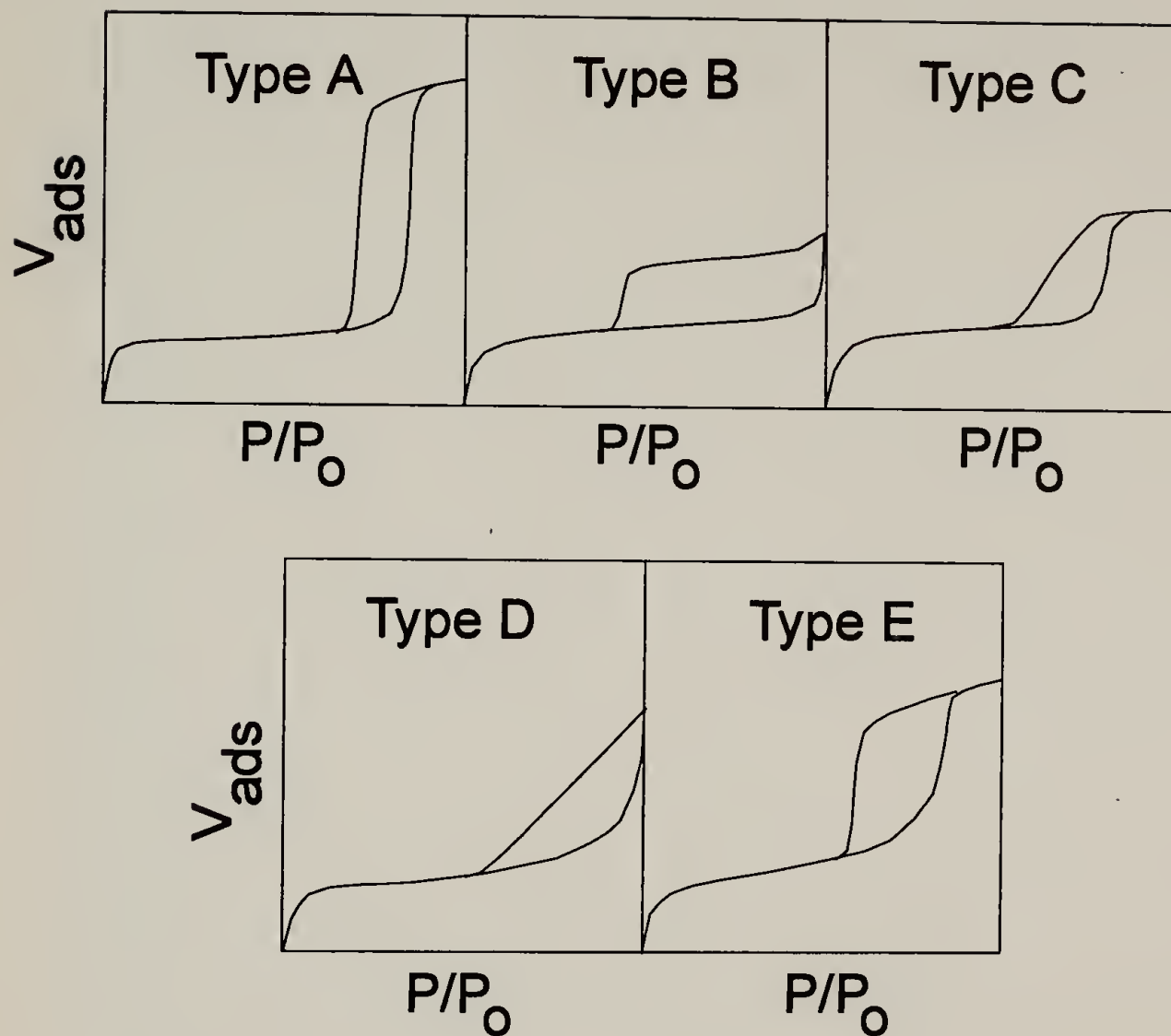


Figure 4.4 Types of Adsorption-Desorption Hysteresis for a Type IV Adsorption Isotherm

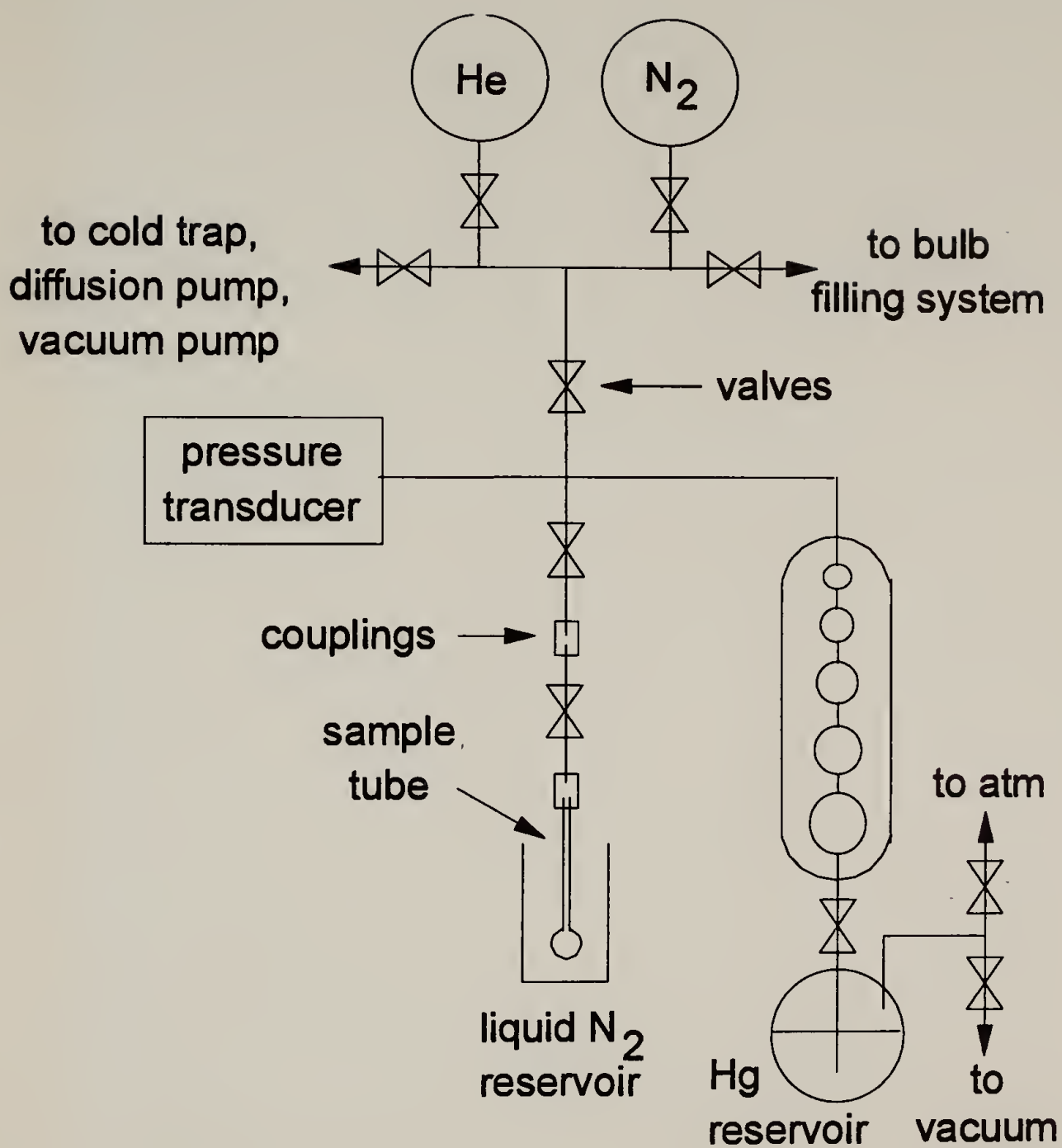


Figure 4.5 Volumetric Static BET Apparatus

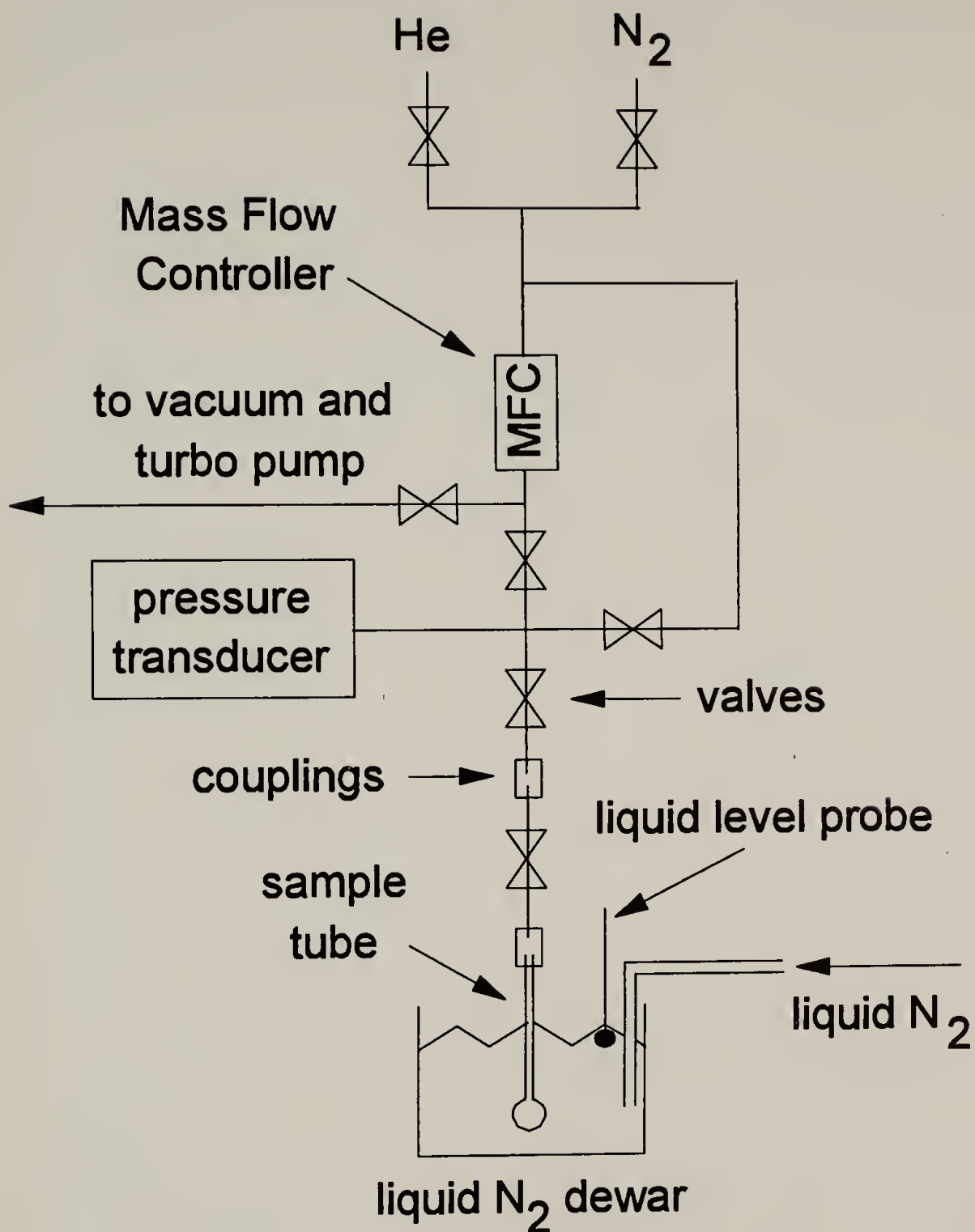


Figure 4.6 Omnisorp™ 100 Adsorption-Desorption Apparatus

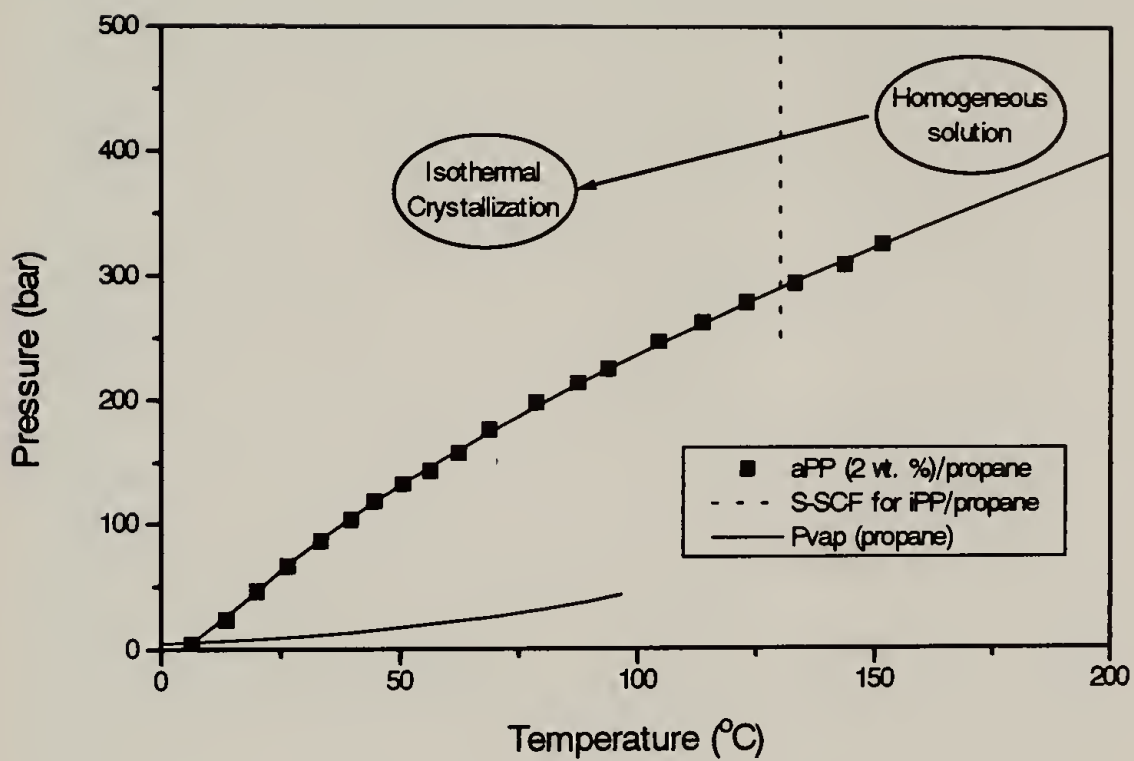
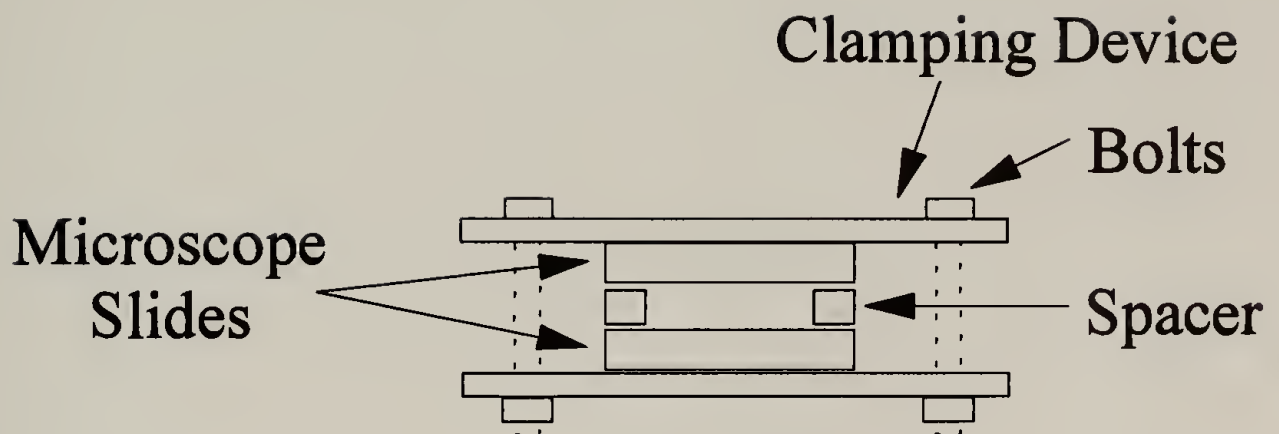


Figure 4.7 Temperature and Pressure Path for Crystallization of Isotactic Polypropylene from Solution in Supercritical Propane



Figure 4.8 Scanning Electron Micrograph for a 20 wt. % iPP Solution in Supercritical Propane Isothermally Crystallized at 80°C



Spacer Material:  
Polyimide or Polycarbonate

Figure 4.9 2-D Crystallization Apparatus

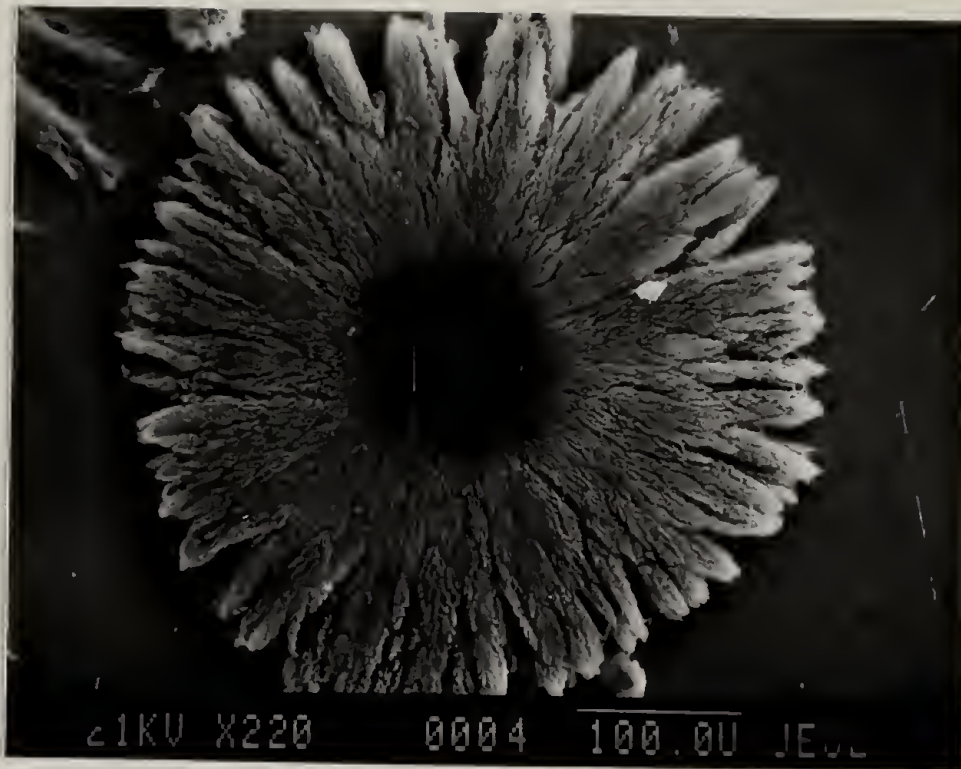


Figure 4.10 Scanning Electron Micrograph for a 20 wt. % iPP Solution in Supercritical Propane Isothermally Crystallized at 80°C in 2-D Crystallization Apparatus (30 $\mu$ m thickness)



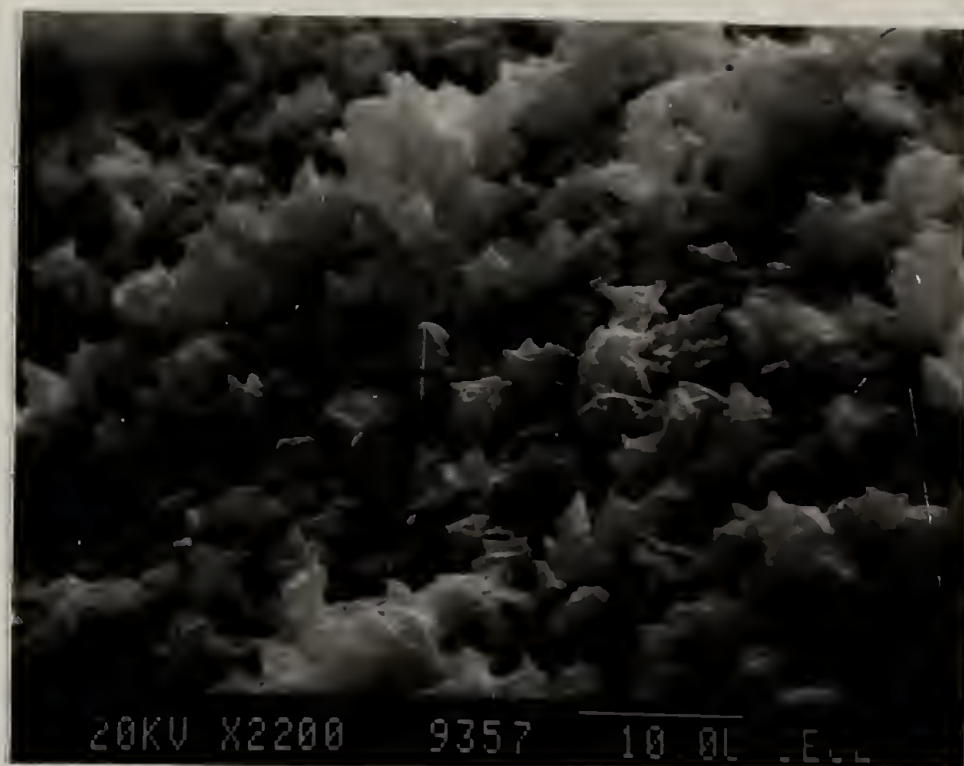


Figure 4.11 Scanning Electron Micrograph for a 20 wt. % iPP Solution in Supercritical Propane Isothermally Crystallized at 100°C

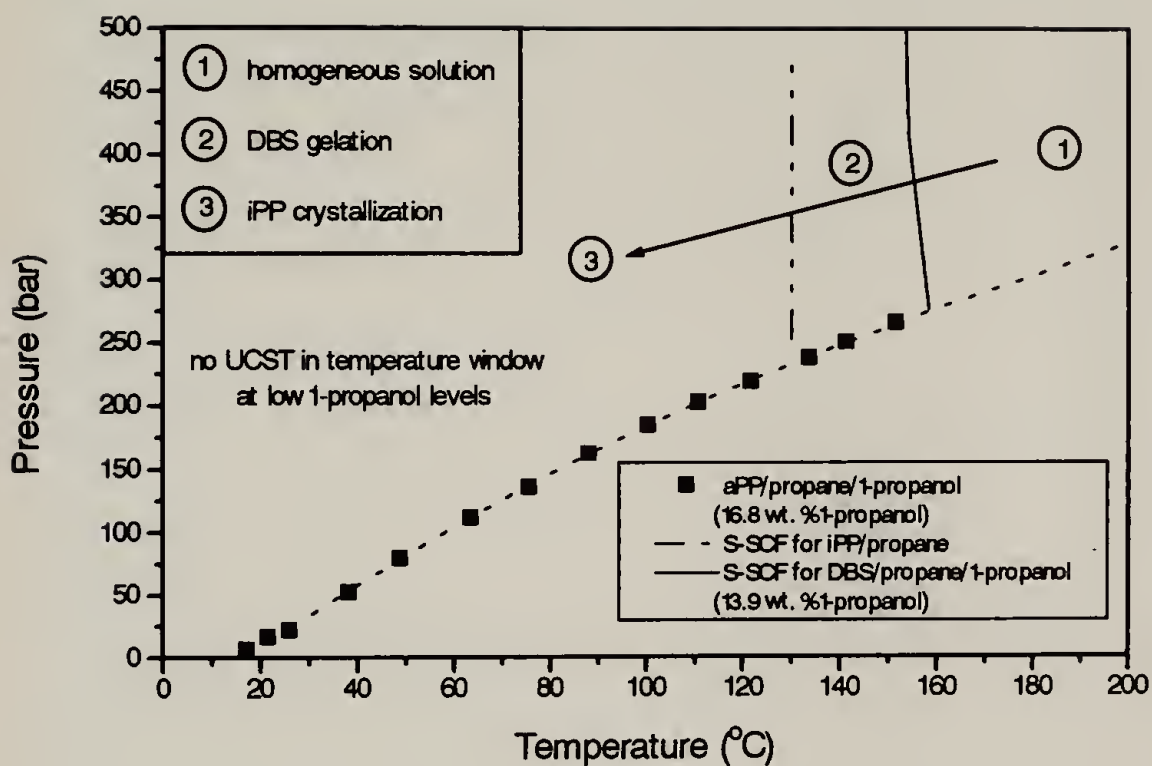


Figure 4.12 Temperature and Pressure Path for Crystallization of Isotactic Polypropylene from Solution in Supercritical Propane/1-Propanol Mixture Containing DBS

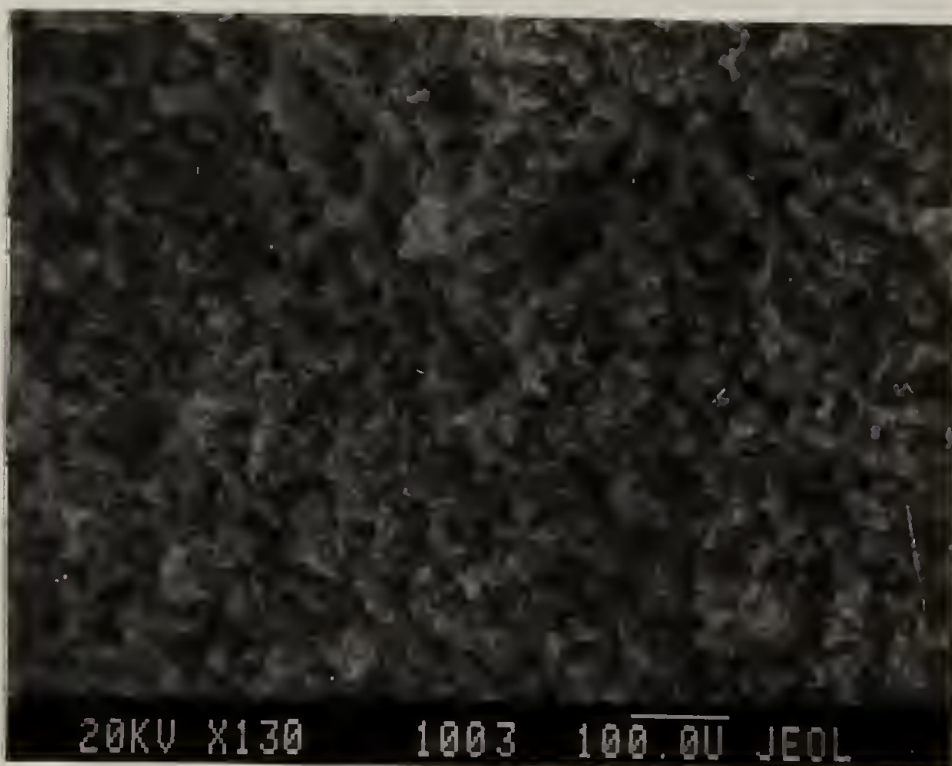


Figure 4.13 Scanning Electron Micrograph for a 20 wt. % iPP Solution in Supercritical Propane/1-Propanol (13.9 wt. % 1-Propanol) Isothermally Crystallized at 80°C Nucleated with DBS

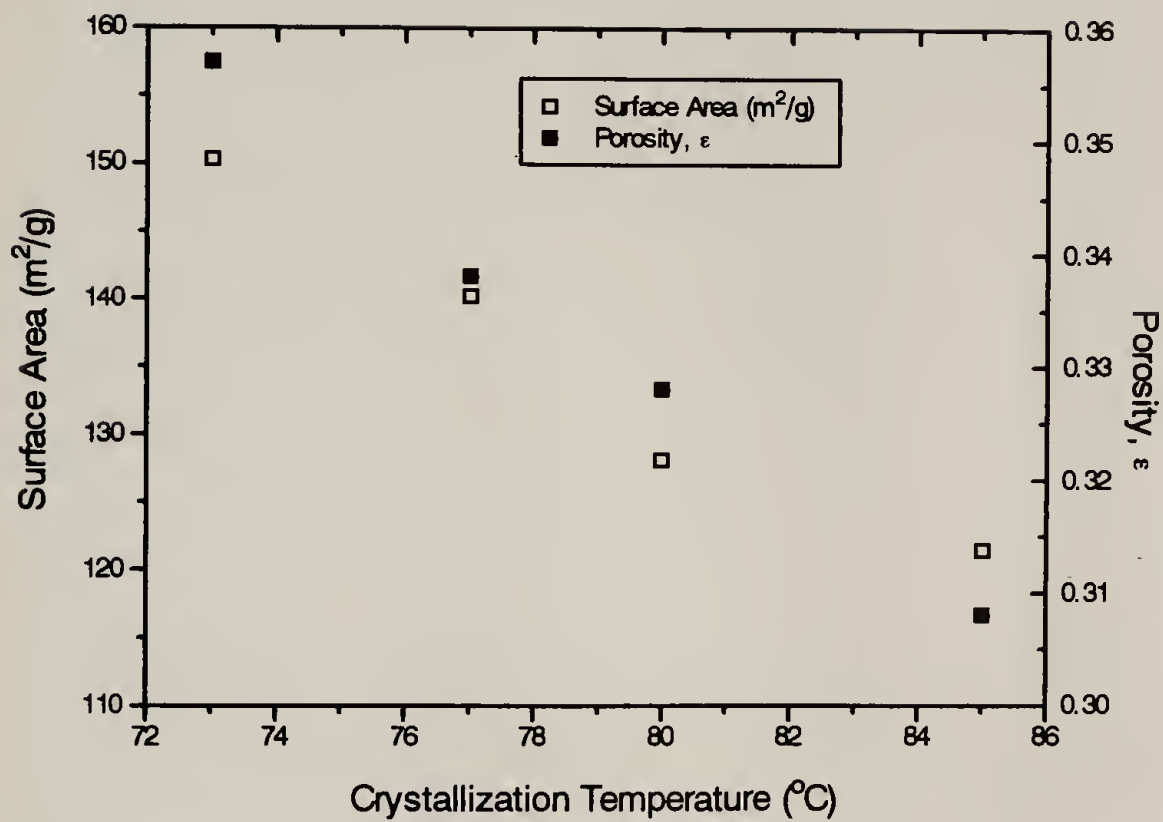


Figure 4.14 Surface Areas and Porosities for Porous iPP Formed by Isothermal Crystallization of 20 wt. % iPP Solutions in Supercritical Propane at Different Temperatures

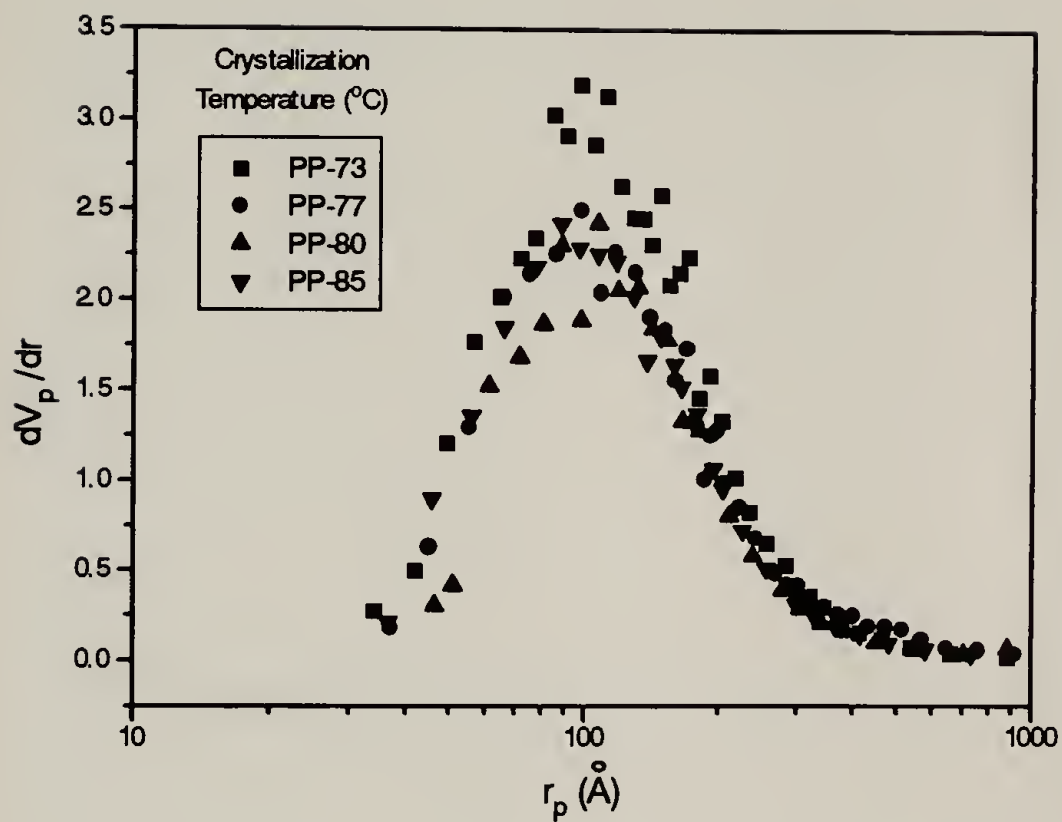


Figure 4.15 Pore Size Distributions for Porous iPP Formed by Isothermal Crystallization of 20 wt. % iPP Solutions in Supercritical Propane at Different Temperatures

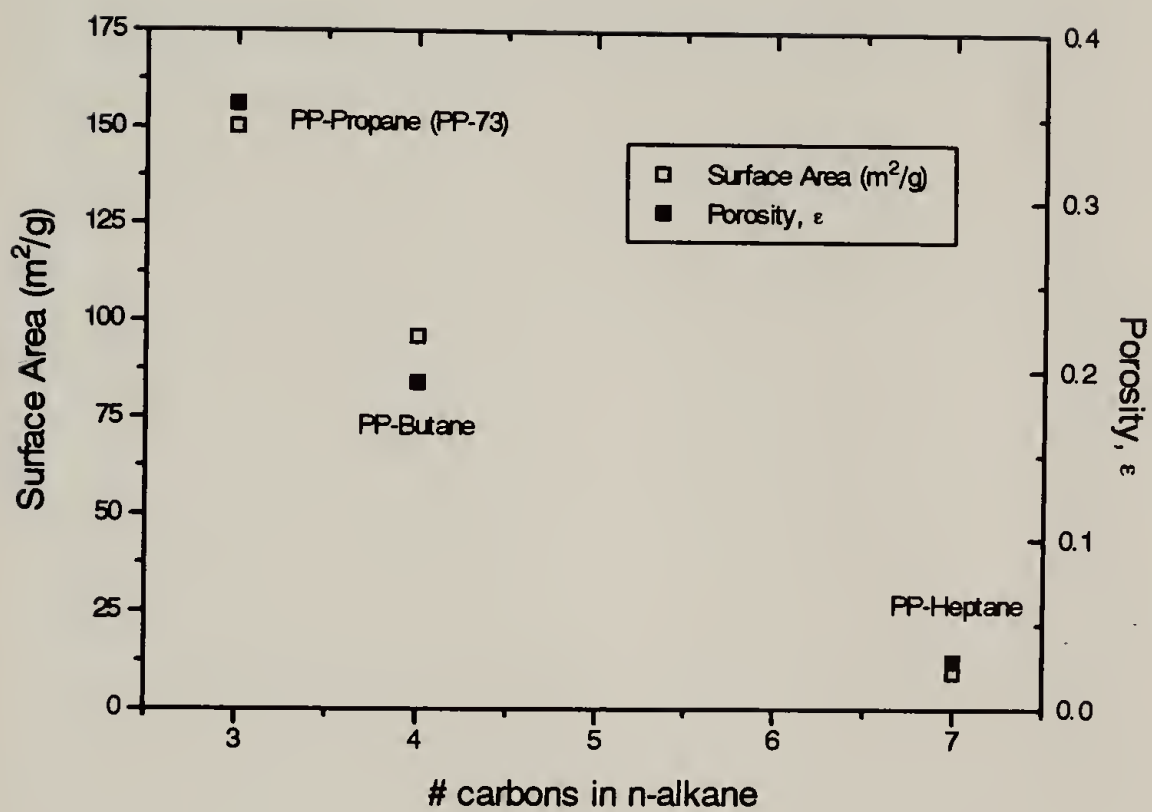


Figure 4.16 Surface Areas and Porosities for Porous iPP Formed by Isothermal Crystallization of 20 wt. % iPP Solutions in Different Alkanes

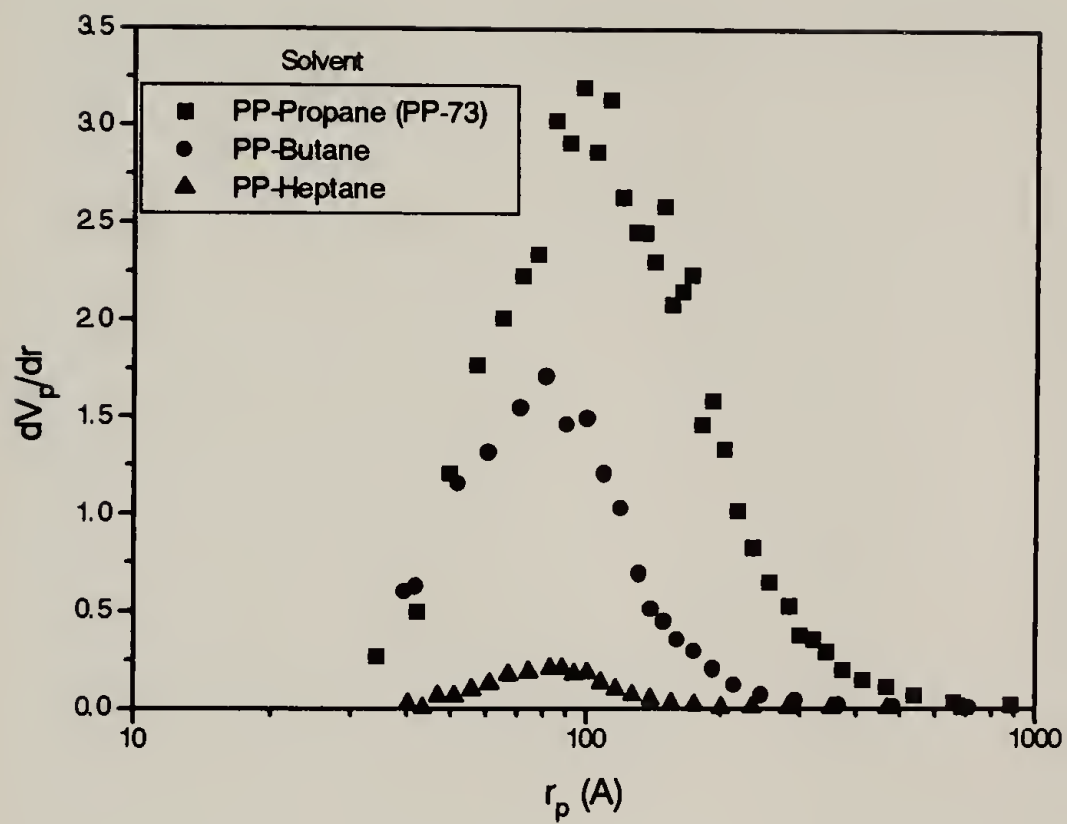


Figure 4.17 Pore Size Distributions for Porous iPP Formed by Isothermal Crystallization of 20 wt. % iPP Solutions in Different Alkanes

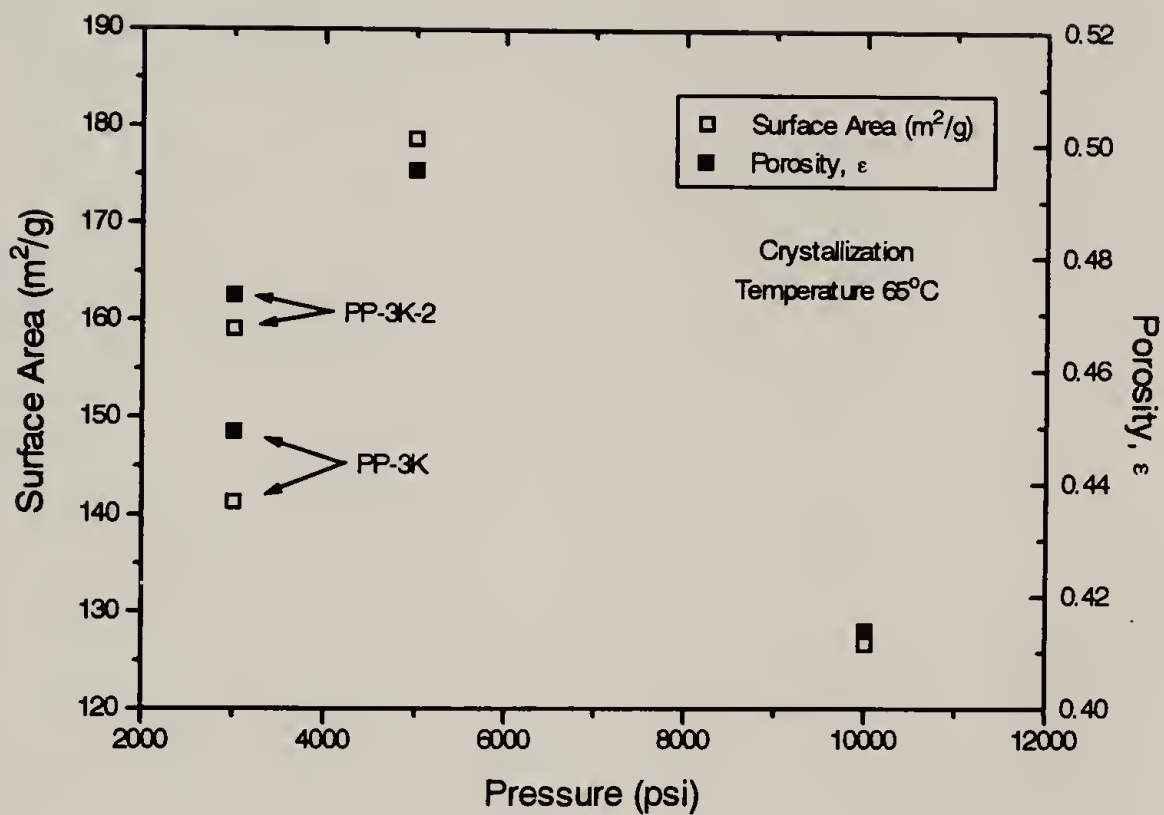


Figure 4.18 Surface Areas and Porosities for Porous iPP Formed by Isothermal Crystallization of 10 wt. % iPP Solutions at 65°C at Different Pressures



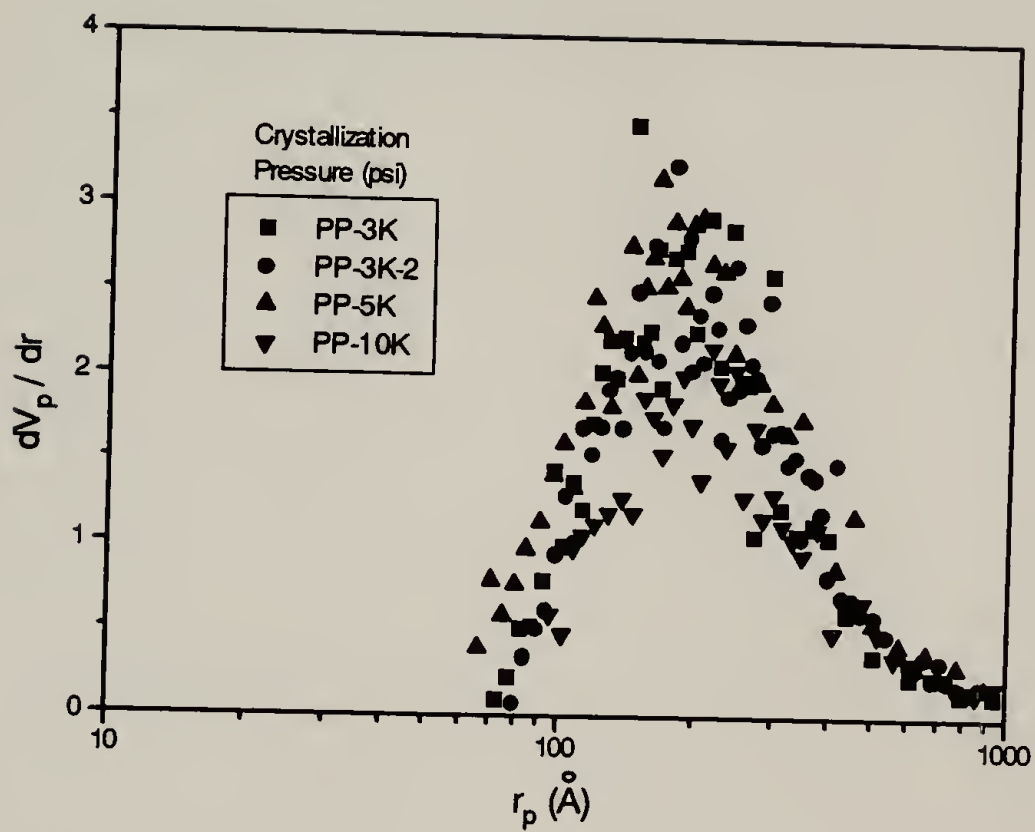


Figure 4.19 Pore Size Distributions for Porous iPP Formed by Isothermal Crystallization of 10 wt. % iPP Solutions at 65°C at Different Pressures

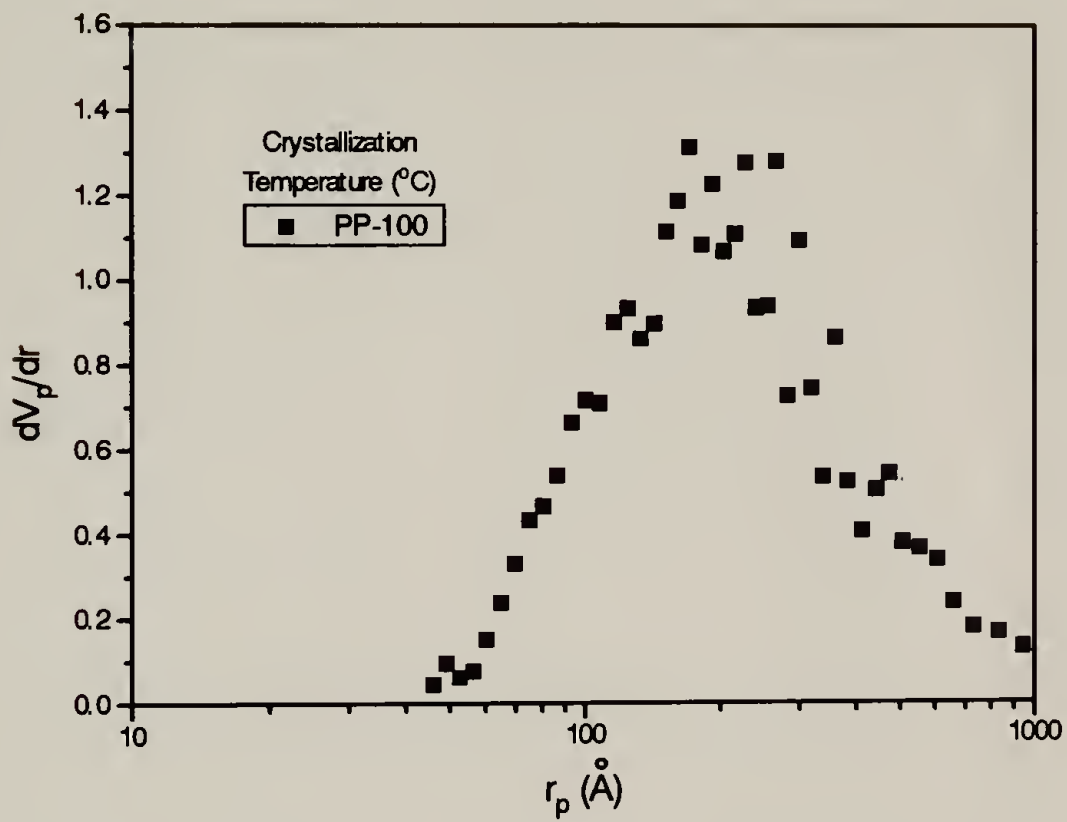


Figure 4.20 Pore Size Distribution for PP-100

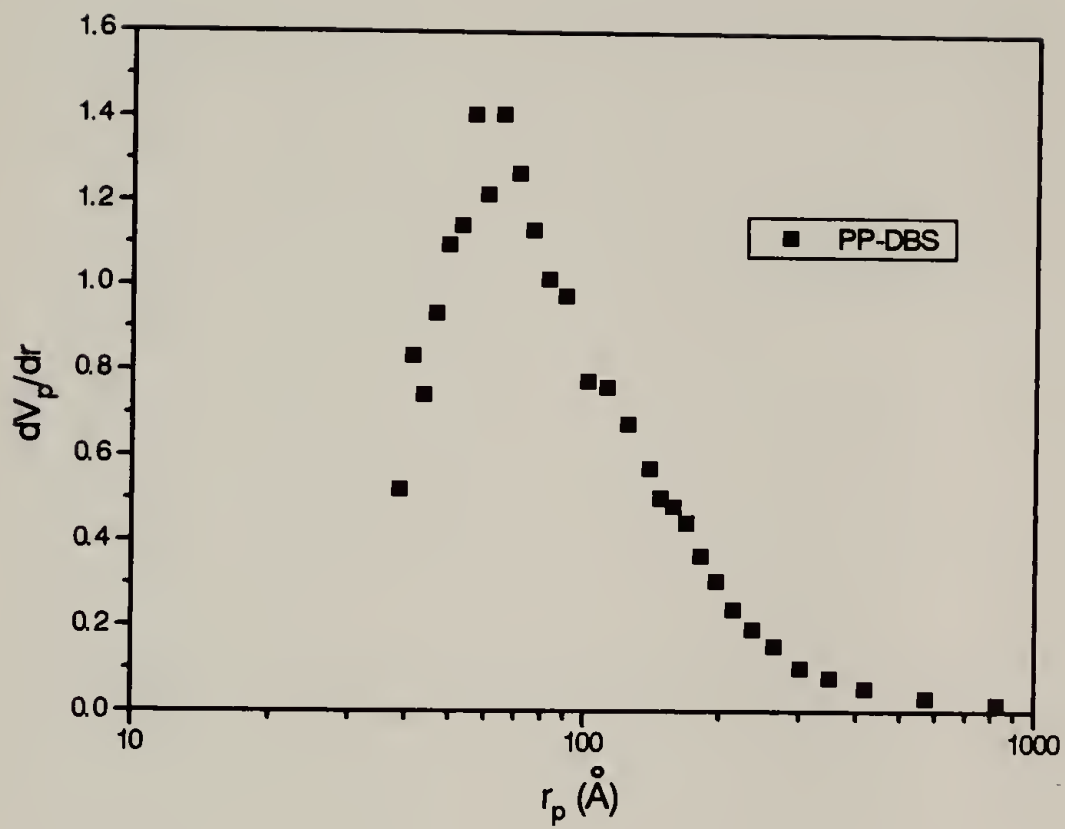


Figure 4.21 Pore Size Distribution for PP-DBS

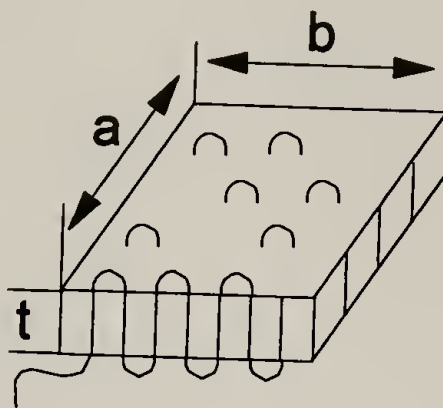


Figure 4.22 Representative Polymer Lamella

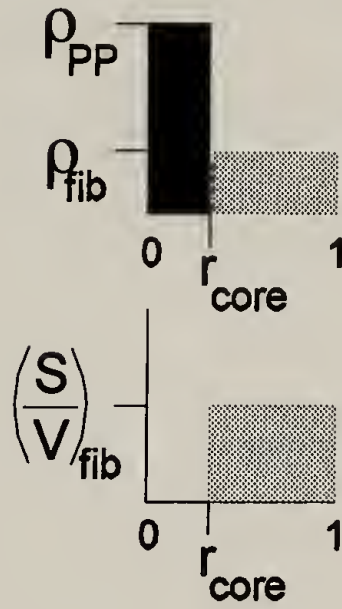
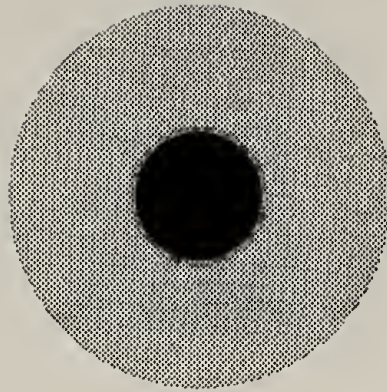


Figure 4.23 Structure for Fibrillation Model

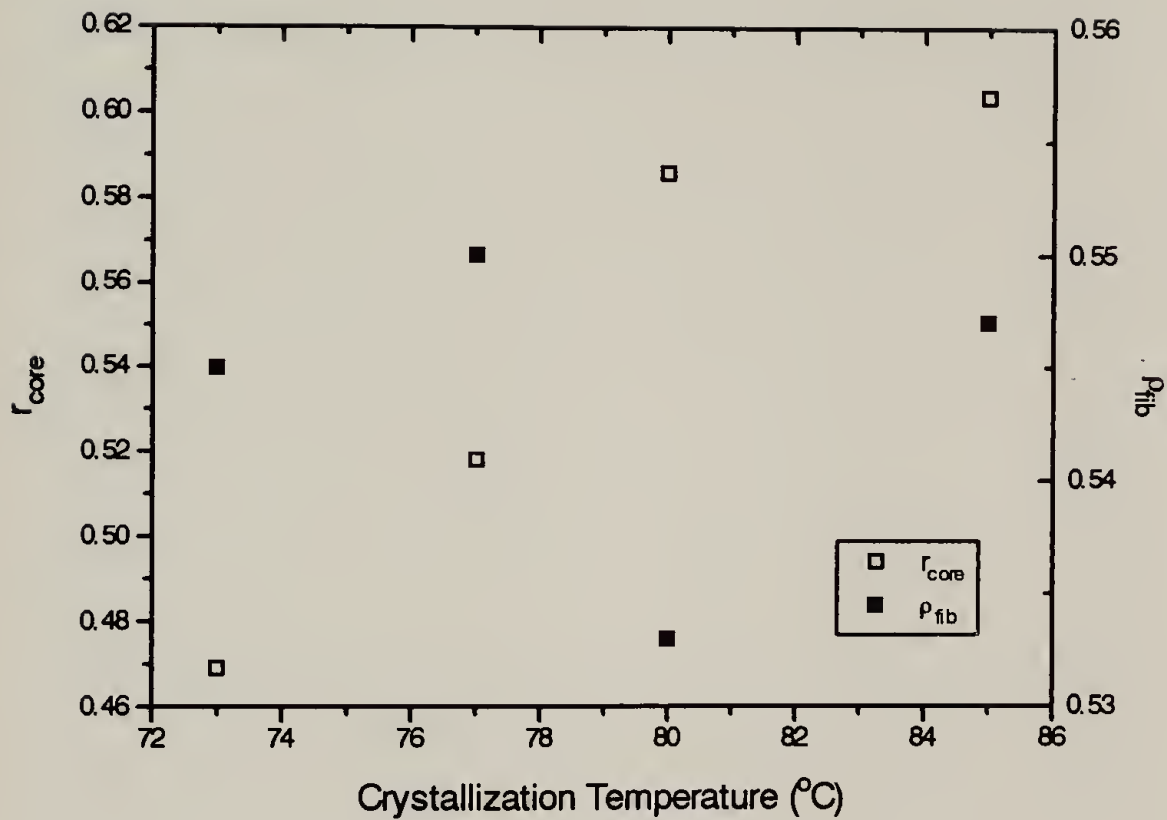


Figure 4.24 Core Radius and Fibrillation Density as Calculated from Fibrillation Model for Porous iPP Isothermally Crystallized from Supercritical Propane at Different Temperatures

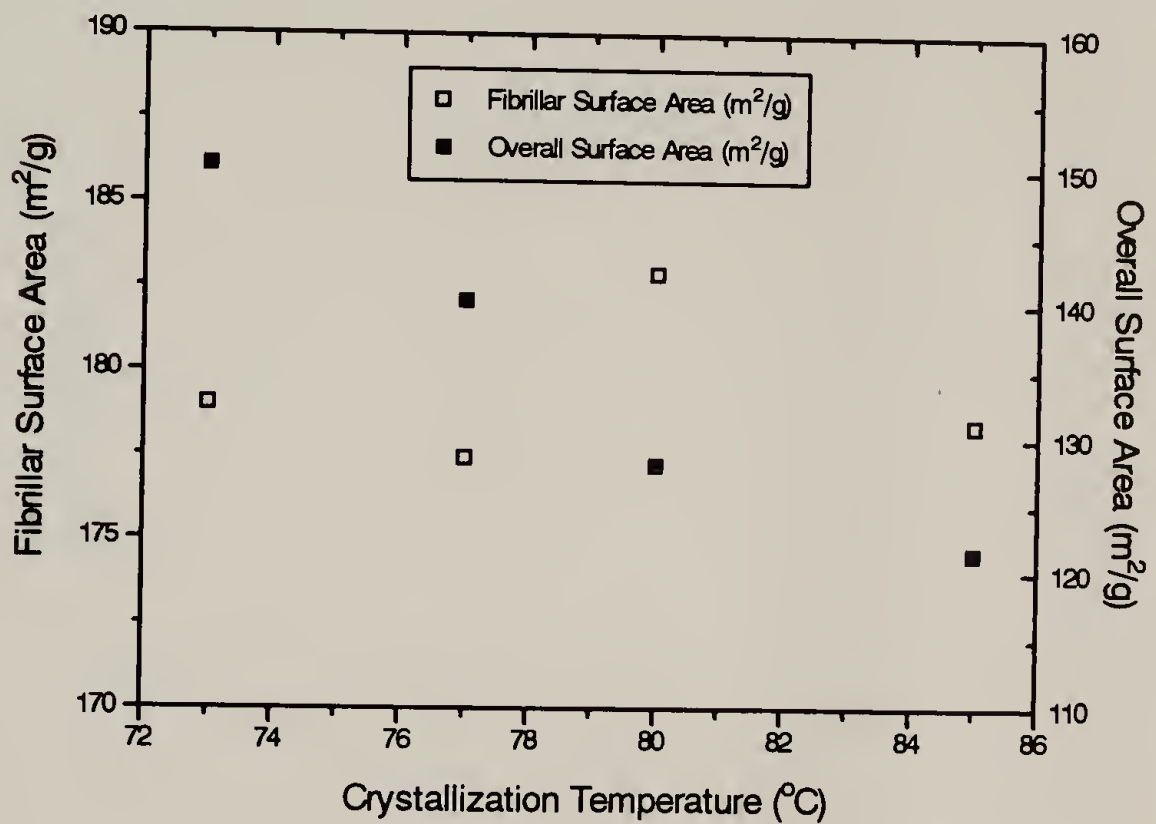


Figure 4.25 Fibrillar Surface Area and Overall Surface Area for Porous iPP Isothermally Crystallized from Supercritical Propane at Different Temperatures

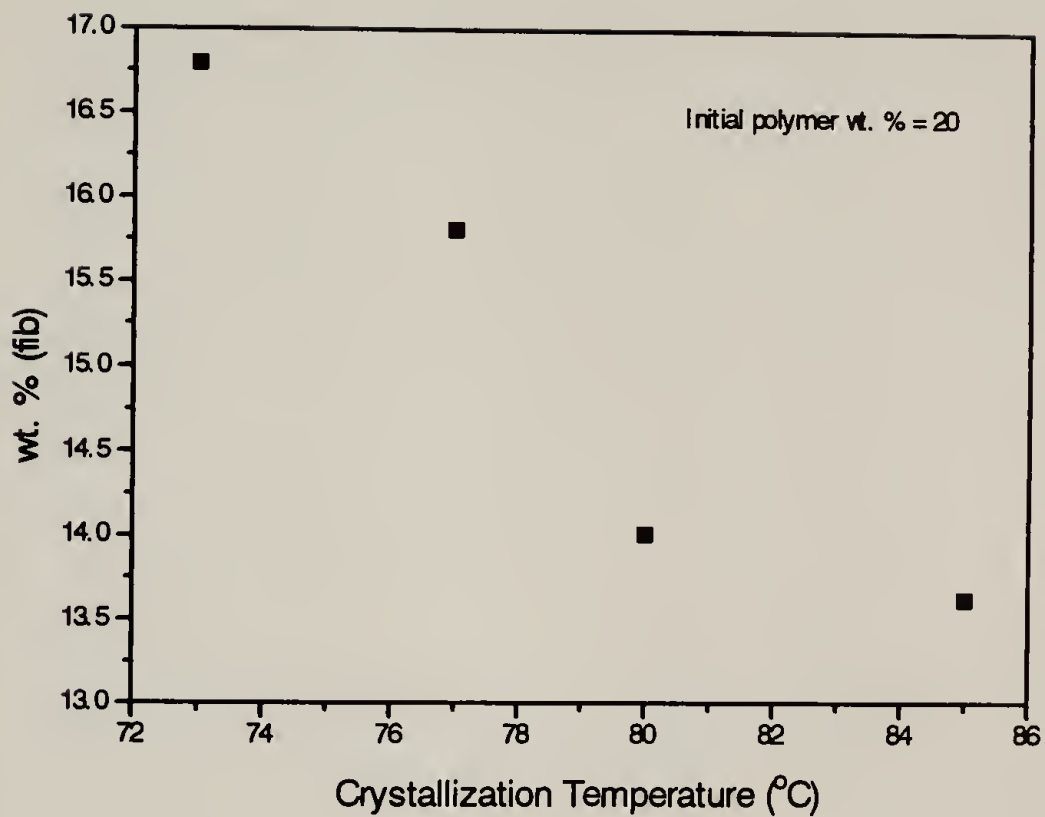


Figure 4.26 Wt. % Polymer Remaining in Solution at the Time of Fibrillation for Porous iPP Isothermally Crystallized from Supercritical Propane at Different Temperatures



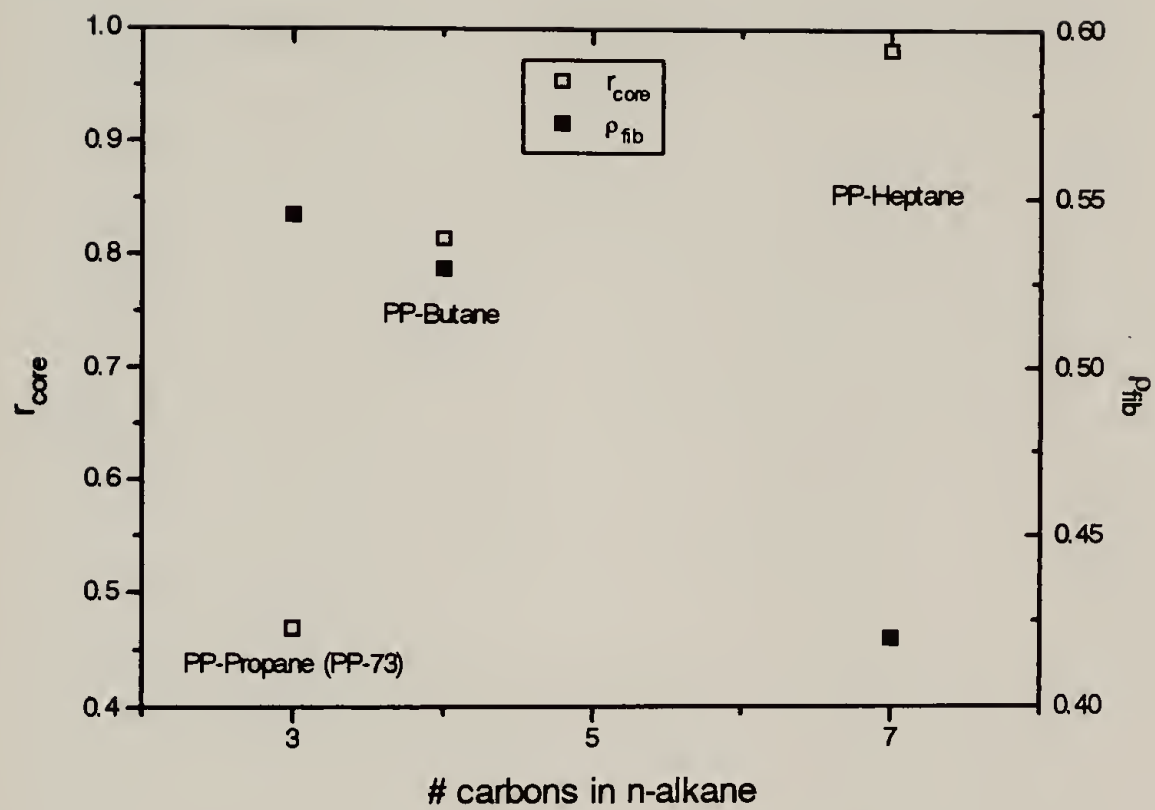


Figure 4.27 Core Radius and Fibrillation Density as Calculated from Fibrillation Model for Porous iPP Isothermally Crystallized from Different Alkane Solvents

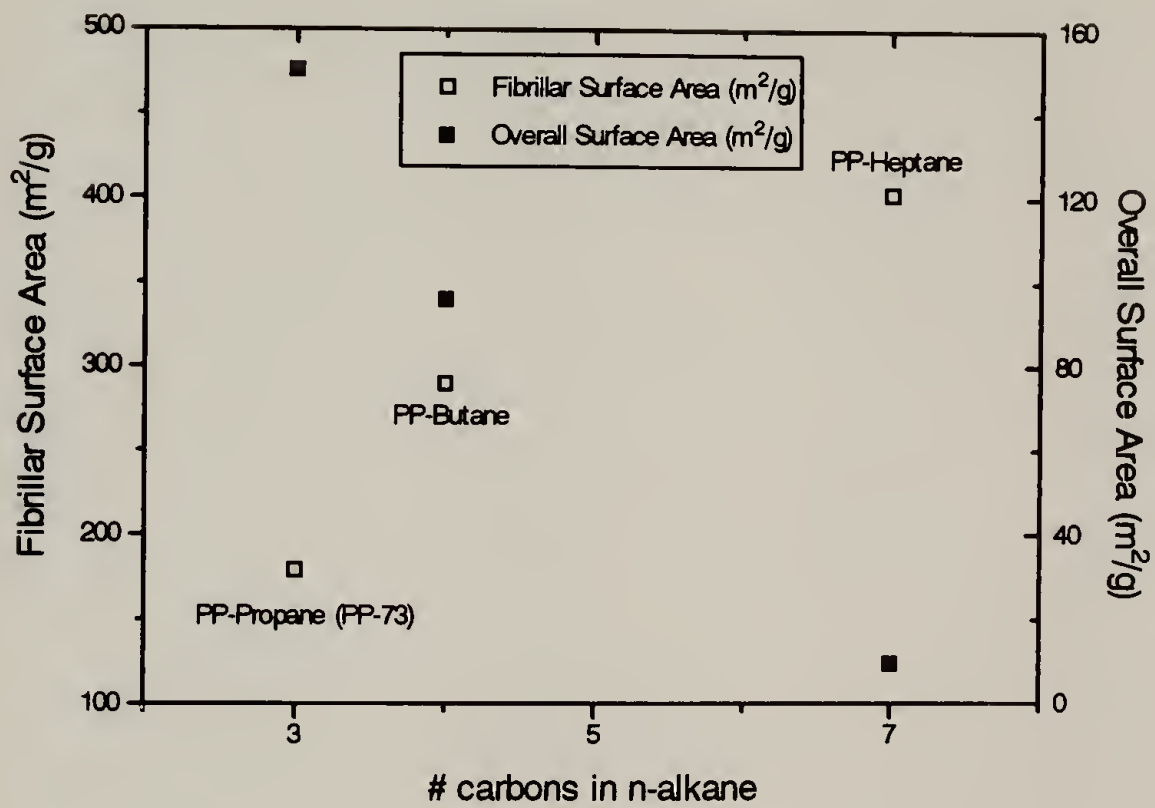


Figure 4.28 Fibrillar Surface Area and Overall Surface Area for Porous iPP Isothermally Crystallized from Different Alkane Solvents

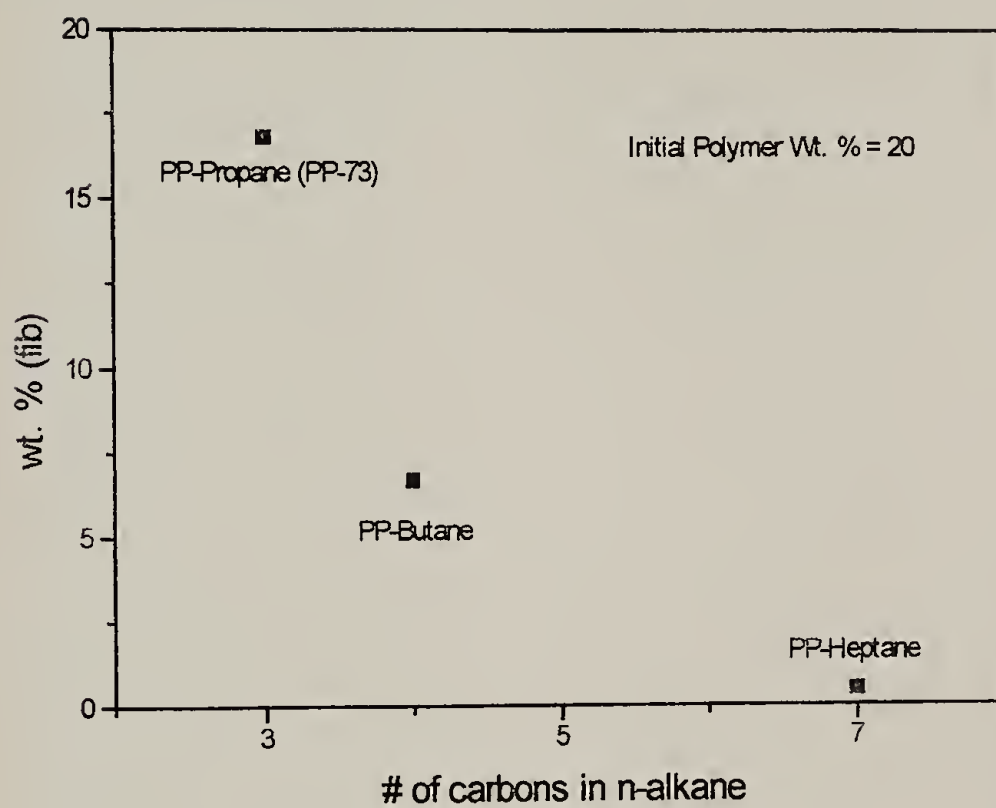


Figure 4.29 Wt. % Polymer Remaining in Solution at the Time of Fibrillation for Porous iPP Isothermally Crystallized from Different Alkane Solvents

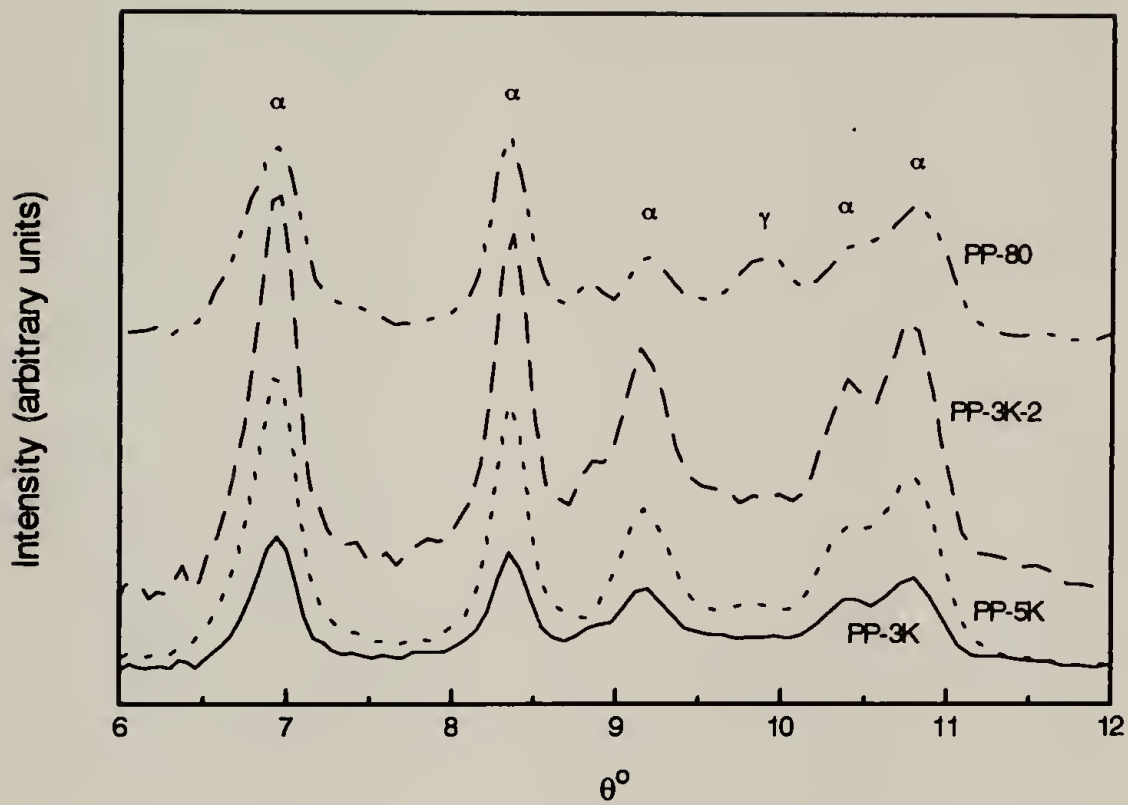


Figure 4.30 Wide Angle X-ray Diffraction (WAXD) Data for Four Porous iPP Samples: PP-80, PP-3K, PP-3K-2, PP-5K

## REFERENCES

- Alwattari, A. A., and D. R. Lloyd, "Microporous Membrane Formation via Thermally-Induced Phase Separation. VI. Effect of Diluent Morphology and Relative Crystallization Kinetics on Polypropylene Membrane Structures," *J. Memb. Sci.*, **64**, 55 (1991).
- Aubert, J. H., "An Objective Characterization of the Cell Size of Microcellular Foams," *J. Cellular Plastics*, **24**, 132 (1988a).
- Aubert, J. H., "Isotactic Polystyrene Phase Diagrams and Physical Gelation," *Macromolecules*, **21**, 3468 (1988b).
- Aubert, J. H., "Structural Coarsening of Demixed Polymer Solutions," *Macromolecules*, **23**, 1446 (1990).
- Beaucage, G., unpublished results, 1995.
- Brunauer, S. L., P. H. Emmett, and E. Teller, "Adsorption of Gases in Multimolecular Layers," *J. Am. Chem. Soc.*, **60**, 309 (1938).
- Brunauer, S., L. S. Deming, W. S. Deming, and E. Teller, "On a Theory of the van der Waals Adsorption of Gases," *J. Am. Chem. Soc.*, **62**, 1723 (1940).
- Bush, P. J., D. Pradhan, and P. Ehrlich, "Lamellar Structure and Organization in Polyethylene Gels Crystallized from Supercritical Solution in Propane," *Macromolecules*, **24**, 1439 (1991).
- Castro, A. J., "Microporous Products," U. S. Patent 4,519,909, (1985).
- Cohan, L. H., "Sorption Hysteresis and the Vapor Pressure of Concave Surfaces," *J. Am. Chem. Soc.*, **60**, 433 (1938).
- Debye, P., and A. M. Bueche, "Scattering by an Inhomogeneous Solid," *J. Appl. Phys.*, **20**, 518 (1949).
- Debye, P., H. R. Anderson, Jr., and H. Brumberger, "Scattering by an Inhomogeneous Solid. II. The Correlation Function and its Application," *J. Appl. Phys.*, **28**(6), 679 (1957).
- Fillon, B., J. C. Wittmann, B. Lotz, and A. Thierry, "Self-Nucleation and Recrystallization of Isotactic Polypropylene ( $\alpha$  Phase) Investigated by Differential Scanning Calorimetry," *J. Polym. Sci. Pt. B. Polym. Phys.*, **31**, 1383 (1993a).

Fillon, B., B. Lotz, A. Thierry, and J. C. Wittmann, "Self-Nucleation and Enhanced Nucleation of Polymers. Definition of a Convenient Calorimetric "Efficiency Scale" and Evaluation of Nucleating Additives in Isotactic Polypropylene ( $\alpha$  Phase)," *J. Polym. Sci. Pt. B. Polym. Phys.*, **31**, 1395 (1993b).

Flory, P. J., *Principles of Polymer Chemistry*, Cornell University Press: Ithaca (1953).

Glatter, O., "Data Treatment," in *Small Angle X-ray Scattering*, O. Glatter and O. Kratky, Eds., Academic Press: London (1982).

Gregg, S. J., and K. S. W. Sing, *Adsorption, Surface Area and Porosity*, 2nd Ed., Academic Press: London (1982).

Halsey, G., "Physical Adsorption on Non-Uniform Surfaces," *J. Chem. Phys.*, **16**(10), 931, (1948).

Hosemann, R., and S. N. Bagchi, *Direct Analysis of Diffraction by Matter*, North-Holland Publishing: Amsterdam (1962).

Keith, H. D., and F. J. Padden, "Spherulitic Crystallization from the Melt. I. Fractionation and Impurity Segregation and Their Influence on Crystalline Morphology," *J. Appl. Phys.*, **35**(4), 1270 (1964).

Khoury, F., "The Spherulitic Crystallization of Isotactic Polypropylene From Solution: On the Evolution of Monoclinic Spherulites From Dendritic Chain-Folded Crystal Precursors," *J. Res. Natl. Bur. Stand.*, **70A**, 29 (1966).

Kim, S. S., and D. R. Lloyd, "Microporous Membrane Formation via Thermally-Induced Phase Separation. III. Effect of Thermodynamic Interactions on the Structure of Isotactic Polypropylene Membranes," *J. Memb. Sci.*, **64**, 13 (1991).

Kim, S. S., G. B. A. Lim, A. A. Alwattari, Y. F. Wang, and D. R. Lloyd, "Microporous Membrane Formation via Thermally-Induced Phase Separation. V. Effect of Diluent Mobility and Crystallization on the Structure of Isotactic Polypropylene Membranes," *J. Memb. Sci.*, **64**, 41 (1991).

Kulkarni, S. K., unpublished results, 1994.

Lauritzen, J. I., and J. D. Hoffman, "Theory of Formation of Polymer Crystals with Folded Chains in Dilute Solution," *J. Res. Nat. Bur. Stand.*, **64A**, 73 (1960).

LeMay, J. D., R. W. Hopper, L. W. Hrubesh, and R. W. Pekala, "Low-Density Microcellular Materials," *MRS Bull.*, **15**, 19 (1990).

Lim, G. B. A., S. S. Kim, Q. Ye, Y. F. Wang, and D. R. Lloyd, "Microporous Membrane Formation via Thermally-Induced Phase Separation. IV. Effect of Isotactic Polypropylene Crystallization Kinetics on Membrane Structure," *J. Memb. Sci.*, **64**, 31 (1991).

Lloyd, D. R., K. E. Kinzer, and H. S. Tseng, "Microporous Membrane Formation via Thermally Induced Phase Separation. I. Solid-Liquid Phase Separation," *J. Mem. Sci.*, **52**, 239 (1990).

Lloyd, D. R., S. S. Kim, and K. E. Kinzer, "Microporous Membrane Formation via Thermally-Induced Phase Separation. II. Liquid-Liquid Phase Separation," *J. Mem. Sci.*, **64**, 1 (1991).

Lopatin, G., L. Yen, and R. R. Rogers, "Microporous Membranes from Polypropylene," U. S. Patent 4,874,567, (1989).

Lotz, B., S. Graff, and J. C. Wittmann, "Crystal Morphology of the  $\gamma$  (Triclinic) Phase of Isotactic Polypropylene and its Relation to the  $\alpha$  Phase," *J. Polym. Sci. Part B: Polym. Phys.*, **24**, 2017 (1986).

Lotz, B., S. Graff, C. Straupé, and J. C. Wittmann, "Single Crystals of  $\gamma$  Phase Isotactic Polypropylene: Combined Diffraction and Morphological Support for a Structure with Non-parallel Chains," *Polymer*, **32**, 2902 (1991).

Lowell, S., and J. E. Shields, *Powder Surface Area and Porosity*, Chapman and Hall: New York (1984).

McGuire, K. S., D. R. Lloyd, and G. B. A. Lim, "Microporous Membrane Formation via Thermally-Induced Phase Separation. VII. Effect of Dilution, Cooling Rate, and Nucleating Agent Addition on Morphology," *J. Memb. Sci.*, **79**, 27 (1993).

Mikhail, R. S., and E. Robens, *Microstructure and Thermal Analysis of Solid Surfaces*, John Wiley & Sons: New York (1983).

Padden, F. J., and H. D. Keith, "Spherulitic Crystallization in Polypropylene," *J. Appl. Phys.*, **30**(10), 1479 (1959).

Padden, F. J., and H. D. Keith, "Crystallization in Thin Films of Isotactic Polypropylene," *J. Appl. Phys.*, **37**, 4013 (1966).

Padden, F. J., and H. D. Keith, "Mechanism for Lamellar Branching In Isotactic Polypropylene," *J. Appl. Phys.*, **44**(3), 1217 (1973).

Pae, K. D., " $\gamma$ - $\alpha$  Solid-Solid Transition of Isotactic Polypropylene," *J. Polym. Sci. Pt. A-2*, **6**, 657 (1968).

Pradhan, D., and P. Ehrlich, "Morphologies of Microporous Polyethylene and Polypropylene Gels Crystallized from Solution in Supercritical Propane," *J. Polym. Sci. Part B: Polym. Phys.*, **33**, 1053 (1995).

Sauer, J. A., D. R. Morrow, and G. C. Richardson, "Morphology of Solution Grown Polypropylene Crystal Aggregates," *J. Appl. Phys.*, **36**, 3017 (1965).

Sawyer, L. C., and D. T. Grubb, *Polymer Microscopy*, Chapman and Hall: New York (1987).

Schmidt, R., E. W. Hansen, M. Stöcker, D. Akporiaye, and O. H. Ellestad, "Pore Size Determination of MCM-41 Mesoporous Materials by means of  $^1\text{H}$  NMR Spectroscopy,  $\text{N}_2$  Adsorption, and HREM. A Preliminary Study," *J. Am. Chem. Soc.*, **117**, 4049 (1995).

Thierry, A., C. Straupé, B. Lotz, and J. C. Wittmann, "Physical Gelation: A Path Towards 'Ideal' Dispersion of Additives in Polymers," *Polym. Comm.*, **31**, 299 (1990).

Thierry, A., B. Fillon, C. Straupé, B. Lotz, and J. C. Wittman, "Polymer Nucleating Agents: Efficiency Scale and Impact of Physical Gelation," *Progr. Colloid Polym. Sci.*, **87**, 28 (1992).

Tsai, F., and J. M. Torkelson, "Roles of Phase Separation Mechanism and Coarsening in the Formation of Poly(methyl methacrylate) Assymmetric Membranes," *Macromolecules*, **23**, 775 (1990a).

Tsai, F., and J. M. Torkelson, "Microporous Poly(methyl methacrylate) Membranes: Effect of Low-Viscosity Solvent on the Formation Mechanism," *Macromolecules*, **23**, 4983 (1990b).

Turner-Jones, A., J. M. Aizlewood, and D. R. Beckett, "Crystalline Forms of Isotactic Polypropylene," *Makromol. Chem.*, **75**, 134 (1964).

Vitzthum, G. H., and M. A. Davis, "0.1 Micron Rated Polypropylene Membrane and Method for its Preparation," U. S. Patent 4,490,431, (1984).

Wunderlich, B., *Macromolecular Physics: Volume 1: Crystal Structure, Morphology, Defects*, Academic Press: New York (1973).



## CHAPTER 5

### CONCLUSIONS AND SUGGESTIONS FOR FUTURE WORK

Conclusions from this work relate to three different areas of research: phase behavior of polymer/supercritical fluid systems, modeling of the phase behavior by the Sanchez-Lacombe lattice fluid theory, and the formation and characterization of porous isotactic polypropylene. The research in all these areas has added to the scientific knowledge base, answering some questions while raising many others. Future work is suggested whose aim is to answer some of these questions.

#### 5.1 Conclusions

##### 5.1.1 Polymer/Supercritical Fluid Phase Behavior

The atactic polypropylene (aPP)/propane system is a Type V system, with a lower critical end point (LCEP) of 279 K, as is the aPP/propylene system in the experimental temperature window. Cloud-point isopleths and solid-supercritical fluid (S-SCF) equilibria for two different molecular weight isotactic polypropylene (iPP) fractions were determined and allowed the estimation of the second critical end point,  $C_2$ . The location of  $C_2$  for iPP/propane systems is at a much lower pressure than that for linear polyethylene/propane [Condo et al., 1992]. Such results are in agreement with previously reported data that suggest that increases in polymer branching decrease the cloud-point pressures in a given supercritical solvent [Chen et al., 1995; Hasch et al., 1993a]. The branching effect was systematically studied by determining the cloud-point pressures for polyolefins with increasing branch length and poly(ethylene-co-octene) copolymers of increasing octene content in supercritical propane. The cloud-point pressures for the various type of polyolefins in supercritical propane studied here and those from the literature [Chen et al., 1995], at constant temperature, correlate well with the percentage of carbon contained in the branches.

Ternary systems of the type aPP/propane/alcohol clearly detail the transition from a Type V system, aPP/propane, to a Type IV system, aPP/alcohol, as a function of the solvent mixture composition. The uniqueness of this system is that the LCEP of the aPP/propane system is at a temperature below the upper critical end point (UCEP) of the aPP/alcohol system. A merging of the upper and lower critical solution temperatures (UCST and LCST) can occur as a function of solvent mixture composition. This merging eliminates the miscibility window along the mixture vapor pressure line which otherwise exists in Type IV systems and has been referred to by some as U-LCST behavior [Chen & Radosz, 1992]. U-LCST behavior depends on the relative shift of the UCST and LCST with solvent mixture composition. In the ternary system with ethanol, U-LCST behavior occurs at low ethanol compositions (<16.8 wt. %). Extrapolating solvent mixture results to the aPP/ethanol system suggests that this binary system would exhibit U-LCST behavior. In the ternary system with 1-propanol, U-LCST behavior occurs at compositions between 16.8 and 31.0 wt. % 1-propanol. A separate UCST and LCST, and corresponding critical end points, are expected to reemerge at 1-propanol compositions above 82.0 wt. % because the aPP/1-propanol system has a separate UCST and LCST. In the ternary system with 1-butanol, U-LCST behavior is not observed for any composition. The shift of the UCEP of the aPP/1-butanol system to lower temperatures and the shift of the LCEP to much higher temperatures, commensurate with the shift in the solvent's critical point, is responsible for the lack of U-LCST behavior. Ternary systems containing higher alcohols are expected to have the same trend with solvent composition as found in the 1-butanol system. Previously, U-LCST behavior had been observed in some systems when the polymer molecular weight reaches a critical value [Zeman & Patterson, 1972; Chen & Radosz, 1992]. This research shows that U-LCST behavior can also occur for certain solvent mixture compositions.

The dissolution of a highly effective polar nucleating agent for iPP, dibenzylidene-d-sorbitol (DBS), in propane/1-propanol mixtures, at low 1-propanol content, shows that

both lower temperatures and pressures are required to achieve dissolution as the 1-propanol content is increased.

### 5.1.2 Modeling of Phase Behavior

For binary systems, the Sanchez-Lacombe lattice fluid (LF) theory has a dimensionless energy and volume parameter which can be adjusted to fit the experimental phase behavior [Sanchez, 1980]. The LCEP for the aPP/propane system predicted by the LF theory, without adjustment to the dimensionless parameters, is 271 K. This is in reasonable agreement with an experimentally determined LCEP of 279 K. However, modeling the LCST over the temperature range investigated requires adjustment to both the dimensionless energy and volume parameters. At a given temperature and pressure, an infinite set of solutions, described by a line, of the dimensionless parameters can appropriately model the phase behavior. A stability analysis of the solution set led to a proposed method for picking a combination of the dimensionless parameters from the solution set. For the aPP/propane system, solutions picked by this method result in the dimensionless volume term,  $\delta$ , obeying a linear function with temperature while the dimensionless energy term,  $\zeta$ , decreases with increasing temperature. The LF theory was selected because previous research on nonpolar polymer/supercritical fluid systems revealed only the need for adjustment of the dimensionless volume parameter [Hasch et al., 1992; Hasch et al., 1993b]. This research shows that this is not universally true for nonpolar systems. Furthermore, modeling of the aPP/propane system suggests that because infinite combinations of dimensionless parameters can describe the experimental phase behavior, additional criteria are required to pick the appropriate dimensionless parameter values. Further information about the system (i.e. density) is required to make more appropriate selections of the dimensionless parameters.

Binodals for two different isotactic polypropylene fractions in supercritical propane were calculated using the LF model and compared to experimental cloud-point isotherms.

The disagreement between the binodal and experimental cloud-point isotherms is probably a result of the polydisperse nature of the isotactic polypropylene fractions [Koningsveld & Staverman, 1968a,b].

Modeling of the ternary system, aPP/propane/1-propanol, was attempted by a pseudo-binary approach proposed by other researchers [Kiran et al., 1993]. This approach involves the formation of a pseudo-solvent from the characteristic parameters of each solvent utilizing mixing rules without dimensionless parameter adjustment. Modeling of the pseudo-solvent/aPP binary system can then be performed. The dimensionless parameters required to fit the observed phase behavior is a complex function of temperature. This is probably a result of having to model both UCST and LCST behavior in that temperature window. Improvements to the modeling of ternary systems by the pseudo-binary approach could be accomplished by modeling the binary solvent system to obtain dimensionless adjustment parameters used in the formation of the pseudo-solvent [Xiong & Kiran, 1994].

### 5.1.3 Formation and Characterization of Porous Isotactic Polypropylene

The morphologies of isotactic polypropylene (iPP) as crystallized from a single phase solution in supercritical propane are qualitatively similar to those obtained by crystallizations from single phase solutions of iPP in high boiling solvents [Lloyd et al., 1990]. The formation of porous microspheres under most conditions from un-nucleated systems agrees with previous researchers results [Lloyd et al., 1990, McGuire et al., 1993]. This suggests that common characteristics of iPP crystallization control the bulk morphology. The absence of information outside of scanning electron micrographs in the literature makes detailed comparisons between the supercritical process and the TIPS process difficult.

One fruitful area for investigation of porous iPP as generated by crystallization from supercritical propane solution was the determination of surface area, porosity, and

pore size distribution by analyzing nitrogen adsorption-desorption isotherms. Surface areas of 90-100 m<sup>2</sup>/g, independent of porosity, were reported for porous iPP formed by liquid-liquid phase separation of n,n-bis(2-hydroxyethyl)tallowamine/iPP solutions [Castro, 1985]. In that study, pore size distributions were obtained by mercury intrusion which is inadequate to determine the dimensions of pores that may account for such surface areas. Analysis of nitrogen adsorption isotherms can yield information about pore sizes of 20-1000 Å which could account for high surface areas. Surface areas in the range of 120-180 m<sup>2</sup>/g and peak pore radii of 100-200 Å were found in almost all porous iPP samples formed by crystallization from supercritical propane. These estimates of pore sizes were supported by small angle x-ray scattering measurements interpreted by a model which treats the pores as a distribution of polydisperse aggregates. The similarity between samples crystallized at a variety of different conditions suggests a common mechanism inherent in iPP crystallization. One possibility is the formation of a lath-like habit for iPP as crystallized from solution which has been observed in thin films [Khoury, 1966; Sauer et al., 1965] and this might be occurring in the three-dimensional structures that are obtained by crystallization from supercritical propane. Another issue is the openness of the spherulite texture as measured by porosity. Porosities increase with increasing degree of supercooling and as the concentration of impurity (solvent) is increased. This dependence of the openness on temperature and with impurity concentration behaves as expected from phenomenological treatments of spherulitic crystallization [Keith & Padden, 1964].

## 5.2 Suggestions for Future Work

Work should be continued investigating the phase behavior of polymers in supercritical fluids. The phase behavior of polyethylene copolymers, particularly those containing polar comonomers, should be studied in greater detail. The effect of comonomer content and cosolvents on the phase behavior should be established. The

study of molecular architecture and its changes in the phase behavior in supercritical solvents should be further elucidated. The phase behavior of a diblock copolymer of ethylene and a branched comonomer should answer questions related to how branch distribution changes the phase behavior. The study of different molecular architectures, perhaps star or dendritic, may also provide interesting results. Changes in the location of the LCEP and LCST of homopolymer polyolefins with long chain branching in supercritical fluids should be studied. This type of study would extend the branching studies presented in this work and suggest whether there is a limiting branch length at which no further decrease in cloud-point pressure is possible. Trends from the polyolefin systems may be applied to structural design of molecules for other supercritical fluids such as CO<sub>2</sub>. Chemical compatibility of polymers in CO<sub>2</sub> is still an issue but the knowledge base of polymers soluble in CO<sub>2</sub> is being expanded [DeSimone et al., 1992].

The work on modeling of polymer/supercritical fluid systems suggests that theories are capable of predicting LCST behavior but good agreement of theory with experiment requires the use of adjustment parameters. Combining rules are used to set values for the interaction parameters but further adjustment is almost always required and is often arbitrary. Additional information on these systems (i.e. density) is required to enhance thermodynamic modeling efforts. With such information, new models can be developed or better criteria for selection of dimensionless parameters can be obtained.

The formation of porous polymeric materials by crystallization from supercritical polymer solutions should be extended to some other crystalline polymers. This would include crystalline polyethylene copolymers, poly(1-butene), and poly(4-methyl-1-pentene). Changes in phase behavior of polar polyethylene copolymers in nonpolar solvents might require the use of cosolvents to modify the phase behavior to obtain desired processing conditions (type of phase separation, pressure, and temperature). Porous materials formed from these systems might require characterization methods, beyond SEM, different from those utilized for porous iPP in this work.

Advances on previously studied systems, such as polyethylene, and polypropylene, requires information during the structure formation. Crystallization rates as well as time-resolved structural features would be very important in elucidating the growth processes. Dilatometric techniques would be ideally suited to the measurement of crystallization rates. This will require the measurement of small volume changes upon crystallization, or alternatively, small pressure drops at constant volume. Special devices would have to be constructed for measuring small volume changes or, alternatively, pressure drops could be magnified by an incompressible system which would magnify small volume changes. Since changes in pressure may change crystallization kinetics or induce a phase separation, processes at constant pressure where volume changes are measured would be preferred. Structural features could be measured by light scattering techniques, however, these efforts would require special cell designs. Transmission of light may depend on the sample conditions and would probably require a scattering path length which could be varied.

Additional studies should investigate, in greater detail, the origins of surface area, porosity, and pore size distribution in porous iPP as generated by crystallization from supercritical propane. The effect of various parameters (i.e. solution concentration, crystallization temperature, and pressure) on the pore characteristics of porous iPP should be investigated in more detail and ideally, would be coupled with crystallization rate measurements. Concentration effects should be determined first and then the influence of molecular parameters such as the stereospecificity of iPP should be investigated. Additional research should also focus on crystallization from supercritical ethane and some nonsupercritical alkanes to determine the effect of solvent. The practical utilization of these materials should be investigated. The reduction of surface area, etc. with elevated temperature should be tested. If surface areas remain high, these materials should be investigated as polymer adsorbents for the removal of organics from gas streams. Surface treatments of such materials should be pursued to evaluate their utility in chromatographic separation applications.

## REFERENCES

- Castro, A. J., "Microporous Products," U. S. Patent 4,519,909, (1985).
- Chen, S., and M. Radosz, "Density-Tuned Polyolefin Phase Equilibria. 1. Binary Solutions of Alternating Poly(ethylene-propylene) in Subcritical and Supercritical Propylene, 1-Butene, and 1-Hexene. Experiment and Flory-Patterson Model," *Macromolecules*, **25**, 3089 (1992).
- Chen, S., M. Banaszak, and M. Radosz, "Phase Behavior of Poly(ethylene-1-butene) in Subcritical and Supercritical Propane: Ethyl Branches Reduce Segment Energy and Enhance Miscibility," *Macromolecules*, **28**, 1812 (1995).
- Condo, P. D., E. J. Colman, and P. Ehrlich, "Phase Equilibria of Linear Polyethylene with Supercritical Propane," *Macromolecules*, **25**, 750 (1992).
- DeSimone, J. M., Z. Guan, and C. S. Elsbernd, "Synthesis of Fluoropolymers in Supercritical Carbon Dioxide," *Science*, **257**, 945 (1992).
- Hasch, B. M., M. A. Meilchen, S. Lee, and M. A. McHugh, "High-Pressure Phase Behavior of Mixtures of Poly(Ethylene-co-Methyl Acrylate) with Low-Molecular Weight Hydrocarbons," *J. Polym. Sci.: Part B: Polym. Phys.*, **30**, 1365 (1992).
- Hasch, B. M., S. Lee, M. A. McHugh, J. J. Watkins, and V. J. Krukonis, "The Effect Of Backbone Structure on the Cloud Point Behavior of Polyethylene-Ethane and Polyethylene-Propane Mixtures," *Polymer*, **34**(12), 2554 (1993a).
- Hasch, B. M., M. A. Meilchen, S. Lee, and M. A. McHugh, "Cosolvency Effects on Copolymer Solutions at High Pressure," *J. Polym. Sci.: Part B: Polym. Phys.*, **31**, 429 (1993b).
- Keith, H. D., and F. J. Padden, "Spherulitic Crystallization from the Melt. I. Fractionation and Impurity Segregation and Their Influence on Crystalline Morphology," *J. Appl. Phys.*, **35**(4), 1270 (1964).
- Khoury, F., "The Spherulitic Crystallization of Isotactic Polypropylene From Solution: On the Evolution of Monoclinic Spherulites From Dendritic Chain-Folded Crystal Precursors," *J. Res. Natl. Bur. Stand.*, **70A**, 29 (1966).
- Kiran, E., Y. Xiong, and W. Zhuang, "Modeling Polyethylene Solutions in Near and Supercritical Fluids Using the Sanchez-Lacombe Model," *J. Supercritical Fluids*, **6**, 193 (1993).



Sanchez, I. C., "Statistical Thermodynamics of Bulk and Surface Properties of Polymer Mixtures," *J. Macromol. Sci.-Phys.*, **B17(3)**, 565 (1980).

Sauer, J. A., D. R. Morrow, and G. C. Richardson, "Morphology of Solution Grown Polypropylene Crystal Aggregates," *J. Appl. Phys.*, **36**, 3017 (1965).

Xiong, Y., and E. Kiran, "Prediction of High-Pressure Phase Behavior in Polyethylene/n-pentane/Carbon Dioxide Ternary System with the Sanchez-Lacombe Model," *Polymer*, **35**, 4408 (1994).

Zeman, L., and D. Patterson, "Pressure Effects in Polymer Solution Phase Equilibria. II. Systems Showing Upper and Lower Critical Solution Temperatures," *J. Phys. Chem.*, **76(8)**, 1214 (1972).

## APPENDIX A

### INDEX OF SUPERCRITICAL FLUID/POLYMER SYSTEMS

The location of lower critical end points (LCEP) as well as the pressure dependence of lower critical solution temperatures (LCST) has been studied in many polymer/solvent systems. The purpose of this appendix is to index systems for which this information is available.

This information is separated into three tables. Table A.1 lists binary systems for which LCEP information only is known. Table A.2 lists binary systems for which LCST data is available. Table A.3 lists ternary systems (solvent/solvent/polymer) for which LCST data is available. When the tables contain multiple entries for both the polymer and the solvent, it does not mean that all polymer/solvent combinations have been studied. In these cases the listed reference will need to be consulted. The remarks column of Tables A.1, A.2, and A.3 details which, if any, important parameters were investigated in a systematic fashion. Table A.4 lists the relationship of the letters found in the remarks column to the parameters investigated in the reference. A list of the abbreviations for the solvents and polymers used in Tables A.1, A.2, and A.3 is found in Table A.5.

Table A.1 LCEP Studies of Binary Polymer/Solvent Systems

Polymer	Solvent(s)	Reference	Remarks*
PE, PP, random P(E-co-P)	various alkanes	Charlet & Delmas, 1981	b,c
PB, P1P, PMP	various alkanes	Charlet et al., 1981	b,c
PP	diethyl ether, pentane, hexane, heptane	Cowie & McEwen, 1974	b
PE, PIB, PDMS, PP, PS	various alkanes, benzene	Freeman & Rowlinson, 1960	b,c

\* - see Table A.4

Table A.2 LCST Studies of Binary Polymer/Solvent Systems

Polymer	Solvent	Reference	Remarks*
P(E-alt-P)	alkenes (propylene, butene, hexene)	Chen & Radosz, 1992	a,b
P(E-co-B)	propane	Chen et al., 1995	c
PE	propane	Condo et al., 1992	a
PEO	water	Cook et al., 1992	a
PE	ethylene	de Loos et al, 1983	a
PE	n-alkanes (C2-C5)	Ehrlich & Kurpen, 1963	b
telechelic PIB (OH endcapped)	ethane, propane, dimethyl ether, carbon dioxide, CDFM	Gregg et al., 1994a,b	d
P(E-co-MA)	ethylene, propylene, ethane, propane	Hasch et al., 1992	b,d
PCL, PMMA	CDFM	Haschets & Shine, 1993	a
PE, P(E-co-MA), P(E-co-AA)	dimethyl ether, butane, butene	Lee et al., 1994	d
P(E-co-MA)	propane, CDFM	Meilchen, et al., 1991	d
PTFE	n-perfluorohexane, perfluorodecalin, Freon <sup>®</sup> 113, Fluorinert <sup>®</sup> FC-75	Tuminello et al., 1995a	
P(TFE-co-HFP)	carbon dioxide	Tuminello et al., 1995b	
PIB, PDMS	alkanes	Zeman et al., 1972	a,b
PS, PPO	methyl acetate, acetone, propane	Zeman & Patterson, 1972	a

\* - see Table A.4

Table A.3 LCST Studies of Ternary Polymer/Solvent/Solvent Systems

Polymer	Solvent System	Reference	Remarks*
P(E-alt-P)	propylene/1-butene ethylene/1-butene ethylene/1-hexene	Chen et al., 1992	
P(E-co-MA)	propane/acetone propane/ethanol	Hasch et al., 1993; Meilchen et al., 1992	d
PS PMMA PBD PVEE	tetrahydrofuran/carbon dioxide	Kiamos & Donohue, 1994	
PE	carbon dioxide/cyclohexane carbon dioxide/toluene carbon dioxide/pentane	Kiran et al., 1993	
P(E-co-P)	ethylene/hexane	McClellan & McHugh, 1985	
P(E-co-P)	hexanes/ethylene hexanes/propylene hexanes/carbon dioxide hexanes/methane	McHugh & Guckes, 1985	
PS	toluene/ethane	Seckner et al., 1988	
Nylon 6	TFEtOH/carbon dioxide	Suresh et al., 1994	

\* - see Table A.4

Table A.4 Definition of Remarks - Relationship to Investigated Parameters

Remark	Parameter Investigated
a	polymer molecular weight
b	solvent
c	polymer structural parameters
d	polarity (solvent or polymer)

Table A.5 List of Solvent and Polymer Abbreviations Used in Tables A.1, A.2 and A.3

<u>Solvent</u>	
CDFM	chlorodifluoromethane
TFEtOH	trifluoroethanol
<u>Polymer</u>	
Nylon 6	polycaprolactam
PB	poly(1-butene)
PBD	polybutadiene
PCL	polycaprolactone
PDMS	polydimethyl siloxane
PE	polyethylene
P(E-alt-P)	poly(ethylene-alt-propylene)
P(E-co-AA)	poly(ethylene-co-acrylic acid)
P(E-co-B)	poly(ethylene-co-butene)
P(E-co-MA)	poly(ethylene-co-methyl acrylate)
P(E-co-O)	poly(ethylene-co-octene)
P(E-co-P)	poly(ethylene-co-propylene)
PEO	poly(ethylene oxide)
PIB	polyisobutylene
PMMA	poly(methyl methacrylate)
PMP	poly(4-methyl-1-pentene)
PP	polypropylene
P1P	poly(1-pentene)
PPO	poly(propylene oxide)
PS	polystyrene
PTFE	polytetrafluoroethylene
P(TFE-co-HFP)	poly(tetrafluoroethylene-co-hexafluoropropylene)
PVEE	poly(vinyl ethyl ether)

## REFERENCES

- Charlet, G., and G. Delmas, "Thermodynamic Properties of Polyolefin Solutions at High Temperature: 1. Lower Critical Solubility Temperatures of Polyethylene, Polypropylene and Ethylene-Propylene Copolymers in Hydrocarbon Solvents," *Polymer*, **22**, 1181 (1981).
- Charlet, G., R. Ducasse, and G. Delmas, "Thermodynamic Properties of Polyolefin Solutions at High Temperature: 2. Lower Critical Solubility Temperatures for Polybutene-1, Polypentene-1, and Poly(4-methylpentene-1) in Hydrocarbon Solvents and the Determination of the Polymer Solvent Interaction-parameter for PB1 and one Ethylene-Propylene Copolymer," *Polymer*, **22**, 1190 (1981).
- Chen, S., and M. Radosz, "Density-Tuned Polyolefin Phase Equilibria. 1. Binary Solutions of Alternating Poly(ethylene-propylene) in Subcritical and Supercritical Propylene, 1-Butene, and 1-Hexene. Experiment and Flory-Patterson Model," *Macromolecules*, **25**, 3089 (1992).
- Chen, S., I. G. Economou, and M. Radosz, "Density-Tuned Polyolefin Phase Equilibria. 2. Multicomponent Solutions of Alternating Poly(ethylene-propylene) in Subcritical and Supercritical Olefins. Experiment and SAFT Model," *Macromolecules*, **25**, 4987 (1992).
- Chen, S., M. Banaszak, and M. Radosz, "Phase Behavior of Poly(ethylene-1-butene) in Subcritical and Supercritical Propane: Ethyl Branches Reduce Segment Energy and Enhance Miscibility," *Macromolecules*, **28**, 1812 (1995).
- Condo, P. D., E. J. Colman, and P. Ehrlich, "Phase Equilibria of Linear Polyethylene with Supercritical Propane," *Macromolecules*, **25**, 750 (1992).
- Cook, R. L., H. E. King, and D. G. Peiffer, "Pressure-Induced Crossover from Good to Poor Solvent Behavior for Polyethylene Oxide in Water," *Phys. Rev. Lett.*, **69**(21), 3072 (1992).
- Cowie, J. M. G., and I. J. McEwen, "Lower Critical Solution Temperatures of Polypropylene Solutions," *J. Polym. Sci.: Polym. Phys. Ed.*, **12**, 441 (1974).
- de Loos, T. W., W. Poot, and G. A. M. Diepen, "Fluid Phase Equilibria in the System Polyethylene + Ethylene. 1. Systems of Linear Polyethylene + Ethylene at High Pressure," *Macromolecules*, **16**, 111 (1983).
- Ehrlich, P., "Phase Equilibria of Polymer-Solvent Systems at High Pressures Near Their Critical Loci. II. Polyethylene-Ethylene," *J. Polym. Sci., Pt. A.*, **3**, 131 (1965).

Ehrlich, P., and J. J. Kurpen, "Phase Equilibria of Polymer-Solvent Systems at High Pressures Near Their Critical Loci: Polyethylene with n-Alkanes," *J. Polym. Sci., Pt. A*, **1**, 3217 (1963).

Folie, B. and M. Radosz, "Phase Equilibria in High-Pressure Polyethylene Technology," *Ind. Chem. Eng. Res.*, **34**, 1501 (1995).

Freeman, P. I., and J. S. Rowlinson, "Lower Critical Points in Polymer Solutions," *Polymer*, **1**, 20 (1960).

Gregg, C. J., F. P. Stein, and M. Radosz, "Phase Behavior of Telechelic Polyisobutylene (PIB) in Subcritical and Supercritical Fluids. 1. Inter- and Intra-Association Effect for Blank, Monohydroxy, and Dihydroxy PIB (1K) in Ethane, Propane, Dimethyl Ether, Carbon Dioxide, and Chlorodifluoromethane," *Macromolecules*, **27**, 4972 (1994a).

Gregg, C. J., F. P. Stein, and M. Radosz, "Phase Behavior of Telechelic Polyisobutylene (PIB) in Subcritical and Supercritical Fluids. 2. PIB Size, Solvent Polarity, and Inter- and Intra-Association Effect for Blank, Monohydroxy, and Dihydroxy PIB (11K) in Ethane, Propane, Carbon Dioxide, and Dimethyl Ether," *Macromolecules*, **27**, 4981 (1994b).

Hasch, B. M., M. A. Meilchen, S. Lee, and M. A. McHugh, "High-Pressure Phase Behavior of Mixtures of Poly(Ethylene-co-Methyl Acrylate) with Low-Molecular Weight Hydrocarbons," *J. Polym. Sci.: Part B: Polym. Phys.*, **30**, 1365 (1992).

Hasch, B. M., M. A. Meilchen, S. Lee, and M. A. McHugh, "Cosolvency Effects on Copolymer Solutions at High Pressure," *J. Polym. Sci.: Part B: Polym. Phys.*, **31**, 429 (1993).

Hasch, B. M., S. Lee, M. A. McHugh, J. J. Watkins, and V. J. Krukonis, "The Effect Of Backbone Structure on the Cloud Point Behavior of Polyethylene-Ethane and Polyethylene-Propane Mixtures," *Polymer*, **34**(12), 2554 (1993).

Haschets, C. W., and A. D. Shine, "Phase Behavior of Polymer-Supercritical Chlorodifluoromethane Solutions," *Macromolecules*, **26**, 5052 (1993).

Kiamos, A. A., and M. D. Donohue, "The Effect of Supercritical Carbon Dioxide on Polymer-Solvent Mixtures," *Macromolecules*, **27**, 357 (1994).

Kiran, E., W. Zhuang, and Y. L. Sen, "Solubility and Demixing of Polyethylene in Supercritical Binary Fluid Mixtures: Carbon-Dioxide-Cyclohexane, Carbon Dioxide-Toluene, Carbon Dioxide-Pentane," *J. Appl. Polym. Sci.*, **47**, 895 (1993).

Lee, S., M. A. LoStracco, and M. A. McHugh, "High-Pressure, Molecular Weight-Dependent Behaviour of (Co)polymer-Solvent Mixtures: Experiments and Modeling," *Macromolecules*, **27**, 4652 (1994).

McClellan, A. K., and M. A. McHugh, "Separating Polymer Solutions Using High Pressure Lower Critical Solution Temperature (LCST) Phenomena," *Polym. Eng. and Sci.*, **25**(17), 1088 (1985).

McHugh, M. A., and T. L. Guckes, "Separating Polymer Solutions with Supercritical Fluids," *Macromolecules*, **18**, 674 (1985).

Meilchen, M. A., B. M. Hasch, and M. A. McHugh, "Effect of Copolymer Composition on the Phase Behavior of Poly(ethylene-co-methyl acrylate) with Propane and Chlorodifluoromethane," *Macromolecules*, **24**, 4874 (1991).

Meilchen, M. A., B. M. Hasch, S. Lee, and M. A. McHugh, "Poly(ethylene-co-methyl acrylate)-solvent-cosolvent Phase Behavior at High Pressures," *Polymer*, **33**, 1922 (1992).

Seckner, A. J., A. K. McClellan, and M. A. McHugh, "High-Pressure Solution Behavior of the Polystyrene-Toluene-Ethane System," *AIChE J.*, **34**(1), 9 (1988).

Suresh, S. J., R. M. Enick, and E. J. Beckman, "Phase Behavior of Nylon 6/Trifluoroethanol/Carbon Dioxide Mixtures," *Macromolecules*, **27**, 348 (1994).

Tuminello, W. H., D. J. Brill, D. J. Walsh, and M. E. Paulaitis, "Dissolving Poly(tetrafluoroethylene) in Low Boiling Halocarbons," *J. Appl. Polym. Sci.*, **56**, 495 (1995a).

Tuminello, W. H., G. T. Dee, and M. A. McHugh, "Dissolving Perfluoropolymers in Supercritical Carbon Dioxide," *Macromolecules*, **28**, 1506 (1995b).

Zeman, L., and D. Patterson, "Pressure Effects in Polymer Solution Phase Equilibria. II. Systems Showing Upper and Lower Critical Solution Temperatures," *J. Phys. Chem.*, **76**(8), 1214 (1972).

Zeman, L., J. Biros, G. Delmas, and D. Patterson, "Pressure Effects in Polymer Solution Phase Equilibria. I. The Lower Critical Solution Temperature of Polyisobutylene and Polydimethylsiloxane in Lower Alkanes," *J. Phys. Chem.*, **76**(8), 1206 (1972).



## APPENDIX B

### ADSORPTION-DESORPTION ISOTHERMS AND SAXS DATA

This appendix contains the original adsorption-desorption isotherms and small angle x-ray scattering data used to obtain surface areas, porosity, and pore size distributions.

Reproducibility of data obtained for BET and pore size distribution analysis from the experimental apparatuses was verified. The reproducibility of adsorption isotherms for BET analysis is very good. For example, surface areas for PP-5K obtained on two consecutive runs were 178.6 and 178.2 m<sup>2</sup>/g with correlation coefficients of 0.9998 and 0.9999, respectively. Multiple BET runs for other samples yielded similar results where the surface area varies by ~ +/- 1%. Adsorption isotherms obtained on the Omnisorp™ 100 agree with the BET isotherms obtained on the static BET apparatus. This is further proof of data reproducibility. The adsorption-desorption hysteresis is also highly reproducible. Figure B.1 shows two separate adsorption-desorption runs determined for a porous isotactic polypropylene membrane (provided by Minnesota Mining and Manufacturing (3M) and denoted as PP-3M) compared to each other along with isotherm points determined on the static BET apparatus.

Porous isotactic polypropylenes prepared by crystallization from supercritical polymer solutions were stored at room temperature which is above  $T_g$  of the polymer. Rearrangement of the amorphous material over time might result in changes in surface areas and pore size distributions. BET surface areas, obtained on the same sample at different times show that the material does not change significantly over time. Table B.1 shows BET surfaces areas, obtained on different dates, from three different samples.

Table B.1 BET Parameters for Porous iPP on Different Dates

Sample	Date	BET Surface Area, (m <sup>2</sup> /g)	BET C Constant	Correlation Coefficient, r <sup>2</sup>
PP-80	12/14/94	129.7	22.6	0.9999
PP-80	3/24/95	128.1	23.1	0.9995
PP-3K-2	2/14/95	159.2	21.8	0.9999
PP-3K-2	3/27/95	160.5	23.1	0.9999
PP-10K	2/8/95	126.2	18.2	0.9999
PP-10K	3/24/95	124.9	16.8	0.9999

The later runs for PP-3K-2 and PP-10K were performed after adsorption of propane at -40°C was attempted. Exposure of the sample to a gas that may have been soluble in the amorphous phase did not change the surface area.

### B.1 Temperature History

The adsorption-desorption isotherms determined with the volumetric static BET apparatus and the Omnisorp™ 100 apparatus are shown in Figures B.2-5 for PP-73, PP-77, PP-80, and PP-85, respectively. Small angle x-ray scattering (SAXS) data is shown in Figure B.6 for PP-73, PP-77, PP-80, and PP-85. The SAXS data on all these samples were provided by Dr. Greg Beaucage of the University of Cincinnati.

The surface areas, BET C constant, and correlation coefficient for the BET plot are included in Table B.2. The Halsey constant, Halsey exponent, and surface area determined from analysis of the adsorption branch with a cylindrical pore model as compared to the BET surface area is shown in Table B.3. Table B.4 contains the Maxwell distribution parameters, and correlation coefficient for fitting the SAXS data to the Hosemann model.

**Table B.2 BET Parameters for Porous iPP Isothermally Crystallized at Different Temperatures**

Sample	BET Surface Area, (m <sup>2</sup> /g)	BET C Constant	Correlation Coefficient, r <sup>2</sup>
PP-73	150.3	22.7	0.99949
PP-77	140.2	22.5	0.99985
PP-80	128.1	23.1	0.99950
PP-85	121.5	22.1	0.99988

**Table B.3 Adsorption-Desorption Parameters for Porous iPP Isothermally Crystallized at Different Temperatures**

Sample	Halsey Constant	Halsey Exponent	PSD Surface Area (m <sup>2</sup> /g)	BET Surface Area, (m <sup>2</sup> /g)
PP-73	4.4	1.83	156.6	150.3
PP-77	4.57	1.84	132.5	140.2
PP-80	5.86	1.65	116.5	128.1
PP-85	4.36	1.80	123.4	121.5

Table B.4 Hosemann Model Parameters for Porous iPP Isothermally Crystallized at Different Temperatures

Sample	$y_0$	n	$A_0$	Correlation Coefficient, $r^2$
PP-73	77.7	2.88	2.75	0.9955
PP-77	66.5	3.77	0.93	0.9959
PP-80	92.1	1.52	1.93	0.9355
PP-85	129.4	0.84	0.35	0.9638

## B.2 Solvent

The adsorption-desorption isotherms determined with the volumetric static BET apparatus and the Omnisorp™ 100 apparatus are shown in Figures B.7-8 for PP-Butane and PP-Heptane, respectively. Small angle x-ray scattering (SAXS) data is shown in Figures B.9 for PP-Propane (PP-73), PP-Butane, PP-Heptane. The SAXS data on all these samples were provided by Dr. Greg Beaucage of the University of Cincinnati.

The surface areas, BET C constant, and correlation coefficient for the BET plot are included in Table B.5. The Halsey constant, Halsey exponent, and surface area determined from analysis of the adsorption branch with a cylindrical pore model as compared to the BET surface area is shown in Table B.6. Table B.7 contains the Maxwell distribution parameters, and correlation coefficient for fitting the SAXS data to the Hosemann model.

Table B.5 BET Parameters for Porous iPP Isothermally Crystallized from Different Alkanes

Sample	BET Surface Area, (m <sup>2</sup> /g)	BET C Constant	Correlation Coefficient, r <sup>2</sup>
PP-Propane (PP-73)	150.3	22.7	0.99949
PP-Butane	96.6	22.4	0.99984
PP-Heptane	10.0	12.9	0.98517

Table B.6 Adsorption-Desorption Parameters for Porous iPP Isothermally Crystallized from Different Alkanes

Sample	Halsey Constant	Halsey Exponent	PSD Surface Area (m <sup>2</sup> /g)	BET Surface Area, (m <sup>2</sup> /g)
PP-Propane (PP-73)	4.4	1.83	156.6	150.3
PP-Butane	5.29	1.50	72.3	96.6
PP-Heptane	5.26	1.17	6.7	10.0

Table B.7 Hosemann Model Parameters for Porous iPP Isothermally Crystallized from Different Alkanes

Sample	$y_0$	n	$A_0$	Correlation Coefficient, $r^2$
PP-Propane (PP-73)	77.7	2.88	2.75	0.9955
PP-Butane	103.3	1.01	0.41	0.9223
PP-Heptane	77.1	1.87	0.19	0.9801

## B.2 Pressure

The adsorption-desorption isotherms determined with the volumetric static BET apparatus and the Omnisorp™ 100 apparatus are shown in Figures B.10-13 for PP-3K, PP-3K-2, PP-5K, and PP-10K, respectively. Small angle x-ray scattering (SAXS) data is shown in Figures B.14 for PP-3K, PP-3K-2, and PP-5K. SAXS data was not obtained for PP-10K. The SAXS data on all these samples were provided by Dr. Greg Beaucage of the University of Cincinnati.

The surface areas, BET C constant, and correlation coefficient for the BET plot are included in Table B.8. The Halsey constant, Halsey exponent, and surface area determined from analysis of the adsorption branch with a cylindrical pore model as compared to the BET surface area is shown in Table B.9. Table B.10 contains the Maxwell distribution parameters, and correlation coefficient for fitting the SAXS data to the Hosemann model.

**Table B.8 BET Parameters for Porous iPP Isothermally Crystallized at Different Pressures**

Sample	BET Surface Area, (m <sup>2</sup> /g)	BET C Constant	Correlation Coefficient, r <sup>2</sup>
PP-3K	141.3	18.2	0.99994
PP-3K-2	159.1	22.0	0.99989
PP-5K	178.7	21.6	0.99990
PP-10K	126.7	18.2	0.99996

**Table B.9 Adsorption-Desorption Parameters for Porous iPP Isothermally Crystallized at Different Pressures**

Sample	Halsey Constant	Halsey Exponent	PSD Surface Area (m <sup>2</sup> /g)	BET Surface Area, (m <sup>2</sup> /g)
PP-3K	5.13	1.72	125.9	141.3
PP-3K-2	5.87	1.66	124.4	159.1
PP-5K	4.84	1.85	150.2	178.7
PP-10K	5.90	1.65	90.2	126.7

Table B.10 Hosemann Model Parameters for Porous iPP Isothermally Crystallized at Different Pressures

Sample	$y_0$	$n$	$A_0$	Correlation Coefficient, $r^2$
PP-3K	120.9	1.66	4.35	0.99393
PP-3K-2	125.9	1.22	6.66	0.9784
PP-5K	133.9	0.97	4.28	0.9895
PP-10K	*	*	*	*

\* - SAXS data not obtained for this sample

### B.3 Miscellaneous

The adsorption-desorption isotherms determined with the volumetric static BET apparatus and the Omnisorp™ 100 apparatus are shown in Figures B.15-16 for PP-100 and PP-DBS, respectively. Small angle x-ray scattering (SAXS) data was not obtained on these samples.

The surface areas, BET C constant, and correlation coefficient for the BET plot are included in Table B.11. The Halsey constant, Halsey exponent, and surface area determined from analysis of the adsorption branch with a cylindrical pore model as compared to the BET surface area is shown in Table B.12.



**Table B.11 BET Parameters for Porous iPP Isothermally Crystallized from Propane at Different Conditions**

Sample	BET Surface Area, (m <sup>2</sup> /g)	BET C Constant	Correlation Coefficient, r <sup>2</sup>
PP-100	125.5	19.7	0.99986
PP-DBS	87.0	23.7	0.99977

**Table B.12 Adsorption-Desorption Parameters for Porous iPP Isothermally Crystallized from Propane at Different Conditions**

Sample	Halsey Constant	Halsey Exponent	PSD Surface Area (m <sup>2</sup> /g)	BET Surface Area, (m <sup>2</sup> /g)
PP-100	5.37	1.63	73.8	125.5
PP-DBS	5.45	1.47	61.2	87.0

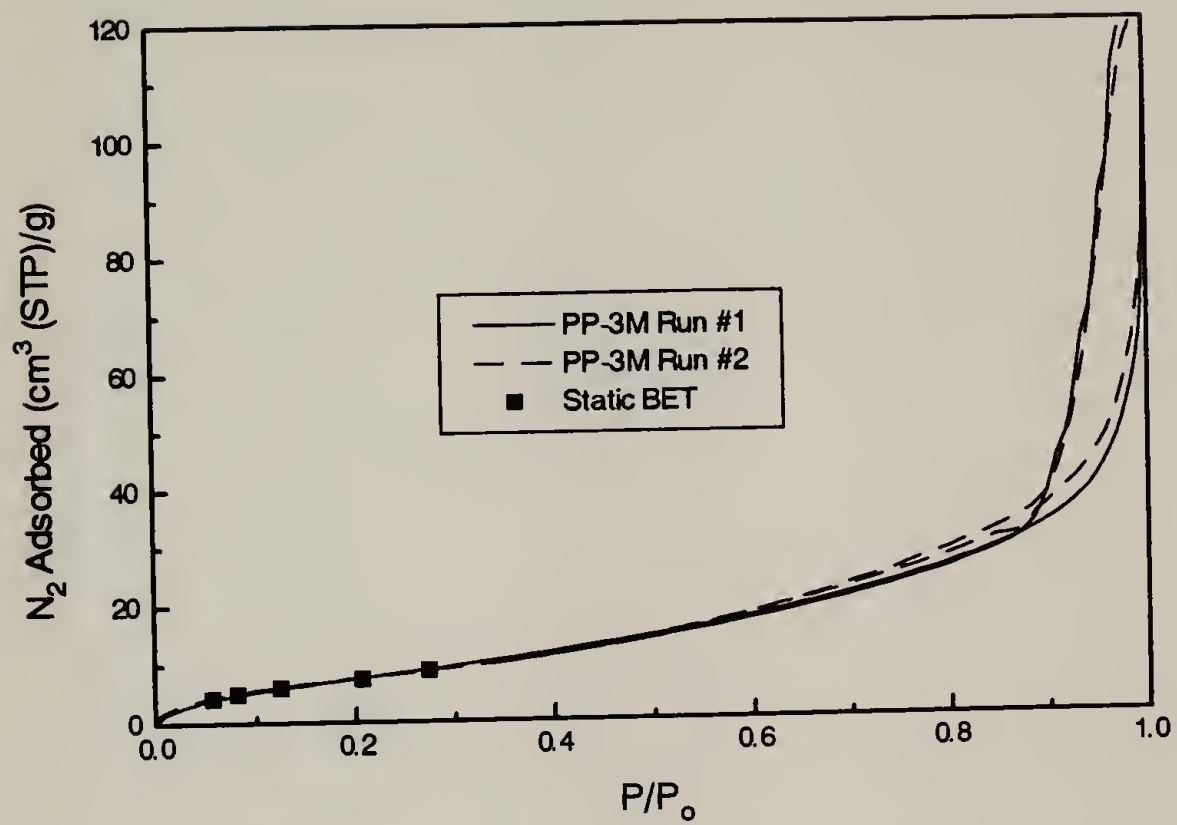


Figure B.1 Reproducibility of Adsorption-Desorption Isotherms for PP-3M

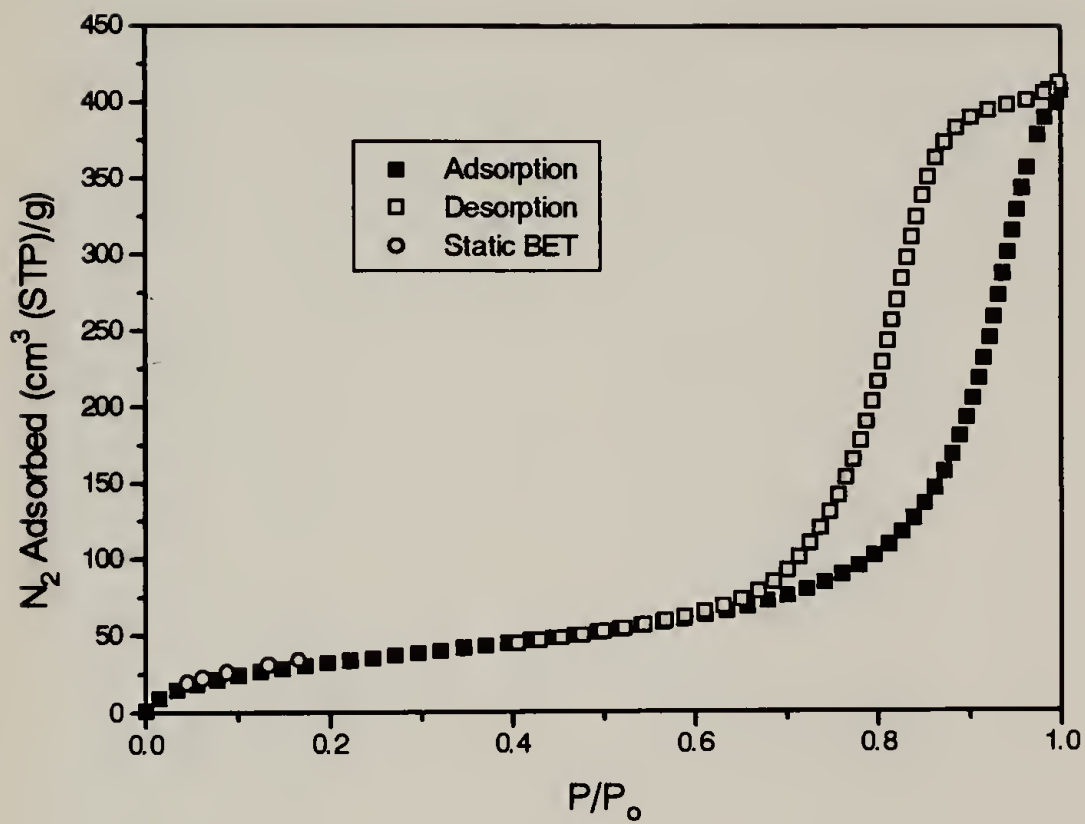


Figure B.2 Adsorption-Desorption Isotherm for PP-73

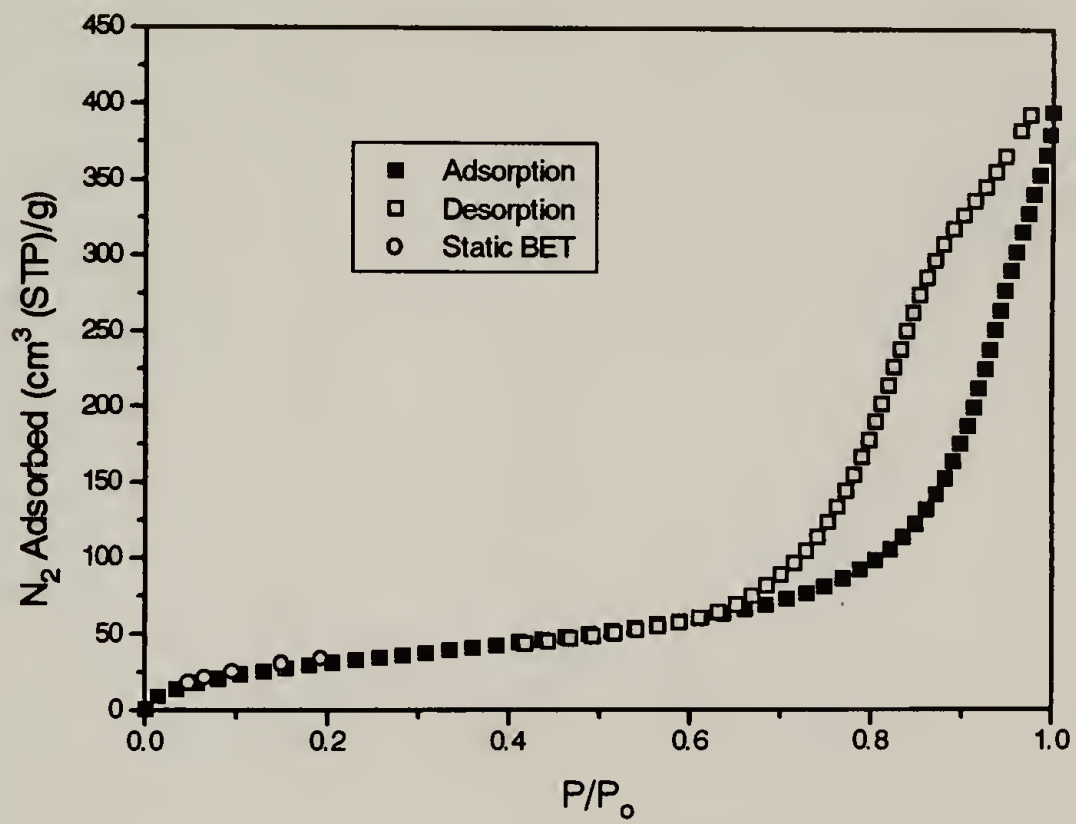


Figure B.3 Adsorption-Desorption Isotherm for PP-77

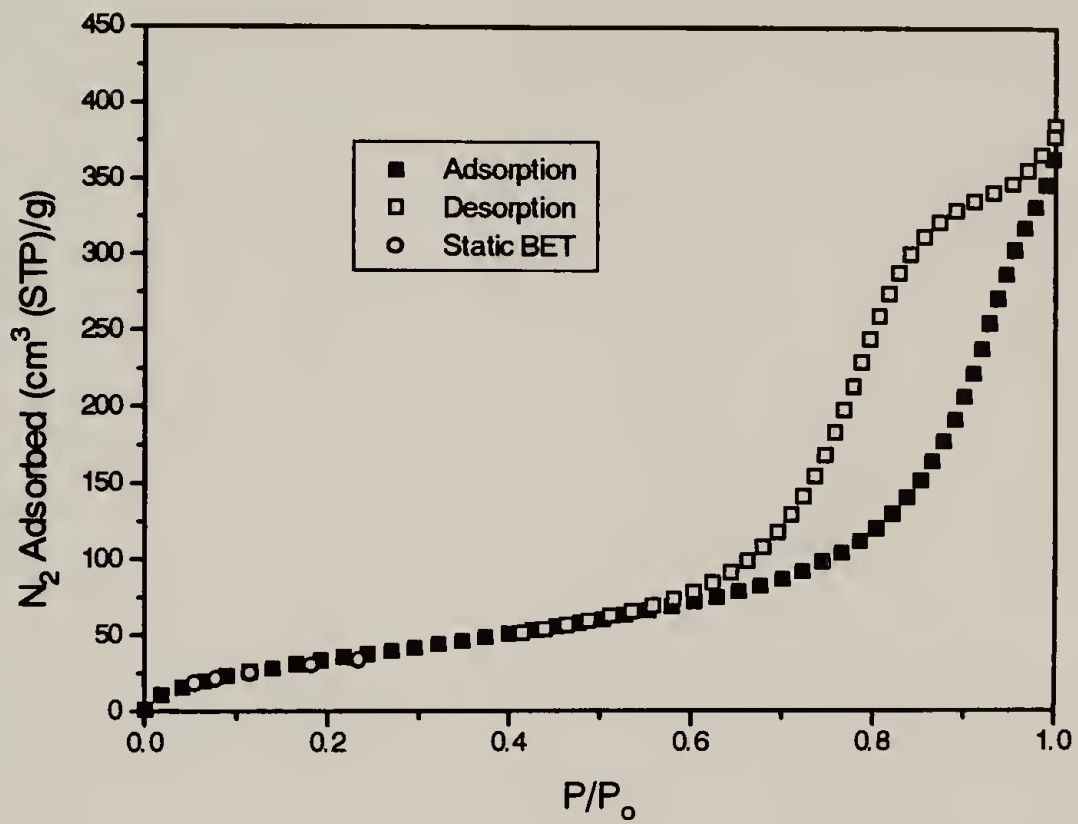


Figure B.4 Adsorption-Desorption Isotherm for PP-80

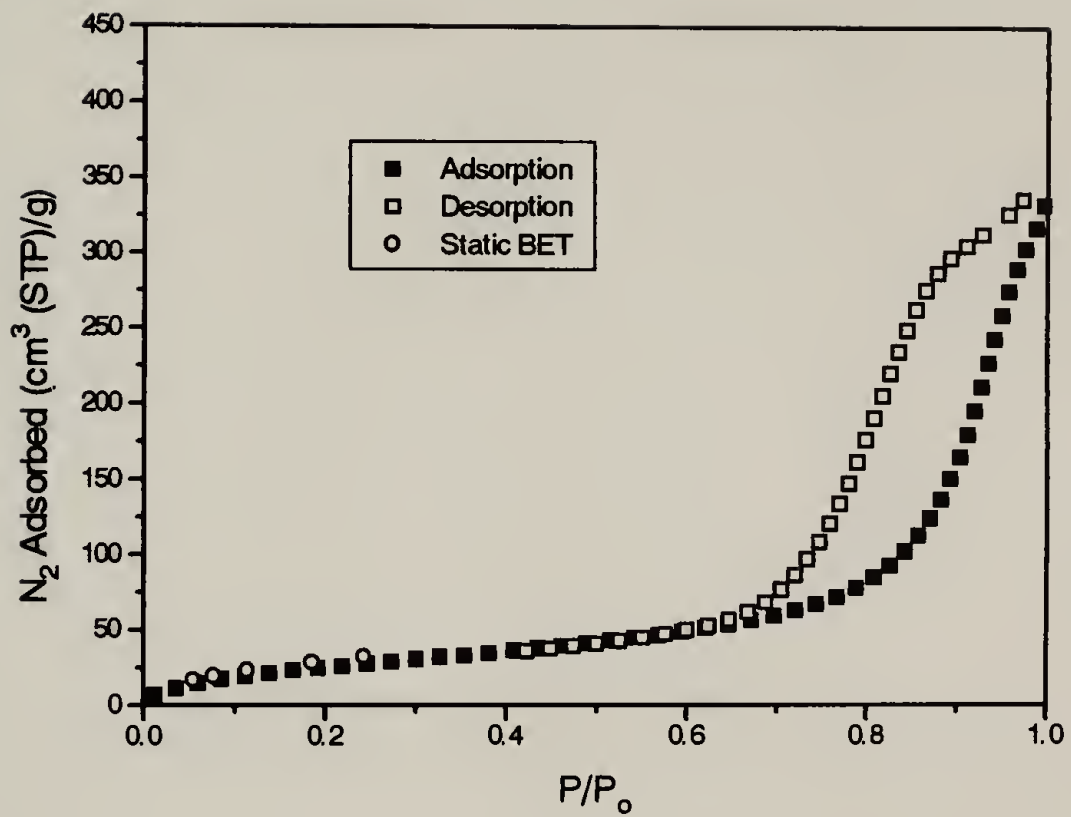


Figure B.5 Adsorption-Desorption Isotherm for PP-85

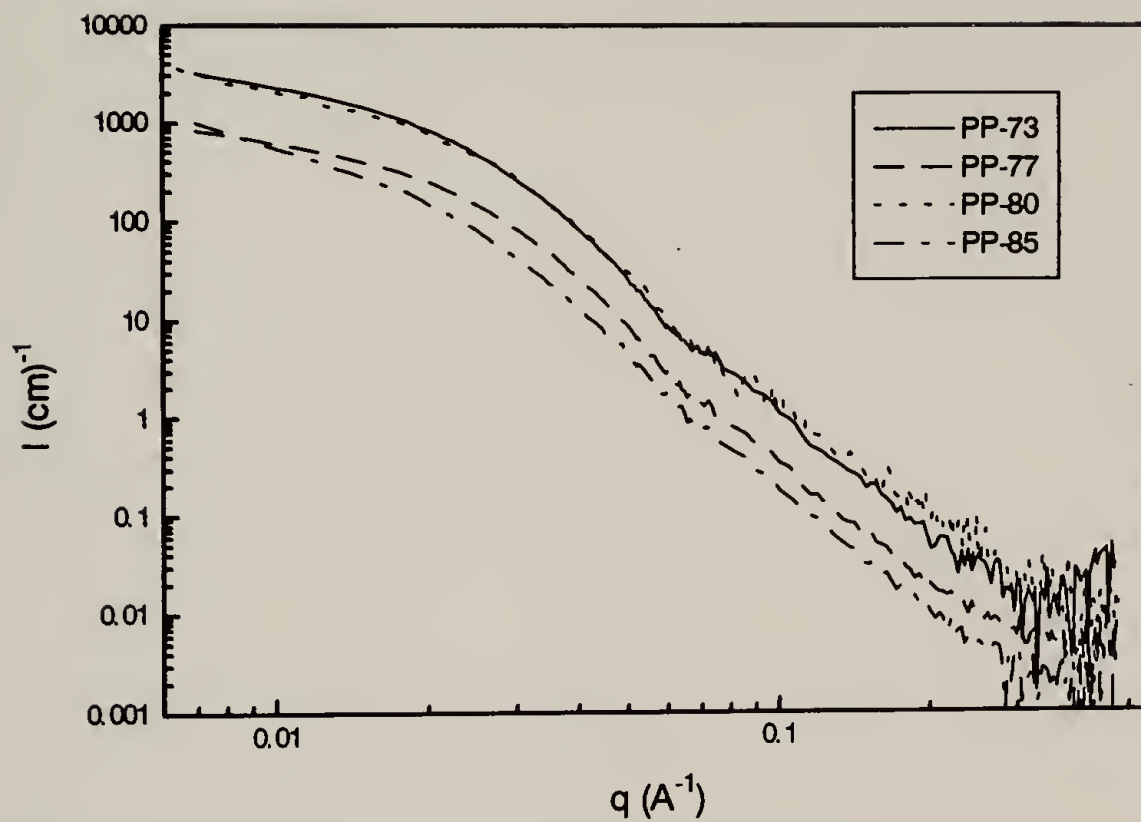


Figure B.6 Small Angle X-Ray Scattering Curves for PP-73, PP-77, PP-80, and PP-85

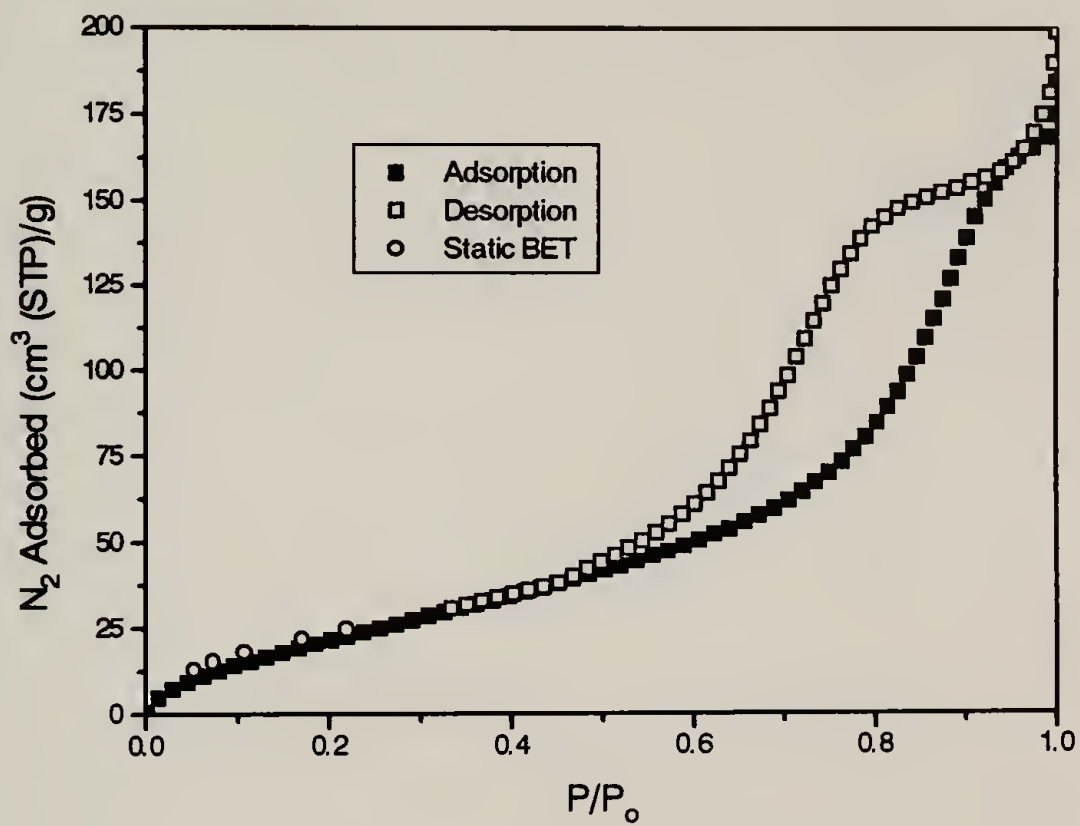


Figure B.7 Adsorption-Desorption Isotherm for PP-Butane



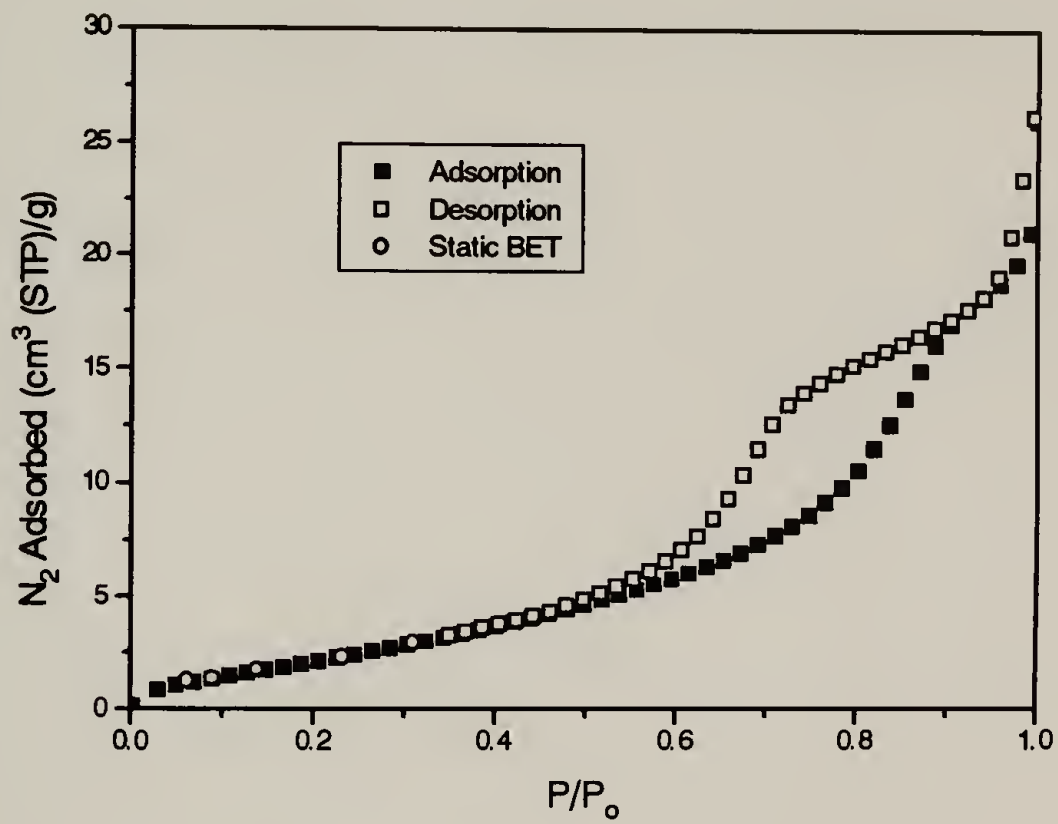


Figure B.8 Adsorption-Desorption Isotherm for PP-Heptane

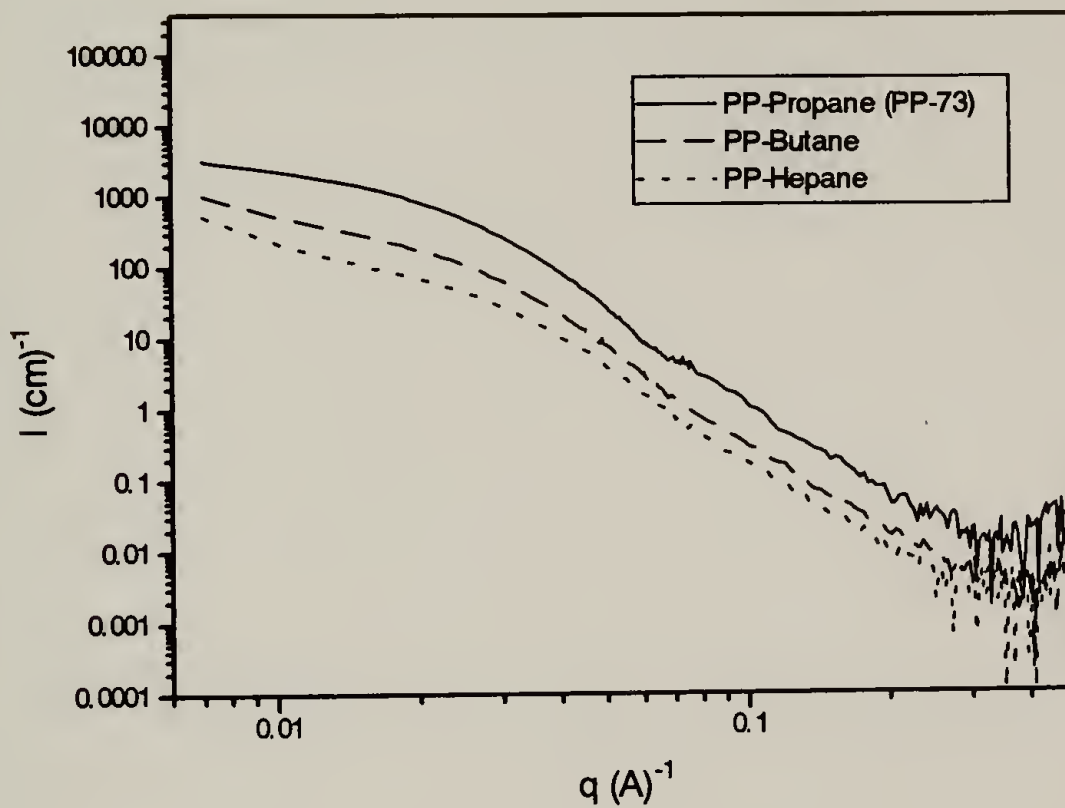


Figure B.9 Small Angle X-Ray Scattering Curves for PP-Propane (PP-73), PP-Butane, and PP-Heptane

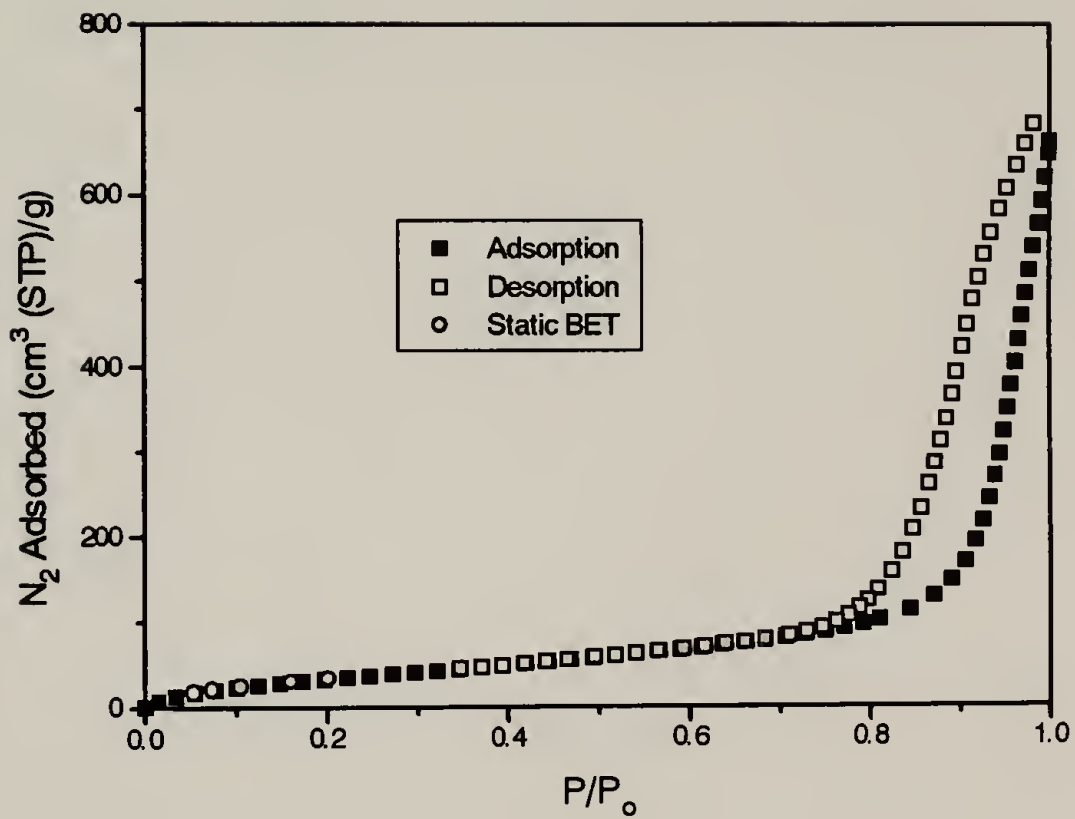


Figure B.10 Adsorption-Desorption Isotherm for PP-3K

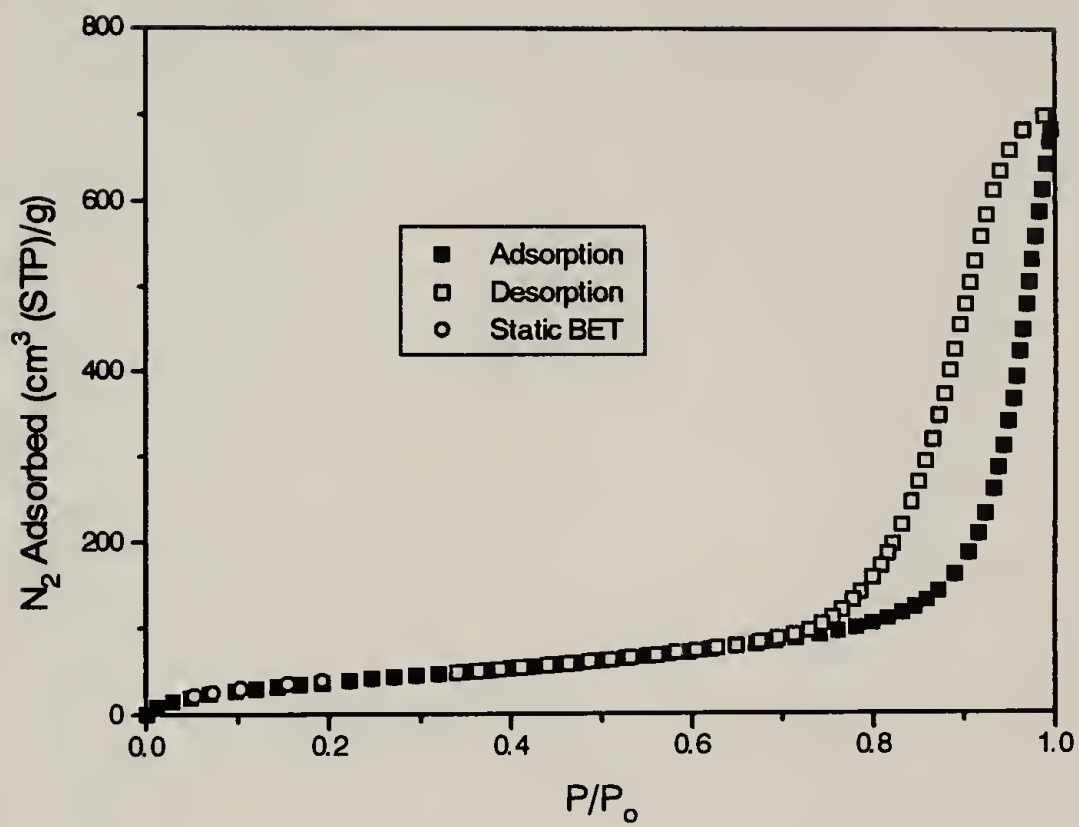


Figure B.11 Adsorption-Desorption Isotherm for PP-3K-2

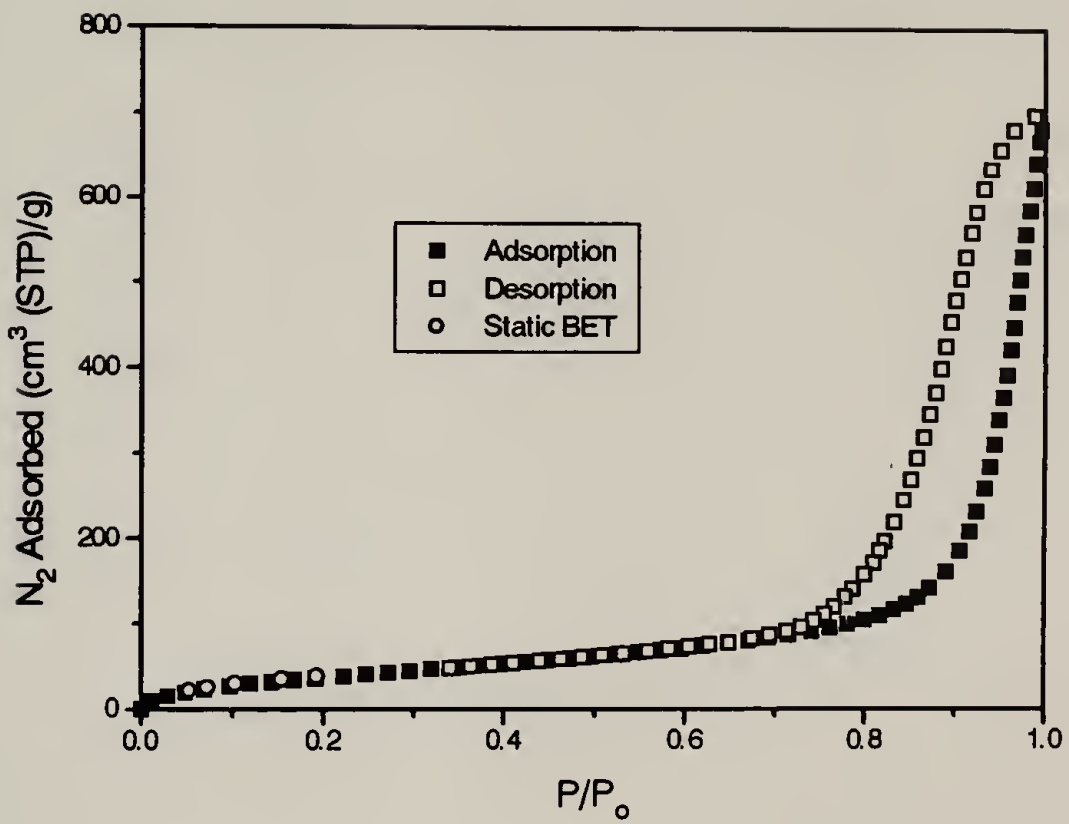


Figure B.12 Adsorption-Desorption Isotherm for PP-5K

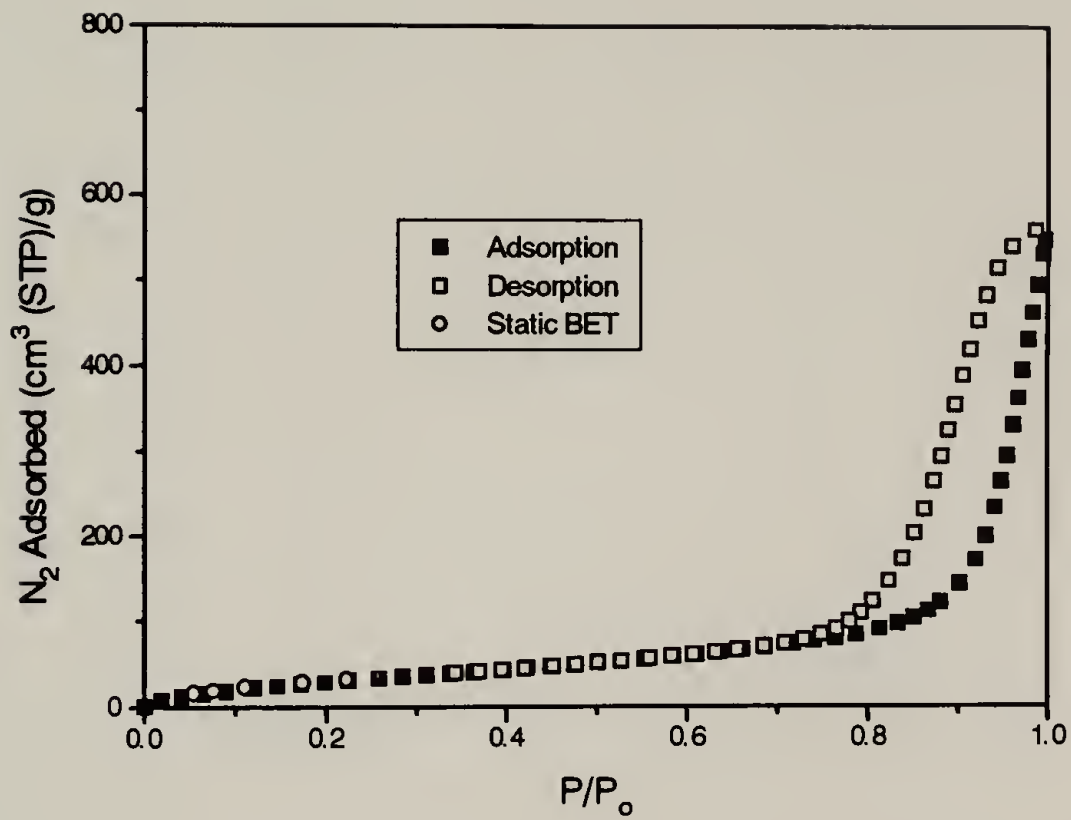


Figure B.13 Adsorption-Desorption Isotherm for PP-10K

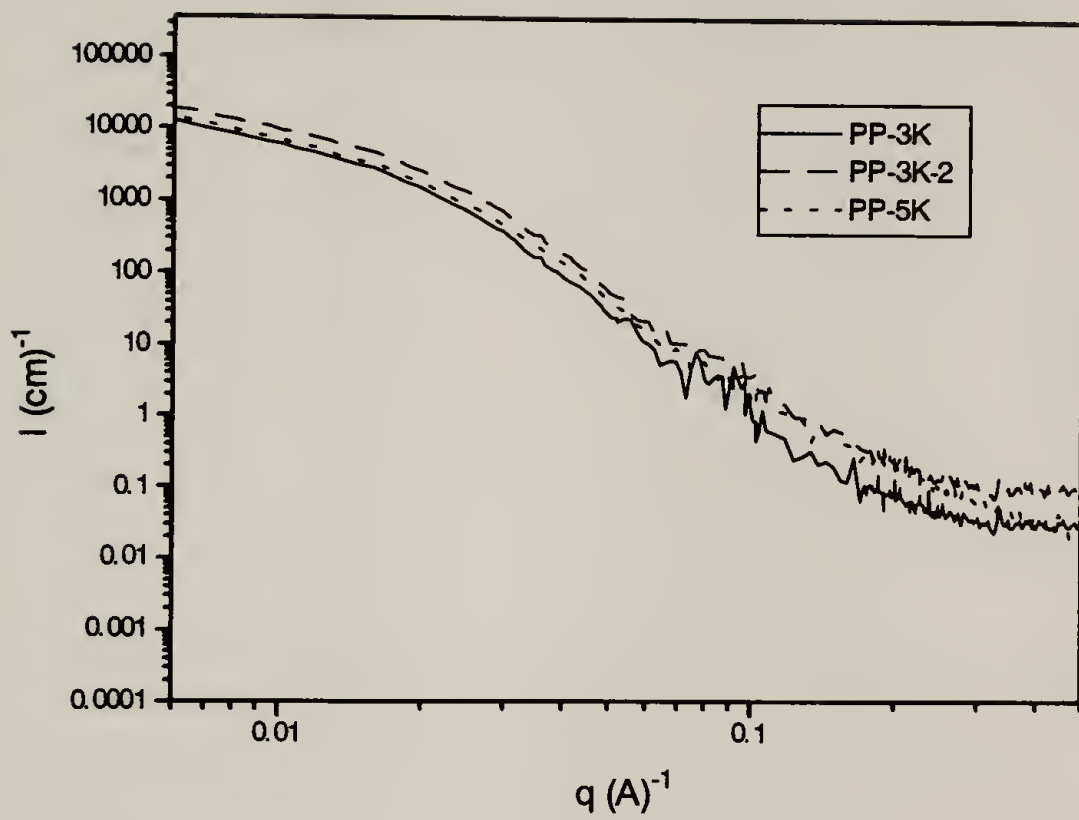


Figure B.14 Small Angle X-Ray Scattering Curves for PP-3K, PP-3K-2, and PP-5K

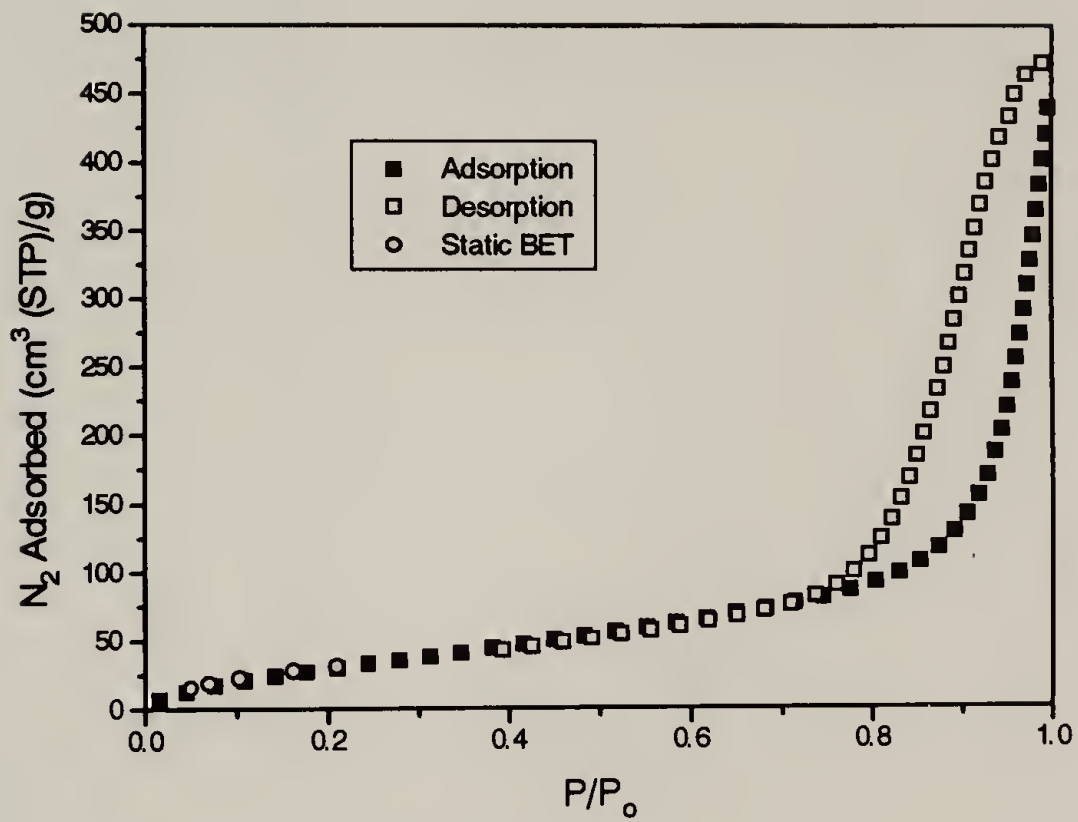


Figure B.15 Adsorption-Desorption Isotherm for PP-100



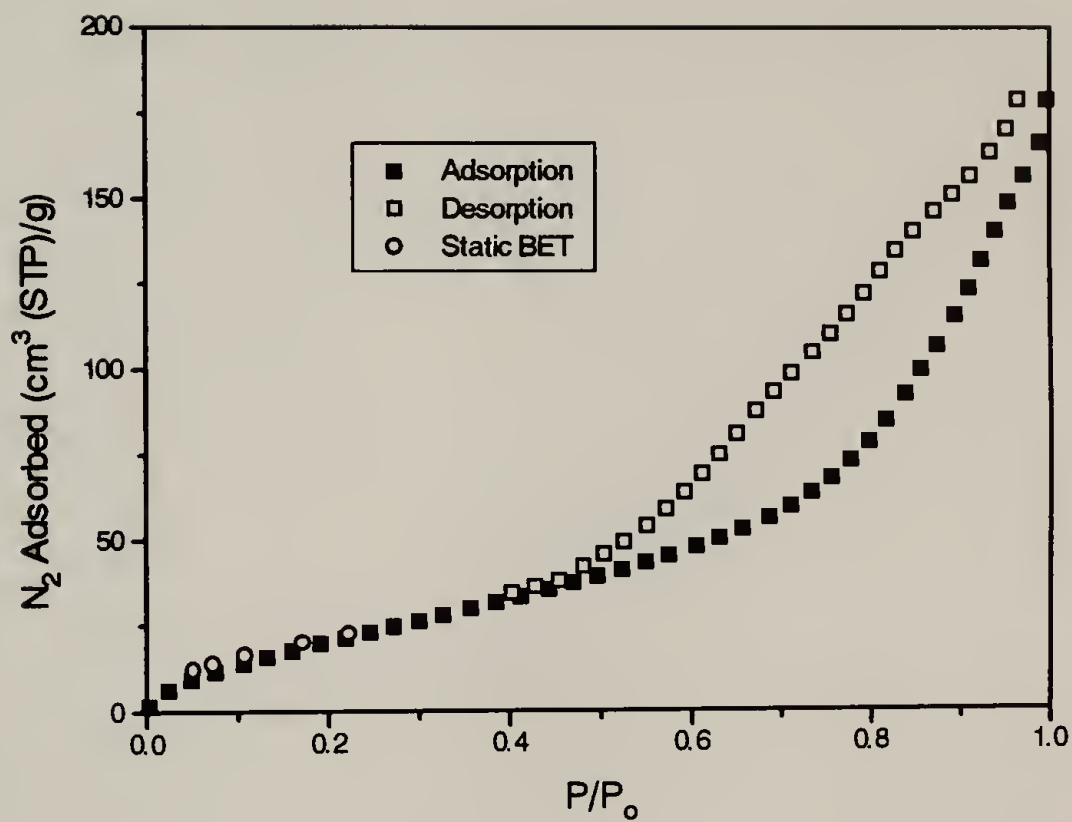


Figure B.16 Adsorption-Desorption Isotherm for PP-DBS

## BIBLIOGRAPHY

Alwattari, A. A., and D. R. Lloyd, "Microporous Membrane Formation via Thermally-Induced Phase Separation. VI. Effect of Diluent Morphology and Relative Crystallization Kinetics on Polypropylene Membrane Structures," *J. Memb. Sci.*, **64**, 55 (1991).

Aubert, J. H., "An Objective Characterization of the Cell Size of Microcellular Foams," *J. Cellular Plastics*, **24**, 132 (1988).

Aubert, J. H., "Isotactic Polystyrene Phase Diagrams and Physical Gelation," *Macromolecules*, **21**, 3468 (1988).

Aubert, J. H., "Structural Coarsening of Demixed Polymer Solutions," *Macromolecules*, **23**, 1446 (1990).

Beaucage, G., unpublished results, (1995).

Brunauer, S. L., P. H. Emmett, and E. Teller, "Adsorption of Gases in Multimolecular Layers," *J. Am. Chem. Soc.*, **60**, 309 (1938).

Brunauer, S., L. S. Deming, W. S. Deming, and E. Teller, "On a Theory of the van der Waals Adsorption of Gases," *J. Am. Chem. Soc.*, **62**, 1723 (1940).

Bush, P. J., D. Pradhan, and P. Ehrlich, "Lamellar Structure and Organization in Polyethylene Gels Crystallized from Supercritical Solution in Propane," *Macromolecules*, **24**, 1439 (1991).

Castro, A. J., "Microporous Products," U. S. Patent 4,519,909, (1985).

Cavanaugh, T. J., and E. B. Nauman, "The Future of Solvents in the Polymer Industry," *Trends Polym. Sci.*, **3**, 48, (1990).

Charlet, G., and G. Delmas, "Thermodynamic Properties of Polyolefin Solutions at High Temperature: 1. Lower Critical Solubility Temperatures of Polyethylene, Polypropylene and Ethylene-Propylene Copolymers in Hydrocarbon Solvents," *Polymer*, **22**, 1181 (1981).

Charlet, G., R. Ducasse, and G. Delmas, "Thermodynamic Properties of Polyolefin Solutions at High Temperature: 2. Lower Critical Solubility Temperatures for Polybutene-1, Polypentene-1, and Poly(4-methylpentene-1) in Hydrocarbon Solvents and the Determination of the Polymer Solvent Interaction-parameter for PB1 and one Ethylene-Propylene Copolymer," *Polymer*, **22**, 1190 (1981).

Chen, S., and M. Radosz, "Density-Tuned Polyolefin Phase Equilibria. 1. Binary Solutions of Alternating Poly(ethylene-propylene) in Subcritical and Supercritical Propylene, 1-Butene, and 1-Hexene. Experiment and Flory-Patterson Model," *Macromolecules*, **25**, 3089 (1992).

Chen, S., I. G. Economou, and M. Radosz, "Density-Tuned Polyolefin Phase Equilibria. 2. Multicomponent Solutions of Alternating Poly(ethylene-propylene) in Subcritical and Supercritical Olefins. Experiment and SAFT Model," *Macromolecules*, **25**, 4987 (1992).

Chen, S., M. Banaszak, and M. Radosz, "Phase Behavior of Poly(ethylene-1-butene) in Subcritical and Supercritical Propane: Ethyl Branches Reduce Segment Energy and Enhance Miscibility," *Macromolecules*, **28**, 1812 (1995).

Cohan, L. H., "Sorption Hysteresis and the Vapor Pressure of Concave Surfaces," *J. Am. Chem. Soc.*, **60**, 433 (1938).

Condo, P. D., E. J. Colman, and P. Ehrlich, "Phase Equilibria of Linear Polyethylene with Supercritical Propane," *Macromolecules*, **25**, 750 (1992).

Cook, R. L., H. E. King, and D. G. Peiffer, "Pressure-Induced Crossover from Good to Poor Solvent Behavior for Polyethylene Oxide in Water," *Phys. Rev. Lett.*, **69**(21), 3072 (1992).

Cotton, N. J., K. D. Bartle, A. A. Clifford, and C. J. Dowle, "Rate and Extent of Supercritical Fluid Extraction of Additives from Polypropylene: Diffusion, Solubility, and Matrix Effects," *J. Appl. Polym. Sci.*, **48**, 1607 (1993).

Cowie, J. M. G., and I. J. McEwen, "Lower Critical Solution Temperatures of Polypropylene Solutions," *J. Polym. Sci.: Polym. Phys. Ed.*, **12**, 441 (1974).

Debye, P., and A. M. Bueche, "Scattering by an Inhomogeneous Solid," *J. Appl. Phys.*, **20**, 518 (1949).

Debye, P., H. R. Anderson, Jr., and H. Brumberger, "Scattering by an Inhomogeneous Solid. II. The Correlation Function and its Application," *J. Appl. Phys.*, **28**(6), 679 (1957).

de Loos, T. W., W. Poot, and G. A. M. Diepen, "Fluid Phase Equilibria in the System Polyethylene + Ethylene. 1. Systems of Linear Polyethylene + Ethylene at High Pressure," *Macromolecules*, **16**, 111 (1983).

de Loos, T. W., W. Poot, and G. A. M. Diepen, "Fluid Phase Equilibria in the System Polyethylene + Ethylene. 2. Calculation of Cloud Point Curves for Systems of Linear Polyethylene + Ethylene," *Macromolecules*, **16**, 117 (1983).

- DeSimone, J. M., Z. Guan, and C. S. Elsbernd, "Synthesis of Fluoropolymers in Supercritical Carbon Dioxide," *Science*, **257**, 945 (1992).
- Ehrlich, P., "Phase Equilibria of Polymer-Solvent Systems at High Pressures Near Their Critical Loci. II. Polyethylene-Ethylene," *J. Polym. Sci., Pt. A.*, **3**, 131 (1965).
- Ehrlich, P., "Supercritical Polymer Solutions and Polymer-Fluid Interactions at High Pressure," *Chemtracts-Macromol. Chem.*, **3**, 1 (1992).
- Ehrlich, P., and J. J. Kurpen, "Phase Equilibria of Polymer-Solvent Systems at High Pressures Near Their Critical Loci: Polyethylene with n-Alkanes," *J. Polym. Sci., Pt. A*, **1**, 3217 (1963).
- Elsbernd, C. S., J. M. DeSimone, A. M. Hellstern, S. D. Smith, P. M. Gallagher, V. J. Krukonis, and J. E. McGrath, "The Application of Supercritical Fluids in the Fractionation and Characterization of Siloxane Oligomers and Graft Copolymers," *Polym. Prepr. (Am. Chem. Soc., Div. Polym. Chem.)*, **31**(1), 673 (1990).
- Fillon, B., J. C. Wittmann, B. Lotz, and A. Thierry, "Self-Nucleation and Recrystallization of Isotactic Polypropylene ( $\alpha$  Phase) Investigated by Differential Scanning Calorimetry," *J. Polym. Sci. Pt. B. Polym. Phys.*, **31**, 1383 (1993).
- Fillon, B., B. Lotz, A. Thierry, and J. C. Wittmann, "Self-Nucleation and Enhanced Nucleation of Polymers. Definition of a Convenient Calorimetric "Efficiency Scale" and Evaluation of Nucleating Additives in Isotactic Polypropylene ( $\alpha$  Phase)," *J. Polym. Sci. Pt. B. Polym. Phys.*, **31**, 1395 (1993).
- Flory, P. J., *Principles of Polymer Chemistry*, Cornell University Press: Ithaca (1953).
- Flory, P. J., R. A. Orwoll, and A. Vrij, "Statistical Thermodynamics of Chain Molecule Liquids. I. An Equation of State for Normal Paraffin Hydrocarbons," *J. Am. Chem. Soc.*, **86**, 3507 (1964).
- Flory, P. J., R. A. Orwoll, and A. Vrij, "Statistical Thermodynamics of Chain Molecule Liquids. II. Liquid Mixtures of Normal Paraffin Hydrocarbons," *J. Am. Chem. Soc.*, **86**, 3515 (1964).
- Folie, B. and M. Radosz, "Phase Equilibria in High-Pressure Polyethylene Technology," *Ind. Chem. Eng. Res.*, **34**, 1501 (1995).
- Freeman, P. I., and J. S. Rowlinson, "Lower Critical Points in Polymer Solutions," *Polymer*, **1**, 20 (1960).
- Glatter, O., "Data Treatment," in *Small Angle X-ray Scattering*, O. Glatter and O. Kratky, Eds., Academic Press: London (1982).

- Gregg, C. J., F. P. Stein, and M. Radosz, "Phase Behavior of Telechelic Polyisobutylene (PIB) in Subcritical and Supercritical Fluids. 1. Inter- and Intra-Association Effect for Blank, Monohydroxy, and Dihydroxy PIB (1K) in Ethane, Propane, Dimethyl Ether, Carbon Dioxide, and Chlorodifluoromethane," *Macromolecules*, **27**, 4972 (1994).
- Gregg, C. J., F. P. Stein, and M. Radosz, "Phase Behavior of Telechelic Polyisobutylene (PIB) in Subcritical and Supercritical Fluids. 2. PIB Size, Solvent Polarity, and Inter- and Intra-Association Effect for Blank, Monohydroxy, and Dihydroxy PIB (11K) in Ethane, Propane, Carbon Dioxide, and Dimethyl Ether," *Macromolecules*, **27**, 4981 (1994).
- Gregg, S. J., and K. S. W. Sing, *Adsorption, Surface Area and Porosity*, 2nd Ed., Academic Press: London (1982).
- Halsey, G., "Physical Adsorption on Non-Uniform Surfaces," *J. Chem. Phys.*, **16**(10), 931, (1948).
- Hasch, B. M., M. A. Meilchen, S. Lee, and M. A. McHugh, "High-Pressure Phase Behavior of Mixtures of Poly(Ethylene-co-Methyl Acrylate) with Low-Molecular Weight Hydrocarbons," *J. Polym. Sci.: Part B: Polym. Phys.*, **30**, 1365 (1992).
- Hasch, B. M., S. Lee, M. A. McHugh, J. J. Watkins, and V. J. Krukonis, "The Effect Of Backbone Structure on the Cloud Point Behavior of Polyethylene-Ethane and Polyethylene-Propane Mixtures," *Polymer*, **34**(12), 2554 (1993).
- Hasch, B. M., M. A. Meilchen, S. Lee, and M. A. McHugh, "Cosolvency Effects on Copolymer Solutions at High Pressure," *J. Polym. Sci.: Part B: Polym. Phys.*, **31**, 429 (1993).
- Hasch, B. M., S. Lee, and M. A. McHugh, "Strengths and Limitations for Calculating Polar Copolymer-Solvent Phase Behavior," *J. Appl. Polym. Sci.*, **59**, 1107 (1996).
- Haschets, C. W., and A. D. Shine, "Phase Behavior of Polymer-Supercritical Chlorodifluoromethane Solutions," *Macromolecules*, **26**, 5052 (1993).
- Hosemann, R., and S. N. Bagchi, *Direct Analysis of Diffraction by Matter*, North-Holland Publishing: Amsterdam (1962).
- Keith, H. D., and F. J. Padden, "Spherulitic Crystallization from the Melt. I. Fractionation and Impurity Segregation and Their Influence on Crystalline Morphology," *J. Appl. Phys.*, **35**(4), 1270 (1964).
- Khoury, F., "The Spherulitic Crystallization of Isotactic Polypropylene From Solution: On the Evolution of Monoclinic Spherulites From Dendritic Chain-Folded Crystal Precursors," *J. Res. Natl. Bur. Stand.*, **70A**, 29 (1966).

- Kiamos, A. A., and M. D. Donohue, "The Effect of Supercritical Carbon Dioxide on Polymer-Solvent Mixtures," *Macromolecules*, **27**, 357 (1994).
- Kim, S. S., and D. R. Lloyd, "Microporous Membrane Formation via Thermally-Induced Phase Separation. III. Effect of Thermodynamic Interactions on the Structure of Isotactic Polypropylene Membranes," *J. Memb. Sci.*, **64**, 13 (1991).
- Kim, S. S., G. B. A. Lim, A. A. Alwattari, Y. F. Wang, and D. R. Lloyd, "Microporous Membrane Formation via Thermally-Induced Phase Separation. V. Effect of Diluent Mobility and Crystallization on the Structure of Isotactic Polypropylene Membranes," *J. Memb. Sci.*, **64**, 41 (1991).
- Kiran, E., Y. Xiong, and W. Zhuang, "Modeling Polyethylene Solutions in Near and Supercritical Fluids Using the Sanchez-Lacombe Model," *J. Supercritical Fluids*, **6**, 193 (1993).
- Kiran, E., W. Zhuang, and Y. L. Sen, "Solubility and Demixing of Polyethylene in Supercritical Binary Fluid Mixtures: Carbon-Dioxide-Cyclohexane, Carbon Dioxide-Toluene, Carbon Dioxide-Pentane," *J. Appl. Polym. Sci.*, **47**, 895 (1993).
- Koningsveld, R., and A. J. Staverman, "Liquid-Liquid Phase Separation in Multicomponent Polymer Solutions. I. Statement of the Problem and Description of Methods of Calculation," *J. Polym. Sci. Pt. A-2*, **6**, 305 (1968).
- Koningsveld, R., and A. J. Staverman, "Liquid-Liquid Phase Separation in Multicomponent Polymer Solutions. II. The Critical State," *J. Polym. Sci. Pt. A-2*, **6**, 325 (1968).
- Koningsveld, R., and A. J. Staverman, "Liquid-Liquid Phase Separation in Multicomponent Polymer Solutions. III. Cloud-Point Curves," *J. Polym. Sci. Pt. A-2*, **6**, 349 (1968).
- Kulkarni, S. K., unpublished results, (1994).
- Lacombe, R. H., and I. C. Sanchez, "Statistical Thermodynamics of Fluid Mixtures," *J. Phys. Chem.*, **80**, 2568 (1976).
- Lauritzen, J. I., and J. D. Hoffman, "Theory of Formation of Polymer Crystals with Folded Chains in Dilute Solution," *J. Res. Nat. Bur. Stand.*, **64A**, 73 (1960).
- Lee, S., M. A. LoStracco, and M. A. McHugh, "High-Pressure, Molecular Weight-Dependent Behaviour of (Co)polymer-Solvent Mixtures: Experiments and Modeling," *Macromolecules*, **27**, 4652 (1994).

- LeMay, J. D., R. W. Hopper, L. W. Hrubesh, and R. W. Pekala, "Low-Density Microcellular Materials," *MRS Bulletin*, **15**(12), 19 (1990).
- Lim, G. B. A., S. S. Kim, Q. Ye, Y. F. Wang, and D. R. Lloyd, "Microporous Membrane Formation via Thermally-Induced Phase Separation. IV. Effect of Isotactic Polypropylene Crystallization Kinetics on Membrane Structure," *J. Memb. Sci.*, **64**, 31 (1991).
- Liu, D. D., and J. M. Prausnitz, "Calculation of Phase Equilibria for Mixtures of Ethylene and Low-Density Polyethylene at High Pressures," *Ind. Eng. Process Des. Dev.*, **19**, 205 (1980).
- Lloyd, D. R., K. E. Kinzer, and H. S. Tseng, "Microporous Membrane Formation via Thermally Induced Phase Separation. I. Solid-Liquid Phase Separation," *J. Mem. Sci.*, **52**, 239 (1990).
- Lloyd, D. R., S. S. Kim, and K. E. Kinzer, "Microporous Membrane Formation via Thermally-Induced Phase Separation. II. Liquid-Liquid Phase Separation," *J. Mem. Sci.*, **64**, 1 (1991).
- Lopatin, G., L. Yen, and R. R. Rogers, "Microporous Membranes from Polypropylene," U. S. Patent 4,874,567, (1989).
- Lotz, B., S. Graff, and J. C. Wittmann, "Crystal Morphology of the  $\gamma$  (Triclinic) Phase of Isotactic Polypropylene and its Relation to the  $\alpha$  Phase," *J. Polym. Sci. Part B: Polym. Phys.*, **24**, 2017 (1986).
- Lotz, B., S. Graff, C. Straupé, and J. C. Wittmann, "Single Crystals of  $\gamma$  Phase Isotactic Polypropylene: Combined Diffraction and Morphological Support for a Structure with Non-parallel Chains," *Polymer*, **32**, 2902 (1991).
- Lowell, S., and J. E. Shields, *Powder Surface Area and Porosity*, Chapman and Hall: New York (1984).
- McClellan, A. K., and M. A. McHugh, "Separating Polymer Solutions Using High Pressure Lower Critical Solution Temperature (LCST) Phenomena," *Polym. Eng. and Sci.*, **25**(17), 1088 (1985).
- McGuire, K. S., D. R. Lloyd, and G. B. A. Lim, "Microporous Membrane Formation via Thermally-Induced Phase Separation. VII. Effect of Dilution, Cooling Rate, and Nucleating Agent Addition on Morphology," *J. Memb. Sci.*, **79**, 27 (1993).
- McHugh, M. A., and T. L. Guckes, "Separating Polymer Solutions with Supercritical Fluids," *Macromolecules*, **18**, 674 (1985).

- McHugh, M. A., and V. Krukonis, *Supercritical Fluid Extraction: Principles and Practice*, Butterworths: Boston (1986)
- Meilchen, M. A., B. M. Hasch, and M. A. McHugh, "Effect of Copolymer Composition on the Phase Behavior of Poly(ethylene-co-methyl acrylate) with Propane and Chlorodifluoromethane," *Macromolecules*, **24**, 4874 (1991).
- Meilchen, M. A., B. M. Hasch, S. Lee, and M. A. McHugh, "Poly(ethylene-co-methyl acrylate)-solvent-cosolvent Phase Behavior at High Pressures," *Polymer*, **33**, 1922 (1992).
- Mikhail, R. S., and E. Robens, *Microstructure and Thermal Analysis of Solid Surfaces*, John Wiley & Sons: New York (1983).
- Padden, F. J., and H. D. Keith, "Spherulitic Crystallization in Polypropylene," *J. Appl. Phys.*, **30**(10), 1479 (1959).
- Padden, F. J., and H. D. Keith, "Crystallization in Thin Films of Isotactic Polypropylene," *J. Appl. Phys.*, **37**, 4013 (1966).
- Padden, F. J., and H. D. Keith, "Mechanism for Lamellar Branching In Isotactic Polypropylene," *J. Appl. Phys.*, **44**(3), 1217 (1973).
- Pae, K. D., " $\gamma$ - $\alpha$  Solid-Solid Transition of Isotactic Polypropylene," *J. Polym. Sci. Pt. A-2*, **6**, 657 (1968).
- Panayiotou C., and I. C. Sanchez, "Hydrogen Bonding in Fluids: An Equation-of-State Approach," *J. Phys. Chem.*, **95**, 10090 (1991).
- Patterson, D., and G. Delmas, "Critical State in Chain-Molecule Mixtures," *Trans. Faraday Soc.*, **65**, 708 (1969).
- Pradhan, D., and P. Ehrlich, "Morphologies of Microporous Polyethylene and Polypropylene Gels Crystallized from Solution in Supercritical Propane," *J. Polym. Sci. Part B: Polym. Phys.*, **33**, 1053 (1995).
- Reid, R. C., J. M. Prausnitz, and B. E. Poling, *The Properties of Gases and Liquids*, 4th. Ed., Mc-Graw Hill: New York (1987).
- Rodgers, P. A., and I. C. Sanchez, "Improvement to the Lattice-Fluid Prediction of Gas Solubilities in Polymer Liquids," *J. Polym. Sci. Pt. B. Polym. Phys.*, **31**, 273 (1993).
- Rowlinson, J. S., and F. L. Swinton, *Liquids and Liquid Mixtures*, 3rd Ed., Butterworths: London (1982).



- Sanchez, I. C., "Statistical Thermodynamics of Bulk and Surface Properties of Polymer Mixtures," *J. Macromol. Sci.-Phys.*, **B17(3)**, 565 (1980).
- Sanchez, I. C., "Equation of State Thermodynamics of Polymer and Related Solutions," in *Models for Thermodynamic and Phase Equilibria Calculations*, S. I. Sandler, ed., Marcel Dekker: New York (1993).
- Sanchez, I. C., personal communication, (1996).
- Sanchez, I.C., and A. C. Balazs, "Generalization of the Lattice-Fluid Model for Specific Interactions," *Macromolecules*, **22**, 2325 (1989).
- Sanchez, I. C., and R. H. Lacombe, "An Elementary Molecular Theory of Classical Fluids. Pure Fluids," *J. Phys. Chem.*, **80**, 2352 (1976).
- Sanchez, I. C., and R. H. Lacombe, "An Elementary Equation of State for Polymer Liquids," *J. Polym. Sci., Polym. Lett. Ed.*, **15**, 71 (1977).
- Sanchez, I. C., and R. H. Lacombe, "Statistical Thermodynamics of Polymer Solutions," *Macromolecules*, **11**, 1145 (1978).
- Sauer, J. A., D. R. Morrow, and G. C. Richardson, "Morphology of Solution Grown Polypropylene Crystal Aggregates," *J. Appl. Phys.*, **36**, 3017 (1965).
- Sawyer, L. C., and D. T. Grubb, *Polymer Microscopy*, Chapman and Hall: New York (1987).
- Schmidt, R., E. W. Hansen, M. Stöcker, D. Akporiaye, and O. H. Ellestad, "Pore Size Determination of MCM-41 Mesoporous Materials by means of  $^1\text{H}$  NMR Spectroscopy,  $\text{N}_2$  Adsorption, and HREM. A Preliminary Study," *J. Am. Chem. Soc.*, **117**, 4049 (1995).
- Scholte, TH. G., H. L. J. Meijerlink, H. M. Schoffeleers, and A. M. G. Brands, "Mark-Houwink Equation and GPC Calibration for Linear Short-Chain Branched Polyolefins, Including Polypropylene and Ethylene-Propylene Copolymers," *J. Appl. Polym. Sci.*, **29**, 3763 (1984).
- Scott, R. L., and P. H. Van Konynenburg, "Van der Waals and Related Models for Hydrocarbon Mixtures," *Disc. Faraday Soc.*, **49**, 87 (1970).
- Seckner, A. J., A. K. McClellan, and M. A. McHugh, "High-Pressure Solution Behavior of the Polystyrene-Toluene-Ethane System," *AIChE J.*, **34(1)**, 9 (1988).
- Shaffer, K. A., and J. M. DeSimone, "Chain Polymerization in Inert Near- and Supercritical Fluids," *Trends. Polym. Sci.*, **5(3)**, 146 (1995).

Siow, K. S., G. Delmas, and D. Patterson, "Cloud-Point Curves in Polymer Solutions with Adjacent Upper and Lower Critical Solution Temperatures," *Macromolecules*, **5**, 29 (1972).

Smith, J. M., and H. C. Van Ness, *Introduction to Chemical Engineering Thermodynamics*, 4th Ed., McGraw-Hill: New York (1987).

Suresh, S. J., R. M. Enick, and E. J. Beckman, "Phase Behavior of Nylon 6/Trifluoroethanol/Carbon Dioxide Mixtures," *Macromolecules*, **27**, 348 (1994).

Thierry, A., C. Straupé, B. Lotz, and J. C. Wittmann, "Physical Gelation: A Path Towards 'Ideal' Dispersion of Additives in Polymers," *Polym. Comm.*, **31**, 299 (1990).

Thierry, A., B. Fillon, C. Straupé, B. Lotz, and J. C. Wittman, "Polymer Nucleating Agents: Efficiency Scale and Impact of Physical Gelation," *Progr. Colloid Polym. Sci.*, **87**, 28 (1992).

Tsai, F., and J. M. Torkelson, "Roles of Phase Separation Mechanism and Coarsening in the Formation of Poly(methyl methacrylate) Assymmetric Membranes," *Macromolecules*, **23**, 775 (1990).

Tsai, F., and J. M. Torkelson, "Microporous Poly(methyl methacrylate) Membranes: Effect of Low-Viscosity Solvent on the Formation Mechanism," *Macromolecules*, **23**, 4983 (1990).

Tuminello, W. H., D. J. Brill, D. J. Walsh, and M. E. Paulaitis, "Dissolving Poly(tetrafluoroethylene) in Low Boiling Halocarbons," *J. Appl. Polym. Sci.*, **56**, 495 (1995).

Tuminello, W. H., G. T. Dee, and M. A. McHugh, "Dissolving Perfluoropolymers in Supercritical Carbon Dioxide," *Macromolecules*, **28**, 1506 (1995).

Turner-Jones, A., J. M. Aizlewood, and D. R. Beckett, "Crystalline Forms of Isotactic Polypropylene," *Makromol. Chem.*, **75**, 134 (1964).

Vitzthum, G. H., and M. A. Davis, "0.1 Micron Rated Polypropylene Membrane and Method for its Preparation," U. S. Patent 4,490,431, (1984).

Walsh, D. J., and G. T. Dee, "Calculations of the Phase Diagrams of Polyethylene Dissolved in Supercritical Solvents," *Polymer*, **29**, 656 (1988).

Watkins, J. J., V. J. Krukonis, P. D. Condo, D. Pradhan, and P. Ehrlich, "Fractionation of High Density Polyethylene in Propane by Isothermal Pressure Profiling and Isobaric Temperature Profiling," *J. Supercritical Fluids*, **4**, 24 (1991).

Wunderlich, B., *Macromolecular Physics: Volume 1: Crystal Structure, Morphology, Defects*, Academic Press: New York (1973).

Xiong, Y., and E. Kiran, "Prediction of High-Pressure Phase Behavior in Polyethylene/n-pentane/Carbon Dioxide Ternary System with the Sanchez-Lacombe Model," *Polymer*, **35**, 4408 (1994).

Xiong, Y., and E. Kiran, "Comparison of Sanchez-Lacombe and SAFT Model in Predicting Solubility of Polyethylene in High-Pressure Fluids," *J. Appl. Polym. Sci.*, **55**, 1805 (1995).

Zeman, L., and D. Patterson, "Pressure Effects in Polymer Solution Phase Equilibria. II. Systems Showing Upper and Lower Critical Solution Temperatures," *J. Phys. Chem.*, **76(8)**, 1214 (1972).

Zeman, L., J. Biros, G. Delmas, and D. Patterson, "Pressure Effects in Polymer Solution Phase Equilibria. I. The Lower Critical Solution Temperature of Polyisobutylene and Polydimethylsiloxane in Lower Alkanes," *J. Phys. Chem.*, **76(8)**, 1206 (1972).

Zhao, X., R. Watkins, and S. W. Barton, "Strategies for Supercritical CO<sub>2</sub> Fractionation of Polydimethylsiloxane," *J. Appl. Polym. Sci.*, **55**, 773 (1995).



